In May 2005, the first International Conference on Polymeric Materials in Automotive was organized in Bratislava followed by the second PMA in 2007. The events reflected steeply rising importance of automotive industry in Slovakia, derived from the presence of dominant investors in Slovakia, namely Volkswagen, PSA and Kia including a number of other companies – suppliers of plastics and rubber parts being a significant part of them – building up their new facilities in the country. Almost 350 participants from 25 countries attended the two conferences which were ranked as successful and interesting. The appreciated feature consisted in a fact that, although targeted to polymeric materials used in automotive industry, the scope of the conference was kept highly scientific. Thus, new ideas have been presented, many of these being far away from industrial application, still contributing significantly to a progress in the area.

Similar to the PMA 2005 and PMA 2007, the upcoming conference PMA 2009 is targeted on various aspects related to plastics and rubber in the automotive industry, with the aim to exchange the innovative approaches towards new polymer products increasingly having a decisive influence on the design and appearance of new generation of cars. Developing goals such as aesthetic appeal and comfort, safety and lightweight construction, as well as quality and cost are affected directly by the material concept and the corresponding processing and product technology.

International scientific conference on rubber, Slovak Rubber Conference, was organized every year by the Rubber Research Institute of Matador Púchov. From 2007 this traditional event was organized as a part of the International Conference on Polymeric Materials in Automotive so that in 2009 the 20th Slovak Rubber Conference will be held.

In this year the International Conference Polymeric Materials in Automotive PMA 2009 for the first time will be connected with International Fair of Plastics, Rubbers and Composites for Car Industry – CARPLAST and International Fair of Producers and Subsuppliers for the Car Industry and Logistics - C.S.I.L.. The 19th International Car Show AUTOSALON which ranks among significant motoring events in Central Europe will be running parallel.

Prof. Ivan Chodák, DSc.
Chairman of the Program Committee

MAIN LECTURES

ML-01
ENGINEERED INTERFACE-INTERPHASE SYSTEMS ON AUTOMOTIVE POLYOLEFINES SURFACE AND THEIR INFLUENCE ON ADHESION

W. (VOYTEK) S. GUTOWSKI*, SHENG LI, ALEX BILYK, and IKO BURGAR

CSIRO Division of Materials Science & Engineering Functional Interphases & Coatings and Intelligent Materials Team, Graham Road (PO Box 56), Melbourne, Highett, Victoria 3190, Australia
Voytek.Gutowski@csiro.au

Abstract

Significant adhesion enhancement of various surface-finishing materials to chemically inert automotive polyolefin blends can be attained through surface grafted connector molecules reactive with oxidized substrate surface. The effectiveness of adhesion improvement through such tethered interfaces is shown to depend on the mode of interaction with the adjacent medium: interpenetration or chemical reaction, as well as surface density and length of grafted molecules.

We have frequently observed that some systems, such as painted or otherwise decoratively coated products, fail through the delamination of the coating from the substrate surface at the stress levels well below the anticipated load-bearing capacity of the tethered interface. Two hypotheses have been formulated to explain the observed phenomenon:

(i) The chain scission in surface oxidized polyolefins takes place not only in the uppermost polymer surface, but may propagate into the sub-surface region, thus creating a weak boundary layer which fails cohesively through its bulk,

(ii) In order to increase the load-bearing capacity of the interphase, the sub-surface region of the substrate needs to be reinforced by short-chain molecules penetrating into and subsequently providing effective crosslinks between individual fragments of excessively oxidized and hence, weaker sub-surface part of the interphase.

In this paper we fully verify the above hypotheses. The oxidized sub-surface layer reinforced by polyethyleneimine becomes an integral part of the effective interphase in addition to the tethered interface and the interpenetrated network of connector molecules and the paint.

Possibility of lignin application in rubber blends based on NR and SBR was studied. Seven types of lignin powder were tested as fillers for rubber blends before and after modification. Influence of lignin on vulcanisation process, mechanical properties, morphological structure as well as dynamical-mechanical properties was investigated. The significant positive effect of modified lignin on properties of model rubber blends was found.

ML-02
POLYMER NANOTECHNOLOGY APPLIED TO POLYMER ALLOYS AND COMPOSITES

TOSHIO NISHI* and KEN NAKAJIMA

WPI Advanced Institute for Materials Research, Tohoku University, 2-1-1 Katahira, Aoba-ku, Sendai 980-8577 Japan
nishi.toshio@wpi-aimr.tohoku.ac.jp

Introduction

Recently, there have been many attempts to develop nano-structured polymeric materials to satisfy the ever-increasing demand of the automotive and electronics industry to accommodate a green and sustainable society. This demand requires such materials to be multi-functional and high performance. Therefore, research and development into structure optimization and related processing development for polymer alloys and polymer-based composites have become more important subjects because single polymeric materials can never satisfy such requirements. This situation accelerates the development of evaluation techniques that have nanometer-scale resolution[1]. To date, transmission electron microscopy (TEM) has been widely used for this purpose. However, TEM technique cannot probe the mechanical properties of such materials in general. The realization of much higher performance materials requires an evaluation technique that enables us to investigate topological and mechanical properties at the same point and the same time. Atomic force microscopy (AFM)[2] is clearly an appropriate candidate because it has almost comparable resolution with TEM. Furthermore, mechanical properties can be readily obtained by AFM due to the fact that the sharp probe tip attached to the soft cantilever directly touches on the surface of the materials in question. Therefore, many polymer researchers have started to use this novel technique to characterize materials properties at the nanoscale[3].

However, there are several drawbacks in AFM usage for soft materials such as polymeric and bio-related materials[4]. For example, the sample deformation caused by the force between the probe tip and the sample can lead to mistaken interpretation of the obtained topography as explained later. The phase contrast image obtained together with the topography image using the so-called tapping-mode is difficult to interpret or provides at most qualitative information. We have been engaged for many years in using AFM with a sufficient understanding of its advantage and disadvantage in order to develop methodology suitable for polymeric soft materials, namely, nanorheology[5] and nanotribology[6,7]. The peculiar feature of these methods is the positive usage of sample deformation, a feature which becomes troublesome in imaging. We are able to extract mechanical information on polymeric materials from the physical quantity, sample deformation. Due to this fact, we may refer to this method as a nano-palpation technique, where a doctor's finger is replaced by the sharp

AFM probe tip. In order to realize this idea, analyses of force-distance curves have proven to be powerful, and correspond to macroscopic stress-strain curves. In the analysis, sample deformation and force exerted are quantitatively estimated to acquire a true topographic image free from the effect of sample deformation together with a Young's modulus image[8] and an adhesive energy image[9] at the same time. In this paper, we applied this method to dynamically vulcanized thermoplastic elastomer (TPE-V) system and newly manufactured non-viscoelastic polymer alloy (NOVA).

Method

As mentioned above, the sample deformation caused by direct touch of the AFM sharp probe is inevitable in AFM usage. If this effect is negligible, an obtained image expresses a true surface topography. However, soft-materials such as polymers and biomaterials are easily deformed even by a very weak force. For example, a 0.1–10 nN force exerted by a 10 nm-diameter punch probe results in a stress of 1.3–130 MPa. Plastic materials with having a GPa-order Young's modulus might not be deformed significantly by this range of force, whereas rubbery materials with a MPa-order modulus and gels with a kPa-order modulus undergo substantial deformation. The sharper the probe tip, the more serious is this effect.

Does this effect become a disadvantage or an advantage? This question can lead to different answers depending on the researcher's viewpoint. In this chapter, our answer is an advantage; we can measure the surface Young's modulus because of this effect. Instrumentation to obtain a measure of "hardness" by pushing some kind of probe onto a surface began their history with a hardness indenter tester and the main stream of recent progress is seen in the nano-indenter system[10]. The recently-developed nano-indenter can provide two-dimensional mechanical mapping, though the lateral resolution achieved is far below that of the AFM. The advantage of the indenter compared to the AFM is: *i*) the probe shape is geometrically similar and therefore the analysis is easier; *ii*) the material of the probe is diamond and thus it has no elastic deformation and is free from wear; *iii*) the force-detection system is independent of the displacement-detection system. In contrast, AFM uses the deflection of the cantilever for the force detection. The sample deformation is also measured from the conversion of this quantity, resulting in a fundamental difficulty in analyzing the mechanical properties of materials. Probes coated with diamond-like carbon are now commercially available, but there remain several problems such as durability and controllability of probe shape. On the other hand, there exist disadvantages in indenter systems. The indenter probes are designed to record plastic deformation from the instant of contact and therefore it becomes difficult to combine a two-dimensional mapping capability. The force range is in the order of μN to mN, not comparable to pN or nN as realized in AFM. In the case of AFM, almost all probes have effective roundness at the top of the probe tip except for a carbon-nanotube (CNT)-attached probe, resulting in measurement in the elastic deformation region below the yield limit. Thus, a two-dimensional mapping capability is easily realized by AFM-based indentation. Like body palpation by medical doctors or masseurs, we can now perform nano-palpation with the AFM sharp probe enabling measurement of surface elasticity.

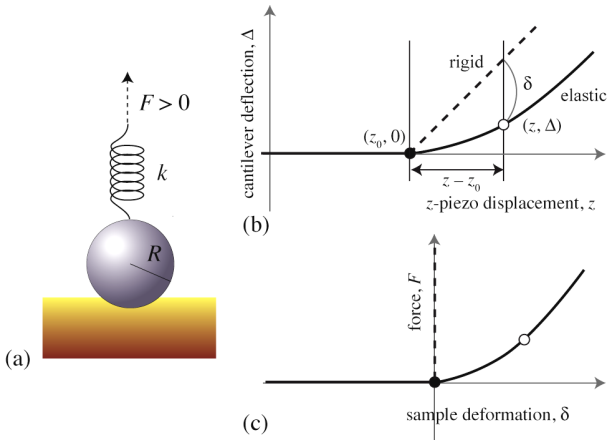

Fig. 1. **Analysis procedure of force-distance curve with and without adhesive force between sample and AFM probe.** (a) The schematics of the contact between two bodies when the applied force is positive (repulsive), (b) the force-distance curve for the contact without adhesive interaction, (c) the corresponding force-deformation plot

The simplest theory for the analysis of surface elasticity based on AFM force-distance curve measurement is Hertzian contact mechanics[11]. As schematically shown in Fig. 1, a force-distance curve is a plot of the displacement, z of the piezoelectric scanner normal to the specimen's surface as the horisontal axis and the cantilever deflection, Δ as the vertical axis. Hertzian contact mechanics cannot treat adhesive force in principle. We need to make some effort to minimize the adhesive force in a practical experiment. Measurement in aqueous conditions is effective for polymeric materials with low water absorbability. A cantilever with a larger spring constant also hides weak van der Waals forces. Fig. 1a shows the force-distance curve measurement on soft-materials during the loading process. The AFM cantilever and probe are treated as a spring with a spring constant of k and a sphere with radius of curvature, R, respectively. The force is expressed by Hooke's law,

$$F = k\Delta \qquad (1)$$

Since recent developments in this field have included several reports on direct measurement of k and R,[12–14] it is expected to realize improved quantitative accuracy.

If the specimen surface is sufficiently rigid, the cantilever deflection, Δ always coincides with the displacement, $(z - z_0)$ of the piezoelectric scanner measured from a contact point $(z_0, 0)$ as depicted in the dashed line in Fig. 1b. However, if the specimen surface undergoes elastic deformation as in the case of the solid line, we can estimate the sample deformation, δ as follows;

$$\delta = (z - z_0) - \Delta \qquad (2)$$

δ-F plot, shown in Fig. 1c, derived from the $z - \Delta$ plot is now fitted with the theory of Hertzian contact to provide the estimated Young's modulus,

$$a=\left(\frac{FR}{K}\right)^{1/3},\ \delta=\left(\frac{F^2}{K^2R}\right)^{1/3}\quad \therefore F=KR^{1/2}\delta^{3/2} \tag{3}$$

where a is contact radius and K is so-called elastic coefficient and expressed using reduced Young's modulus E^* as follows,

$$K\equiv\frac{4}{3}E^*=\frac{4}{3}\left[\frac{1-\nu_s^2}{E_s}+\frac{1-\nu_p^2}{E_p}\right]^{-1} \tag{4}$$

where E_i and ν_i are Young's modulus and Poisson's ratio, respectively. The subscript suffix i stands for sample (s) and probe (p).

AFM is widely used in the world as an imaging tool for soft-materials like polymers and biomaterials. Contact and tapping-mode operations are known as major imaging modes. Specimens are scanned over their surfaces with mechanical contact in both modes. Thus, it has been said among researchers that topographic images from both modes are affected by the deformation of the sample itself due to contact or tapping forces. The users might be also able to qualitatively understand the influence of a contact or tapping forces for obtained topographic images in the past. However, the imaging with constant force condition never results in quantitative estimation of such influences.

Now, here will be demonstrated the quantitative method to obtain accurate topographic images of deformable samples together with Young's modulus distribution images. Especially, our interest in this paper exists in soft-materials that are commonly difficult for AFM to deal with. The final goal is to understand peculiar properties of soft-materials, i.e., mechanical and rheological properties at nano-meter scale. The value of a cantilever spring constant, k is an important factor to detect mechanical properties from a sample surface as mentioned above. If k is very small, the cantilever approaching to the surface cannot deform the sample. If k is very large, instead, the cantilever can deform the sample, without any deflection. Therefore, necessary information about the sample is lacking. Thus, we need to choose a cantilever with an appropriate value for k.

To obtain the mapping of the local mechanical properties of soft-materials, force-volume (FV) measurement would be the most appropriate method. In this mode, force-distance curve data are recorded until a given cantilever deflection value (trigger set-point), Δ_{trig} is attained for 64 × 64 (or 128 × 128 for the latest condition) points over two-dimensional surface. At the same time, z-displacement, z_{trig} corresponding to the trigger set-point deflection was recorded to build an apparent topographic image. The topographic image taken in this mode is basically same from that by conventional contact mode if contact force set-point and trigger set-point are identical. If all the points over the surface are rigid enough, the set of recorded displacements, z_{trig} represents the topographic feature (true height) for the sample. However, if the surface deforms as discussed, it is no more valid to regard an obtained data as the real topographic information. However, since we have a force-distance curve for each point, we can estimate the maximum sample deformation value for each point referring to Eq. (*2*),

$$\delta=\left(z_{trig}-z_0\right)-\Delta_{trig} \tag{2}$$

Then, two-dimensional arrays of sample deformation value can be regarded as sample deformation image. The force-distance curve analyses for 4,096 or 16,384 data give the sets of Youngs modulus distribution images at the same time and the same place. We now have apparent height (z_{trig}) and sample deformation (δ) images taken at the same time and Δ_{trig} is the preset value and therefore constant for all of force-distance curves. Then, the appropriate determination is performed for contact point (the array of (z_0, 0)), this realizes the reconstruction of "true" surface topography free from sample deformation[8].

Results & Discussion

During dynamic vulcanization process, thermoplastic matrix materials as well as rubber components are generally blended in an extruder resulting in so-called co-continuous morphology. A cross-linking agent can be also added into the extruder. During the cross-linking of the rubber-rich phase the viscosity of the rubber increases, which results in the increased blends viscosity ratio, since the viscosity of the thermoplastic matrix remains the same. The shear stress causes rubber-rich phase to break up into fine dispersed rubber particles in a thermoplastic matrix. The formation of the characteristic matrix-particle morphology is essentially influenced by the kinetics of the vulcanization and the cross-linking density of the rubber phase[15,16]. Due to the nanometer-scale dispersion, TPE-V, thus, can be regarded as one of the most promising polymer nano-alloys.

If the cross-linking density of the rubber phase is very poor, the phase will be able to undergo large deformation and remains co-continuous. On the other hand, if the cross-linking

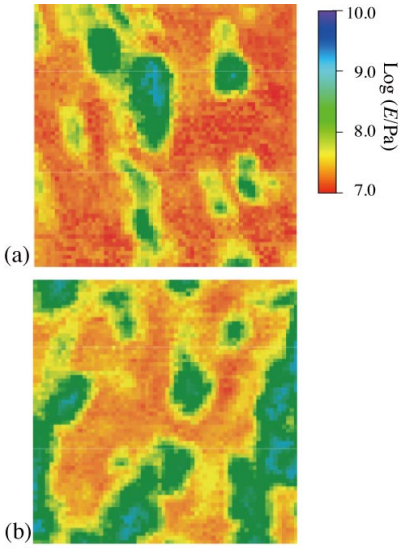

Fig. 2. **Young's modulus mappings of crystalline EVA/EVA rubber 3:7 reactive blend.** The scan size was 2 μm. (a) without dynamic vulcanization and (b) with dynamic vulcanization

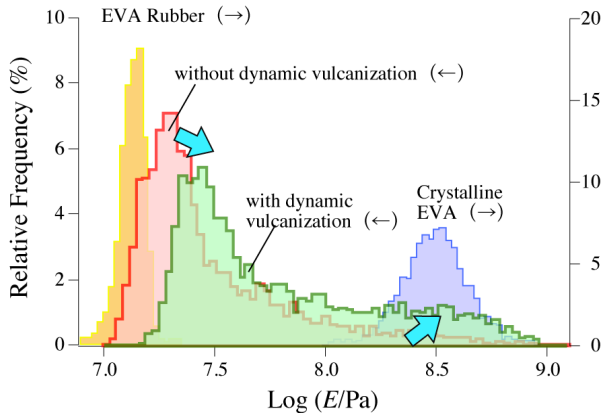

Fig. 3. **Young's modulus distribution obtained from Fig. 1.** The distribution for each pure component is also superimposed

density is too high, the rubber phase can only be deformed under shear stress without ripping. Therefore an optimum of cross-linking density should exist. To date, there have been many researches conducted to elucidate the complicated dynamic vulcanization process. However, many of researches only treated structural information obtainable by microscopic techniques together with macroscopic mechanical property testing. Here, we introduce the results obtained by our nano-mechanical mapping for a TPE-V specimen. TPE-V specimens were prepared as follows[17]; A vinyl silane was firstly grafted on rubbery ethylene vinyl acetate copolymer (EVA rubber) to obtain silylated rubber. Then, the product was mixed with crystalline EVA in a twin-screw extruder. The masterbatch was put in a mixer with or without cross-linking catalyst to realize dynamic vulcanization.

Fig. 2 shows the Young's modulus mapping images for crystalline EVA/EVA rubber 3:7 reactive blend. As explained above, EVA rubber is designed to be cross-linked if cross-linking catalyst exists in the vulcanization process. Fig. 2a is for the blend without dynamic vulcanization and 2b is for that with dynamic vulcanization. In the case of Fig. 2a, the see-island structure was observed. However, as one can see from Young's modulus distribution shown in Fig. 3, both phases had the modulus different from their pure constituents. This was attributed to the fact that this blend system was composed of partially miscible polymers. Especially, crystalline EVA rich phase perfectly lost crystalline hardness (~GPa). On the other hand, dynamically vulcanized sample showed co-continuous structure that could not be expected from original blend ratio. In addition, Fig. 3 indicated two important findings. The first one was the increase of Young's modulus in rubber rich phase. This could be easily explained as the consequence of the vulcanization of EVA rubber. The second, more interesting one was the recovery of crystalline hardness in the crystalline EVA rich phase. We speculated that this was due to vulcanization-induced phase separation. This kind of observation cannot be realized by TEM or even by conventional AFM.

Another application example of this technique is non-viscoelastic polymer alloy (NOVA)[18]. This materials shows soft response to high-speed input which never be explained by conventional idea of viscoelasticity. We performed this technique to pursue the mechanism of this strange property. Fig. 4 shows the apparent height and Young's modulus images of NOVA manufactured by twin-screw extruder with L/D=100. NOVA is composed of a certain resin and a certain rubber and rubbery phases are dispersed at nano-meter scale. The manner of dispersion is essentially same as other polymer-based nano-alloys looking at Fig. 4a, while Young's modulus image implied us a very interesting phenomena. The hollows in apparent height image (of course due to pressure by AFM sharp probe) correspond to rubber-rich phases. Then, the matrix phase is corresponding to resin-rich phase. However, in the Young's modulus image, intermediate phases appear where the Young's modulus is lower than that of matrix. Furthermore, this intermediate phase appears as co-continuous phase. The existence of intermediate phase could not be observed for other nano-dispersed polymer alloy systems and it is uniquely observed in NOVA. More detailed discussion will be made at the site.

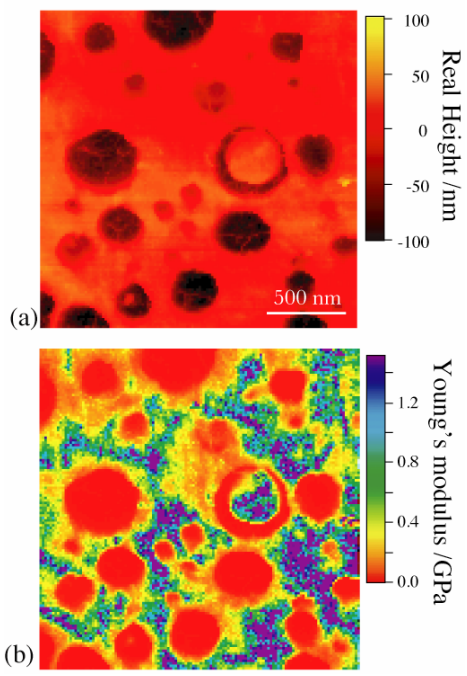

Fig. 4. **(a) apparent height and (b) Young's modulus images of NOVA.** The scan size was 2 μm. The intermediate phase is clearly visible in Young's modulus image

We thank for the financial support from New Energy Development Organization (NEDO) as one of the projects in the Nanotechnology Program by the Ministry of Economy, Trade, and Industry (METI) of Japan.

REFERENCES

1. Nishi T., Nakajima K.: *Kobunshi Nano Zairyo,* (Kobunshi Gakkai, ed.). Kyoritsushuppan, Tokyo 2005.
2. Binnig G., Quate C. F., Gerber Ch.: Phys. Rev. Lett. *56*, 930 (1986).
3. Magonov S. N., Whangbo M. H.: *Surface Analysis with STM and AFM*. VCH, Weinheim 1996.

4. Nakajima K., Fujinami S., Nukaga H., Watabe H., Kitano H., Ono N., Endoh K., Kaneko M., Nishi T.: Kobunshi Ronbunshu *62*, 476 (2005).
5. Nakajima K., Yamaguchi H., Lee J. C., Kageshima M., Ikehara T., Nishi T.: Jpn. J. Appl. Phys. *36*, 3850 (1997).
6. Terada Y., Harada M., Ikehara T., Nishi T.: J. Appl. Phys. *87*, 2803 (2000).
7. Komura M., Qiu Z., Ikehara T., Nakajima K., Nishi T.: Polym. J. *38*, 31 (2006).
8. Nukaga H., Fujinami S., Watabe H., Nakajima K., Nishi T.: Jpn. J. Appl. Phys. *44*, 5425 (2005).
9. Nagai S., Fujinami S., Nakajima K., Nishi T.: Compos. Interf. *16*, 13 (2009).
10. Oliver W. C., Pharr G. M.: J. Mater. Res. *7*, 1564 (1992).
11. Landau L., Lifchitz E.: *Theory of Elasticity*. Mir, Moscow 1967.
12. Butt H. J.: J. Colloid Interface Sci. *180*, 251(1996).
13. Hutter J. L., Bechhoefer J.: Rev. Sci. Instrum. *64*, 1868 (1993).
14. Wang T., Ikai A.: Jpn. J. Appl. Phys. *38*, 3912 (1999).
15. Radusch H.-J., Pham T.: Kautsch. Gummi Kunstst. *49*, 249 (1996).
16. Abdou-Sabet S., Puydak R. C., Rader C. P.: Rubber Chem. Technol. *69*, 476 (1996).
17. Sugita K., Watanabe K., Inoue T.: to be published.
18. Inoue T.: to be published.

ML-03
POTENTIALS OF RUBBER NANO-COMPOSITES IN AUTOMOTIVE APPLICATIONS

KATHARINA BRANDT, HAGEN LORENZ, LUCIANE KLAFKE DE AZEREDO SCHNEIDER, and ROBERT H. SCHUSTER

Deutsches Institut für Kautschuktechnologie e. V., Eupener Str. 33, 30519 Hannover
Robert.schuster@dikautschuk.de

Introduction

For technical and ecological reasons there is nowadays a keen interest in saving oil resources and translating into action innovative concepts for efficient engines and global CO2 reduction. For the rubber technology the urgent challenges are to use more conscious the raw materials. Taking into consideration that reinforcing fillers used in the rubber industry are oil based and/or produced by high energy consumption processes one urgent demand is to develop strategies for alternative fillers made from natural sources. In these regards, it has been recognized that natural nano-fibers and natural occur-ring plate-like fillers have the potential to play a similarly graded role alongside conventional filler. The present contribution is meant to introduce new concepts for *in-situ* manufacturing of Cellulose, Rubber/Cellulose and Rubber/Clay-nanocomposites, respectively as well as for polymeric nano-particles. Morphological features and physical properties of the corresponding rubber nanocomposites will be discussed in the following.

Methodology

Cellulose nano-fibers are *in-situ* formed by applying the "continuous dynamic latex compound-ding" (CDLC) proprietary process based on a co-coagulation of cellulose xanthate and rubber latex (NR, SBR, NBR, ACM) in an elongation flow jet. Rubber/clay nano-composites are obtained by submitting aqueous slurry of pristine montmorillonite and rubber latex to an elongational/turbulent flow followed by coagulation. Morphological investigations were performed on vulcanized composites by TEM, XRD, AFM. Standard mechanical properties, dynamic cut growth resistance, swelling and permeation of model fuel were measured.

Results and discussion

A more unexplored field is the reinforcement by short and long nano-fibers. Rubber composites containing *in-situ* formed cellulose nano-fibers display an opposite behavior to composites containing carbon black, silica and polymeric nano-particles. By applying the CDLC technique the fibers are well incorporated and dispersed in the rubber matrix and do not show an agglomeration and flocculation tendency during storage of unmodified mixes. The high aspect ratio (130–250) and fiber density increases with the elongational flow prior to co-coagulation. In addition the cellulose fibers can be linked to the rubber matrix by covalent bonds. As a result the composites relax shortly after the breakdown of the storage modulus during an amplitude sweep (non-linear viscoelasticity). The recovery of 95–98 % of the initial properties is unique for elastomer nano-composites. The large solid-rubber interface is probed by a larger reduction of equilibrium swelling than the one shown by silica and carbon black at constantφ. The specific fiber network formed at relatively low concentrations lead to dynamic-mechanical properties which are superior to those of generated by silica and carbon black at the same loading (Fig. 2). The reinforcing effect can be explained by accuring an effective aspect ratio of ca. 20. The results show. That the reinforcement obtained by silica can be achieved by employing only half volume fraction of *in-situ* formed cellulose fibers. The same beneficial effects can be reported for tensile properties whre anisotropic effects come into function for calendared nanocomposites.Considering rubber/clay nanocomposites obtained without any modification of MMT by the new CDLC process well dispersed and partly fanned out (intercalated?) factoids be-

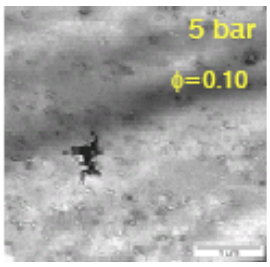

Fig. 1. ***In-situ* formed cellulose fibres**

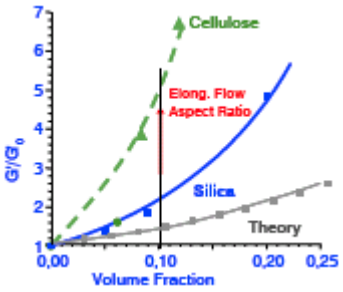

Fig. 2. **Normalized storage modulus as a function of φ,** 1) Cellulose, 2) Silica, 3) Guth-Gold prediction

come obvious from TEM and XRD investigations (Fig. 3). This underlines the advantages of the CDLC process which is short, effective, requires less energy than mechanically mixing and is inexpensive. The improvement of the mechanical properties level increases significantly in nano-composites produced by CDLC compared to composites obtained by melt mixing. The polarity of the rubber matrix however plays an important role. As far barrier properties are concerned, the reduction of permeation coefficient reduction by 51 % generated by a volume fraction 0.04 MMT is in accordance to theoretical expectations for an aspect ratios of ca. 50.

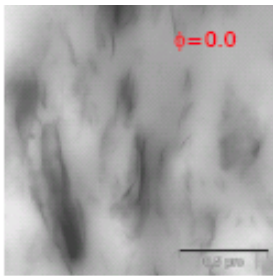

Fig. 3. **Morphology of rubber/MMT**

Conclusion

New processing techniques permit the use of new and competitive types of fillers. The polymeric fillers, long and short nanofibers as well as well dispersed plate-like fillers offer a reliable base to reduce conventional properties of the elastomers.

ML-04
LANXESS - INNOVATIVE SOLUTIONS FOR SUSTAINABLE ECONOMIC GROWTH

FLEMMING B. BJOERNSLEV

LANXESS Central Eastern Europe s.r.o., Chief Executive Officer, Štetinova 4, 811 06 Bratislava, Slovak Republic
flemming.bjoernslev@lanxess.com

KEY LECTURES

KL-01
FROM GUM ELASTOMERS TO FILLED VULCANIZED RUBBER: RHEOLOGICAL MODELING OF THE NON-LINEAR BEHAVIOR

FABIO BACCHELLI, and SALVATORE COPPOLA

ENI - POLIMERI EUROPA, Centro Ricerche Elastomeri
via Baiona 107, 48100 Ravenna, Italy,
fabio.bacchelli@polimerieuropa.com

Processing of rubber compounds involves the application of rapid and large deformations in both shear and elongation. This indicates that transient flow and a large degree of stretching are actually prevalent. Nevertheless, the analysis of unit operations is usually performed on the basis of the rheological response to steady state, mild shear flow. Moreover, commonly used constitutive equations for rubber elasticity do not point out the contribution of the raw elastomer in the vulcanizate response.

Commercial rubbers possess more complex structures with respect to model polymers and the non-linear rheology of a compound is strongly affected by changes in the relaxation time spectrum of its polymer matrix as a consequence of variations in molar mass distribution or branching patterns, together with filler loading and filler dispersion.

Up to now, there is a lack of a comprehensive theory, which can simultaneously describe the rheology of the raw elastomer, the response of filled rubber and its behavior in the final cured state. Then, the problem of describing and modeling the nonlinear behavior of rubber at different processing stages should be approached by collecting various theoretical and experimental contributions.

The non-linear behavior of the polymer matrix can be described using micro-rheological models accounting for reptation together with the contribution of chain stretch and dissipative convective constraint release. The time-dependent response of the filled polymer with a particle loading above the percolation threshold can be approached by introducing terms describing the filler-polymer dynamics under flow. Rheological modeling can be extended to the post-cure state to describe Mullins stress-softening-hysteresis and other aspect of the vulcanizate with a very limited number of parameters.

A commercial high-*cis*-polybutadiene (*cis*-BR) was investigated in the present work (Neocis BR40, Polimeri Europa), characterized by a 1,4-*cis* content of 97 %. The polymer, nearly linear, has an average molecular weight of 420 000 g mol^{-1} and a polydispersity index of 3.8. Carbon black compounds (N990, N330) were prepared in a Brabender Plasticorder with a filler volume fraction of 0.2. A Rheometric Scientific ARES A11 was used to determine the dynamic properties of *cis*-BR and related cured and uncured compounds.

Elongational measurements on cured and uncured rubber were performed with a detachable commercial fixture for rotational rheometers, which incorporates dual wind-up drums

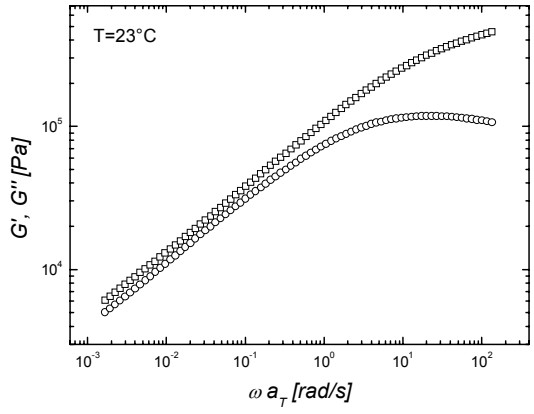

Fig. 1. **Linear viscoelastic data of a nearly linear *cis*-BR at 23 °C**

to ensure a truly uniform extensional deformation during uniaxial extension. A SER-HV-P01 (ref.[7]) platform was hosted by a Anton Parr Physica MCR 501. Uncured cylindrical specimens with an effective length of 12.7 mm were prepared by means of a Göttfert Rheograph 6000 capillary rheometer and relaxed for at least three days. Flat specimens were used for vulcanized rubber.

The linear viscoelastic behavior of a typical high-*cis*-BR is reported in Fig. 1. The crossover point was not observed in the investigated frequency range, accounting for the presence

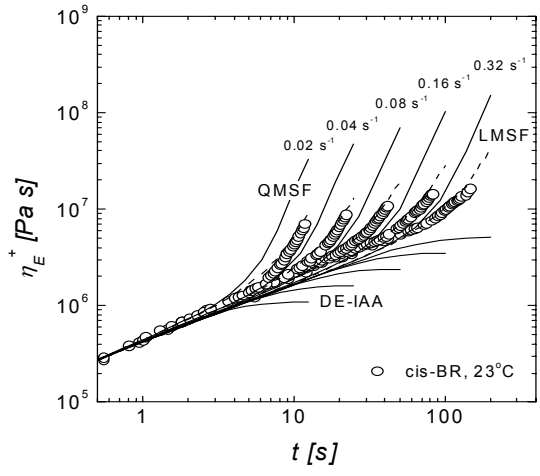

Fig. 2. **Startup flow of a nearly linear *cis*-BR in uniaxial extension at 23 °C.** Lines represent the linear (LMSF) and quadratic (QMSF) form of the Molecular Stress Function theory and the prediction of the Doi-Edwards theory under the assumption of independent alignment (DE-IAA)

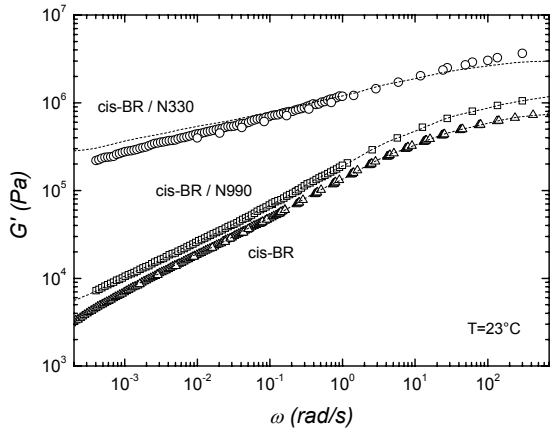

Fig. 3. **Elastic modulus of *cis*-BR and related carbon black compounds at 23 °C.** Dashed lines represent the model prediction

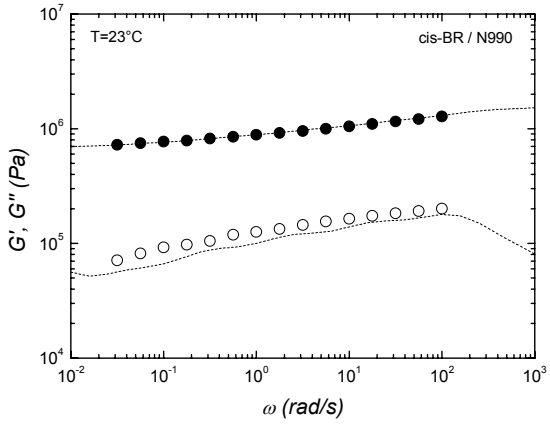

Fig. 5. **Dynamic moduli of vulcanized carbon black filled *cis*-BR (N990) at 23 °C.** Dashed lines represent the model prediction

of very long relaxation dynamics affecting many important processing parameters.

Data were used to access micro-rheological models for the prediction of the nonlinear response to different kinds of deformation. These models prove essential for understanding, for example, the important contribution of the strain hardening associated with the elongation of the polymer matrix in a compound. The extensional behavior of *cis*-BR at room temperature is reported in Fig. 2 for different Hencky strain rates.

Data are compared with the model known as Molecular Stress Function, accounting for reptation together with the contribution of chain stretch. An extended version of this generalized tube model with strain-dependent tube diameter was considered, to include the CCR contribution[3,5]. The prediction of the Doi-Edwards theory based on pure orientational contribution is also reported[4].

Industrial filled polymer compounds represent highly concentrated suspensions with complex interactions between filler particles and the polymer. Unlike the concentrated suspensions with low viscosity matrices the rheological behavior of rubber compounds can be described in terms of a single medium approach, though with complicated properties, because the high viscosities of the polymer matrices make the typical two-phase effects, such as internal rotations of the particles, presumably insignificant.

In comparison with the rheology of polymer melts and solutions, filled polymers display very long relaxation phenomena which reflect the processes of structurization (flocculation and aggregation) of particles in the medium.

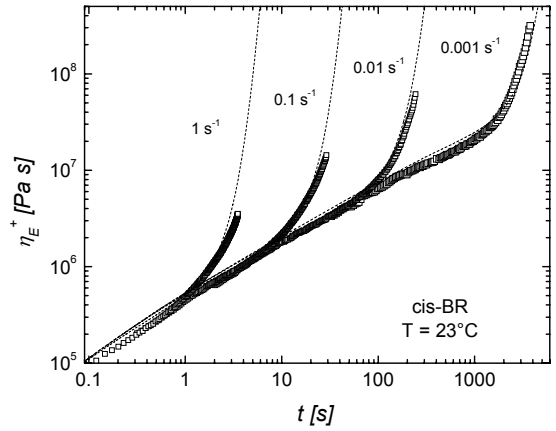

Fig. 4. **Startup flow of *cis*-BR in uniaxial extension at 23 °C and Hencky strain rates of 1, 0.1, 0.01 and 0.001 s^{-1}.** Lines represent the prediction of the Leonov's model

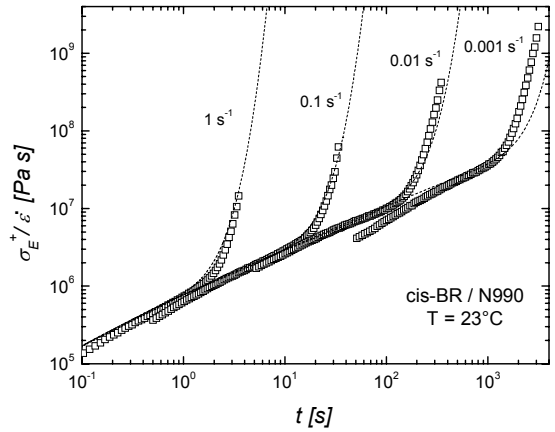

Fig. 6. **Startup flow of carbon black filled *cis*-BR in uniaxial extension at 23 °C and Hencky strain rates of 1, 0.1, 0.01 and 0.001 s^{-1}.** Lines represent the prediction of the Leonov's model

Tube models are not suitable for describing the relaxation dynamics of filled, uncured rubbers. Also the typical continuum mechanics approach commonly used for the modeling of polymer melts (K-BKZ, rubber-like liquid[2]) results largely unsatisfactory.

A set of thermodynamically consistent and stable constitutive/kinetic equations was proposed by Leonov and coworkers[1,6] to describe manifestations of particle-matrix interactions and polymer viscoelasticity.

Though not being a first-principles theoretical approach, the Leonov's model proves valid in describing almost the whole phenomenology of polymer nonlinear viscoelastic behavior. The model is based on two tensorial differential equations accounting for the stress carried by the free and trapped chains, respectively. A scalar kinetic equation is also necessary to describe the process of bonding/debonding of the polymer chains on the filler particles. Besides a discrete spectrum of relaxation times for the linear Viscoelastic behavior, the model just needs the determination of 4 parameters, two of them for describing the nonlinear viscoelasticity and two structural/kinetic parameters for the filler-matrix interaction.

Fig. 3 shows the dynamic elastic modulus for *cis*-BR and related uncured carbon black compounds. As expected, a significant effect of the different filler surface area (N330>N990) is observed in terms of linear Viscoelastic response for these compounds with the same filler loading. The linear Viscoelastic spectrum is extracted for each material from dynamic moduli. With an appropriate choice of the parameters for the nonlinear viscoelasticity, the strain hardening behavior in uniaxial extensional flow start-up is very well described for the pure polymer (Fig. 4). A similar procedure has been applied to the uncured compounds and to the vulcanized rubber (Fig. 5).

The Leonov's model predictions for filled uncured compounds were successfully compared with experimental data in in Fig. 6.

The application of the Leonov's model to the vulcanized compound is reported in Fig. 7, 8 in terms of Mullins stress-softening-hysteresis measured at constant Hencky strain rate. The model is able to predict the thixotropy effects of cyclic extensional deformations and results are in satisfactory agreement with model predictions. Interestingly, the Mullins effect predicted by the Leonov's model is reduced with respect to the experimental data. This suggests that filler-filler interactions, not modeled by Leonov's approach, cannot be fully neglected for these *cis*-BR/CB compounds.

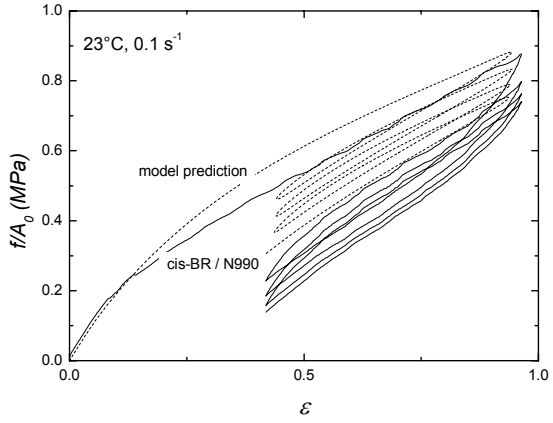

Fig. 7. **Mullins stress-softening-hysteresis of vulcanized carbon black filled *cis*-BR (N330) at 23 °C and |Hencky strain rate of 0.1 s^{-1}.** Dashed lines represent the Leonov's model prediction

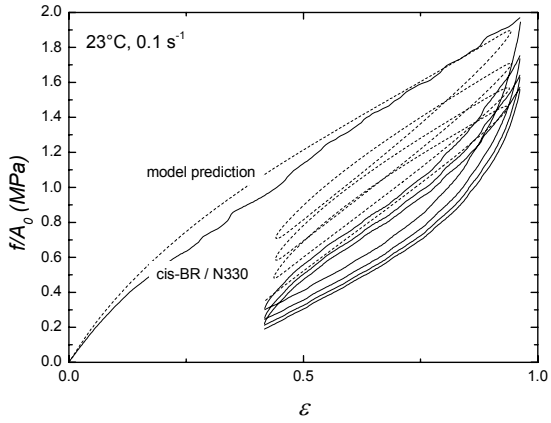

Fig. 8. **Mullins stress-softening-hysteresis of vulcanized carbon black filled *cis*-BR (N990) at 23 °C and |Hencky strain rate of 0.1 s^{-1}.** Dashed lines represent the Leonov's model prediction

The approach presented in this paper could be extended for capturing a wide range of rheological behavior of filled elastomers in a wide range of stresses and strain rates, for the description of various unit operation in rubber processing.

REFERENCES

1. Joshi G. P., Leonov A. I.: Rheol. Acta *40*, 350 (2001).
2. Larson R. G., in: *Constitutive Equations for Polymer Melts and Solutions*. Butterworth, Boston 1988.
3. Wagner M. H., Rubio P., Bastian H.: J. Rheol. *45*, 1387 (2001).
4. Doi M. Edwards S., in: *The Theory of Polymer Dynamics*, Oxford Science Publications, 1986.
5. Ianniruberto G., Marrucci G.: J. Non-Newtonian Fluid Mech. *65*, 241 (1996).
6. Leonov A. I.: J. Rheol. *34*, 1039 (1990).
7. Sentmanat M. L.: Rheol. Acta *43*, 657 (2004).

KL-02
AUTOMOTIVE APPLICATIONS OF THERMOPLASTIC ELASTOMERS

JIŘÍ GEORGE DROBNY

Drobny Polymer Associates
Merrimack, NH 03054 USA

Thermoplastic elastomers (TPEs) are rubbery materials with fabrication characteristics of conventional thermoplastics and many performance properties of thermoset (vulcanized) rubber. TPEs can be processed by the same methods such as injection molding, extrusion, blow molding, rotational molding, thermoforming as most thermoplastic materials, including polyethylene, polypropylene, and polyvinyl chloride. On the other hand, their basic properties are very similar to those of vulcanized rubber materials based on natural rubber, SBR, EPDM, NBR, and polychloroprene. Thermoplastic elastomers offer a variety of practical advantages over vulcanized rubber, such as simple processing with fewer steps, shorter fabrication times, and the possibility of recycling of production and post-consumer scrap. These and other advantages are the main reasons why the applications of TPEs in the automotive industry have been growing at a constantly increasing rate during the past two decades and currently automotive applications represent the largest single market for these materials. This contribution will discuss properties of the thermoplastic elastomers that are widely used in automobiles and their specific applications as well as the most recent developments.

The author of this contribution is an international consultant and university educator. His book “Handbook of Thermoplastic Elastomers” was published by Plastics Design Library/William Andrew Publishing in 2007.

KL-03
RUBBER REINFORCEMENT BY CARBON NANOTUBES BETWEEN MYTH AND REALITY

N. DURENT, M. OWCZAREK, and B. HAIDAR

Institut de Chimie des Surfaces et Interfaces, ICSI-CNRS UPR 9069, Université de Haute Alsace, Mulhouse, France
b.haidar@uha.fr

Carbon nanotubes have attracted much attention for their unique structure, as well as for their excellent mechanical, electrical and thermal properties. Most properties of carbon nanotubes are closely related with its anisotropic structure, their form factor and their nano-scale size are critical for understanding their behavior in solutions as well as in polymer composites. However, in the case of polymer-based composites, polymer/solid interactions, rubber adsorption, chain conformation… are just a few of numerous factors affecting the development of the interphase which controls the overall macroscopic behavior of such materials. Polymer-carbon nanotube, NTC's, blends are no exception of this frame but with an additional specific factor that has to be considered. In fact, when the scale of the solid surface approaches the scale of a polymer chain, or its segment, the opportunity of an efficient adsorption ought to be different from those identified on quasi-infinite even surfaces. Only when the length of the chains is significantly smaller than the tub radius, the curved surface is approximately even on a local scale so that the concept for flat surfaces can be applied. However, such considerations should not apply for significantly curved nanotube surfaces.

Stable physisorption, at a given temperature, is known to be achieved thanks to a high number of weak physical adsorption sites. Such mechanism is conceivable with even surfaces, or any surface considered as such. The establishment of stable polymer-nanotube links depends also on the number of interaction sites between the two partners that depends, on its turn, essentially on the polymer chain conformation. The goal of this work is to tempt an experimental measurement of the adsorption enthalpy on NTC's of macromolecules with variable natures and sizes, MW's.

In the present work three series of a commercial PDMS with different and distributed molecular weights (MW in the 4000 to 420 000 g mol^{-1} range), a polybutadiene, PB, of different molecular weights (in the 3,000 to 120,000 g mol^{-1} range) but of identical microstructure (1,2-PB content equal to about 80 %) and a polyethylene HDPE with different Melt Flow Index were selected. The chosen CNT's belong to the multi-walls carbon nanotubes family were purchased from Nanocyl (France). Rubbers adsorption measurements were performed from solution a flow micro calorimetric technique, FMC. Adsorption can be monitored by the determination of the amount of adsorbed polymer and the measurement of its heat (enthalpy) of adsorption.

Results show that for linear amorphous polymer adsorption takes place exclusively in a relatively small window of MW's; adsorption, in this case, is permanent and associated with a substantial amount of heat. Outside this window, adsorption is reversible and heat exchange is low. High MW's molecules do not adsorb presumably because of their failure to wind around the nanotube and low MW's because of their incapacity to yield a sufficient number of adsorption contact-points to insure permanent adhesion and to overcome thermal agitation, kT. Only intermediate MW's are short enough to be unfolded over the surface without too much entropic penalty but with enthalpic gain which still high enough to link these intermediate chains permanently to the nanotube surface. Semi-crystalline polymers adsorption on NTC's was found to depend on the same molecular forces, the adsorption stability in this case, however, is achieved by adsorption nucleating crystal growth and the formation of the so-called nano hybrid “shish-kebab”.

Results are discussed in term of entropic penalty, enthalpic gain, polymer to tube scale-matching and radius of curvature of the NTC's surfaces.

KL-04

POWDER INJECTION MOULDING FOR AUTOMOTIVE APPLICATIONS - AN ALTERNATIVE TO TRADITIONAL PROCESSING ROUTES

BERENIKA HAUSNEROVÁ

Polymer Centre, Faculty of Technology, Tomas Bata University in Zlin, TGM 275, 762 72 Zlin, Czech Republic
hausnerova@ft.utb.cz

The possibility to use a forming method for plastics – injection moulding – to produce metallic and ceramic parts is still not widely spread information within polymer processing society.

Powder Injection Moulding (PIM) technology is a state of art process allowing the large-number production of relatively small parts of complex shapes with reduced cost and increased efficiency by avoiding the use of extra processes comparing to traditional metallurgical processes as machining or investment casting.

During the process (Fig. 1), powder is mixed with suitable polymers (called binder) into a homogeneous compound. In the next step, compound in the form of granules is formed in conventional injection moulding machines for thermoplastics into the final shape. This stage is followed by debinding, where the binder is extracted from the green part. Finally, compact is sintered so as to obtain the final part, which is purely metallic (Metal Injection Moulded – MIM) or ceramic (Ceramic Injection Moulded – CIM).

PIM process concerns several steps, and therefore the number of process variables is very high and their interactions are only partially understood. In this presentation, the important factors of the particular steps to the successful PIM processing will be briefly discussed.

Step 1: Mixing. During mixing the powder selected for the particular application is mixed together with a suitable polymer binder. Binder has usually a multicomponent character for the two reasons: good adhesion to powder at reasonable price during moulding, and different decomposition temperatures or chemical stability of its components during debinding.

Thermoplastics based binders predominate, but usage of thermosets, water based and gellation systems have been also

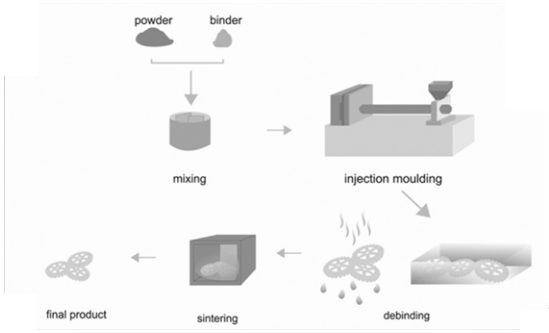

Fig. 1. **PIM processing steps**

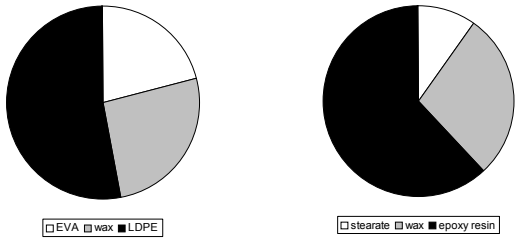

Fig. 2. **Examples of polymer binder compositions**

reported[1]; for examples see Fig. 2. The major part of a thermoplastic binder is typically low molecular weight polymer – a wax. However, due to its low viscosity, the shear forces necessary to disperse the particles and break up agglomerates may not be sufficient.

Additionally, as a consequence of the non-polar character, wax (when used alone) tends to migrate from the feedstock during moulding due to its poor adhesion to powder as we have demonstrated for cemented carbides compounds[2].

The other binder components, containing higher-molecular-weight polymers and additives, should provide suitable interactions with powder, and thus prevent the separation from powder during the flow. Block copolymers are often used for this purpose since they can be made of polymer blocks soluble in the dispersion medium and blocks with high affinity to powder imparting steric stabilisation of a compound. When we compared three types of polymer binders differing in the block copolymer used[3] (ethylene-butyl acrylate, ethylene-vinyl acetate, ethylene-acrylic acid) the influence of the flow properties of the particular binder composition diminished as the volume concentration of a solid component increased to 30 vol. %.

Mixing is carried out under high shear forces in order to break up agglomerates and disperse polymer binder efficiently on the powder surface as demonstrated in Fig. 3.

The crucial point during mixing is an adjustment of optimal loading (powder-binder ratio). Optimal loading refers[4] to powder concentration for which compound exhibits good flow properties (viscosity less than 10^3 Pa s) as well as homogeneity and stability in the shear rate range from 10^2 to 10^5 s^{-1}. It occurs slightly below a maximum (critical) packing fraction

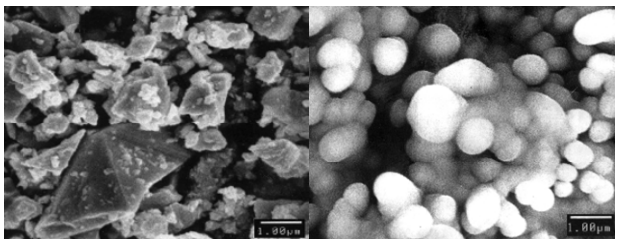

Fig. 3. **SEM of pure carbide powder and carbide powder-based PIM compound**

attainable for a given system; according to Dihoru et al.[4] it should be set 6–14 % lower than the maximum value.

In order to obtain maximum packing fraction for the particular powder/binder system, relative viscosity (ratio of the mixture viscosity to the viscosity of pure polymer) as a function of volume fraction of solids is often employed. The method is based on the assumption that powder particles stay mobile only to some filling degree (a cluster model). As the particles loading reaches the maximum a melt is confined among powder particles and the motion of the compound is made impossible, which results in a sharp increase of viscosity beyond all limits due to the friction between small hard powder particles[5].

The value of the maximum packing fraction depends strongly not only on the materials properties, but also on the packing conditions. Nielsen[6] proposed that the value of maximum packing ranges from 0.601 to 0.637 for random packed spheres, Chong et al.[7] used the value 0.605 for monodispersed glass beads in PIB matrix, e.t.c.

More than hundred empirical and theoretical relations have been proposed in order to obtain the value of maximum packing fraction from the viscosity data. Often a simple empirical Maron-Pierce relation[8] is employed to calculate maximum loading level for PIM compounds. In cases, where the Maron-Pierce model departs from experimental data, as shown e.g. by Jorge et al.[9] for the description of alumina powder and PEG/PE wax binder, its modification proposed by German and Bose[1] offers the good accordance with experimental data, predicting the maximum loading degree value with high accuracy.

Recently, we tested[10] a set of most often recommended relations in the PIM literature and found that the values predicted with the models were rather overestimated or underestimated, when compared to the experimental data. Further, the predicted values of the maximum volume fraction of the same powder varied with the model used (Table I) even though the maximum loading levels of PIM compounds, established using these models, followed well the powder characteristics: the highest value of maximum loading belonged to the powder with the broadest distribution of particle sizes, while the lowest value was attained for powder with high portion of small particles.

Table I
Predicted values of maximum volume fraction of solids for three carbide powders (UNI 1, UNI 2, BI) differing in their powder characteristics[10]

Model	Maximum volume fraction of powder, ϕ_m		
	UNI 1	UNI 2	BI
Eilers	0.60	0.56	0.63
Chong	0.60	0.56	0.62
Fedors	0.68	0.60	0.70
Frankel-Acrivos	0.60	0.53	0.61
Quemada	0.64	0.58	0.66
Graham	0.58	0.53	0.59
Krieger - Dougherty	0.66	0.57	0.59
Sengun - Probstein	0.71	0.70	0.61

Another rheological method to obtain critical powder volume concentrations has been proposed by Barreiros and Vieira[11], which employed torque rheometry to set optimal compositions of feedstocks based on powders having non-conventional characteristics for PIM. The optimal particle loading was evaluated as the highest value resulting from the intersections of the adjustment of linear functions of the mixing torque as a function of powder loading plots. The product coming from the feedstock selected by this method showed high density and flexural strength.

Recently, Dihoru et al.[4] demonstrated a possibility to determine optimal solid loading by the help of neutral network modeling. Consequently, they proposed an idea of combining neural networks with knowledge-based systems to optimize PIM process.

It should be mentioned that volume fraction of particles also slightly varies due to pressurization, because of a great discrepancy between bulk moduli of powder and binder[5]. Except of the pressure affected flow behaviour of PIM compounds reported by Hausnerova et al.[12] for the system consisting carbide powder and three-component binder (polyethylene, polyethylene based copolymer, paraffin wax), the effect of pressure is still omitted in the rheological characterization of filled polymers.

Step 2: Injection Moulding. Moulding of PIM compounds does not essentially vary from the processing of pure polymer melts. Both the screws and the barrels should be made from a wear resistant material. The screws are equipped with a non-return valve[13], which prevents feedstock's pressing backwards into the barrel.

Temperature is the most important variable – too high temperature can lead into the binder separation from the melted compound, on the other hand insufficiently high temperature would cause freezing of the feedstock before the mould filling or creation of weld lines. Computer aided engineering (CAE) gives the predictions of pressure, velocity and temperature profiles throughout the flow region via commercially available PIMSolver (Cetatech, South Korea), which is a 2.5D FEM software package developed for the simulation of the injection moulding process[14].

Nevertheless, a key to successful injection moulding lies in understanding of their rheological properties. A priori application of the fundamental theories on the suspensions in predicting the flow properties of PIM compounds should be taken with an extreme caution, because it brings a number of obstacles and limitations.

The rheology of such an extreme type of filled polymers has been documented in a far from sufficient manner. Majority of researchers concentrated on the effect of binder composition on rheological properties of feedstocks, but the role of the particular binder components and their interrelationship remain still unclear. One of the rare systematic investigations has been presented by Hsu and Lo[15]. They used McLean-Anderson statistic method[16] to study fluidity (inverse of viscosity) and pseudoplasticity (in terms of power-law index) of 15 binder formulations and presented contour maps showing how these two rheological variables vary with binder components at a constant value of the fourth.

PIM compounds generally show high sensitivity to variations in shear rate. Newtonian plateau becomes reduced or even disappear in the measured range of shear rates. It has been widely accepted that the change into non-Newtonian flow arises from the disruption of agglomerates formed by particles[17].

Depending on the type of the dispersed particles, especially on their particle size, yield point may appear for highly concentrated compounds at low shear rate as an indication of particle network structure within the melt, which is relatively stable at lower shear rates, e.g.[18]. At higher shear rates, however, this structure is broken, and the viscosity is dominated by hydrodynamic interactions[19] resulting in shear thinning as particles and polymer orientate and order in the flow direction to allow interparticle motion.

At still higher powder loading, with further rise of shear rate, volume increases because particles cannot form layers and slide over each other[20]. Then, depending on the binder wetting characteristics, shear thinning may turn into dilatant flow, as shown in Fig. 4.

There is still considerable uncertainty about the source of such behaviour. An increase in viscosity with shear rate may be indicative of particle disordering[20] or dilation.

The mechanism proposed by Barnes[21] is that with increasing shear stress (rate) the layers formed in the pseudoplastic flow region becomes disrupted, and at a certain (critical) shear stress or rate are fully eliminated and the flow turns into dilatant. It implies that each highly concentrated suspension exhibits dilatant flow at the proper flow conditions depending on filler concentration, particle size distribution, and also viscosity of a polymer component.

Finally, highly concentrated compounds (about 50 vol.% solids and higher) may exhibit a radical change on their flow curves accompanied by distortions of the extrudate surface called melt flow instabilities. Hausnerova and coworkers[2,22] recorded flow instabilities of a "pressure oscillations" type for carbide compounds and showed that temperature is the key factor limiting their onset almost independently of the filler concentration. At higher temperatures the formation and reformation of particles mat at the capillary entrance is enhanced by lower binder viscosity, which supports the mechanism of filtration effect, as a possible explanation.

Phenomenon considered as typical to occur during flow of highly concentrated suspensions is wall slip. Mooney method is a common approach to detect presence of wall slip during rheological measurements. The later approach to evaluate wall slip given by Hatzikiriakos and Dealy[23] is based on the slip velocity dependence on the wall normal stress.

For cemented carbides in a three-component binder (PEG, PMMA, stearic acid) the existence of a crisscross slip has been reported by Chunkrerkkul et al[24]. It is phenomenon occurring typically for clays in water, where the flow occurs on sets of slip bands (mobile binder) formed on planes near to the planes of maximum shear tress. The slip bands are composed of aligned particles layers of a plate shape, which slip one past another, lubricated by water. The authors propose a "slip band model" resulting in equation similar to the empirical relations of Maron-Pierce[8] or German and Bose[1] bearing relative viscosity to the volume fraction of filler.

Step 3: Debinding. Debinding is the most time consuming stage, depending mainly on the compact thickness and binder composition. A typical wall thickness of a PIM parts ranges from 2 to 3 mm, generally down to 0.1 mm (ref.[25]).

The binder has to be extracted from the pores as a fluid without distorting or contaminating the compact. There are two general ways of debinding (Fig. 5) – thermal and solvent, which are often combined in order to accelerate the process[1]. The first one proceeds by degradation and evaporation or liquid extraction. Thermal debinding in gaseous form is run under low (diffusion) or high pressure (permeation). Liquid extraction is carried out at a temperature high enough for the binder to reach sufficiently low viscosity to flow out of the compact into the pores of the wick material. The other type of debinding, solvent debinding, involves immersing the compact in a fluid that selectively dissolves some components of the polymer binder, thereby leaving an open pore structure for subsequent debinding by evaporation[5].

In general, thermal debinding should be carried out by sequential diffusion of the binder components, and therefore the binder should consist of at least two components with different diffusion temperatures.

In Fig. 6 thermogravimetric analysis of a paraffin wax is shown[2]. Debinding time increases with the chain length and paraffin wax has only between 18 and 32 carbon atoms; it has a narrow decomposition range (Fig. 6a). In contrast, binder containing components differing in molecular weights, melting and decomposition temperatures facilitates a step-by-step debinding. As it is evident from the results shown in Fig. 6b, PEG and paraffin wax move (by diffusion and viscous flow) to the surface of the part before PE and EVA, creating pores which enable easier evaporation of the rest of the binder[2].

Step 4: Sintering. The demands on PIM powders during moulding, debinding and sintering are contradictory. Small particles allow faster sintering, but on the other hand increase

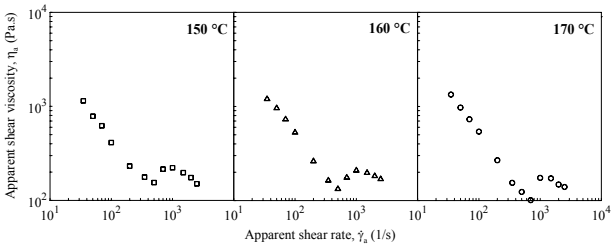

Fig. 4. **Flow curves of ceramic compound at various temperatures**

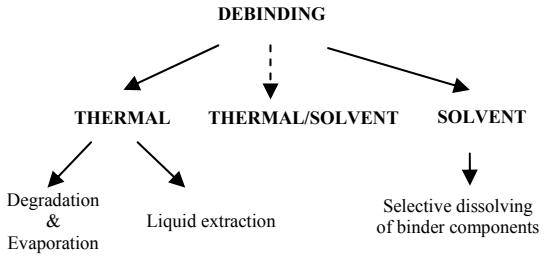

Fig. 5. **Schema of debinding techniques**

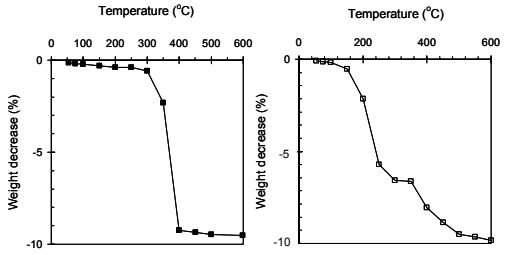

Fig. 6. **Thermo-gravimetric analysis of binders containing;** (a) paraffin and (b) paraffin, PE, PEG 6000, and EVA copolymer[2]

sintering shrinkage, give slower debinding compared to larger particles, and are considerably more expensive. A broad particle size distribution offers higher packing density, less sintering shrinkage, but it causes slower debinding[26]. The disadvantages of spherical particles are slumping during debinding and lower compact strength[5]. In this view, new alloys with improved tailored properties should be developed to further advance the PIM applications as well as to help to attain prices competitive to "conventional" ones.

Concluding remarks. The automotive sector has become a major consumer of PIM parts in Europe. Metallic parts of high complexity are used in ignition locks, as gearbox components, in the steering, in engines, in sensors, car seats, turbochargers, convertible bonnet driving and locking mechanisms, etc.[27] In Japan major automotive applications consist in steering systems components being produced in quantity of 400 000 parts/month[28] (PIM technique is usually competitive to metallurgic processes starting with production of 50 000 parts/year). PIM components for applications at the extreme low temperatures with the potential use in the hydrogen storage tank of the BMW Hydrogen 7 are currently developed in Austria[29].

At present demands on multiphase PIM materials are stringent. It is obvious that reliable simulations of the PIM process can only be performed when the material parameters are known with sufficient accuracy. Processing of PIM materials is clearly an interdisciplinary challenge, combining metallurgy with plastic processing and material science of polymer resins. However, the design methodology currently developed in the PIM industry is based on the trial and error approach. The present state might be partly affected by the fact that majority of PIM realizations is patented, and the research groups involved do not will to publish their findings.

This work has been financially supported by the Grant Agency of the Czech Republic (project 103/08/1307) and Ministry of Education, Youth and Sports of the Czech Republic (project no. MSM 7088352101). B.H. is the laureate of the national section "For Women in Science", being financially supported by L´Oréal during the year 2007.

REFERENCES

1. German R. M., Bose A., in: *Injection Molding of Metals and Ceramics*. MPIF, Princeton 1997.
2. Hausnerová B., Sáha P., Kubát J.: Int. Polym. Proc. *14*, 254 (1999).
3. Hausnerová B., Sáha P., Kubát J., Kitano T., Becker J.: J. Polym. Eng. *20*, 237 (2000).
4. Dihoru L. V., Smith L. N., German R. M.: Powder Metall. *43*, 31 (2000).
5. German R. M., in: *Powder Injection Moulding*. MPIF, Princeton 1995.
6. Nielsen L. E., in: *Polymer Rheology*. Marcel Decker, New York 1977.
7. Chong J. S., Christiansen E. B., Baer A. D.: J. Appl. Polym. Sci. *15*, 2007 (1971).
8. Maron S. H., Pierce P. E.: J. Colloid Sci. *11*, 80 (1956).
9. Jorge H. R., Correia A. M., Cunha A. M.: ANTEC *2005*, 605.
10. Honek T., Hausnerová B., Sáha P.: Polym. Comp. *26*, 29 (2005).
11. Barreiros F. M., Vieira M. T.: Ceram. Int. *32*, 297 (2006).
12. Hausnerova B., Sedlacek T., Slezak R., Saha P.: Rheol. Acta *45*, 290 (2006).
13. Schlieper G.: Powder Injection Mould. Int. *2*, 21 (2008).
14. Urval L., Lee S., Atre S. V., Park S.-J., German R. M.: Powder Metall. *51*, 133 (2008).
15. Hsu K. C., Lo G. M.: Powder Metall. *39*, 286 (1996).
16. Murray J. S. Jr., in: *X-Stat Statistical Experiment Design/ Data Analysis/Nonlinear Optimization*. John Wiley, New York 1984.
17. Kurzbeck S., Kaschta J., Münstedt H.: Rheol. Acta *35*, 446 (1996).
18. Hausnerová B., Honek T., Sáha P., Kitano T.: J. Polym. Mat. *21*, 1 (2004).
19. Husband D. M., Aksel N.: J. Rheol. *37*, 215 (1993).
20. Hoffman R. L.: Trans. Soc. Rheol. *16*, 155 (1972).
21. Barnes H. A.: J. Non-Newtonian Fluid Mech. *56*, 221 (1995).
22. Honek T., Hausnerová B., Sáha P.: Appl. Rheol. *12*, 72 (2002).
23. Hatzikiriakos G. S., Dealy J. M.: J. Rheol. *36*, 703 (1992).
24. Chuankrerkkul N., Messer P. F., Davies H. A.: Powder Metall. *51*, 72 (2008).
25. German R. M.: Powder Injection Mould. Int. *2*, 18 (2008).
26. Dowson G., Williams B., in: *Metal Injection Moulding*. EPMA, Shrewsbury 1995.
27. http://www.piminternational.com/aboutpim/application
28. Williams N.: Powder Injection Mould. Int. *2*, 37 (2008).
29. Williams N.: Powder Injection Mould. Int. *1*, 5 (2007).

KL-05
PLASTICIZATION IN COMPLEX, PHASE-SEPARATED POLYMERS

E. BRUCE ORLER[a], REX. P. HJELM[b]*, JOSEPH T. MANG[c], DEBRA A. WROBLESKI[a], DAVID A. LANGLOIS[a], and MARILYN E. HAWLEY[a]

[a] Materials Science and Technology Division, Los Alamos National Laboratory; [b] Los Alamos Neutron Science Center, Los Alamos National Laboratory, H-805, Los Alamos New Mexico 87455, USA, [c] Dynamic Experimentation Division, Los Alamos National Laboratory*
hjelm@lanl.gov

Plasticizers reduce the bulk modulus and T_m of polymer materials; thus, they are of commercial importance as processing aids. A nitroplasticizer (NP) is used to soften a polyurethane binder, Estane, to lower the temperature at which Estane bound composites can be molded. The effect of NP on Estane mechanical properties is significant. Young's modulus, for example, for Estane is 5 MPa (ref.[1]), whereas the value for plasticized Estane is 0.7 MPa (ref.[2]). We aim to determine the poorly understood nanoscale mechanisms that lead to the softening of a thermoplastic, such as Estane.

Segmented polyurethanes, such as Estane, consist of crystalline aromatic, hard segments, randomly covalently linked with soft, rubbery segments. Previously we showed in, Estane, which has a low, 23 % by weight, hard segment content, that the hard segments partially phase segre-gate into small, discrete domains embedded in a matrix rich in rubbery segments. We postulated that the discrete domains act as reinforcing fillers[3].

We used small-angle neutron scattering (SANS) data and the difference in scattering between NP mixtures containing different fractions of NP and deuterated NP (d-NP), f_D, to determine the distribution of NP in Estane and its effect on the nano-scale structure. The method was the same used to extract the composition and structure of neat Estane by swelling with mixtures of protonated and deuterated solvents[3].

SANS data was analyzed assuming that the discrete domain structure is described by a micelle model[3], in which the dis-crete domains have a uniform core, surrounded by a corona of tethered polymer intermixed with the matrix. Whereas the core consists mainly of hard segment, it contains a significant component of soft seg-ment. Conversely, the matrix consists mostly of soft segment, but also contains a significant amount of hard seg-ment. The corona is chemically identical to the matrix, but is distnquished by taking up less solvent when Estane is swollen with different solvents.[3]

With increasing content of NP from 10 to 50 % by weight the T_g associated with soft segments decreased from ca −35 C to −50 C. The endotherm associated with T_m of the discrete do-mains decreased slightly from ca 60 C and its integrated area decreased by roughly a factor of 2. Young's modulus decreased by an amount that was far greater than predicted by dilution effects of the matrix. When d-NP is used, a peak in the Estane SANS data was seen to decrease in intensity with the amount of d-NP present up to about 20 % by weight, then increase. These results indicated that the NP interacts with the matrix and has an effect on the discrete domains.

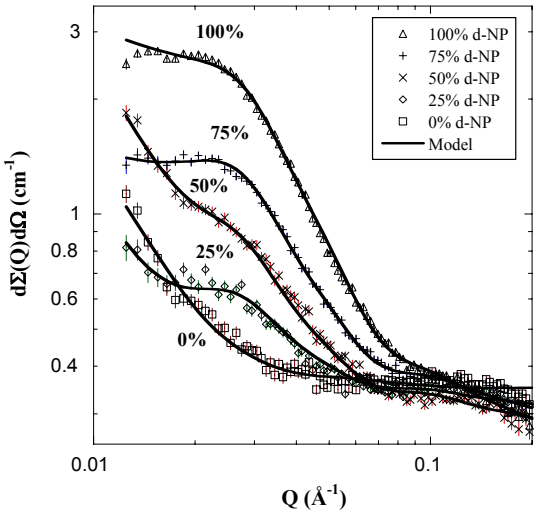

Fig. 1. **Contrast-dependent SANS**

In Estane formulated with 50 wt.% NP a SANS peak appears and its intensity becomes larger with increasing f_D (Fig. 1). The peak is positioned at lower Q than in Estane[3], consistent with a greater concentration of NP in the matrix and increased spacing between the domains in plasticized Estane.

Analysis of the data by the micelle model, (Fig. 1), showed that the bulk of the NP was taken up by the matrix and that there was a significant plasticizer in the core. However, there was no change in either the core radius, 2.95±0.01 nm or in soft segment content, 0.37±0.01, in plasticized Estane compared to Estane[3]. There was less hard segment content in the core, 0.34±0.01, relative to neat Estane, 0.7±0.1 (ref.[3]). The corona included less NP than the matrix, suggesting that the core in plasticized Estane affects the micromechanics of the surrounding volume in the same way as observed in Estane[3].

We gain insight on the effect of NP in Estane by comparing the discrete domain density corrected for the volume change due to NP, $5.1 \pm 0.3 \cdot 10^{16}$ cm^{-3}, with that for neat Estane, $1.0 \pm 0.1 \cdot 10^{17}$ cm^{-3} (ref.[3]). Thus, the effect of NP on Estane is consistent with the hypothesis that the mechanism of softening by NP is by inhibiting the forma-tion of the filler-like discrete domains.

This work benefited from the use of LQD at the Manuel Lujan, Jr. Neutron Scattering Center of the Los Alamos National Laboratory and was supported by the US. Department of Energy.

REFERENCES

1. Banergee B., Cady C. M., Adams D. O.: Modeling Simul. Mater. Sci. Eng. *11*, 457 (2003).
2. Cady C. M., Blumenthal W. R., Gray G. T. III, Idar D. J.: Polym. Sci. Eng. *46*, 812 (2006).
3. Mang J. T., Hjelm R. P., Orler E. B., Wrobleski D. A.: Macromolecules *41*, 4358 (2008).

KL-06

POLYCAPROLACTONE – WOOD PARTICLES BIODEGRADABLE COMPOSITES MODIFIED BY THERMAL DECOMPOSITION OF ORGANIC PEROXIDE

IVAN CHODÁK*, ZUZANA NÓGELLOVÁ, and IVICA JANIGOVÁ

Polymer Institute, Slovak Academy of Sciences, Dúbravská cesta 9, 842 36 Bratislava, Slovakia
upolchiv@savba.sk

Biodegradable plastics attract an increased interest as environmentally friendly materials. The high volume applications can be also considered for automotive especially for interior parts. Besides natural look and light weight, simple waste management is also important in this case since recycling of cars is of rising consent recently. However, a broad application is partially hindered by unsuitable properties and by the high price of biodegradable plastics, compared to conventional materials, especially polyolefins. Rather inexpensive way consists in a preparation of two – phase materials via either blending with another polymer or preparation of composites by addition of a filler[1]. Both routes usually require certain level of adjustment of interactions on the phase boundaries by an addition of compatibilizers as a separate component of the mixture[2] or by chemical modification of either matrix or filler surface[3]. Certainly, when dealing with environmentally degradable plastics, any modification can be only considered if the resulting material is also environmentally degradable. From this point of view, the mixing with various types of cellulose – based particles is an obvious option. In this case, besides modification of certain properties, a decrease of the price of the material can be expected as well.

In this paper, biodegradable matrix filled with organic filler has been discussed. Polycaprolactone (PCL) was used as the biodegradable matrix. The disadvantages connected with this polymer can be summarized as low melting temperature resulting in a low deflection temperature, relatively low tensile strength and modulus, and rather high price compared to high volume common plastics, e.g. polyolefins. On the other hand, high toughness and elongation at break, biodegradability and resistance towards thermal degradation as well as good processability can be mentioned as advantages of PCL.

If organic fillers such as sawdust or switchgrass are used as a composite component, usually a compatibilizer has to be used to improve the interaction between hydrophobic polymer matrix and hydrophilic surface of the filler. Various compatibilizers have been used, the most common being the parent matrix polymer functionalized by maleic anhydride[4]. In the past we investigated the crosslinking initiated by thermal decomposition of an organic peroxide to achieve a compatibilizing effect in a composite based on low density polyethylene as a model matrix and various organic fillers such as birch wood particles[5], aspen fibers, recycled paper, rubber crumb etc.[6]. A formation of covalent bonds leading to grafting of the polyethylene chains onto filler surface was proposed based on SEM observation[7]; this model is in accordance with mechanical properties, especially with an unexpected large increase in Young's modulus for crosslinked composites in spite of a decrease in the crystallinity of the matrix due to crosslinking[8].

The effect similar to crosslinking regarding mechanical properties was observed also if 10 to 30 wt.% of functionalized polyethylene was added to LDPE / wood flour composite. In this case a copolymer polyethylene – co – acrylic acid was found as an efficient modifier[9].

In this paper, a formation and properties of biodegradable composites with polycaprolactone matrix were investigated. A mixture of polycaprolactone (CAPA 6800, Solvay) with switchgrass (supplied by Univ. Québec Trois-Rivières) was chosen as an example of biodegradable filler in biodegradable matrix. 2,5-dimethyl-2,5-ditertbutyl peroxyhexyne (Luperox 130, Luperco, Germany) was used as the initiator of crosslinking.

The composites were prepared by melt mixing all components in a Plasti-Corder kneading machine PLE 330 (Brabender, Germany) at 120 °C for 10 minutes. Test specimens were prepared by compression molding at 120 °C for 2 minutes and at 180 °C for 20 minutes for uncrosslinked and crosslinked materials, respectively. The peroxide has been completely decomposed under given conditions. The dog – bone specimens for testing the mechanical properties were cut at room temperature using a specially shaped knife. Mechanical properties were measured using the Universal testing machine INSTRON 4301 at RT at deformation rate 10 mm / minute. Thermal parameters of samples were measured using DSC 821^e (Mettler-Toledo) in nitrogen atmosphere. Heat of fusion and melting temperature was determined from the second heating scan. Brittle fracture surfaces of notched samples for SEM observation were prepared at a liquid nitrogen temperature. Scanning electron microscope JSM 6400 (JEOL, Japan) was used for micrographing.

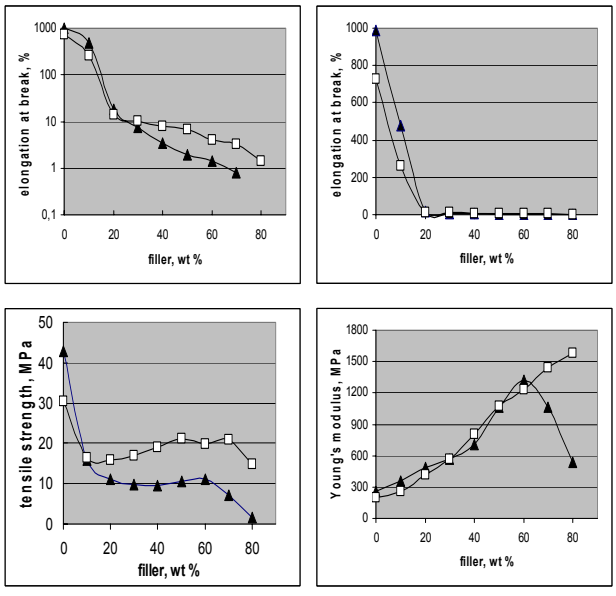

Fig.1. **The dependences of mechanical properties on the filler content for uncrosslinked (full triangles) and crosslinked (open squares) polycaproplactone filled with switchgrass**

The effect of the filler content for uncrosslinked and crosslinked mixtures is seen in Fig. 1. The effect of both the filler content increase and the crosslinking is similar to the one observed for polyethylene filled with organic fillers[5,6]. The increase in the filler content leads to an increase in Young's modulus and a decrease in the elongation at break. This behaviour is generally common for most of two-phase polymeric systems if a stiff component is mixed into a ductile matrix.

Crosslinking results in certain changes in the dependences of mechanical properties on the filler content. First, it is seen that crosslinking leads to a decrease in Young's modulus, tensile strength and elongation at break for PCL without filler. The decrease in modulus can be ascribed mainly to the drop in the crystallinity degree in the virgin polymer (see Fig. 3). As seen in Fig. 1, the same effect regarding both mechanical properties and melting parameters was observed also for composites with low amount of the filler. With rising filler content, the effect of crosslinking on mechanical properties is changing. In spite of decreased crystallinity, modulus of crosslinked PCL / switchgrass composite with the filler content above 30 wt.% is higher compared to the uncrosslinked composites with the same concentration of the filler.

This behaviour is similar to that observed for LDPE / organic filler composites and has been ascribed to a formation of covalent bonds between polymeric chains and the filler surface. Grafting of the polymer occurs on the filler surface, leading to an increased adhesion on the phase boundaries. Consequently, more compact material is formed with fewer voids formed during the sample preparation, containing smaller number of weak units where crack could be easily formed. This is clearly seen especially at filler content above 60 wt.% where uncrosslinked composites suffer from many defects, resulting in a decrease of modulus (presumably due to a formation of number of voids leading to a decrease in effective cross section of the specimen) while a permanent increase in the modulus values for crosslinked samples is observed, up to impressive 1.5 GPa. Obviously, improved adhesion of the part of polymeric matrix onto filler surface results in a formation of much more compact materials with lower number of defects.

The increased adhesion of the matrix polymer onto filler surface due to crosslinking was directly observed by SEM, as seen in Fig. 2, where fracture surfaces of composites containing 50 wt.% of the filler are shown. The filler surface of uncrosslinked material is almost clean from the polycaprolactone, while for crosslinked composite remnants of the polymer attached to the surface is clearly observed.

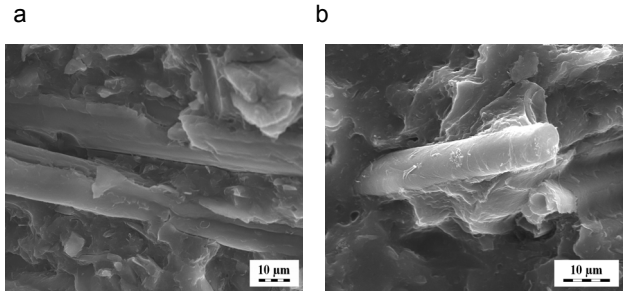

Fig. 2.

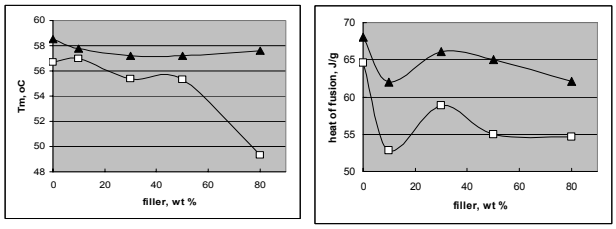

Fig. 3. **Melting temperature and heat of fusion of uncrosslinked (full triangles) and crosslinked (open squares) polycaprolactone composites in dependence on the switchgrass filler content**

On the other hand, a decrease in elongation at break as a result of crosslinking can be ascribed to a decrease in the chain mobility due to cross bonds introduced. These tendencies are observed for the unfilled PCL and composites with low amount of the filler, up to about 20 wt.%. With rising filler content, the behaviour is changing. In this case, crosslinking results in an increase in deformability partially due to lower crystallinity but mainly resulting from higher resistance to crack formation on the polymer – filler phase boundaries as discussed in[10].

Tensile strength curves shown in Fig. 1 indicate that this parameter depends on both modulus and deformation values. Growing modulus contributes to an increased strength but the same is true for elongation at break, namely due to possible elongation strengthening at high deformation, but generally simply because at similar modulus more energy is required to break the sample if deformation is higher. A decreased number of defects on the polymer – filler boundaries contributes to an increased tensile strength as a result of crosslinking.

The melting parameters (melting temperature and heat of fusion proportional to overall crystallinity) are shown in Fig. 3 in dependence on the filler content for crosslinked and uncrosslinked samples. Crosslinking leads to lower melting temperature obviously due to the fact that crosslinking represents a defect in the polymeric chain, resulting in shorter folds forming crystals. It is understandable that lower amount of the polymer can crystallize if more defects are introduced in the chains leading to lower values of the heat of fusion.

Thus, it can be concluded that treating the polycaprolactone / switchgrass composites with organic peroxide results in an increase of polymer adhesion on the filler surface as indicated by mechanical properties, scanning electron microscopy and melting parameters. The observed changes in mechanical properties are interpreted as a uperposition of improved interactions on the phase boundaries and a decrease in crystallinity.

The research was supported by the Slovak Research and Development Agency APVV, grant No 51-010405.

REFERENCES

1. Biodegradable Polymers, Principles and Applications, (Scott G., ed). Kluwer Acad. Publ., Dordrecht 2002.
2. Zuchowska D., Steller R., Meissner W.: Polym. Degrad.

Stab. 60, 471 (1998).
3. Bikiaris D., Prinos J., Koutsopoulos K., Vourotzis N., Pavlidou E., Frangis N., Panayiotou C.: Polym. Degrad. Stab. 59, 287 (1998).
4. Maldas D., Kokta B. V.: J. Adhes. Sci. Technol. 8, 1 (1994).
5. Nógellová Z., Kokta B. V., Chodák I.: J. Macromol. Sci., A, Pure Appl. Chem. 35, 1069 (1998).
6. Chodák I., Nógellová Z., Kokta B. V.: Macromol. Symp. 129, 151 (1998).
7. Janigová I., Lednický F., Nógellová Z., Kokta B. V., Chodák I.: Macromol. Symp. 169, 149 (2001).
8. Chodák I.: Progr. Polym. Sci. 20, 1165 (1995).
9. Sedláčková M., Lacík I., Chodák I.: Macromol. Symp. 170, 157 (2001).
10. Chodák I., Chorváth I.: Macromol. Symp. 75, 167 (1993).

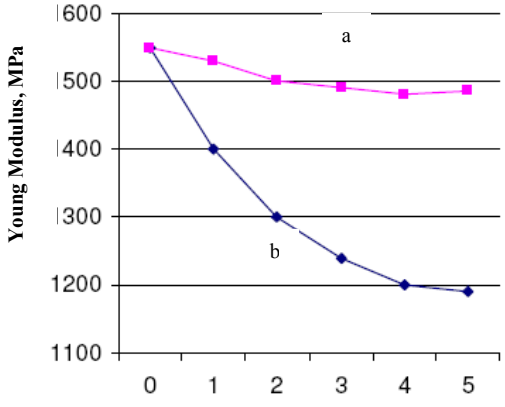

Fig. 1. **Young modulus of recycled polycarbonate:** a) dryed; b) wet

KL-07
RECYCLING OF PLASTIC COMPONENTS IN THE CAR LAMPS

MAREK KOZLOWSKI and STANISLAW FRACKOWIAK

Wroclaw University of Technology, Faculty of Environmental Engineering, Laboratory of Advanced Polymeric Materials and Recycling, Wybrzeze Wyspianskiego 27, 50-370 Wroclaw, Poland
marek.a.kozlowski@pwr.wroc.pl

Introduction

Plastics represent a steadily increasing share among the materials used for construction of automobiles. These materials are advantageous in comparison to metals because plastics do not rust, are easily processable, highly aesthetic, safe and comfortable in use. However, a main merit is that a density of plastics is a few time lower than that of steel or cast iron. With a vehicle mass saving one can reduce a fuel consumption, thus contributing to an improvement of environment by means of reducing CO_2 emissions and by savings the natural resources (crude oil). The material savings are related to recovery and recycling of plastic parts from the end of use vehicles. This possibility is directly related to the required quota of the materials re-use and recycling according to the ELV Directive 2000/53/CE (currently 85 wt.% and 95 wt.% till 2015). Among recovery methods the mechanical recycling (reprocessing) has a well established position for its simplicity and economy. However, the economical profits depend on a kind of the polymer to be recycled. As a rule, recycling of the commodity plastics is hardly profitable (besides large, easy to dismantling parts), because the costs of technology are higher than the difference in price between the virgin resin and recylate. Much more profits one can expect from the mechanical recycling of engineering plastics, which price of a virgin polymer is high. To this group of plastics belong polycarbonate (PC), polyamide (PA), ABS, POM, PMMA, PBT. Among the parts constructed with these polymers are the front and rear lamps. The headlamps are made of polycarbonate, whereas in the tail lights besides PC also ABS and PMMA is used. Recycling of these plastic has been discussed in this paper.

Teh easiest way of waste management is regrinding and reprocessing into a form of pellets. Unfortunatelly, during these processes a degradation of polymers takes place. This results in a deterioration of the mechanical properties of recyclates. The extent of degradation depends both on the equipment used for recycling (grinders, dryers, extruders), operating parameters and on a nature of the polymer. Some polymers are sensitive to moisture, whereas others can reprocessed several times without any visible influence on their properties.

Possible changes have been presented in Fig. 1 for polycarbonate. While recycled in dry conditions, PC retains high stiffness even after five recycling stages. If avoiding drying, the mechanical properties of polycarbonate drop dramatically after each recycling. Deterioration of properties can be reduced by blending of a recyclate with other polymers or fillers. Such possibilities have been attempted and the results have been presented in this paper.

Experimental

The polymers used for the study were: polycarbonate Makrolon (Bayer), polymethyl methacrylate PMMA 920 (Altuglas) and ABS copolymer. For compatibilization of blends a maleated copolymer Kraton SEBS-g-MA was used.

Polymer composites were manufactured by addition of following fillers: unmodified montmorillonite Nanomer PGW (Nanocor), organically modified montmorillonites Nanomer I30.P, Nanomer I44.P (Nanocor) nanometric calcium carbonate NPCC (NanoMaterials Technology).

Composites manufactured with PC, ABS, PMMA and respective fillers (5 wt.%) were prepared by melt mixing with a periodic mixer Haake (220–235 °C depending on a matrix polymer).

Melt rheology was measured with HAAKE Rotovisco RT20 rheometer. Mechanical properties were evaluated with a tensile machine Lloyd LR10k or an impact tester Resil 5.5 (Ceast).

Results

Rheological measurements have revealed that reprocessing does not influence markedly ABS and PMMA – the viscosity curves remain almost at the same level after four recycling stages (Fig. 2 and 3). This finding are contradictory to that received for recycling of polycarbonate, especially if the polymer was not dryed.

Application of silica and $CaCO_3$ as fillers have revealed that the properties of composites are related to a kind of the inter-gallery modifier in a montmorillonite filler. The shape of a filler (cubic versus platelet) also plays a role for a final characteristics of composites.

Polycarbonate has revealed as an extremely sensitive polymer to a degradation caused by the thermal and mechanical stresses.

More promising results have been received for the blends prepared from the polymers studied (Fig. 4). Combination of different viscoelastic characteristics od PC and ABS resulted in a high impact of blends, especially after compatibilization with a maleated copolymer SEBS-g-MA.

Conclusions

Waste plastics form the vehicle lightings may serve as a source of promissing materials for new blends of attractive properties.

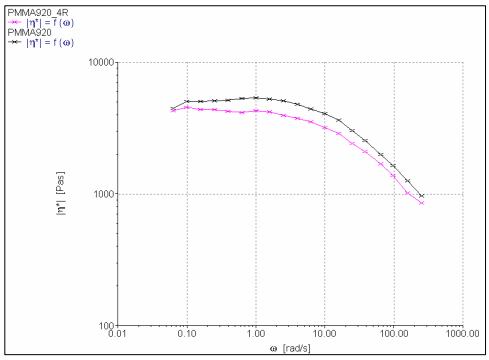

Fig. 2. **Melt viscosity of virgin PMMA and after 4 reprocessings**

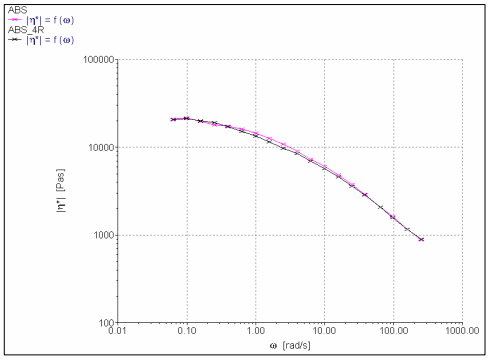

Fig. 3. **Melt viscosity of virgin ABS and after 4 recycling stages**

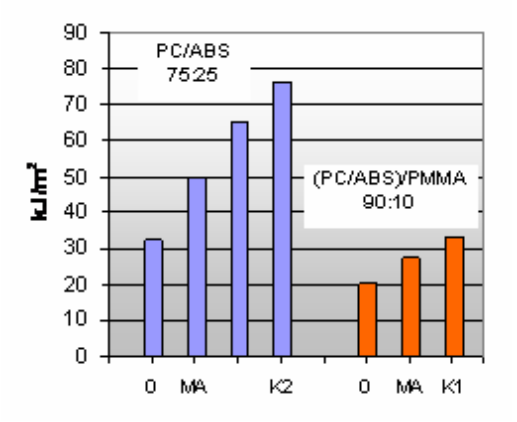

Fig. 4. **Charpy impact strength for PC/ABS blends and alloys**

Polymer composites based of engineering polymers filled with the fillers of nanometric size do not guarantee the mechanical properties of high interest to automotive industry. For a successful application of the composites made of waste polymers used for automotive lightings a thorough design and sophisticated materials science knowledge should be applied.

KL-08
VERY FAST VULCANISING SYSTEMS

ANTONÍN KUTA, ZDENĚK HRDLIČKA, and VRATISLAV DUCHÁČEK

Institute of Chemical Technology, Department of Polymers, Technická 5, 166 28 Praha 6, Czech Republic
antonin.kuta@vscht.cz

Abstract

Sulphur vulcanising systems with zinc isopropyl xanthate (ZIX) and zinc diethyl dithiocarbamate (ZDEC) have been used for dry natural and synthetic rubbers (NR and SR). Curing process of NR has been faster than that of SR. The biggest difference has been found for standard emulsion type of styrene-butadiene rubber (E-SBR). Retarding influence of acids originated from an emulsifier could play a role. A solution type of SBR (S-SBR) and other SR without acidity have been tested as well. Curing process was still slower than that of NR. Good results for E-SBR have been obtained when combinations of tetramethylthiuram disulfide (TMTD) with thiourea (TU) without elementary sulphur were used.

Xanthate and carbamate accelerators cure common types of NR reasonably faster than common highly unsaturated types of synthetic rubbers. Cure rate and cure efficiency of conventional and efficient vulcanising systems with ultra accelerators depend on “impurities” in raw NR.

Introduction

Very fast vulcanising sulphur systems due to their high activity are used for vulcanisation of highly unsaturated rubbers at low temperatures or low unsaturated rubbers at common (higher) temperatures.

Very fast rubber vulcanisation is usually achieved by vulcanising systems with ultra accelerators. Zinc salts of xanthates and dithiocarbamates are typical representatives of them. It has been also suggested that thiourea can be used as a secondary accelerator to the primary one, such TMTD to reach fast vulcanisation[1,2].

Ultra accelerators are typically used for vulcanisation of natural rubber in the latex form. Vulcanisation of latex products is usually carried out at lower temperatures compared to dry rubber products. Cure activity of ultra accelerators in highly unsaturated synthetic rubbers (SR) is expected also to be high, however, lower than in natural rubber (NR), e.g. in emulsion type of SBR (E-SBR).

Material and methods

Rubbers:
Natural Rubber (NR)*;* Malaya Rubbers, Malaysia
SMR 20, SMR 10, pale crepe
deprotenized NR (DPNR)
Isoprene rubber (IR)
SKI-3, Nizhnekamskneftechim Inc., Russia
Butadiene rubber (BR),
SKD, Efremov Synthetic Rubber Enterprise Join Stock Co., Russia
Buna cis 132 - Schkopau, Dow Plastics
Styrene-butadiene rubber, emulsion type (E-SBR)
Kralex 1500, Synthos Kralupy a.s., Czech Republic
Buna SB 1500 Schkopau, Dow Plastics
Styrene-butadiene rubber, solution type (S-SBR),
Calprene 1204B, Dynasol Elastomers, S.A., Spain
BUNA VSL 5025-0 HM, Lanxess, Germany
SE SLR-4601, Dow Plastics

Accelerators:
Zinc diethyl dithiocarbamate (ZDEC), *Robac ZDEC*; Robinson Brothers, UK
Zinc isopropyl xanthate (ZIX), *Robac ZIX*; Robinson Brothers, UK

Formulation of rubber compounds were as simple as possible, to allow clearly observe the rubber curing nature. "Conventional" (C) and "efficient" (EV) vulcanising systems were used. The formulations are shown in Table I.

The course of vulcanisation has been recorded by Rubber Process Analyzer 2000 (Alpha Technologies) at temperature range from 140 °C to 80 °C.

Rubber vulcanisation activity was evaluated as cure rate and cure efficiency.

The term cure rate R_v means an average cure rate, which has been calculated via the simplest method:

$$R_v = \frac{1}{t_{90} - t_{10}}$$

where t_{90} (t_{10}) is time required to reach 90 % (10 %) of maximum cure degree.

Table I
Formulation of rubber compounds

	ZIX-C	ZIX-EV	ZDEC-C	ZDEC-EV
Rubber	100	100	100	100
ZnO (phr)	5	5	5	5
Stearic acid (phr)	1	1	1	1
ZIX (phr)	1	4	–	–
ZDEC (phr)	–	–	1	4
Sulphur (phr)	2.5	1	2.5	1

Table II
Ash content and the relative absorption *I* of NR and SR at selected bands

Rubber	Ash [wt.%]	I_{1541}	I_{1633}
SMR 20	1.36	0.020	0.046
SMR 10	1.40	0.009	0.024
Crepe	1.25	0.004	0.021
DP NR	0.05	0.002	0.062
SKI-3	< 0.05	0	–

Cure efficiency has been expressed as a difference between maximum and minimum values of modulus (torque) $M_{max} - M_{min}$.

Impurities in NR have been quantified (Table II) as an ash content and by infrared spectroscopy as the relative absorption *I* (related to vibration C=C bond) at 1541 cm^{-1} band, if it was accompanied with the absorption band at 1633 cm^{-1} as a measure of protein content.

Results and discussion

Very low activity of xanthate ultra-accelerators in common SBR was the main reason for this study. Faster sulphur vulcanisation of NR compare to E-SBR is well known. However, the cure rate differences have been much larger when mercaptobenzothiazole (MBT) or sulphenamide accelerators are used. For example, cure rate at 140 °C of NR with MBT is 0.14 min^{-1} and E-SBR 0.018 min^{-1}, NR/SBR cure rate ratio is 7.8. For the ultra-accelerator studied (ZIX) this ratio was around 100. Cure rate values at 140 °C are summarized in Table III.

Main reason for cure rate differences is the presence of "impurities" or some additives in rubber. Acids are typical vulcanisation retarders, basic substances on the contrary accelerate vulcanisation. Organic acids in E-SBR originated from emulsifier are an example of the first group. Nitrogen containing bases (trigoneline, stachydine, choline, trimethyl amine)[3] which are present in fresh NR latex or are generated from proteins during latex processing and rubber storage are the examples of the second group.

Acidity of E-SBR has been our first explanation of dif-

Table III
Average cure rate R_v (min^{-1}) of NR and SR at 140 °C

Rubber	ZIX-C	ZIX-EV	ZDEC-C	ZDEC-EV
NR (*SMR 20*)	1.36	0.93	0.52	1.08
NR (*SMR 10*)	1.40	0.76	0.55	0.95
NR (*crepe*)	1.25	0.89	0.42	0.51
DP NR	0.83	0.52	0.48	0.35
IR (*SKI-3*)	0.86	0.56	0.52	0.38
E-SBR (*Kralex 1500*)	0.010	0.013	0.101	0.041
E-SBR (*Buna SB 1500*)	0.011	0.034	0.101	0.096
S-SBR (*Calprene*)	0.35	0.32	0.121	0.126
S-SBR (*Buna VSL*)	0.181	0.31	0.116	0.133
S-SBR (*SLR-4601*)	0.57	0.36	0.25	0.198
BR (*SKD*)	0.72	0.72	0.20	0.149
BR (*Buna cis*)	0.47	0.35	0.169	0.157

Table IV
Maximum cure degree M_{max}–M_{min} (dNm) of NR and SR at 140 °C

Rubber	ZIX-C	ZIX-EV	ZDEC-C	ZDEC-EV
NR (*SMR 20*)	10.7	10.9	14.3	9.7
NR (*SMR 10*)	10.4	8.4	14.0	9.2
NR (*crepe*)	3.3	7.4	12.7	9.1
DP NR	4.6	5.0	10.4	6.9
IR (*SKI-3*)	3.4	9.3	9.4	5.7
E-SBR (*Kralex 1500*)	5.6	0.7	20.9	10.6
E-SBR (*Buna SB1500*)	2.8	0.5	19.6	8.6
S-SBR (*Calprene*)	10.9	14.2	22.2	9.0
S-SBR (*Buna VSL*)	2.5	1.1	18.4	7.0
S-SBR (*SLR-4601*)	3.5	2.9	17.0	7.5
BR (*SKD*)	13.8	17.5	20.3	14.4
BR (*Buna cis*)	5.1	5.6	18.4	8.6

ferences in curing activity of NR and E-SBR. To prove it, 2 phr of sodium carbonate or triethanol amine were added to a Kralex based compound to neutralise acids. The cure rate with ZDEC-C system at 140 °C increased from 0.1 min^{-1} to 0.12 min^{-1} and 0.21 min^{-1}, respectively.

The preparation of rubber compounds based on a solution type of SBR is another way how to obtain SBR compounds without acid emulsifier residues. The S-SBR compounds cured faster than E-SBR ones, especially with ZIX accelerator. However, the cure rate has been still lower then in NR.

S-SBR is not a simple copy of E-SBR without acids. Styrene units are also randomly distributed in macromolecular chains and their amount is similar (25 % in S-SBR and 23.5 % in E-SBR), but due to different polymerisation chemistry, butadiene units are more frequently bonded in 1,2 positions in polymer chains. Content of vinyl groups arising via this 1,2 addition is higher in S-SBR than in E-SBR, in our case 30 % compare to 18 %. That difference can also influence vulcanisation reactions.

To eliminate vinyl group effects and diluting effect of the inert comonomer, next rubber compounds have been prepared from high *cis*-1,4-polybutadiene. Although the cure rate of BR compound has been higher than S-SBR, the level of NR has not reached.

Cure rate of isoprene rubber (IR) as real synthetic analogue of NR has been the closest to NR. However, there are cure rate differences between NR grades. Cure rate of NR grades has increased in order DPNR < crepe < SMR 10 < SMR 20, i,e, with impurities content. Polyisoprenes with very low content of impurities (DP NR and SKI-3) have showed almost the same cure rates.

Conventional system with ZIX accelerator was always faster than EV system. On the other hand, the same system with carbamate accelerator was slower, except SKI and crepe at low temperatures.

Cure rate generally decreased with temperature decreasing. The effect of "impurities" and molecular structure at temperature range 140 °C to 80 °C was very similar – cure rate of NR increased with N content, E-SBR has been the slowest. It cured so slowly, that carbamate system has not been able to vulcanise below 120 °C, xanthate even below 140 °C. Good results have been obtained with another vulcanising system based on the combination of tetramethylthiuram disulfide (TMTD) with thiourea (TU) without elementary sulfur. Optimum dosage is 4 phr TMTD and 5 phr TU. Cure rate at 120 °C was 0.44 min^{-1}, at 100 °C 0.09 min^{-1} and at 90 °C still 0.03 min^{-1}. Curing time (t_{95}) of carbon black filled SBR compounds vulcanized at 100 °C lies in the range from 50 to 60 min (ref.[4]).

Maximal cure degree of rubbers has been also influenced by "impurities" content. The lowest cure degree of NR was reached in case of DP NR. Conventional carbamate system was the most efficient system in polyisoprenes. Cure degree reached with EV systems was mostly lower. Higher curative dosage could decrease system sensitivity on impurities. But very low cure degree and cure rate of ZIX-EV system in E-SBR is probably a result of accelerator decomposition by acidity due to low chemical stability of xanthates. M_{max}–M_{min} data at 140 °C as the maximal cure degree are summarized in Table IV.

Conclusions

Vulcanising activity of xanthate systems in emulsion type of SBR is very low, probably due to accelerator decomposition. Good result has been obtained with system based on the combination of tetramethylthiuram disulfide with thiourea.

Xanthate and carbamate accelerators based vulcanising systems cure NR reasonably faster than common highly unsaturated types of synthetic rubbers. There are cure rate differences between NR grades, cure rate increases with non-rubber substances content, namely with proteins.

The support of the Ministry of Education, Youth, and Sports of the Czech Republic (through research grant MSM 6046137302) is gratefully acknowledged.

REFERENCES

1. Ducháček V.: J. Appl. Polym. Sci. *22*, 227 (1978).
2. Mathew G., Kuriakose A. P.: J. Appl. Polym. Sci. *49*, 2009 (1993).
3. Suchiva K., Kowitteerawut T., Srichantamit L.: J. Appl. Pol. Sci. *78*, 1495 (2000).
4. Kuta A., Hrdlička Z., Ducháček V.: In: *IRC 2007*, Paper No. 161. Cleveland, OH, USA (2007).

KL-09
X-RAY NANO CT: 3D ANALYSIS OF COMPOSITE AND RUBBER MATERIALS WITH SUBMICROMETER RESOLUTION

JENS LUEBBEHUESEN and OLIVER BRUNKE

GE Sensing & Inspection Technologies GmbH (phoenix|x-ray), Niels-Bohr-Str. 7, 31515 Wunstorf, Germany
Jens.Lubbehusen@ge.com, www.phoenix-xray.com

During the last decade, Computed Tomography (CT) has progressed to higher resolution and faster reconstruction of the 3D-volume. Most recently it even allows a three-dimensional look into the inside of materials with submicron resolution. High-resolution X-ray CT allows the 3D visualization and failure analysis of the internal microstructure of composite materials – even where 2D X-ray microscopy would give only the integral information of the overlaying bundles of fibers. By means of nanofocus® tube technology, nanoCT®-systems are pushing forward into application fields that were exclusive to expensive synchrotron techniques. But their potential, convenience and economy of these lab systems is often underestimated.

Especially for modern composite and rubber materials which are used in very expensive or safety relevant applications, CT is ideal to accompany the product from development to final quality control. The tube based CT measurements for the study were performed with a granite-based phoenix|x-ray nanotom®-CT system (GE Sensing & Inspection Technologies GmbH, Wunstorf, Germany) equipped with a 180 kV / 15 W high-power nanofocus® tube with Tungsten or Molybdenum-Targets. The tube offers a wide range of applications from scanning low absorbing samples in nanofocus® mode with voxel resolutions <500 nm and high absorbing objects in high power mode with focal spot and voxel sizes of a few microns. The nanotom® is the first 180 kV nanofocus computed tomography system which is tailored specifically to high resolution applications in the field of material science and micro electronics. Therefore it is particularly suitable for nanoCT-examinations e.g. of polymeric and composite materials, metals and metal foams, ceramics etc.

The CT volume data set can be displayed in various ways; it can be sectioned and sliced in all directions, rotated and viewed from any desired angle. Highly applicable to a variety of fields, nanoCT can be a viable substitute for destructive mechanical slicing and cutting. Any internal difference in material, density or porosity within a sample can be visualized and data such as distances can be measured. Some of the many applications of nanoCT include the analysis of fiber textures, air inclusions or cracks in composite materials with voxel resolutions down to less than one micrometer.

The presentation will outline the hard- and software requirements for high resolution tube based CT and compare CT results of sophisticated conventional tube-based with synchrotron radiation based scans. It will showcase several quality control applications of different composite and rubber materials that were inspected with high resolution nanofocus® and microfocus CT.

KL-10
MODIFICATION OF POLYAMIDES PROPERTIES BY IRRADIATION

MIROSLAV MANAS, MICHAL STANEK, DAVID MANAS, MICHAL DANEK, and ZDENEK HOLIK

Tomas Bata University in Zlin, Faculty of Technology, Department of Production Engineering, TGM 275, 762 72 Zlin, Czech Republic
manas@ft.tub.cz

Abstract

Radiation processing involves the use of natural or man-made sources of high energy radiation on an industrial scale. The principle of the radiation processing is the ability of the high energy radiation to produce reactive cations, anions, and free radicals in materials. The industrial application of the radiation processing of plastic and composites includes polymerization, cross-linking, degradation and grafting. Radiation processing involves mainly the use of either electron beams from electron accelerators or gamma radiation from Cobalt-60 sources.

Radiation processing does not make the product radioactive. The majority of industrial applications of radiation processing are a cross-linking of wire and cable insulations, tube, heat shrink cables, components of tires, composites, moulded products for automotive and electrical industry etc. Another significant application of radiation processing is the sterilization of medical disposables. A comparison of the mechanical properties of natural and irradiated polyamide PA6 and PA6.6 (unfilled and filled – 30 % GF) is presented in this article.

Introduction

The cross-linking of rubbers and thermoplastic polymers is a well-proven process of the improvement of the mechanical and thermal properties. The chemical cross-

linking or rubber vulcanization is normally induced by the effect of heating after processing with the presence of a curing agent. The cross-linking process for thermosets is very similar. In thermosets the polymer molecules are also chemically linked due to heat after processing.

The irradiation cross-linking of thermoplastic materials via electron beam or cobalt 60 (gamma rays) is proceeding separately after the processing. The cross-linking level can be adjusted by the irradiation dosage and often by means of a cross-linking booster.

The main deference between beta and gamma rays lies in their different abilities of penetrating the irradiated material. Gamma rays have a high penetration capacity. The penetration capacity of electron rays depends on the energy of the accelerated electrons.

Due to electron accelerators, the required dose can be applied within seconds, whereas several hours are required in the gamma radiation plant.

The ability of penetrating the irradiated material are given in the Fig. 1.

The palleted products are conveyed trough the radiation field. The radiation dose is applied gradually, that is to say, in several stages, whereby the palleted products are conveyed around the radiation sources several times. This process also permits the application of different radiation doses from one product type to another. It can be used for irradiation of polyolefines, polyesters, halogen polymer and polyamids from thermoplastics group, elastomers and thermoplastic elastomers. Some of them need the addition of crosslinking agent.

The dimensional stability, strength, chemical resistance and wear of polymers can be improved by irradiation[2]. Irradiation cross-linking normally creates higher strength as well as reduced creep under load if the application temperature is above the glass transition temperature (T_g) and below the former melting point. Irradiation cross-linking leads to a huge improvement in resistance to most of the chemicals

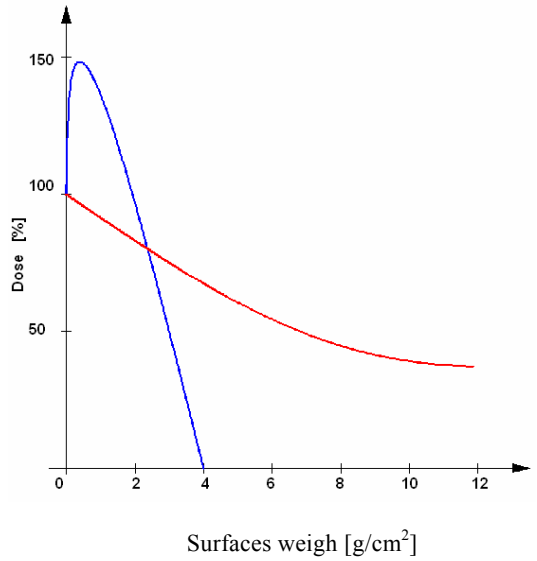

Fig. 1. **Ability of penetrating of electron – β and gamma – γ radiation**

and it often leads to the improvement of the wear behaviour.

The thermoplastics which are used for production of various types of products have very different properties. The main group presents standard polymers which are easy obtainable with favourable price conditions[3]. Limited level of both mechanical and thermal properties is big disadvantage of standard polymers. The group of standard polymers is the most considerable one and its share in the production of all polymers is as high as 90 %.

The engineering polymers are a very important group of polymers which offers much better properties in comparison to standard polymers. Both mechanical and thermal properties are much better than in case of standard polymers. The production of these types of polymers takes less than 10 %.

High performance polymers have the best mechanical and thermal properties but the share in production and use of all polymers is less than 1 %.

Still, it is necessary to say that in the decision-making process (which kind of polymers will be used) the application area and price are important. The differences in price are exorbitant – from unit euros (standard polymers) to tens or hundred euros per kg in case of some types of high performance polymers.

In connection with these data we have to ask if it is necessary to use engineering polymers or even high performance polymers in some application. In many cases it would be possible to use standard or engineering polymers and improve their properties, e.g. by irradiation.

The main objective of this study is investigation of influence of dose of irradiation on mechanical properties of polyamides PA6 and PA6.6 both without reinforcement and reinforced by 30 % of glass fibres.

Experimental

The properties not irradiated PA6 and PA6.6, both unfilled and filled 30 % glass fibres have been compared. The injection molding machine Arburg Allrounder 420C Advanced has been used for sample preparation.

Irradiation was carried out in the company BGS Beta Gamma Service GmbH & Co, KG, Saal am Donau, Germany with the electron rays, electron energy 10MeV, doses minimum of 66, 99, 132, 165 and 198 kGy.

Used polymers:
PA 6 – Frianyl B63 (unfilled)
PA 6 – Frianyl B63 GV30 (filled by 30 % glass fibers)
PA 6.6 – Frianyl A63 (unfilled)
PA 6.6 – Frianyl A63 GV30 (filled by 30 % glass fibers)

The tensile test with the use of stated equipment has been carried out:

Tensile test, according to standard CSN EN ISO 527 – 1, 527 – 2.
Equipment: Tensile test machine ZWICK 1456
SW – Test Xpert Standard
Temperatures: 23, 80 °C

To be able to state the effect of irradiation on net creation in the polymer structure the cross – linking grade has been determined (measured by Xylos gel test) for each type of

tested polyamide and the doses of irradiation. The results of gel test are given in the Fig. 2.

The irradiation radically improves the crosslinking grade of both filled and unfilled polyamides. The cross – linking grade of filled polyamides is about 15 to 20 % higher in comparison with the unfilled polyamides. The cross – linking improves the tensile strength and E modulus. The results on tensile strength of unfilled polyamides PA6 and PA6.6 are given in Fig. 3 and 4.

The results show the improvement of the ultimate tensile strength after irradiation by the dose of 66 kGy and its further slow increasing with the higher dose of irradiation.

The improvement of tensile properties is remarcable also in case of PA6 and PA6.6 both filled by 30 % glass fibres (Fig. 5 and Fig. 6). All test were carried out the temperature 23 °C.

The results of tensile tests at the temperature 80 °C are given in the Fig. 7 and Fig. 8. There are visible differences of ultimate tensile strength between irradiated and not irradiated tested polyamides.

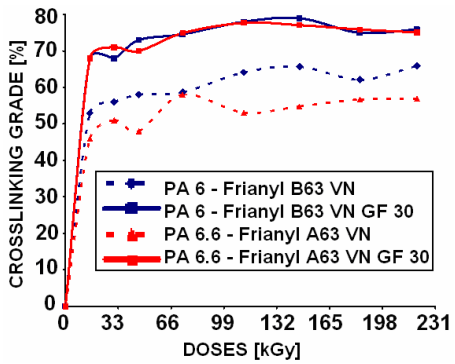

Fig. 2. **Comparison of Gross – linking grade of tested polymers**

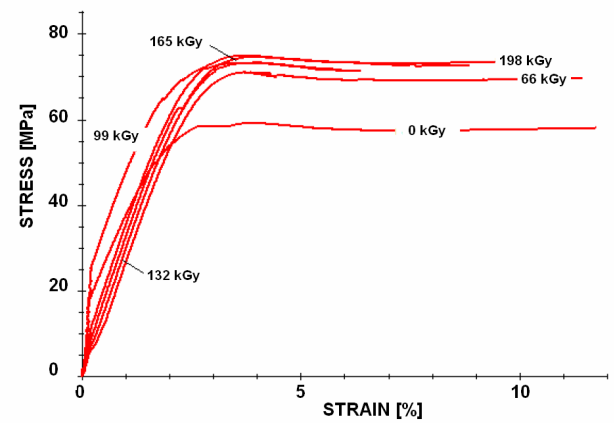

Fig. 3. **Tensile test** (PA6 at 23 °C)

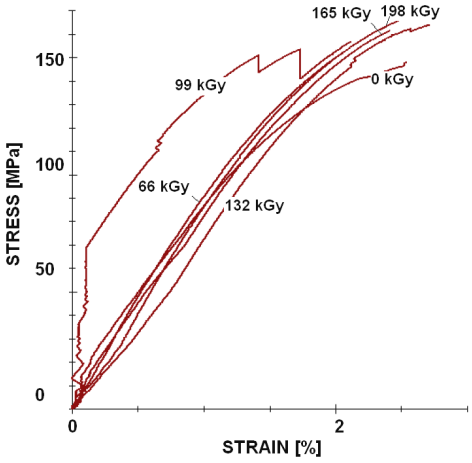

Fig. 4. **Tensile test** (PA6, 30 % GF at 23 °C)

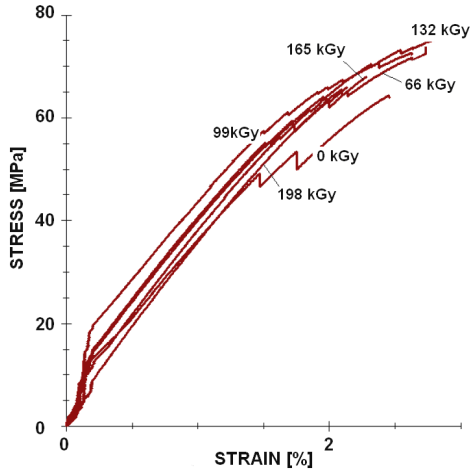

Fig. 5. **Tensile test** (PA6.6 at 23 °C)

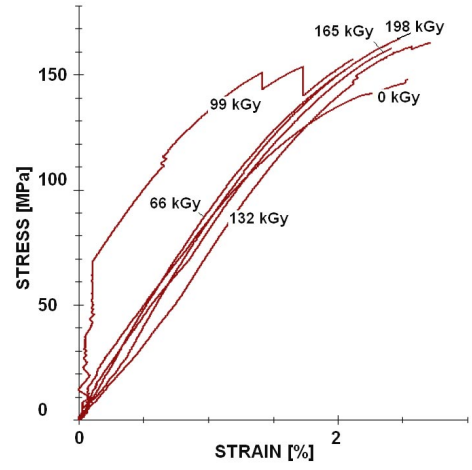

Fig. 6. **Tensile test** (PA6.6, 30 % GF at 23 °C)

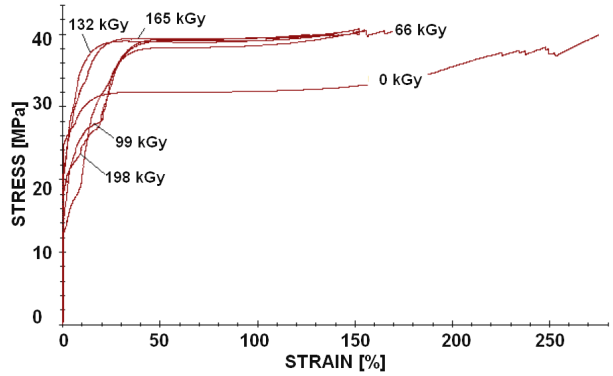

Fig. 7. **Tensile test** (PA6 at 80 °C)

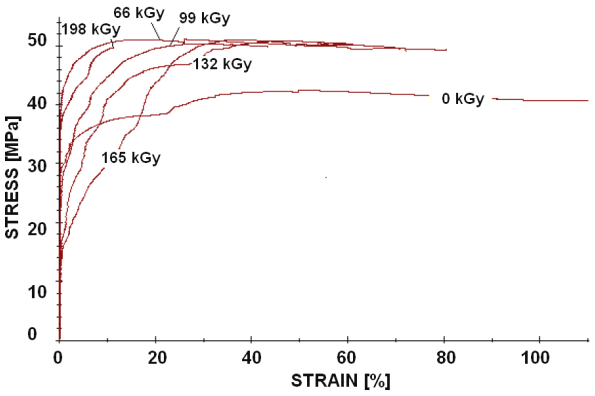

Fig. 8. **Tensile test** (PA6.6 at 80 °C)

Discussion

Generally said the irradiation of polyamides catalyzes the tensile strength and E modulus. Irradiation of PA6 (unfiled) bring improvement both the tensile strength and E modulus of about 22 % by the dose of 66 kGy, measured by room temperature (Fig. 9). Higher doses of irradiation are conductive to soft growth of value of ultimate tensile strength but the difference in these values with doses from 66 to 198 kGy is very low (max. 3 %). The value of E modulus drop with increasing doses of irradiation and the fall of E modulus reaches up to 11 %. By irradiation with the dose of 198 kGy is this property of about 10 % higher than in case of not irradiated polymer (Fig. 10). In case of not filled PA6.6 the irradiation gives only small improvement of tensile strength. Maximum value is reached by the dose of 132 kGy and after that it sinks.

The same tendency is remarkable also by E modulus. The increases of ultimate tensile strength of PA 6 filled by 30 % of glass fibres reaches cca 8 % and do not change with the doses of irradiation. The improvement of E modulus after irradiation with the dose of 66 kGy changes the reinforced PA6. The of E modulus of reinforced PA6 after irradiation with the dose of 66 kGy reaches to 23 % and there is a dorp of

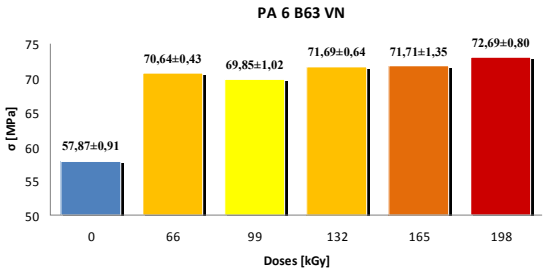

Fig. 9. **Tensile test** (PA6 at 23 °C)

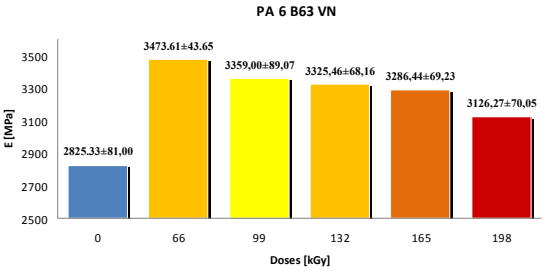

Fig. 10. **E modulus** (PA6 at 23 °C)

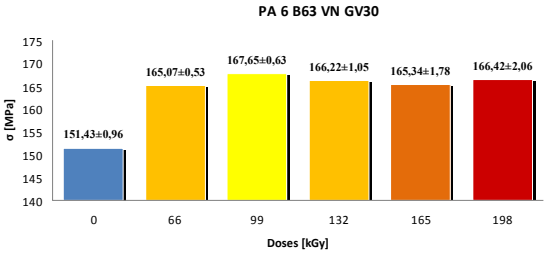

Fig. 11. **Tensile test** (PA6.6, 30 GF at 23 °C)

E up to 10 % bellow the value of not irradiated polymer. The ultimate tensile strength of reinforced PA6.6 will be improved by irradiation of about 10 % and it is going up with the higher dose of radiation. The growth of E modulus is marked already by the doses of 66 kGy and it is going up with the higher dose of irradiation.

By the temperature of 80 °C the ultimate tensile strength grows of about 7 % by PA6 and 15 % by PA6.6. Further increasing of dose of irradiation brings no changes. E modulus rises of 21 % (PA6) respectively 44 % (PA6.6). With growing dose of irradiation the E modulus does not change. The growth of ultimate tensile strength of PA6 and PA6.6 filled by 30 % of glass fibres reaches 7 % (PA 6) resp. 13 % (PA6.6) and is going up with the dose of irradiation. The same tendency is remarkable in case of E modulus.

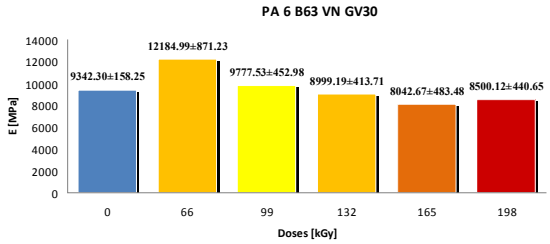

Fig. 12. **E moduilud** (PA6.6, 30 GF at 23 °C)

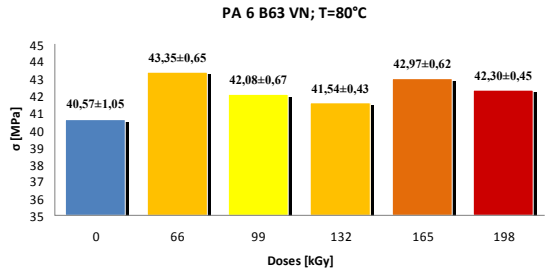

Fig. 13. **Tensile test** (PA6 at 80 °C)

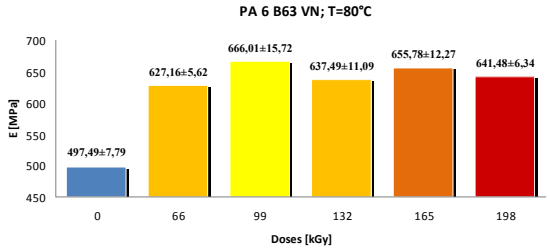

Fig. 14. **E modulus** (PA6 at 80 °C)

Conclusion

Irradiation improves mechanical properties of filled an unfilled PA6 and PA6.6. Substantial improvement was found already by the dose of irradiation 66 kGy. Higher doses have only limited effect on the follow up properties.

This article is financially supported by the Czech Ministry of Education, Youth and Sports in the R&D project under the title 'Modelling and Control of Processing Procedures of Natural and Synthetic Polymers', No. MSM 7088352102.

REFERENCES

1. Zyball A.: *Strahlungsenergie zur Modification von Kunststoffen – Industrielle Anwendungen der Bestrahlungstechnik*. In: Strahlenvernetzte Kunstoffe, Springer Verlag, Dusseldorf 2006.
2. Drobný J. G.: *Radiation Technology for Polymers*. CRC Press, Boca Raton 2003.

KL-11
THE RELATION BETWEEN MECHANICAL AND THERMAL PROPERTIES OF POLYPROPYLENE FIBRES

ANTON MARCINČIN*,MARCELA HRICOVÁ, KONŠTANTÍN MARCINČIN, and ALENA HOFERÍKOVÁ

Slovak University of Technology in Bratislava, FCHFT, IPM, Department of Fibres and Textile Chemistry, Radlinského 9, 812 37 Bratislava, SK
anton.marcincin@stuba.sk

A relation between mechanical properties and structure of polymers is permanently actual mainly from the point of view of development of tailored polymeric materials[1,2], including textile and technical fibres[3]. The effect of structure on mechanical properties is very actual for characterization of the classical and new developed fibres based on polypropylene produced from Ziegler-Natta (zniPP) and metallocene (miPP) catalyzed processes. The melt spinning of miPP and standard zniPP to compare processing of both kinds of PP and selected properties of fibres was studied by E. B. Bond, J. E. Spruiell and others[4–8]. The effect of the spinning speed on the density of fibres, crystallinity, crystalline and non-crystalline orientation functions, was investigated. The mechanical properties of fibres were explained on the basis of the nature and orientation of noncrystalline portions. The impact of orientation of PP composite fibres on their thermal and mechanical properties was studied also in our previous research[9].

In this paper, the spinning and selected mechanical and thermal properties of PP fibres were studied. The two kinds of the equivalents of commercial miPP and conventional-based zniPP were used in experimental work. Both zniPP and miPP resins were spun at the same spinning conditions within the 190–290 °C. The thermal and mechanical properties of zniPP and miPP fibres are presented and correlated in the paper as well

Experimental

Materials and procedure used

a) Ziegle-Natta isotactic polypropylene (zniPP) PP Moplen 561R (PP561R), MFR 25 g/10 min and PP Moplen HP561N (PP561N), MFR 11 g/10 min,

b) Metallocene isotactic polypropylene (miPP) PP Moplen 562R (PP562R), MFR 25 g/10 min, PP Moplen HP562N

(PP562N), MFR 11 g/10 min and PP Moplen 562S (PP562S) MFR 30 g/10 min.

All PP resins are produced and delivered by Lyondel-Basell Polyolefins

Melt spinning of PP fibres

The laboratory single-screw extruder D = 16 mm, L/D = 30 and spinneret with 13 orifices, d = 0.5 mm. was used for melt spinning of fibre grade PP. The spinning temperature was within 190–290 °C. Metering of the melt was 15 g min^{-1}, spinning speed 210 m min^{-1}. Fibres were drawn using laboratory drawing machine at 120 °C for the scale of draw ratio up to maximum draw ratio.

Methods used

Rheological measurements: Rheological properties of PP and PP composites were measured using capillary extrusiometer Göttfert N 6967 with extruder ϕ = 20 mm at 190–290 °C. The diameter of capillary was 2 mm and length was 30 mm. The Newton and Oswald de Waele laws were used for calculation of basic rheological parameters: apparent viscosity $\eta = \tau/\gamma$ and power law index n ($\tau = k.\gamma^{\cdot n}$), where τ-shear stress, γ – shear rate, η – apparent viscosity, n – power law index, k – coefficient.

Mechanical properties of the blend fibres: The Instron (Type 3343) was used for the measurements of the mechanical properties of fibres (according to ISO 2062:1993).

DSC measurements: The measurements were performed using Perkin Elmer DSC 7 in the temperature range 30–200 °C. The standard heating rate was 10 °C min^{-1}. The measurements were carried out using classic method (CM) and constant length method (CLM) in which the fibres with constant length during measurement were assured. The melting peak temperature T_p and melting enthalpy ΔH_m were evaluated.

Results and discussion

Rheological properties of PP resins

The melt viscosity and deviation from the Newtonian behaviour, expressed by power law exponent n are very similar for zniPP and miPP resins (Fig. 1 and Table I).

In general, the results of rheological measurements reveal that melt viscosity of miPP is moderately higher in average in comparison with zniPP equivalent. The difference is higher for couple with lower MFR. of PP. In spite of higher viscosity, mentioned miPP exhibited lower deviation from the Newtonian behaviour. The lowest deviation from the Newtonian flow is characteristic mainly for miPP562S from the tested polymers.

Table I
The power law exponent n and viscosity η for the selected shear rate for PP at various temperatures

PP/T [°C]		n	η [Pa s] γ =100 [s^{-1}]
PP 561R	230	0.44	327
	250	0.48	261
	280	0.50	195
PP 561N	230	0.39	476
	250	0.43	400
	280	0.44	314
PP 562R	190	0.39	550
	230	0.46	357
	250	0.49	289
	280	0.61	177
PP 562N	230	0.42	511
	250	0.45	426
	280	0.55	295
PP 562S	190	0.40	493
	230	0.52	284
	250	0.57	217
	280	0.65	146

Mechanical properties of PP fibres

The basic mechanical properties of the examined zniPP and miPP fibres spun at the various temperatures and cold

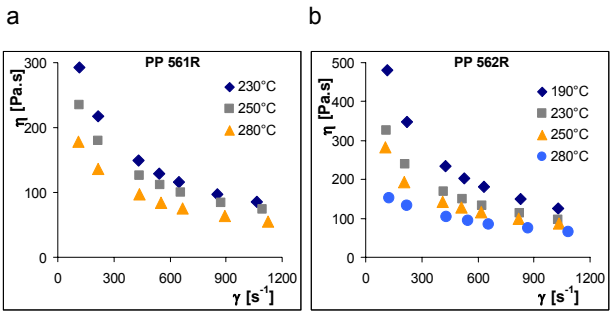

Fig. 1. **Dependences of dynamic viscosity on shear rate for zniPP561R (a) and miPP562R (b) at various temperatures**

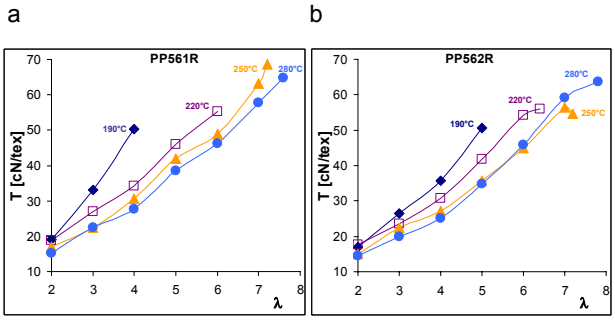

Fig. 2. **Dependence of the tenacity T on draw ratio λ for PP fibres spun at various spinning temperature. a. PP561R, b. PP562R, c. PP562S**

Table II
Tenacity T and Young's modulus YM for zniPP and miPP fibres spun at the temperatures 220 °C and 280 °C for constant elongation of fibres E = 20 % and E = 35 %

Sample		220 °C		280 °C	
		T [cN/tex]	YM [N/tex]	T [cN/tex]	YM [N/tex]
E 20 %	PP561R	54.0	6.88	58.4	7.98
	PP562R	54.0*	7.50*	54.1	7.56
	PP561N	42.0*	4.90*	53.2*	7.55*
	PP562N	56.0*	6.50*	59.3	7.46
	PP562S	57.6	8.10	50.5	7.87
E 35 %	PP561R	34.5	4.02	43.1	6.16
	PP562R	46.5	5.82	38.0	5.07
	PP561N	41.2	4.39	45.3	5.76
	PP562N	41.9	4.88	44.0	5.48
	PP562S	43.4	5.82	34.4	4.86

* extrapolated values

drawn are presented on the Fig. 2. The dependences on the Fig. 2 give information regarding the effect of drawing on tenacity of conventional and metallocene PP fibres spun at various spinning temperatures within 190–290 °C. The negative effect of the low spinning temperature (190–220 °C) on tenacity of fibres was found for zniPP561N and zniPP561R. The less sensitive resins to low spinning temperature were miPP562R and miPP562N. The spinning temperature 220 °C without any negative effect on tenacity of fibres was found for miPP562S. The high tenacity of fibres based on all investigated resins was obtained at high spinning temperature (280–290 °C).

To compare the mechanical properties of zniPP and miPP spun within the spinning temperatures of 190–290 °C and drawn at the same conditions, the tenacity and Young's modulus of the fibres were calculated and extrapolated for constant elongation E = 20 % and for E = 35 % (Table II).

The results reveal that the highest tenacity and Young's modulus of fibres for elongation of 20 %, were obtained for zniPP561R and miPP562N, both spun at 250 °C. The fibres are suitable for technical (industrial) textiles. The highest tenacity and Young's modulus of fibres for elongation of 35 %, were found for zniPP561N, spun at 250 °C and 280 °C and for miPP562N, spun at 280 °C. The fibres are suitable for common textiles when higher tenacity and elastic modulus are required.

Thermal properties of PP fibres

The DSC measurements were carried out using classic method (CM) and constant length method (CLM) at which the constant length fibres during measurement were assured. The results of thermal measurements of the zniPP561N as well as for miPP562N and miPP562S are given in the Tables III and IV. The DSC CLM method provides thermograms with different shape for fibres of different nature, MFR and also for fibres spun at various temperatures. Besides, the peak temperature increases with draw ratio (orientation) of fibres what is important result of DSC CLM method.

Table III
The peak melting point T_p and melting enthalpy ΔH_m for PP fibres spun at 220 °C and 280 °C, for various draw ratio λ, obtained using DSC CM method

PP	220 °C			280 °C		
	draw ratio λ	T_p [°C]	ΔHm [J g^{-1}]	draw ratio λ	T_p [°C]	ΔH [J g^{-1}]
PP 561N	1	162.6	80.6	1	161.5	77.2
	4.3	162.8	92.4	6	163.3	90.5
PP 562N	1	144.3	62.5	1	143.8	62.9
	5	144.5	81.1	6.8	147.0	76.9
PP 562S	1	144.5	59.8	1	143.8	63.2
	7.2	146.8	81.9	7.2	146.0	77.4

Both, melting temperature and melting enthalpy increase with higher draw ratio (orientation) of fibres. According to expectation, the metallocene resins provide lower melting temperature, especially miPP562S and lower melting enthalpy in comparison with zniPP561N (Table IV). The lower melting enthalpy of indicates the lower crystallinity of miPP compared to zniPP equivalent.

The gradually increase of the melting temperatures of both conventional and metallocene PP in dependence on draw

Table IV
The peak melting temperature T_p and melting enthalpy ΔH_m for PP fibres spun at 220 °C and 280 °, for various draw ratio λ, obtained using DSC CLM method

PP	220 °C			280 °C		
	draw ratio λ	T_p [°C]	ΔHm [J g^{-1}]	draw ratio λ	T_p [°C]	ΔH [J g^{-1}]
PP 561N	3	169.6	87.7	3	167.3	80.8
	4	182.1	85.8	5	179.2	85.3
	4.1	188.0	90.6	5.5	183.8	93.0
	4.3	184.0	86.3	6	185.2	91.7
PP 562N	3	157.0	68.8	3	151.3	68.2
	4	168.2	76.6	5	168.5	77.8
	4.7	173.0	77.2	6	173.5	77.4
	5	180.3	72.5	6.8	176.0	84.2
PP 562S	3	149.0	68.3	3	147.0	61.0
	5	156.5	77.7	5	154.2	76.7
	6	160.1	80.4	6	159.8	78.9
	6.5	161.8	83.6	7	165.6	86.9
	7.2	166.6	85.1	6.8	165.3	83.1
	7.5	169.2	85.4	7.2	165.5	86.2

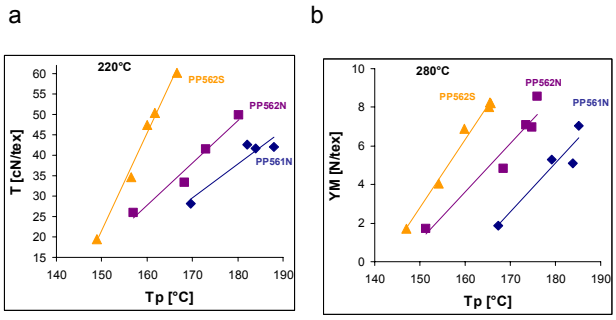

Fig. 3. **Dependence of tenacity T (a) and Young's modulus YM (b) on melting (peak) temperature T_p of PP fibres.** The multifilaments were drawn at draw ratio within2–7

ratio (orientation of fibres) results probably from increase of the total crystallinity of fibres and the higher height of crystals which grows in the fibres under tension at the relative high temperature in DSC pan. From this point of view, the increase of melting temperature of oriented fibres can result from the molecular orientation of fibres and can be correlated with their tensile properties such as tenacity or Young's modulus.

Correlation of the mechanical and thermal properties of PP fibres

Correlations of the tenacity and Young's modulus of fibres spun at 220 °C and 280 °C on their melting (peak) temperature are on the Fig. 3. The same correlations for tenacity and Young's modulus on melting temperature for fibres spun within the 190–290 °C were found. The correlations reveal that there is unambiguous straight-line dependence between tenacity and melting (peak) temperature as well as between Young's modulus and melting (peak) temperature of fibres, both obtained by DSC CLM method. These dependences were found for fibres based on both zniPP and miPP resins. The similar dependences but not such clear were obtained for tensile properties and melting enthalpy of fibres.

In the any case the melting (peak) temperatures of oriented PP fibres, obtained by DSC CLM method provide important information regarding the average orientation of fibres. Further analysis can give an answer on correlation of this melting temperature values with molecular orientation of fibres.

Conclusions

The following points of conclusion can be drawn:

The melt viscosity of miPP is moderately higher in average in comparison with zniPP equivalents. In spite of higher viscosity, miPP exhibited lower deviation from the Newtonian behaviour.

The DSC CLM method provides thermograms with different shape for fibres of different nature, MFR and also for fibres spun at various temperatures. Besides, the peak temperature increases with draw ratio (orientation) of fibres.

The unambiguous straight-line dependences between tenacity and melting (peak) temperature as well as between Young's modulus and melting (peak) temperature of miPP and zniPP fibres, obtained by DSC CLM method, were found.

Based on experimental results, from the point of view of the basic mechanical properties of miPP fibres and their zniPP equivalents there is not possible to prefer unambiguously conventional or metallocene PP. The advantages of higher deformability of miPP fibres could appear at higher spinning speed.

Experimental works were supported by Slovak Grant Agencies: APVV 0226-06 and VEGA 1/4456/07.

REFERENCES

1. Meijer H. E. H., Govaert L. E.: Prog. Polym. Sci. *30*, 915 (2005).
2. Boger A., Heise B., Troll C., Marti O., Rieger B.: Eur. Polym. J. *43*, 634 (2007).
3. Gregor-Svetec D., Sluga F.: Jour. Appl. Polym. Sci. 98, 1 (2005).
4. Misra S., Lu F. M., Spruiell J. E., Richeson G. C.: J. Appl. Polym. Sci. *56*, 761 (1995).
5. Andreasen E., Myhre O. J., Hinrichsen E. L., Gronstad K.: J. Appl. Polym. Sci. *57*, 1075 (1995).
6. Sundell T., Fagerholm H., Crozier H.: Polymer *37*, 3227 (1996).
7. Spruiell J. E., Lu F. M., Ding Z., Richeson G. C.: J. Appl. Polym. Sci. *62*, 1965 (1996).
8. Bond E. B., Spruiell J. E.: J. Appl. Polym. Sci. *82*, 3237 (2001).
9. Marcinčin A., Hricová M., Marcinčin K., Hoferíková A., Legéň J.: Fibres & Textiles in EE *15*, 64 (2007).

KL-12
VALORISATION OF WAST TYRE MATERIAL

WANDA PARASIEWICZ, MAREK TULIK, and JAN MĘŻYŃSKI

IMPIB Elastomers& Rubber Technology Div.
Ul. Harcerska 30; 05-820 Piastow
w.parasiewicz@impib.pl

Over a billion tires are sold worldwide each year and subsequently just as many fall into the category of end-of-life tires. European Landfill of the Waste Directive from 1999 introduced a ban of the landfills of used tires (since 2003) and shredded tires (2006). It was the obligation of member countries to create the proper legislation for implementation to the Directive. The key point was the acceptance of the 'Producer Responsibility' strategy. It created the challenge for producers and users of tires to develop efficient ways for end-of-life tires recovery. Material recycling is the one of more preferable methods of recovery of the valuable material. The results of this activity are shown by the data of different ways of recovery.

In 2006, there were approximately 3.2 million tons of used tires in the enlarged Europe. For the EU-15 alone, the annual volume increased from 2.1 million tons in 1994 to 2.7

million tons in 2006. However, in the same time frame, the EU's total recovery rate rose from 38 % to 87 **%**. This positive achievement clearly demonstrates that end-of-life tires are being sustainably diverted from landfills. The major markets benefiting from this are the material recycling (34 %) and energy recovery (32 %) sectors, which show that the market for end-of-life tire-derived products has become sustainable and economically viable. Encouraging results in 2007 are close to 90 % of ELTs in Europe are recovered[1].

The first step of tire recycling is size reduction, usually by grinding. Rubber crumb of different sizes received in such kind of processes have limited the area of application, because its admixing to new rubber compounds result in a significant drop of mechanical properties[2]. The next stage of process is the valorisation, which allows obtaining new rubber material with satisfactory properties.

Many ways the valorisation of rubber crumbs exist now but only a few are commercialized. The most popular since the late 90's have surface modification of rubber granules, like Sucrum introduced by Vredestin[3],or De – Link[4] or modification with functionalized polymers[5].

Another way of upgrading the material is by devulcanization commercialized as reclaiming. This is the process of cleaving the monosulfidic, disulfidic, and polysulfidic crosslinks of vulcanized rubber, without cleavage of polymer chains. The product can be re-vulcanized/re-cured to form new rubber articles.

In practice, a pure devulcanization process is very difficult to achieve since many problems are caused by accompanying chemical transitions such as depolymerization, thermal destruction and oxidation, which worsen the properties of the recovered elastomers.

The main problem hampering the appropriate running of the devulcanization process is the very low thermal conductivity of rubber resulted, an extremely difficult selective regulation of the quantity of energy carried to the cross-linking bonds.

Theoretically, the energy input should be sufficient for the dissociation of the S-S bonds (271.7 kJ mol^{-1}) and C-S bonds (301 kJ mol^{-1}), but at the same time too low for dissociation of the C-C bonds (347 kJ mol^{-1}) of the polymer chains. In practice, it's virtually impossible to achieve such an exact level of energy evenly distributed within the material. It's necessary to experimentally find the optimal devulcanization process and conditions, under which devulcanized products with good properties can be obtained.

One of the oldest and simplest devulcanization methods in the rubber reclaiming industry is called the ''pan process''[6].

In this process, finely ground rubber powder mixed with oils and devulcanizing agents are heated with steam in a pressure vessel at a temperature of ca. 200 °C for more than 5 h. Moreover, this process must usually be followed by several procedures (refining and straining) for obtaining the final devulcanized rubber. The devulcanized rubber obtained by this method is much more inferior in physical properties to a virgin (new) rubber, due to the occurrence of breakages of both the crosslinking points and main chain (C–C) bonds unselectively.

Hence, new material recycling technologies such as microwave devulcanization[7,8] and ultrasonic devulcanization[9] methods have been developed with the aim of shorter reaction times and optimizing the parameters in the reactor such as shear stress, temperature, pressure[6]. However, the devulcanized rubber obtained by these methods still was not good enough in quality to be widely applicable in practical use.

The new approach is continuous devulcanization performed on a modular twin screw extruder.

In the first zone of this process, roughly crashed rubber material is made into fine particles by high shearing and heating to the devulcanization-reaction temperature quickly. The principle of this method is the difference of the elastic constant for -C-C- and the crosslinking sulfur bonds, estimated to be 1/30 of C-C bonds[10]. This phenomena is responsible for the selective cleavage in a high shear condition in the extruder. The residence time is assured to be enough to complete the devulcanization reaction under the shear flow in the next zone. In this reaction zone, the fine particles of the vulcanized rubber become highly elongated by filling and shearing with the kneading disk elements, and thus eventually result in plasticizes of devulcanized rubber. After the process, the devulcanized rubber is extruded from the head of the reactor and cooled in the water bath.

The result of the process depends on the feeding rate, design of screws and temperature distribution along the extruder. The proper optimization of these parameters is the key for the good properties of received material.

The efficiency of devulcanization could be improved by admixing the peptizer and or reclaiming agent which accelerate the process. The most common reclaiming agents are disulfides, e.g. aryl disulfides such as diphenyldisulfide, thiophenols and their zinc salts and mercaptanes. These compounds are radical scavengers; they react with the radicals generated by chain or crosslink scission and prevent recombination of the molecules.

In the frame of this project the optimization of processing parameters in specially designed twin screw extruder was performed.

The extruder with co-rotating screws 40 mm diameter L/D 39 with 7 heating zones with max. screw speed 500 rpm was used to devulcanize buffing rubber material with an output 80 kg hr^{-1}.

The devulcanized material obtained shows Mooney plasticity 50+/−5 ML(1+4)×100, and tensile strength in the range of 10–12 MPa.

The 20 phr of this material was admixed to tread tire compound used for retreading truck tires. The experimental tires are actually tested.

The overview of the valorization methods of tire material and experimental trials made with the use of a prototype of the twin screw extruder made in IMPIB confirm that it is a promising way of the valorization of tire rubber granulate and to open the possibility of up-scaling the technology.

The overview of the valorization methods of tire material and experimental trials made with the use of a prototype of the twin screw extruder made in IMPIB confirm that it is a promising way of the valorization of tire rubber granulate and to open the possibility of up-scaling the technology

The work is financially supported by Polish Ministry of Science and Higher Educations the Research Project nr R08 029 03 carry out in the years2007-2010.

REFERENCES
1. Cineralp F.: ETRMA Report, "End of life tyres-avaluable 117 resorce with growing potential" 2007 Edition.
2. Pysklo L., Parasiewicz W., Stępkowski R.: Elastomery *4*, 15 2 (2000).
3. Dirkes W.:Elastomery *3*, 18 (1999).
4. Parasiewicz W., Pysklo L., Wilkonski P.: A New simple method of mechanochemical devulcanization of rubber wastes. *Conference proceedings, Polymers-Environment-Recycling, Szczecin-September 1995*.
5. Parasiewicz W., Stępkowski R., Ostaszewska U., Tulik M.: Elastomery *10*, 14 (2006).
6. Myhre M., Mackillop D. A: Rubber Chem. Technol. *75*, 429 (2002).
7. Novotony D. S.: Microwave devulcanization of rubber, US Patent 4,104,205, 1978.
8. Parasiewicz W., Adamski W., Kleps T., Stępkowski R.: Elastomery *2*, 23 (1998).
9. Isayev A. I., Tukachinsky A.: Rubber Chem. Technol. *68*, 267 (1995).
10. Fukumori K., Matsushita M.: Tech. J. R&D Rev. of Toyota *38*, 39 (2003).

KL-13
SHAPE-MEMORY BEHAVIOR OF PEROXIDIC CROSS-LINKED POLYETHYLENE BASED BLENDS

HANS-JOACHIM RADUSCH and IGOR KOLESOV

Martin Luther University Halle-Wittenberg, Chair of Polymer Technolog,y, D-06099 Halle, Germany
hans-joachim.radusch@iw.uni-halle.de

Abstract

Shape-memory (SM) polymers are characterized by a specific temperature and load controlled deformation behavior. They can be advantageously used e.g. in cable and packaging industry, medicine or automotive. Precondition for proper appearance of the thermal induced SM effect (SME) is the existence of stable physical or covalent molecular network and glass or phase transition, respectively, at relevant temperatures.

The thermally induced SME of binary and ternary peroxidic cross-linked blends from several ethylene-1-octene copolymers (EOC) and/or nearly linear polyethylene (HDPE) was investigated. The SME behavior of the prepared materials was evaluated by the characteristic parameters strain recovery (R_t), strain fixity ratio (R_f) and SM recovery rate ($d\varepsilon(T)/dt$) in dependence on programming conditions.

It was found that triple and quadruple SME could be observed after two- and accordingly three-step programming of binary and ternary HDPE/EOC blends, respectively, at suitable temperatures and durations. The effects correlate with multiple melting/crystallization behavior of HDPE/EOC blends.

Introduction

For covalent (e.g. peroxidic) cross-linked semi-crystalline polymers the SM behavior with high performance can be achieved, firstly, if this polymeric material possesses a resistant network with suitable high cross-link density and as a consequence of this produces sufficiently large elastic and viscoelastic forces under load at programming temperature $T_{pr} > T_{trans}$ and preferably lowest residual strain as well as shows high enough break strain, and secondly if its crystalline phase formed after cooling of the programmed (loaded) sample is able to fix efficiently the strain and elastic and viscoelastic forces stored in the network. The ability of SM polymers to strain fixation and to form regeneration is characterized by strain fixity (R_f) and strain recovery ratios (R_r), respectively, which are defined according to Lendlein and Kelch[1] as:

$$R_f = \frac{\varepsilon_v}{\varepsilon_{pr}}, \qquad R_r = \frac{\varepsilon_{pr} - \varepsilon_{rec,m}}{\varepsilon_{pr}} \qquad (1)$$

where ε_{pr} is the strain caused by programming, ε_v is the strain that remains after programming, cooling, unloading and recovery at lowest temperature of experiment of specimen and $\varepsilon_{rec,m}$ is the residual strain that resides after thermal-induced recovery (shrinkage) at maximum temperature of experiment. The objective of the presented work was the production of peroxidic cross-linked binary and ternary blends on the basis of HDPE and two EOCs with medium and high degree of branching as well as the investigation on their multiple SM behavior and their characterization by the relevant thermal and mechanical properties.

Experimental

Polyethylenes used were HDPE (KS 10100 UE) and EOCs (AFFINITY TM PL 1280G and ENGAGE 8200) (Dow Chemical) with 30 and 60 hexyl branches per 1000 C (EOC30 and EOC60). As cross-linking agent 2,5-dimethyl-2,5-di-(*tert*.butylperoxy)-hexane (DHBP) (Degussa) was used. The mechanical mixes of DHBP impregnated polymer pellets in desired ratio (Table I) were blended by a single-screw mixing extruder (Brabender) at 130 °C. As reference object a HDPE was prepared in the same manner.

Designation	HDPE [%]	EOC30 [%]	EOC60 [%]
100HDPE	100	–	–
50HDPE/50EOC30	50	50	–
33HDPE/33EOC30/34EOC60	33	33	34
10HDPE/45EOC30/45EOC60	10	45	45
10HDPE/25EOC30/65EOC60	10	25	65
50EOC30/50EOC60	–	50	50
30EOC30/70EOC60	–	30	70

The extrudates were processed to 1 and 2 mm films at 140 °C and cross-linked at 190 °C. The tensile tests in the

temperature range of SM tests programming (120 and 140 °C) has been carried out using a testing machine Zwick 1425 (Zwick) with heating chamber and a load cell 10 N at a crosshead speed of 50 mm min^{-1}. Test bars were used with the cross-section area 2.0×2.0 mm^2. Thermal analysis was performed by DSC 820 (Mettler-Toledo) at a heating and cooling rate of 20 and 10 K min^{-1}, respectively. For the characterization of the shape memory behavior the samples came at first under a specific temperature-deformation program. The samples were programmed at a stretching strain of $\varepsilon_{pi} \leq 100$ % during a dwell period of 120 s at the programming temperature T_{p1}, and cooled down to T_{p2} with an average cooling rate of approx. 11 K min^{-1} in a constant deformed state. Before loading of the next programming strain ε_{pi} the sample temperature was kept constant for 10 min. After last programming step the specimen was cooled down to 10 °C at the programming strain of 100 %, thermal equilibrated for 10 min and unloaded. The recovery strain was measured first after a delay of 10 min at 25 °C (ε_v) and than in the course of a heating run with a rate of 2 K min^{-1} and 'zero' stress of 70 Pa ($\varepsilon_{rec}(T)$). Complete SM investigations were carried out in tensile mode using a mechanical spectrometer measuring head Mark III (Rheometric Scientific).

Results and Discussion

From the results of stress-strain measurements and the Mooney-Rivlin equation as well as rubber elasticity theory the degree of cross-linking and average molar mass of the polymer chains between two neighboring network nodes were calculated. All investigated materials with the exception of HDPE evidence a small increase of ν_c and consequently decrease of $\bar{M}_c$ values at higher temperature. The ν_c values change not significantly and varies approx. from 110 to 140 mol m^{-3} at 120 °C and from 80 mol m^{-3} for HDPE as well as 150 to 170 mol m^{-3} for blends at 140 °C, respectively.

The melting and crystallization behavior of HDPE and HDPE/EOC30/EOC60 blends is displayed in Fig. 1.

Only second heating runs at a cooling rate of 10 K/min were used for the analysis of melting behavior. All blends demonstrate multiple behavior for both melting and crystallization (Fig. 1). In 10HDPE/45EOC30/ 45EOC60 and 10HDPE/25EOC30/ 65EOC60 blends the HDPE phase crystallizes at 97.7 °C and 100.3 °C, respectively. Moreover, the local cross-linking degree in the HDPE phase is by all means lower than the average cross-linking degree of the blend as a whole. Obviously, the described behavior of blends suggests the crystallization of the main part of HDPE phase together with the EOC30 at significantly lower temperature. Interestingly, the melting of the HDPE phase in 10HDPE/45EOC30/ 45EOC60 and 10HDPE/25EOC30/65EOC60 blends occurs also stepwise in two stages (see Fig. 1).

T_m and T_c of the HDPE phase decrease markedly with decreasing HDPE content in the blend compared to the values for 'bulk' cross-linked HDPE. At the same time, T_m and T_c values of the EOC30 phase can increase in blends containing HDPE or decrease in binary blends with high branched EOC60. In blends both nucleating effect of HDPE crystallites and molecular interaction are available only in uncross-linked crystalline domains which consist of ethylene sequences of blend components with suitable length. Due to the existence of several populations of PE crystallites of different stability and correspondingly with different melting temperatures in the described blends the thermograms in Fig. 1 show nearly continuous melting by that the SM behavior of these blends is affected.

The SM behavior and especially the temperature dependence of SM recovery strain and recovery strain rate of HDPE and HDPE/EOC30/EOC60 blends and their components having a network with similar cross-linking degree are demonstrated in Fig. 2. Here, the findings of the first cycle of SM tests are demonstrated. The sharp step of SM recovery strain and high, well separated peaks of SM recovery rate can be generated only by melting of a phase with sufficient crystallinity and relatively perfect crystallites.

For the explicit appearance of SME the availability of stored sufficiently high visco-elastic forces is important no less than suitable melting behavior. These visco-elastic forces caused by network deformation during programming must be efficiently stored by the crystalline structure formed in the actual temperature range. As expected, the blends having a higher average crystallinity exhibit the high strain fixity ratio R_f and SM recovery rate $-d\varepsilon_{rec}/dt$. Correspondingly, these parameters increase with increasing HDPE (and partly EOC30) content in the blends. The single-step programming of all blend types results in appearance of only one step and accordingly one peak in the temperature dependences of the SM recovery strain and SM recovery rate, respectively, i.e. in

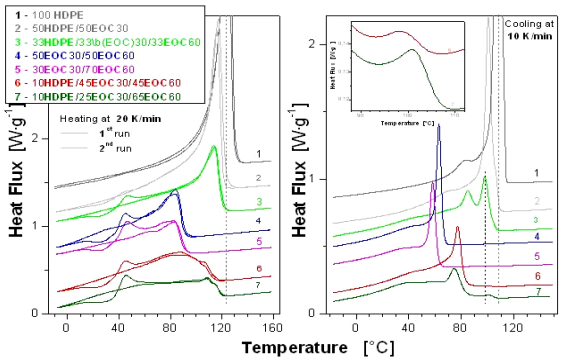

Fig. 1. **Melting (left) and crystallization (rigth) of cross-linked HDPE and HDPE/EOC blends**

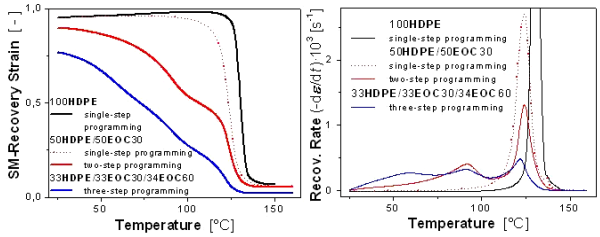

Fig. 2. **Effect of composition and programming conditions on the temperature dependence of SM recovery strain (left) and recovery strain rate (rigth) of HDPE and binary and ternary HDPE/EOC blends**

dual-shape behavior. The blends after two- or three-step programming show significantly lower R_f and $-d\varepsilon_{rec}/dt$ values and particularly $[-d\varepsilon_{rec}/dt]_{max}$ values at melting temperatures of the components (see Fig. 2). The decrease of R_f values as a result of multi-step programming is caused by the partial deformation of already crystallized (fixed) phase/phases by each next programming step at lower temperature. All investigated blends and their components independent from programming mode demonstrate relatively high values of strain recovery ratio (R_r) that amounts approx. 93 to 98 %. Presumably, the multi-shape behavior by single-step programming may be carried out only in a heterogeneous polymer material having a phase morphology with preferred orientation of planar phase layers perpendicularly to the load direction (Kolesov and Radusch[3]).

REFERENCES
1. Lendlein A., Kelch S.: Angew. Chem., Int. Ed. Engl. *41*, 2034 (2002).
2. Li F., Chen Y., Zhu W., Zhang X., Xu M.: Polymer *39*, 6929 (1998).
3. Kolesov I. S., Radusch H.-J.: eXPRESS Polymer Letters *2*, 461(2008).

KL-14
APPLICATION OF ALIPHATIC POLYAMIDES AS ENGINEERING PLASTICS

JAN RODA

Institute of Chemical Technology, Department of Polymers, Technická 5, CZ16628 Praha 6, Czech Republic
jan.roda@vscht.cz

KL-15
NEW ELASTOMER MATERIALS MADE OF ELASTOMER BLENDS MODIFIED BY SPECIFIC INTRA- OR INTERELASTOMER REACTIONS

WLADYSLAW M. RZYMSKI*, KINGA BOCIONG, and MAGDALENA KMIOTEK

Technical University of Lodz,Institute of Polymer & Dye Technology, 90-924 Lodz, Stefanowskiego 12/16, Poland
rzymski@p.lodz.pl

The lack of thermodynamic miscibility of the rubbers (A, B) causes that the crosslinking reactions in rubber blends occur mostly independently in the microphases of each component (in intermolecular, intraelastomer reactions in rubber A and B respect.) and – to some extent – in interelastomer crosslinking reactions, resulting in interelastomer crosslinks *X* between rubber A and B, *e.g.* in A-*X*-B structures. It is caused by the curing agent solubility in A and B, its reactivity to A and B, and by the existence of interphase layer of different thickness and structure[1].

However, epoxy groups of epoxidized natural rubber (ENR) react with ~SO_2-Cl groups of CSM (chlorosulfonated polyethylene), with ~CO-OH groups of XNBR (carboxylated nitrile) or with allyl Cl groups in chloroprene rubber (CR). It leads to interelastomer crosslinks in ENR-CSM, ENR-XNBR ENR-CR and CSM-XNBR blends, even if no curing agent was used (self-vulcanizable elastomer blends SVEB)[2,3]. However, curing of such blends needs long heating time and results in products of limited curing degree and of poor mechanical properties.

From the other side, selective, dynamic curing of a rubber (in intraelastomer reactions), connected with its dispersion during mixing with a selected plastomer, results in valuable engineering materials, thermed thermoplastic vulcanizates[4–6].

In our studies we found new cured, elastomer materials prepared from elastomer blends modified by the specific intra- and/or interelastomer reactions, governed by other factors than in the SVEB case.

Elastomer blends modified by specific intraelastomer reactions

Such modification occurs due to the neutrali-zation of ~CO-OH groups in XNBR with metal compounds during rubber dynamic curing and dispersion in other elastomer, followed by static (conventional) curing of the blend obtained. In our studies[7] hydrogenated nitrile rubber (HNBR, bound acrylonitrile content: 42.5 %; hydrogenation degree: 99 %) was modified with XNBR (bound acrylonitrile: 27 %; bound acid: 7 %). XNBR was dispersed in HNBR and cured with MgO during blend mixing in micromixer. To dynamically prepared blends DCP (dicumyl peroxide) was added on two roll mill and the blends were than compression moulded in press and cured. The properties of dynamically and conventionally (all ingredients mixed on two roll mill only) prepared blends were than compared.

The properties of the prepared blends depend on the XNBR/HNBR-ratio, mixing time, amount of MgO used for selective XNBR curing and on the DCP amount used for static curing.. The dynamically prepared HNBR/XNBR blends (80/20 wt./wt.) are heterogenous systems with continuous phase formed by HNBR, in that microsized droplets and rod-like particles of cured XNBR are dispersed. In blends prepared conventionally each of elastomers forms its own continuous phases (two co-continuous phase morphology). The dynamically cured blends exibit higher crosslinking degree and higher tensile strenth (12–15 MPa) but lower swelling (~10 vol.%) in hexane than prepared conventionally (~15 vol.%).

The rective mixing of HNBR/XNBR blends connected with dynamical curing of dispersed, cheaper XNBR lead to compounds showed the properties of cured HNBR. Similar results were obtained for NBR/HNBR blends in that NBR was selectively, dynamically cured with sulfur-system during its mixing with HNBR.

Elastomer blends modified by specific interelastomer reactions

Such blends consist elastomers that can be cured due to the action of *in situ* generated initiators or due to its specific activity to the elastomers.

Blends containing styrene-butadiene rubber

The reactivity of α-methylene groups and >C=C< bonds in the styrene-butadiene rubber (SBR) is used for its curing with sulfur containing systems. From the other side, phenyl rings in SBR can be alkylated by halides or olefines in the Friedel-Crafts' reaction catalyzed with Lewis acids. We found[8–10] that the SBR/CSM blends undergo curing, when heated in the presence of ZnO, SnO or Fe_2O_3. The curing rate and degree, and the properties of cured blends can be modified by the CSM/SBR-ratio, the kind of CSM added (bound Cl: 24, 29 or 43 wt.%, CSM24, CSM29 and CSM43 respectively) and by the amount and kind of metal oxide incorporated, Table I.

Table I
Selected properties of SBR/CSM/ZnO blends (85/15/0.90 by wt.) cured at 423 K for 50 min

CSM	$2C_1$ [MPa]	Q_v^T [vol.%]	TS_b [MPa]
CSM24	< 0.05	3180	1.62
CSM29	0.304	470	4.12
CSM43	0.334	424	7.25

$2C_1$ – Mooney-Rivlin elasticity constant; Q_v^T – equilibrium swelling degree in toluene; TS_b – tensile strength

The curing is a result of the alkylation of SBR phenyl rings by CSM chains (thus – CSM bonding on the SBR) and by SBR chains containing vinyl side groups. The curing reaction is catalyzed by $ZnCl_2$ (Lewis acid) generated *in situ* from ZnO and CSM. The heating of CSM with ZnO leads to no curing.

The decrease of absorption intensity at 1164 and 1352 cm^{-1} (~SO_2-Cl groups), at 1639 cm^{-1} (vinyl side groups of SBR) and the changes in IR-spectra at 1700–1940 cm^{-1} (substitution in phenyl rings), the content of the fraction soluble in 2-butanone and the bound Cl content in cured and purified SBR/CSM blends confirm the proposed curing mechanism.

Recent investigations[11] indicate that chlorinated butyl rubber can replace CSM in such blends.

Blends containing CSM and XNBR

XNBR/CSM blends are self-vulcanizable, but the reached curing degree and the mechanical properties of cured blends are poor. We found that the heating of such blends at T < 440 K, if they contain up to 40 wt.% of selected CSM, metal compound and stearic acid, leads to cured products of high curing degree and high tensile strength[12]. The content of soluble fraction, bond Cl content in cured and than purified samples and the IR analysis indicate that the curing reactions include hydrolysis of ~SO_2-Cl groups to ~SO_2-OH and neutralization of ~CO-OH + ~SO_2-OH groups by metal oxide. Intra- [^{X}R~CO-O$^{(-)(+)}$Me$^{(+)(-)}$O-CO~R^{X}] and interelastomer [^{X}R-CO-O$^{(-)(+)}$Me$^{(+)(-)}$O-SO_2-R^{CSM}] ionic crosslinks are formed (Table II); ^{X}R = XNBR, ^{CSM}R = CSM.

The extent of such curing and the properties of cured blends depend on the CSM amount and kind, and the amount and kind of metal compound used.

Table II
Selected properties of CSM35/XNBR blends cured with 12 phr MgO and 2 phr stearic acid at 433 K for 30 min

CSM/XNBR	100/0	40/60	20/80	0/100
S_{e100}, MPa	–	3.2	4.4	5.5
TS_b, MPa	–	23.0	30.2	41.7
E_b, %	–	610	565	550
$2C_1$, MPa	–	0.37	0.34	0.35
Q_v^M, vol. %	∞	550	470	395
Cl^b, wt. %	–	7.4	7.6	0
S^M, wt. %	100	11	5	4

S_{e100} – stress at 100 % elongation; TS_b – tensile strength; E_b – elongation at break; $2C_1$ – Mooney-Rivlin elasticity constant; Q_v^M – volume swelling in 2-butanone, Cl^b – bound Cl content in samples extracted with 2-butanone; S^M – fraction soluble in 2-butanone

Summary

The proposed new curing method of the blends makes it possible to prepare new elastomer materials of interesting properties. The properties of such blends can be further modified with the reinforcing fillers or with the selected plastificators.

REFERENCES

1. Corish P. J., in: (Mark J. E., Erman B., Eirich F. R., ed.): *Science and Technology of Rubber*, Elastomer Blends, Chapter 12, p. 545, 2nd Edition. Academic Press, San Diego 1994.
2. Antony P., De S. K., van Duin M.: Rubber Chem. Technol. *74*, 376 (2001).
3. Rzymski W. M.: Polimery *39*, 422 (1994).
4. Coran A. Y., in: (Mark J. E., Erman B., Eirich F. R., ed.): *Science and Technology of Rubber*, Vulcanization, Chapter 7, p. 339, 2nd Edition. Academic Press, San Diego 1994.
5. Radusch H.-J., Rzymski W. M.: Elastomery *5*, 11 (2001); *5*, 3 (2001).
6. Rzymski W. M., Radusch H.-J.: Polimery *47*, 229 (2002).
7. Bociong K., Rzymski W. M.: Elastomery *12*, 21 (2008); Polimery *in press.*
8. Rzymski W. M., Wolska B.: Polimery *48*, 520 (2003); *49*, 524 (2004); Gummi Fasern Kunstst. *58*, 518 (2005).
9. Rzymski W. M., Wolska B., Wawrzecka A.: Ann. Pol. Chem. Soc. *2*, 146 (2003).
10. Rzymski W. M., Wolska B., Wawrzecka A.: Polish Patent 198303 (2007).
11. Rzymski W. M., Bociong K., Gietka K.: Polish Patent Declaration P-385040 (2008).

12. Kozioł M., Rzymski W. M.: Ann. Pol. Chem. Soc. *3*, 1015 (2004); Polimery *50*, 587 (2005); *52*, 511 (2007).

KL-16
POLYMER ADDITIVES AS ONE OF THE KEY FACTORS OF SUCCESS OF PLASTICS IN AUTOMOTIVE APPLICATIONS

LEONID SMOLIAK

Division PA, Clariant International Ltd, Rothausstrasse, 61, CH-4132, Muttenz, Switzerland leonid.smoliak@clariant.com

Plastics are widely used for automotive applications due to their low weight, mechanical characteristics, corrosion resistance and large variety of other properties compared to metals and glass. The major plastic parts of a modern car are made from such plastics as Polypropylene (bumpers), Polyamide (elements in under hood), and Polycarbonate (transparent roofing elements, head and rear light elements).

Polymer materials are affected by such factors as heat and UV light which initiate their oxidative degradation. Such consequences of polymer degradation as polymer chain breakage (loss of mechanical properties) and color formation are ones of the most important limitations of plastics utilization's in the demanding automotive applications.

However, there are ways to prevent and inhibit the reactions of photo- and thermal oxidative degradation of polymer materials and therefore to enhance their utilization options and service life. The most important way is the utilization of polymer additives, in particular, thermal and light stabilizers for polymers.

Main classes of polymer stabilizers are Phenolic Antioxidants, Processing Stabilizers, Light stabilizers (HALS) and UV-absorbers. Each class works through its own mechanism (chemical or physical polymer protection), very often one can observe a synergism between different stabilizers[2].

Role and need for stabilization varies depending on polymer resin type and end application requirements. For example, a Polypropylene grade (general purpose or specific PP) is always stabilized by phenolic AO and processing stabilizer whereas Polycarbonate macromolecules are more stable by themselves and require stabilization in very specific applications.

We will study some examples how polymer additives contribute the final performance of plastics for automotive industry.

Polypropylene stabilization

Polypropylene can be used for car exterior parts (like bumpers), interior and under hood elements. An under hood application requires as a must a long term heat stability (high exploitation temperatures in the engine compartment), while exterior and interior elements require both light stability and some heat stability.

The most efficient way of long term heat stabilization (LTHS) of PP is a combination of high efficient phenolic antioxidant and thio-synergist, with such a formulation you can increase LTHS of PP in times. Thio-synergists (peroxide decomposers) is a group of thermal stabilizers which gives strong synergetic effect to phenolic antioxidants under long term heat treatment of PP. Scheme 2 illustrates the effect of thio-compound on LTHS of Polypropylene.

Thus, due to combination of proper phenolic antioxidant and thi-synergist, Polypropylene materials can work under long term heat exposure.

Another very important application of PP in automotive is such parts of car exterior as bumper elements. Requirements in terms of light stability are normally include at least five years outdoor stabilization (means no dramatic changes in mechanical properties and color). This light stabilization level can be obtained with utilization of proper light stabilizer, like substances of Hindered Amine Light Stabilizer (HALS) class. Typical compound of HALS chemistry is product known as HALS-770 (bis(2,2,6,6-tetramethyl-4-piperidyl) sebaceate) which is quite efficient for PP thick article like

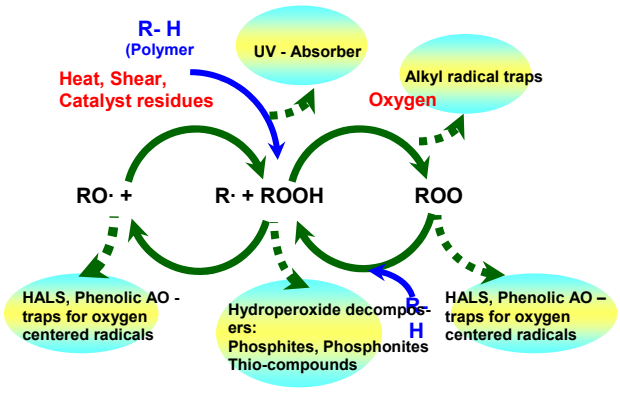

Scheme 1. **Mechanism of Polymer Stabilization**[1]

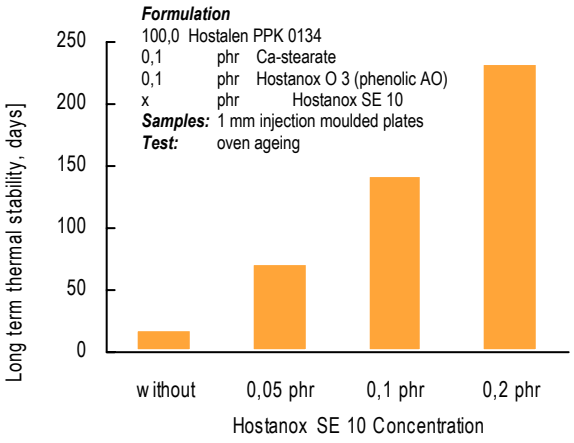

Scheme 2. **Enhancement of Long Term Thermal Stability of Polypropylene co-polymer with thio-synergist**

bumpers. However, there are secondary aspects of utilization of additives in polymers like poor solubility and diffusion of light stabilizers[3]. Solubility of HALS-770 additive in PP is on the level of tenths of a per cent which is exactly the level of effective concentration of HALS in PP for bumper application. Presence of HALS on its edge of solubility in PP creates so called physical effects (migration of the additive onto the surface) which lead to visible surface chalking. The 'state-of – the art' solution to this problem is the utilization of HALS with high solubility in PP matrix (such as Hostavin N845) or oligomeric HALS with low migration (such as Hostavin N30). Hostavin N845 has an excellent solubility (more than 3 %).

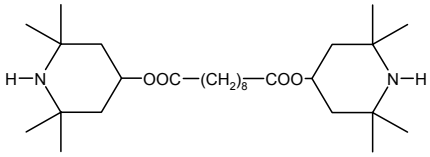

HALS-770 (bis(2,2,6,6,-tetramethyl-4-piperidyl)sebaceate)

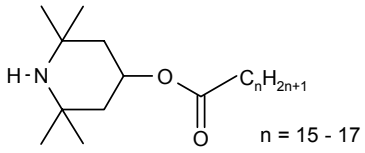

Hostavin N845

As one can observe from the Scheme 3, the higher solubility of Hostavin N845 is directly correlated to its efficiency at higher concentration, whereas Tinuvin 770 effect is limited by concentration of 0.3–0.5 %.

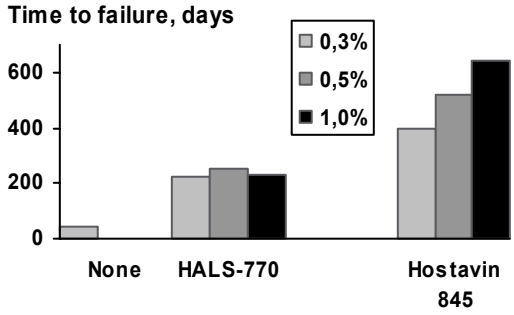

Scheme 3. **Comparison of low and high soluble HALS efficiency in PP.** Sample: EPDM Modified and Talc Filled PP; Test: Atlas WOM (DIN 53 357 A); Time to failure is calculated by visible chalking (increase of L value from 76 (original) to 80 or more)

Polyamide stabilization

Polyamide is widely used for glass-reinforced and filled engineering compounds for automotive parts (made by Injection Moulding) due to its higher mechanical properties, abrasion resistance and thermal stability. We can often find polyamide textile and technical yarns as a base material for safety belts, airbags and car seat covers. Polyamide tire cord is also one of the basic elements of a modern tire construction. Standard systems for thermal stabilization of Polyamides are copper based inorganic complexes (Copper Chloride based); these systems are quite efficient in terms of polymer protection. However, apart from efficiency in polymer, copper salts can give unfavorable discoloration of polyamide (green-blue shade) and they can be easily extracted since they are water-soluble. This is the first reason why polyamide industry looks for organic alternatives to Copper which are Phenolic Antioxidants. The second reason is the fact that for high demand applications of polyamide like automotive industry, there is a need for higher efficiency of stabilization of polyamide. Such a higher level of stabilization can be obtained with utilization of special stabilization agent like Nylostab S-EED ( ).

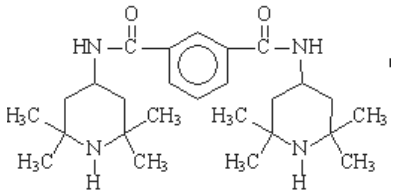

Nylostab S-EED

Nylostab S-EED can influence the processability, surface properties, heat and light stability of injection moulded parts and fibers (see Scheme 4 and 5).

Nylostab S-EED is a unique additive for polyamide which can be used during polymerization of Polyamide as well as during compounding and injection moulding processes. Apart from its excellent surface modification and filler dispersion aid effect, Nylostab S-EED work as a highly efficient light stabilizer for polyamides (because of its hindered amine structure). Best results of light stabilization (no color change) can be achieved by combination of Nylostab S-EED with a UV-absorber (Hostavin VSU).

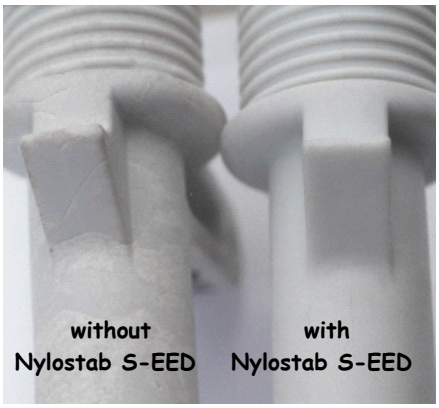

Scheme 4. **Surface modification of PA** (IM shaft) **by Nylostab S-EED** (additive of HALS class)

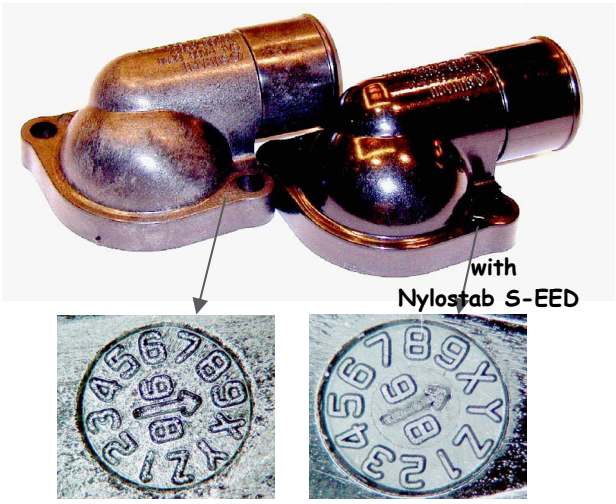

Scheme 5. **Surface quality of the Black Pigmented GF PA 6.6** (Circular marks on the molded parts)

Yellowness Index

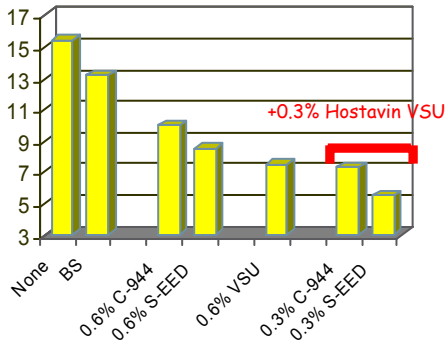

Scheme 6. **Light Stability of Polyamide** (Injection Moulding 1 mm plaques, Accelerated Weathering Conditions: 1500 hours in Atlas WOM (DIN 53 387 A)

Polycarbonate stabilization

A main application for Polycarbonate in automotive industry is a replacement of glass parts since Polycarbonate resin has excellent transparency and impact resistance. Stabilization of Polycarbonate articles is required for exterior parts of car like head lights and transparent roofs. A proper stabilization from UV light allows us to maintain mechanical properties and transparency of PC and the same time to prevent discoloration of PC which is essential for optical elements.

Conclusion

Automotive industry is a high demand application for polymer materials, utilization of polymer additives enables polymer producers to meet and overcome the specific requirements to plastic elements of cars such as long term heat stability and light stability.

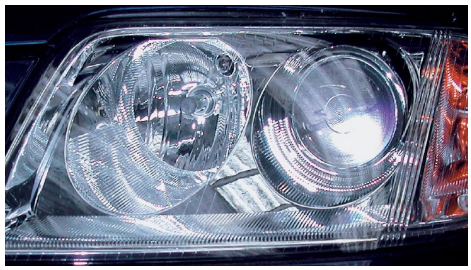

Scheme 7. **Head Light Element made from Polycarbonate requires high level of UV- and heat stabilization**

Stabilization is an essential and very often the only way to maintain mechanical, optical, aesthetical and other important characteristics of such plastics as PP, PA, PC, ABS during conditions of exploitation of a modern car.

REFERENCES

1. Zweifel H.: *Polymer Additives Handbook*, 5th edition, Hanser Gardner Publications (2001).
2. Malik J., Kröhnke C.: Comptes Rendus Chimie *9*, 1330 (2006).
3. Malik J., Hrivik A., Tomova E.: Polym. Degrad. Stab. *35*, 61 (1992).

KL-17
AUTOMOTIVE MATERIALS FROM PTS

WALTER BAUMANN

PTS Marketing- & Vertriebs-GmbH
Hautschenmühle 3
D-91587 Adelshofen-Tauberzell

1. Supertough glass fibre reinforced PP
PP + glass fibre is standard for automotive interior structural parts. The limit is dimension stability, impact and warping combined with not sufficient surface quality. Therefore PTS Group has developed a wide range of special compounds with super impact, good dimension stability and excellent surface.

2. Semi-aromatic highly glass reinforced polyamide for metal replacement
These special PA grades with typically 50-60 % glass fibre show excellent aesthetical surface, high impact and ultraflow properties for thin-wall-applications.

3. Cross-linkable polymers
With cross-linkable PA, PBT and other semi-crystalline materials, the gap between engineering plastics and expensive special polymers can be filled.

CONTRIBUTED LECTURES

CL-01
APPLICATION OF LIGNINS IN RUBBER BLENDS

PAVOL ALEXY[a], JOZEF FERANC[a], ZUZANA KRAMÁROVÁ[a], MARTINA HAJŠOVÁ[a], SYBILL ILISCH[b], MIROSLAV ĎURAČKA[c], DANIELA MOŠKOVÁ[d], and IVAN CHODAK[d]

[a] Slovak University of Technology in Bratislava, Faculty of Chemical and Food Technology, Radlinskeho 9, 812 37 Bratislava, Slovakia, [b] Martin-Luther University Halle-Wittenberg, Institute of Material Science,Merseburg, Germany, [c] VUCHTa.s. Nobelova 34, 836 03 Bratislava, Slovakia, [d] Polymer Institute, Slovak Academy of Sciences, 842 36 Bratislava, Slovakia

Possibility of lignin application in rubber blends based on NR and SBR was studied. Seven types of lignin powder were tested as fillers for rubber blends before and after modification. Influence of lignin on vulcanisation process, mechanical properties, morphological structure as well as dynamical-mechanical properties was investigated. The significant positive effect of modified lignin on properties of model rubber blends was found.

Introduction

Lignin biopolymer is dominant component of waste in wood – processing technologies. Most frequently way for its utilization is combustion. In the last years, technical lignins are investigated for their utilization in material recycling technology. Application of some types of lignins for preparation of crosslinked resins is described in ref.[1,2]. Also application of lignin for modification of some properties of thermoplastics as well as rubber blends was investigated in many works[3–8]. Addition of lignin to both types of polymer matrixes (thermoplastic as well as rubber) has positive effect on thermal stability of resulting materials. In rubber blends, lignin is able to improve abrasion resistance, but it exhibit partially negative effect on tensile properties. Some types of lignins can interact with vulcanization agents. Application of lignin can modify dynamical-mechanical properties which can be used for modification of driving properties of tires for example. Improving of thermoxidation stability of NR blends was described in work[8]. Lignin create synergic effect with IPPD in this case. In our work seven types of commercial lignins were tested in NR and SBR model blends. Influence on vulcanization parameters, mechanical and dynamical properties was studied together with phase arrangement and morphology of vulcanisates.

Experimental

Chemicals

Seven types of lignin powder were tested. Borrement CA 120 (Calcium lignosulfonate, Ca content 5 %, pH of 10 % sol. = 4.5) as well as Calcium lignosulfonate with pH 4.2, 7.3, 9.1, 6.7, Borresperse NA 220 (Natrium lignosufonate, Na content 8 %, pH of 10 % sol. = 8.0) and Vianultra (Magnesium lignosulfonate, pH of 10 % sol. = 5.5) were kindly supplied by company Borregaard, Germany. Narural Rubber SMR 20 and SBR rubber Kralex 1500 were used. Sulphenamide and diphenylguanidine accelerators with sulphur, ZnO and mixture of stearic and palmitic acid were used as vulcanization system. Glycerol (99.8 % purity) was used as plasticizer for lignin.

Processes

All rubber blends were prepared in 75 cm^3 Plasticorder Brabender chamber in two mixing steps, both at 80 °C and 70 rpm. Vulcanization curves were recorded using Rheometer Monsanto 100 at 150 °C. Samples were cured at 150 °C at time corresponding with optimum of vulcanization. Pressure was 20 MPa. Tensile test of prepared samples was done according to ISO 37 at cross head speed 500 mm min^{-1} using TIRATEST 27025 machine. Crosslinking density was determined based on kinetic of swelling and calculated according to Flory-Rehner equation. For morphological study, SEM pictures of fracture surface were done using microscope TESLA BS 300 with TESCAN digitalized unit and software WINTIP 3.1.

Results and discussion

Studied lignins were tested in SBR as well as NR matrix in concentration range up to 40 phr. Lignins have significant influence on vulcanization process of both types of blends. In general, scorch time as well as optimum of vulcanization decreases with increasing of lignin concentration. Calcium and Magnesium types of lignin exhibit only moderate decreasing of both parameters in contrast to Natrium type which causes more significant shortening of vulcanization process. Small changes were observed also in crosslinking density of prepared vulcanisates. Participation of lignins on vulcanization process can be assumed based on obtained results. Much more strong effect of lignin on mechanical properties was observed, mainly in case of NR matrix. Dependency of tensile strength and elongation at break for NR vulcanisates on lignin concentration is shown in Fig. 1.

Addition of lignins causes moderate modification of dynamical-mechanical properties. Peak value of dependency of tg δ on temperature is slightly decreases to lower values with increasing of lignins concentration for both rubber matrixes. Simultaneously can be observed increasing of tg δ at

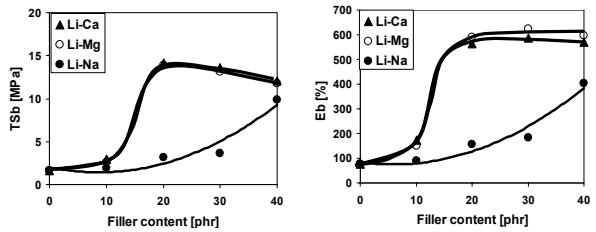

Fig. 1. **Dependency of tensile strength and elongation at break on lignin content in NR matrix for Calcium (Li-Ca), Magnesium (Li-Mg) and Natrium (Li-Na) lignosulfonate**

0 °C, particularly in case of Calcium type of lignin. In case of Calcium type of lignin addition of plasticizer was tested. Dependencies of observed properties on glycerol content were studied in the blend containing 30 phr of lignin. Scorch time as well as optimum of vulcanization decrease with increasing of glycerol concentration. Maximum was observed on curve of dependency of tensile strength on glycerol concentration around 20 % of glycerol content. Elongation at break slightly continuously increases in whole concentration range of glycerol. Positive effect of glycerol on mechanical properties of both types of vulcanisates containing various amount of lignin is evident from Fig. 2 and 3.

Morphology of rubber blends containing lignin is also positively influenced by glycerol addition. As an example the

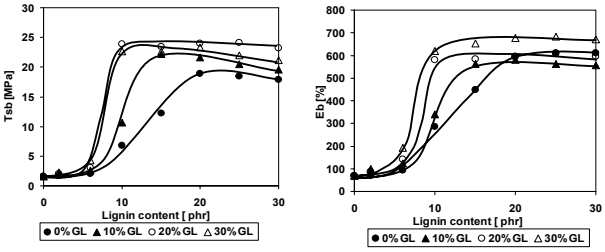

Fig. 2. **Dependency of tensile strength and elongation at break on lignin content in NR matrix for Calcium lignosulfonate at various concentration of glycerol (GL)**

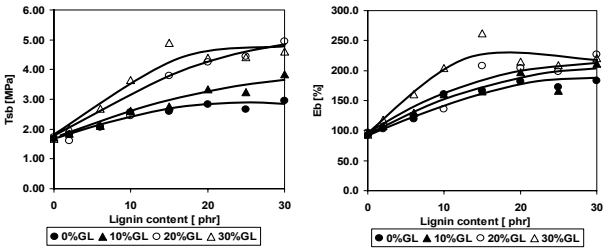

Fig. 3. **Dependency of tensile strength and elongation at break on lignin content in SBR matrix for Calcium lignosulfonate at various concentration of glycerol (GL)**

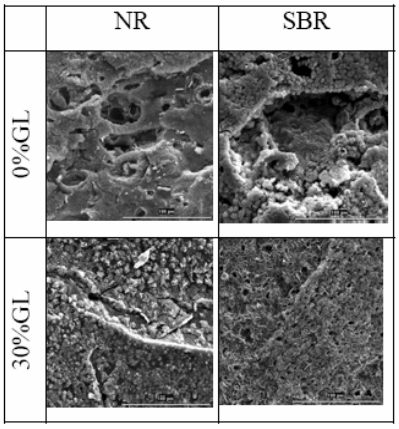

Fig. 4. **Extracted fracture surfaces of NR and SBR vulcanizates containing 30 phr of Ca lignin at 0 and 30 % of glycerol**

fracture surfaces of blends containing 30 phr of Calcium lignin are shown in Fig. 4. All samples were extracted in 60 °C distilled water before SEM measurements for removing of lignin from the fracture surface for better resolution of phase arrangement.

Finelly the influence of molecular weigth of lignin on properties of NR model blends was studied. Strong influence of Mw (together with pH value of 10 % lignosulfonate solution) on vulcanisation process as well as on mechanical properties was found. Tensile strength and elongation at break decrease with Mw in studied range of Mw from 20 000 to 90 000. Vulcanisation parameters (scorch time and optimum of vulcanisation) were influenced as well.

Conclusions

Obtained results shown positive influence og lignin preparates on properties of rubber/lignin blends. Especially in case of NR strong improving of mechanical properties by lignin addition can be achieved particularly in case of simultaneous application of plasticizer. Positive effect of plasticiser was confirmed. The required properties of rubber blend can be also adjusted by selection of suitable type of lignin – type of ion as well as Mw of lignin derivate is important.

This work was supported by Slovak grant agencies, grants No. VEGA 1/4455/07 and APVV -99-038805.

REFERENCES

1. Kuom M., Hse C. Y., Huang D. H.: Holzforschung *45*, 47 (1991).
2. Glasse W. G., Barnett C. A., Sano Y. J.: J. Appl. Polym. Sci. *37*, 441 (1983).
3. Ljubeshkina E. G., Belova L. J., Fribman M. L.: Mech. Polimerov *3*, 353 (1977).
4. Alexy P., Košíková B., Podstránska G.: Polymer *41*, 4901 (2000).
5. Košíková B., Alexy P., Gregorová A.: Wood Research *48*, 62 (2003).

6. Kumaran M. G., De Sadhan K.: J. Appl. Polym. Sci. *22*, 1885 (1978).
7. Gregorová A: *Aplication of Lignin in Polymer Blends*, Institue of Chemistry, Slovak Academy of Sciences, Bratislava 2005.
8. Gregorová A., Košíková B., Moravčík, R.: Polymer Degrad. Stab. *91*, 229 (2006).

CL-02
IMPROVEMENT OF HOMOGENEITY OF EPDM/NBR RUBBER BLENDS

SAMIR BOTROS*, AHMED MOUSTAFA, and MOHAMED ESSA

National Research Center, Polymers Department, Tahrir St., Dokki 12622, Giza, Egypt.
botros-1@hotmail.com

Synthesis and characterization of EPDM-g-PDMAEMA

The graft copolymerization of poly 2-dimethylamino ethylmethacrylate (PDMAEMA) onto ethylene propylene diene mononer rubber (EPDM) was carried out in toluene via solution polymerization technique at 70 °C, using dibenzoyl peroxide (BPO) as initiator. EPDM-g-PDMAEMA was characterized with ^{1}HNMR spectroscopy, gel permeation chromatography (GPC), differential scanning calorimetry (DSC), and thermal gravimetric analysis (TGA).

Fig. 1 shows the ^{1}H NMR spectroscopy of EPDM-g-PDMAEMA together with proposed structure and peaks assignment. Fig. 2 illustrates the GPC trace of the modified EPDM. It has a higher PI due to branching caused by PDMAEMA moieties. Fig. 3 represents the DSC scan of EPDM-g-PDMAEMA; the two *T*g's of EPDM and PDMAEMA segments appear at –49.91 °C and 114.6 °C respectively. The T_g of PDMAEMA segment is lower than its respective homopolymer due the reduction in molecular weight of PDMAEMA in the copolymer which is 18 K and that of homopolymer is 52 K. Fig. 4 represents the TGA scan of EPDM-g-PDMAEMA. It is obvious that the material is stable up to 150 °C as it loses only 4.9 % of its original weight.

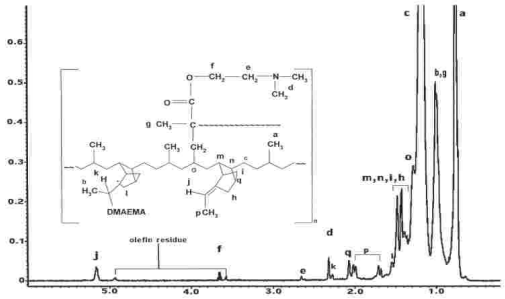

Fig. 1. **^{1}HNMR spectrum of EPDM-g-PDMAEMA**

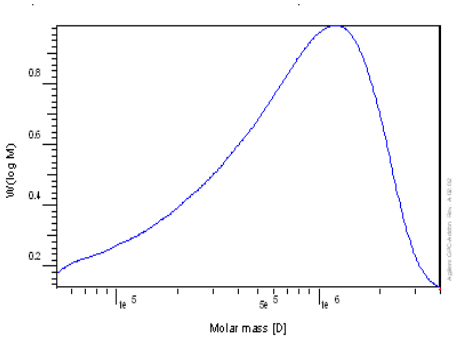

Fig. 2. **GPC trace of EPDM-g-PDMAEMA**

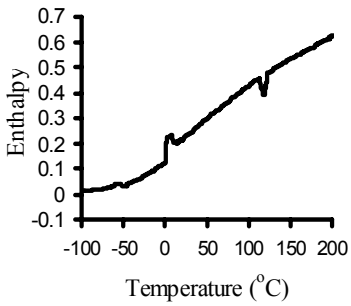

Fig. 3. **DSC scan of EPDM-g-PDMAEMA**

Homogeneity of EPDM/NBR Blend

The EPDM-g-PDMAEMA was incorporated into EPDM/butadiene acrylonitrile rubber (EPDM/NBR) blends where the homogeneity of such blends was examined with scanning electron microscopy (SEM) and DSC. The DSC traces of EPDM/NBR (50/50) blends with and without EPDM-g-PDMAEMA (10 phr) are illustrated in Fig. 5 and 6. Glass transition temperatures ($T_{g's}$) of EPDM and NBR in the blend without EPDM-g-PDMAEMA appear at −30 °C and −60 °C respectively with T_g difference of 30 °C. However, T_g of EPDM/NBR rubber blend with EPDM-g-PDMAEMA appears at −50 °C. These data illustrate that EPDM/NBR rubber blend possessed one T_g upon incorporation of EPDM-g-PDMAEMA. This can be attributed to the reduction of interfacial energy and to the increase of adhesion between phases[31]; as a result of the dipole-dipole interaction between the acrylonitrile group of nitrile rubber and the amino group of EPDM-g-PDMAEMA. EPDM/NBR blends of (50/50) blend ratio with and without EPDM-g-PDMAEMA (10 phr) were prepared for microscopy examination. The micrograph (Fig. 7a) of the blend without EPDM-g-PDMAEMA illustrates two different phases for the individual rubbers indicating phase separation and incompatibility of EPDM/NBR blend. However the micrograph (Fig. 7b) of the blend containing EPDM-g-PDMAEMA shows one phase and

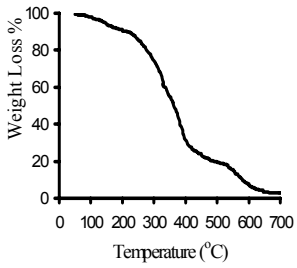

Fig. 4. **TGA scan of EPDM-g-PDMAEMA**

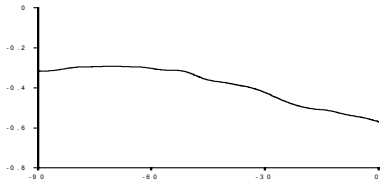

Fig. 5. **DSC scan of EPDM/NBR (50/50) without EPDM-g-PDMAEMA**

no phase separation takes place indicating change in the morphology and enhancement of the homogeneity of EPDM/NBR rubber blend.

Effect of EPDM-g-PDMAEMA on the physico-mechanical properties of EPDM/NBR blends

EPDM/NBR rubber blends with different blend ratios, namely 100/0, 75/25, 50/50, 25/75, and 0/100, were prepared in presence and absence of EPDM-g-PDMAEMA. The formulations and the rheological properties of EPDM, NBR and their blends are listed in Table I. Cure times (t_{c90}) of the EPDM/NBR (25/75) blends with and without EPDM-g-PDMAEMA were shorter and cure rate indices were greater than those of the individual rubbers. The rubber mixes were then vulcanized at their cure times. Physico-mechanical properties of EPDM, NBR and their blends with different blend ratios in presence and absence of EPDM-g-PDMAEMA were measured after and before thermal aging and plotted *vs*. NBR content in the blend (Fig. 8 and 9). It is clearly seen from Fig. 8 that the tensile strength and elongation at break (%) of EPDM/NBR blends decrease with increasing of NBR content in the blends till EPDM/NBR ratio of 50/50, beyond which (25/75 blend) the physico-mechanical properties remain unchanged. However, both tensile strength and elongation at break (%) increase with further increase of NBR content up to 100 parts (NBR vulcanizate). From the same Fig. 8, it is obvious that both tensile strength and elongation at break (%) of EPDM/NBR blend vulcanizates with different blend ratios were improved as a result of incorporation of EPDM-g-PDMAEMA (10 phr). The improvement in the mechanical properties can be attributed to the improved interfacial adhesion of EPDM/NBR blends by reducing the interfacial energy between phases; as a result of incorporation of EPDM-g-PDMAEMA. Also, the tensile strength and elongation at

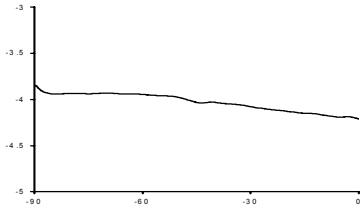

Fig. 6. **DSC scan of EPDM/NBR (50/50) with EPDM-g-PDMAEMA**

Table 1. Formulations and rheological properties of EPDM/NBR rubber blends of different blend ratios with and without EPDM-g-PDMAEMA, at 162°C.

EPDM	100	75	50	25	75	50	25	0
NBR	0	25	50	75	25	50	75	100
EPDM-g-PDMAEMA	0	0	0	0	10	10	10	0
Rheological properties								
Minimum torque, Nm	16	13	11	10.5	9.5	9.5	8	8
Maximum torque, Nm	86	91	79	77	78	72	60	71
Cure time (tc_{90}), min	16.5	11.5	11.5	5.5	13	12	7	10
Scorch time (ts2), min	3	2	2	1.5	2	2	1.5	1.75
Cure rate index (CRI),min-1	7.4	10.5	10.5	25	9	10	18	12

*High abarasion furnace black.

**N-cyclohexyl 2-benzothiazole sulfenamide.

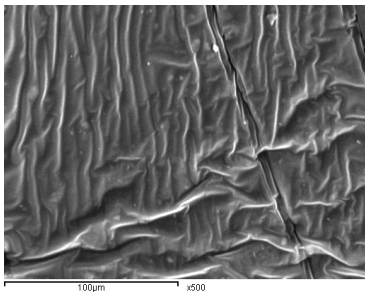

Fig. 7a. **SEM micrograph of EPDM/NBR (25/75) rubber blend, without EPDM-g-DMAEMA, M= 500X**

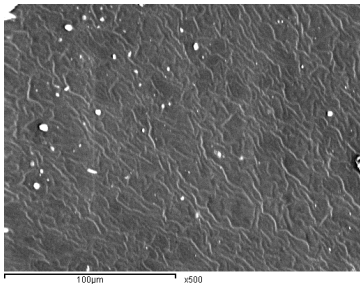

Fig. 7b. **SEM micrograph of EPDM/NBR (25/75) rubber blend, with EPDM-g-DMAEMA, M= 500X**

break (%) of EPDM/NBR homogeneous blends after 7 days of thermal aging, showed superior performance to that of the inhomogeneous blends. EPDM/NBR (50/50) blend as well as 25/75 blend showed more pronounced effect of EPDM-g-PDMAEMA. On the other hand, the elongation at break and tensile strength data agree with one another and confirm homogeneity of EPDM/NBR as a result of incorporation of EPDM-g-PDMAEMA.

Swelling behavior

Weight swell (%) in toluene, motor oil and brake fluid of the EPDM/NBR rubber blend vulcanizates *vs* NBR content in those blends, in presence and absence of EPDM-g-PDMAEMA, are illustrated in Fig. 10. Weight swell (%) in toluene, in absence of EPDM-g-PDMAEMA, shows S shape behavior. However, it shows linear behavior with incorporation of EPDM-g-PDMAEMA, this linearity in turn confirms the homogeneity of EPDM/NBR rubber blends as a result of incorporation of EPDM-g-PDMAEMA. Also, Fig. 10 illustrates that weight swell % of the EPDM/NBR rubber blend vulcanizates decreased in motor oil while increased in brake fluid with increasing NBR content in the blend. This can be attributed to the increase of the number of the polar acrylonitrile groups due to the increase of NBR content. Generally, weight swell % of the homogeneous EPDM/NBR blends in motor oil and in brake fluid is less than that of the inhomogeneous blends (desired phenomena). Of all blend ratios explored EPDM/NBR (25/75) exhibited the best swelling behavior in motor oil while EPDM/NBR (75/25) possessed the best swelling behavior in brake fluid. Therefore, EPDM/NBR blends (25/75) and (75/25) can be recommended to be used in industry of oil seal and hoses subjected to motor oil and brake fluid respectively.

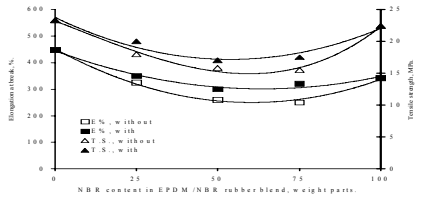

Fig. 8. **Tensile strength, MPa and elongation at break, % of EPDM/NBR rubber blend vulcanizates with and without EPDM-g-PDMAEMA *vs* NBR content in the blend**

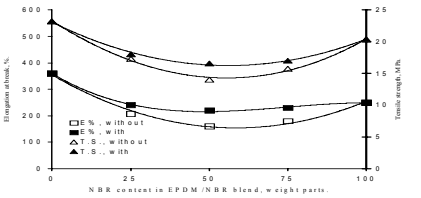

Fig. 9. **Tensile strength, MPa and elongation at break, % of EPDM/NBR rubber blend vulcanizates, with and without EPDM-g-PDMAEMA *vs* NBR content in the blend, after thermal aging at** 90° **C for 7 days**

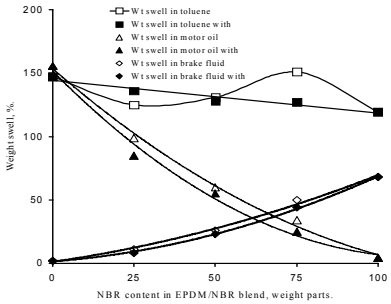

Fig. 10. **Weight swell, % of EPDM/NBR rubber blend vulcanizates with and without EPDM-g-PDMAEMA in toluene, motor oil and brake fluid, *vs* NBR content in the blend**

Conclusions

1. The results obtained from the SEM micrographs and DSC traces confirmed that EPDM-g-PDMAEMA (10phr) can be used successfully to improve the homogeneity of EPDM/NBR rubber blends.
2. 75/25 EPDM/NBR rubber blend possesses good mechanical properties together with the best swelling be-

havior in brake fluid.

3. NBR and NBR rich blend showed the best weight swell % in toluene and motor oil. This can be attributed to the great number of polar acrylonitrile groups.

REFERENCES

1. Oliveira M. G., Gomes A. O., Almeida M. M., Soares, B. G.: Macromol. Chem. Phys. *205*, 465 (2004).
2. Hellens W. V.: Kautsch Gummi Kunstst *47*, 124 (1994).
3. Hess W. M., Herd C. R., Vegvari P. C.: Rubber Chem. Technol. *66*, 329 (1993).
4. Duin M. V., Kranas J. C., Smedinga J.: Kautsch Gummi Kunstst. *46*, 445 (1993).
5. Coran A. Y.: Rubber Chem. Technol. *61*, 281 (1988).
6. Johnston J.: Pressure Sensitive Adhesive tapes, PSA council 2514 Stonebridge Lane NorthBrook. IL, 2003, 60065-0609 USA.
7. Rudin A. ed., in: *The Elements of Polymer Science and Engineering*, pp 428. Academic Press, 1982.
8. Schuster R. H.: Angew. Makromol. Chem. *202/203*, 159 (1992).
9. Shonik G. O., Simon G. P. (ed.), in: *Polymer Blends and alloys*. Marcel Dekkar, New York 1999.
10. Wetton R. E., Corish P. J.: Polym. Testing *8*, 303 (1989).
11. El Sheemy H.: Kautsch. Gummi. Kunstst. *52*, 586 (1999).
12. Coran A. Y., Legge N. R., Holden G., Shroder H. E. (ed.), in: *Thermoplastic Elastomers*. pp 133. Hanser Publishers, Munich 1991.
13. Lohmar L.: Kuatsch. Gummi. Kunstst. *39*, 1065 (1986).
14. Setua D. K., White J. L.: Polym. Eng. Sci. *31*, 742 (1991).
15. Setua D. K., Pandey K. N., Saxena A. K., Mathur G. N.: J. Appl. Polym. Sci. *74*, 480 (1999).
16. Botros S. H., Tawfic M. L.: Polym. Plast Technol. Eng. *44*, 209 (2005).
17. Koning C., Duin M. V., Pagnoulle C., Jerome R.: Prog. Polym. Sci. Jpn. *23*, 707 (1998).
18. Oliveira M. G., Soares B. G.: J. Appl. Polym. Sci. *82*, 38 (2001).
19. Oliveira M. G., Soares B. G.: J. Appl. Polym. Sci. *91*, 1404 (2004,).
20. Botros S. H, Moustafa A. F.: J. Elastomers Plast. *34*, 15 (2002).
21. Botros S. H., Tawfic M. L.: J. Elastomers Plast. *38*, 349 (2006).
22. Botros S. H., Tawfic M. L.: J. Elastomers Plast. *37*, 299 (2005).
23. Botros S. H., Moustafa A. F.: J. Appl. Polym. Sci. *89*, 3143 (2003).
24. ASTM designation D 2084-95 (1998).
25. ASTM designation D 412-98a (1998).
26. ASTM designation D 471-97 (1997).
27. Oliveira P. C., Oliveira A. M., Garcia A., Barboza J. C. S., Zavaglia C., Santos A. M.: Eur. Polym. J. *41*, 1883 (2005).
28. Selvam P., Victor Babu K., Penlidis A, Nanjundan S.: Eur. Polym. J. *41*, 831 (2005).
29. Botros S. H., Moustafa A. F., Ibrahim S. A.: J. Appl. Polym. Sci. *99*, 1559 (2006).
30. Fox T. G., Flory P. J.: J. Polym. Sci. *14*, 315 (1954).
31. Okieimen F. E., Urhoghide I. N.: J. Appl. Polym. Sci. *59*, 1803 (1996).

CL-03

NEW POTENTIAL IN POLYMER ARCHITECTURE ANALYSIS USING DYNAMIC MECHANICAL ANALYSIS BY COMBINING LINEAR AND NON-LINEAR VISCO-ELASTICITY

HENRI G. BURHIN

Alpha Technologies UK, 98 rue longue, B-1320 Beauvechain, Belgium
henri.burhin@dynisco.com

Introduction

Since decades, most polymers have been characterised by simple although robust instruments. For elastomeric materials, the Mooney viscometer has been the reference instrument and will probably remain as such for some time. Meanwhile, experienced rubber technologists admit that identical Mooney viscosity for two polymers of identical nature but, for instance, from different producers, do not guarantee identical processability. For thermoplastic, a similar situation exists with the Melt Flow Indexer (MFI).

Both instruments have an identical limitation. They provide only a single point measurement while polymer specialists know that, due to their pseudo-plasticity nature, polymers demand testing at variable speed to capture this important characteristic. Nevertheless, due to their intrinsic simplicity, both instruments are still largely used in polymer plant quality control.

Capillary rheometry is another technique for polymer analysis providing pseudo-plasticity index. Unfortunately, if it is highly valuable for thermoplastic materials and rubber compounds, it is hardly used in testing pure elastomers. This limitation is essentially due to the high elastic character of these polymers providing very early appearance of melt fracture phenomenon, thus preventing valuable characterisation at high shear. Finally, capillary rheometer requires extensive cleaning after each test. This drawback prevents high productivity testing hence general use of capillary rheometers in plant QC operation.

Since the original work by Weisenberg on the first Dynamic Mechanical Analyser, the Rheogoniometer, linear visco-elasticity has developed itself as the preferred polymer characterisation tool in the world research laboratories.

The reasons behind this success reside in the ability of this technique to quickly and precisely assess two of the most important polymer characteristics, Average Molecular Weight (AMW) and Molecular Weight Distribution (MWD). Unfortunately, linear visco-elasticity failed to provide unambiguous information and measurements on the third most important polymer characteristic, Long Chain Branching (LCB). It is essential to mention that polymer LCB content is largely responsible of often observed processability problems such as die swell. It is worth mentioning the fact that very small variations of LCB have very large effect on processability.

This paper will review the latest approach to fast, reli-

able and precise measurement of these three polymer characteristics by the combination of linear visco-elasticity and non-linear visco-elasticity measurements.

Theory and practice

Contrary to simple liquids such as water, oils etc… having a constant viscosity versus shear rate, polymer melt exhibits a different behaviour. At low to very low shear rate, they behave as simple liquids. This viscosity value is called η_0, or Newtonian viscosity. Over a given shear rate, they exhibit a sharp decrease of viscosity called pseudo-plasticity region. This behaviour is highly interesting for processing polymer melts and especially rubber compounds as it makes processing possible with reasonably powered machinery. Without it, high speed extrusion or injection would not be possible. The machinery power required for processing materials having viscosity level equal to their Newtonian viscosity would simply not be economical or even feasible. Therefore, a precise measurement of this complex behaviour over a wide range of shear rate is highly recommended. Several non-linear mathematical flow models have been successfully used to fit polymer response to shear rate (Cross, Carreau, Carreau-Yasuda etc…). All these models have in common to simplify the response to a very limited number of parameters. The following graph represents the "Cross model" (Fig. 1).

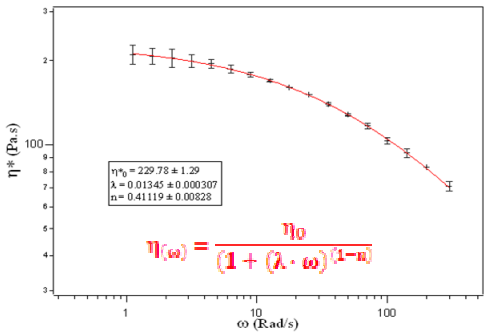

Fig. 1.

These parameters not only enable powerful flow simulation software to predict complex flow patterns in injection moulding but also permit to calculate polymer simple characteristic such as Mw or average molecular weight by weight using the following mathematical relationship

$$\eta_0 = k \cdot M_w^{3.5} \qquad (1)$$

Newtonian viscosity is rarely measured by capillary rheometry. Typically, this technique accuracy is very limited in the shear rate range corresponding to polymer Newtonian behaviour.

Only linear visco-elasticity is sensitive and accurate enough to measure in this domain. In order to overcome the limitations of dynamic measurements in the high shear rate range, the "Time-Temperature Superposition" principle (TTS) enables to convert temperature in frequency. Lower test temperature is equal to higher shear rate.

When visco-elasticity measurements are performed within the linear domain, no melt facture can occur thus testing at high shear is feasible.

Depending upon the temperature sensitivity of the polymer, even very high shear rate are achievable.

Fig. 2. illustrates this possibility on polystyrene.

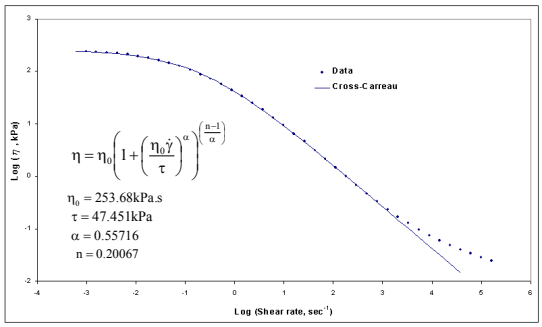

Fig. 2.

The second most important polymer characteristic is molecular weight distribution (MWD). Usually, it is measured by Gel Permeation Chromatography (GPC) or Size Exclusion Chromatography (SEC). This technique is well established but is rather expensive, time consuming and not very accurate and repeatable. In addition, it involves the use of large quantity of organic solvents which may soon be banned for toxicity ("REACH" norms in EU).

Linear visco-elasticity can sometimes be a very useful replacement for GPC/SEC. For linear polymers such as PIB, Poly dimethyl siloxane (PDMS), polypropylene (PP), LLDPE, IIR etc…, the crossover point coordinates (G'=G") in frequency and modulus can be used for the direct determination of AMW and MWD in a single test. The principle is illustrated in Fig. 3.

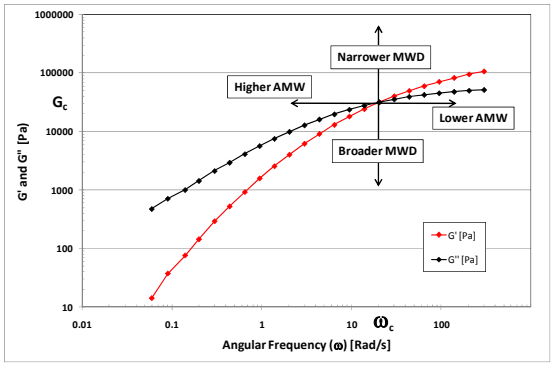

Fig. 3.

The fact that linear visco-elasticity test can easily be automated, re-emphasizes the interest for this technique as the most productive test for plant quality control. Unfortunately, this technique is useless for branched polymers. Branching, even at low level, is moving the crossover point coordinates towards lower frequencies thus preventing meaningful AMW and MWD measurements.

Linear visco-elasticity testing is performed at strain where dynamic modulus depends on frequency only. In the non linear visco-elasticity domain, modulus depends on both frequency and strain. This implies that the stress signal in this condition is no longer a pure sine wave although the strain remains perfectly sinusoidal. Strictly speaking, one shall not test in this domain as the traditional mathematics will not apply unless the signal analysis is performed by Fourier Transform (FT).

It has been found that some polymers exhibit large distortion of the stress signal when submitted to strain superior to 1000 % strain (γ_0=10). In addition, it was found that the distortion can vary between samples. Fig. 4 illustrates this behaviour.

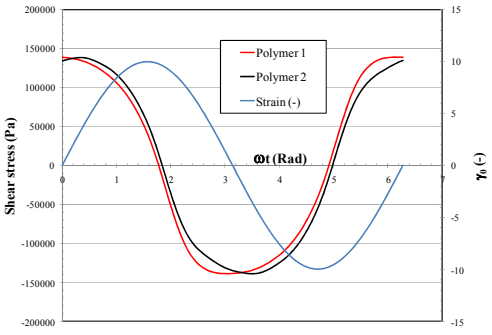

Fig. 4.

FT analysis enabled precise quantification of the stress signal distortion. We were than able to relate the distortion to the level of LCB in the polymer.

The results are expressed as a series of moduli at all odd harmonics (G'_n & G''_n). The series is limited to the 9th harmonics as the values for the higher harmonics can be considered as not significant. The response can also be expressed under the form of Lissajou figures with shear stress ($\tau_{(t)}$) versus shear rate ($\dot{\gamma}$) over one cycle.

The separation of the stress signal is illustrated in Fig. 5 and Fig. 6.

From the Lissajou figures, it has been found that linear polymers exhibit a pronounced secondary loop at each end of the distorted ellipse. These loops have been found on ALL polymers known to be linear. These loops disappear as soon

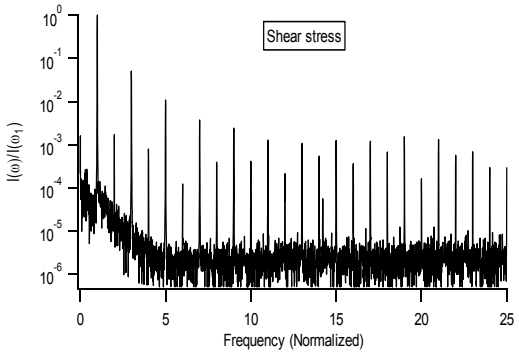

Fig. 5.

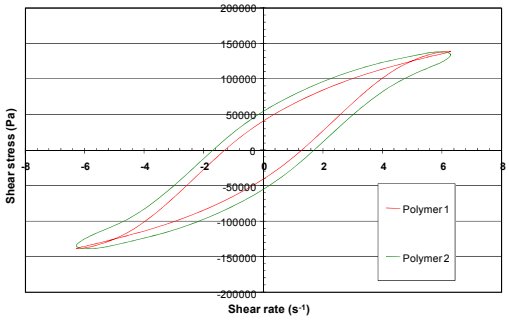

Fig. 6.

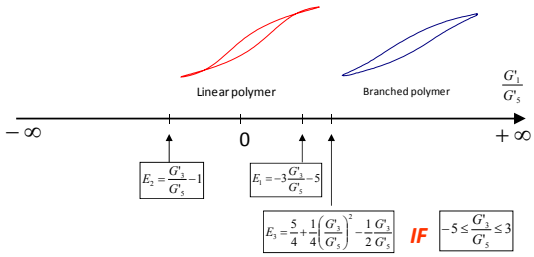

Fig. 7.

as LCB are present even at very low level. We were able to detect on polypropylene level as low as 1 LCB per 500,000 carbons. No other technique currently available is capable of this sensitivity. A comprehensive mathematical analysis of the shear stress curve in relation to G'_n and G''_n.

It has found that the LCB content can be expressed as a simple ratio of $\frac{G'_3}{G'_5}$. It is remarkable that the mathematical analysis shows the significance of elastic moduli only. All viscous moduli of the all harmonics simply disappear.

A graphical representation of this ratio is given in Fig. 7.

This approach for LCB detection and quantification was successful on the following polymers, BR,EPDM, NR, FKM, IIR, PIB, PP, LDPE, LLDPE, PP, PC and PS. We can reasonable believe that this approach is general and could be applied to all polymer types.

Summary and conclusion

From all modern polymer characterisation techniques, visco-elasticity is the most efficient. AMW and MWD can be easily measured and polymer discrimination is possible which very high confidence.

Traditionally, only linear visco-elasticity was considered as traditional signal analysis did not allow meaningful analysis in the non linear regime. The use of modern signal analysis based on Fourier transforms enables not only testing in the non linear regime but as well the quantification of the stress signal higher harmonics.

From these higher harmonics, a simple moduli ratio $\{\frac{G'_3}{G'_5}\}$

has been found to quantify the presence and level of LCB. This has been found valid on a very large selection of polymers.

Due to the second normal stress difference, this technique is only valid in a closed chamber Dynamic Mechanical Analyser (DMA) such as the RPA2000 from Alpha Technologies. Traditional open boundary DMA's are unable to perform this test. The polymer sample tends to escape from the test chamber with the appearance a melt fracture at the edge.

The combination of linear and non linear visco-elasticity is the only technique providing unambiguous separation between MWD effects from LCB effects thus guaranteeing the most efficient polymer discrimination.

The efficiency of the technique is further enhanced by automation of linear visco-elasticity tests and very short test time of non linear visco-elasticity (< 4 minutes).

CL-04

AN INNOVATIVE METHOD TO INVESTIGATE POLYMER LONG CHAIN BRANCHING WITH FT-RHEOLOGY AND LARGE AMPLITUDE OSCILLATORY SHEAR (LAOS)

HENRI G. BURHIN[a] , NICOLAS ROSSION[c], CHRISTIAN BAILLY[b], ADRIEN LEYGUE[c], and ROLAND KEUNINGS[c]

[a] Alpha Technologies UK, 98 rue longue B-1320 Beauvechain, Belgium, [b] Université Catholique de Louvain (UCL), Département POLY, Bâtiment Boltzmann 1 Place Croix du Sud, B-1348 Louvain La Neuve, Belgium, [c] Centre for Systems Engineering and Applied Mechanics (CESAME), Université catholique de Louvain, B-1348 Louvain-la-Neuve, Belgium henri.burhin@dynisco.com

Introduction

The most commonly used shear data used for characterisation of viscoelastic melt is generated at low amplitude to give linear properties to agree with accepted visco-elasticity theory.

Steady shear viscosity or transient elongational viscosity data, are used in the case of non-linear characterisation. Such measurements can also be used to give indications of the macromolecular structure of polymer melts.

Large Amplitude Oscillatory Shear (LAOS) can provide useful non-linear characterisation of polymers even in absence of a widely agreed theoretical base. LAOS, or the non-linear visco-elasticity domain can be described as the oscillatory strain domain where the shear complex modulus (G*) is not a function of angular frequency (ω) only but a function of both ω and strain, (γ_0)

The use of LAOS in experimental studies has been reported initially by Philippoff W [9] (1966), Tee & Dealy[1] (1975) and Mac Sporran & Spiers[2] (1982, 1984). Later, Giacomin and Dealy reported results using a special measuring device called "sliding plate rheometer". At present, the group of M. Wilhelm appears to be one of the most active in this field. Wilhelm et al.[3,4] (1998, 1999) developed a methodology for high sensitivity Fourier transform rheology applied to linear polymer melt and polymer solutions. Additional work on comparing simulation and experimental results in LAOS on HDPE melt was also published[11].

The aim of the present work is to investigate the influence of Long Chain Branching (LCB) on LAOS experiments and evaluate the potential of this technique in detecting LCB content in polymers. In addition, to evaluate this technique as potential replacement of other well documented LCB probing techniques such as NMR, dynamic viscosity activation energy and SEC with light scattering.

This study was performed using a non-conventional rheological instrument and Fourier Transform analysis for precise quantification of the stress signal distortion. The stress signal analysis in this work was performed using the method proposed by Giacomin & Dealy[5].

Experimental

All experimental work was performed using the VTM theometer commercialised by Dynisco. The VTM rheometer is based on the RPA2000 from Alpha Technologies. It is a dynamic testing instrument initially developed for visco-elastic property measurements of elastomers and uncured rubber compounds, Dick and Pawlowski[6] (1992).

The instrument is working under controlled strain amplitude. A periodic shear deformation with amplitude γ_0 and frequency ω is applied, given by

$$\gamma = \gamma_0 \sin \omega t \qquad (1)$$

According to Giacomin and Dealy, the shear stress signal was considered as a Fourier series.

$$\tau_t = \gamma_0 \sum_{n=1}^{\infty} G'_n(\sin\, n\omega t) + G''_n(\cos\, n\omega t) \qquad (2)$$

$$G'_{n(\omega)} = \frac{\varpi}{\pi} \int_0^{\frac{2\pi}{\omega}} \frac{\tau_t}{\gamma_0} (\sin n\varpi t) \cdot dt \qquad (3)$$

$$G''_{n(\omega)} = \frac{\varpi}{\pi} \int_0^{\frac{2\pi}{\omega}} \frac{\tau_t}{\gamma_0} (\cos n\varpi t) \cdot dt \qquad (4)$$

Note: Only odd harmonics ≠ 0

Virgin polypropylene (PP) and chemically modified PP were used to study the effect of LCB on $\tau_{(t)}$ function. PP samples with different LCB level were obtained by reactive extrusion with Per-Oxy-Dicarbonate (PODIC) as per Lagendijck et al.[7] (2001). As reported, this treatment enables the formation of increasing level of LCB as a function of amount of PODIC. An additional sample of high viscosity (HV) linear PP has been used to study the effect of Average Molecular weight (AMW). Molecular Weight Distribution (MWD) was investigated as well by mixing fraction of high viscosity linear PP in

Table I
Polypropylene molecular characteristics as per[7]

Mmol/100 g PP	Mn Kg mol^{-1}	Mw Kg mol^{-1}	Mn/Mw	λ	B_n
0 (virgin PP)	74	410	5.54	–	–
0.5	69	400	5.74	0.00	0.03
1	62	410	6.56	0.01	0.15
2	68	460	6.81	0.01	0.23
3	71	485	6.81	0.02	0.36
High visc. PP	150	1150	7.66	–	–

low viscosity linear PP at 5 % and 50 % by weight through solution mixing.

Polymer molecular characteristics are listed in Table I. For comparison purposes, a commercially available β irradiated PP (ref.[8]) was tested in the same conditions. This polymer is used for improvement of PP melt strength. LCB were produced through radical reaction induced by β irradiation.

Both parameters B_n and λ describe LCB level. B_n is the number of branched polymer chain per polymer chain (0.03 = 3 % branched molecules). λ is the number of long branches per 1000 monomers. These values can be considered as very low level of LCB.

Results and Discussion

When testing polymer melt under large amplitude, far in the non linear viscoelasticity domain (γ_0 >>1), although the strain signal is perfectly sinusoidal, the stress signal as a function of time appears largely distorted. Depending upon polymer characteristics, this distortion can vary as illustrated in Fig. 1.

This behaviour can also be illustrated using Lissajou figure plotting shear stress versus shear strain or better shear rate as used by Giacomin and Dealy. The plot of shear stress (τ) versus shear rate ($\dot{\gamma}$) for the polymers in Fig. 1 is illustrated in Fig. 2.

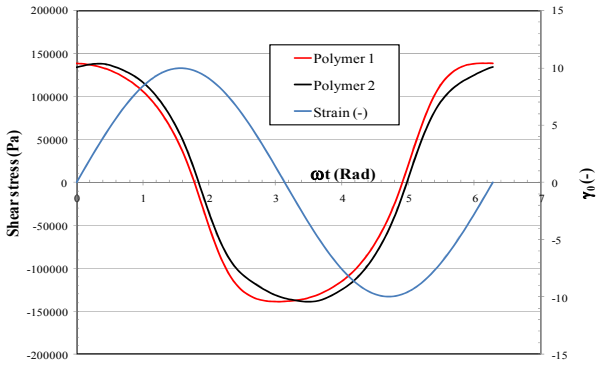

Fig. 1. **Shear stress and shear rate signal for two** generic polymers at 190 °C, 0.1 Hz, γ_0 = 10

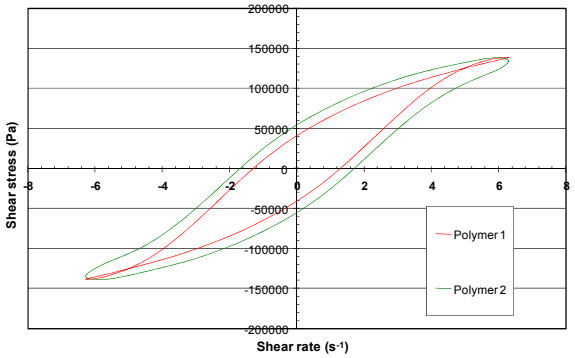

Fig. 2. **Lissajou figure** ($\tau = f(\dot{\gamma})$) of two generic polymers as per Fig. 1

PP and PODIC modified PP

Lissajou figures ($\tau = f(\dot{\gamma})$) on these polymers highlight a very interesting effect of the distortion. This plot is illustrated in Fig. 3. The presence of secondary loops at the highest shear rate values are observed only for linear polymer molecules (Virgin PP and High viscosity PP).

We can also observe that increasing level of LCB separates the loading part of the stress signal from the unloading part, increasing the loop surface.

To confirm this observation, τ was plotted against shear rate for virgin PP, HV PP, mixture of 5 % and 50 % HVPP in virgin PP, all being linear molecules. The results are illustrated in Fig. 4. In all cases, secondary loops appear demonstrating that this rather peculiar effect can be attributed to polymer linearity only, irrespective of AMW and MWD effects.

Changing from the time domain to the frequency domain by Fourier transform enables the calculation of G'_n and G''_n for all polymers. These modulus results are listed in Table II.

The most pronounced effect of LCB is observed on G'_1 or on the ratio G''_1/G'_1 (Tangent δ_1), which takes into account viscosity effects. Unfortunately, Tangent δ_1 is not totally inde-

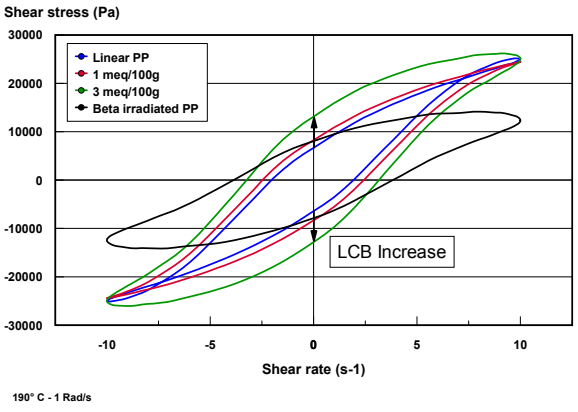

Fig. 3. **Lissajou figures of variable LCB level PP,** 190 °C, 1 Rad/s, γ_0=10

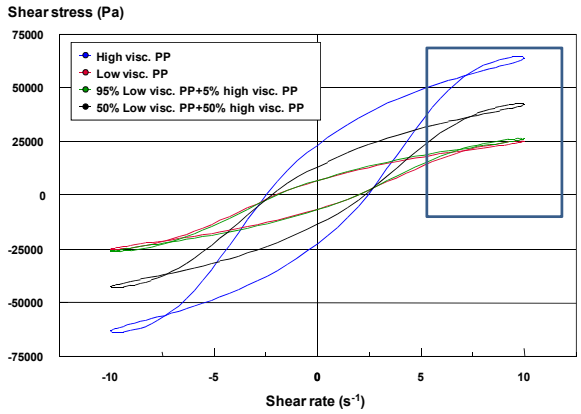

Fig. 4. **Lissajou figure** [$\tau = f(\dot{\gamma})$] for Linear LV PP, Linear HV PP, Mix of 5 %/95 % HV PP in LV PP and mix of 50 %/50 % HV PP in LV PP samples at 190 °C, γ_0=10, ω=1 Rad/s. All samples exhibit distinct secondary loops at highest $\dot{\gamma}$ values

pendent of the MWD. An unambiguous mathematical parameter was therefore necessary to provide a clear ranking of LCB content of the tested polymers.

This parameter was found by deep mathematical analysis of the Lissajou figures[10].

Lissajou figures are forming loops in the two dimensional space (τ and $\dot{\gamma}$). Within one complete cycle, we can easily observe two identical shear rate values not automatically having the same value of shear stress. We can therefore calculate the difference of shear stress at a given value of shear rate in each half loop. This difference is given by equation (*5*)

$$\Delta\tau(t) = \tau(t) - \tau(t_2) = \gamma_0 \sum_{n=0}^{\infty} G'_n(\sin n\omega t) + G''_n(\cos n\omega t) - \gamma_0 \sum_{n=0}^{\infty} G'_n(\sin n\omega t_2) + G''_n(\cos n\omega t_2) \qquad (5)$$

This analysis is illustrated in Fig. 5.

Table II
G'n and G"n for all PP samples. ω=1Rad/s, γ_0=10, 190 °C

γ_0 = 1000%	G'$_1$	G'$_3$	G'$_5$	G'$_7$	G'$_9$
Virgin PP	333.2	-258.0	67.4	-9.2	-0.8
1 mmol/100g	512.0	-254.2	69.1	-10.0	-1.7
3 mmol/100g	937.2	-274.0	88.7	-15.9	-2.7
Beta PP	648.0	-112.1	35.9	-6.6	-0.3
PP HV	1176.3	-890.2	258.0	-21.3	-14.9
LV+HV (5%)	338.0	-272.4	74.1	-11.0	-0.5
LV+HV (50%)	688.1	-518.1	143.3	-16.5	-3.7
	G"$_1$	G"$_3$	G"$_5$	G"$_7$	G"$_9$
Virgin PP	2695.5	-185.0	-24.6	20.1	-9.1
1 mmol/100g	2627.7	-175.5	-24.9	21.4	-10.5
3 mmol/100g	2724.4	-220.0	-15.5	23.7	-13.1
Beta PP	1353.2	-112.2	-6.6	7.8	-6.1
PP HV	6995.2	-596.1	-111.9	85.9	-32.0
LV+HV (5%)	2833.7	-202.7	-24.1	22.5	-11.1
LV+HV (50%)	4620.3	-354.8	-54.5	43.9	-19.0

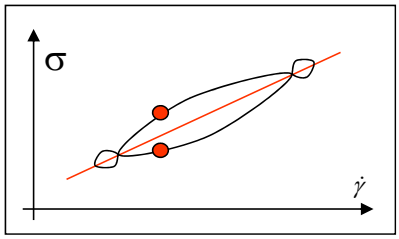

Fig. 5. **Lissajou figure mathematical analysis**

The appearance of secondary loops in the Lissajou figure is represented by a crossing of the loading and unloading part of the Δτ function.

Substituting t_2, using simple trigonometric relations and even harmonic nullity, we obtain the following equation.

$$\Delta\tau(t) = \gamma_0 \sum_{n\ odd} 2G'_n \sin n\omega t \qquad (6)$$

This equation means that only the in-phase part of the response will have an impact on the Lissajou figure surface hence the appearance of secondary loops.

First, it must be noticed that the An parameters are respectively G'n.

As equation (*6*) is a trigonometric function, it can be transformed into an algebraic function using Tchebychev polynomial (eq. (*7*)).

$$qx\prod_k (x^2 - a_k^2) = \sum_{iodd} (-1)^n A_i T_i(x) \qquad (7)$$

Considering the Fourier series limited to 3rd harmonic, the condition of existence of secondary loop will be

$$-3 \le \frac{A_1}{A_3} \le 1$$

Repeating the analysis up to the 5th harmonics provides a more sensitive parameter in the form of another harmonic ratio A_1/A_5 to be between values depending upon another harmonic ratio (A_3/A_5).

The extreme limits of the values for appearance of secondary loops are as follow:

$$E_1 = -3\frac{A_3}{A_5} - 5$$

$$E_2 = \frac{A_3}{A_5} - 1$$

$$E_3 = \frac{5}{4} + \frac{1}{4}\left(\frac{A_3}{A_5}\right)^2 - \frac{1}{2}\left(\frac{A_3}{A_5}\right) \quad \text{if} \quad -5 \le \left(\frac{A_3}{A_5}\right) \le 3$$

This rather complex analysis is better illustrated in Fig. 6.

Applying this new harmonic ratio A_1/A_5 or G'_1/G'_5 to the polypropylene and PODIC modified PP, we can detect and quantify extremely low level of LCB by the mathematical value of this last ratio. In addition, it was proven that this harmonic ration is NOT affected by MWD.

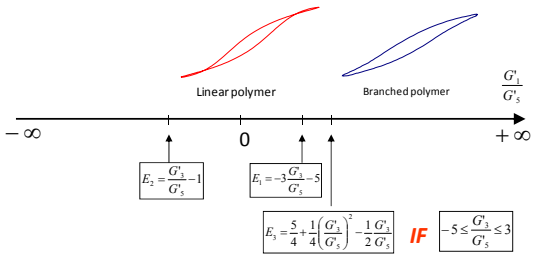

Fig. 6. **Schematic of the LCB index using G'1/G'5** harmonic ratio

Summary and conclusions

The level of LCB in polymer can be investigated using LAOS measurements with Fourier transform of the stress signal. The appearance of multiple loops in the function $\tau = f(\dot{\gamma})$ can be considered as the signature of linear polymer molecules. The use of modern signal analysis based on Fourier transform enables the quantification of the stress signal higher harmonics.

From these higher harmonics, a simple modulus ratio (G'_1/G'_5) has been found to quantify the presence and level of LCB. This has been found valid on a very large selection of polymers.

Due to the second normal stress difference, this technique is only valid in a closed chamber Dynamic Mechanical Analyser (DMA) such as the VTM from Dynisco. Traditional open boundary DMA's are unable to perform this test. The polymer sample tends to escape from the test chamber with the appearance a melt fracture at the edge.

The combination of linear and non linear visco-elasticity is the only technique providing unambiguous separation between MWD effects from LCB effects thus guaranteeing the most efficient polymer discrimination.

A complete polymer analysis for LCB using LAOS can be performed in test time smaller than 5 minutes.

The author wishes to thank A.D. Gotsis and AKZO Nobel for providing the virgin and modified polypropylene samples.

REFERENCES

1. Tee T. T., Dealey J. M.: Trans. Soc. Rheol. *19*, 595 (1975).
2. Mac Sporran W. C., Spiers R. P.: Rheol. Acta *21*, 184 (1982) and *23*, 90 (1984).
3. Wilhelm M., Maring D., Spie H. W.: Rheol. Acta *37*, 339 (1998).
4. Wilhelm M., Reinheimer P., Ortseifer M.: Rheol. Acta *38*, 349 (1999).
5. Giacomin A. J., Dealy J. M., in: *Techniques in rheological measurements*. pp. 99–121. Collyer & Clegg, Elsevier, Burking 1992.
6. Dick J. S., Pawlowski H. A.: Rubber World *1992*, 35.
7. Lagendijck R. P., Hogt A. H., Buijtenhuijs A., Gotsis A. D.: Polymer *42*, 10035 (2001).
8. Himont Inc., Scheve B. J., Mayfield J. W., DeNicola A. J.: US Patent 4916198 (1980).
9. Philippoff W.: Trans. Soc. Rheol. *10*, 317 (1966).
10. Nicolas Rossion: *Master thesis*. Université Catholique de Louvain (UCL), Faculty of Applied Sciences, Department of mathematical engineering (2004–2005).
11. Debbaut B., Burhin H.: J. Rheol. *46*, 1155 (2002).

CL-05
TEXTILE MATERIALS WITH NANO TiO_2 COATING

ĽUDMILA ČERNÁKOVÁ, RENÁTA SZABOVÁ, MAGDALÉNA WOLFOVÁ, and MILAN MIKULA

Slovak Technical University in Bratislava, Faculty of Chemical and Food Technology, Department of Polymer Materials, Radlinského 9, 812 37 Bratislava
renata.szabova@stuba.sk

Industrial utilisation of the photocatalytic effect of nano-scale TiO_2 has already found its way into various applications, especially for self-cleaning and anti-fogging purposes like, self-cleaning windows or self-cleaning textiles, anti-fogging mirrors, etc. The anti-microbial and deodorizing effect has been demonstrated as well[1]. The commercial potential for such coatings are also in automotive industry (cleaner technologies, air filters, carpets, seats, non-fogging glass and mirrors).

Studies have shown that, when exposed to ultraviolet rays in the sub 400 nm range, nano TiO_2 will actively begin creating hydroxyl radicals and superoxide ions which will decompose all micro-sized air pollutants that land on it, including petro fumes, smog, diesel smoke, exhaust gases, industrial smoke, VOCs from car fabric, air toxins, cigarette odor and many other hydrocarbon molecules in the atmosphere into nontoxic materials, such as CO_2 and water. Air purified with TiO_2 can prevent smoke and soil, pollen, bacteria, virus and harmful gas as well as seize the free bacteria in the air by filtering percentage of 99,9 %. The titanium dioxide photocatalyst has been found to be more effective than any other antibacterial agent, because the photocatalytic reactions work even when there are cells covering the surface and while the bacteria are actively propagating. Generally speaking, disinfections by titanium oxide is three times stronger than chlorine, and 1,5 times stronger than ozone. Titanium dioxide does not deteriorate and shows a long-term anti-bacterial and air-purifying effect[2].

Well-known is use of nano-enhanced TiO_2 as automotive protectant which delivers sun protector factor of up to SPF 50 to prevent fading and cracking on rubber, vinyl, and leather automotive surfaces.

In our work we studied possibilities to immobilize nanoparticles of TiO_2 at the surface of polypropylene textile after plasma activation. Diffuse Coplanar Surface Barrier Discharge (DCSBD) which was developed for treatment of textile materials at atmospheric pressure was used for activation[3]. In our previous experiments we found that this plasma source can be very effectively used for hydrophylisation of polypropylene nonwoven and consequently immobilization of iron oxide nanoparticles[4].

Experimental

Polypropylene nonwoven (PPNW) with surface area 50 g m^{-2} were used in our research. Nanoscaled titanium dioxide (Hombitec S-100, content of TiO_2 = 88 wt.%, particle size = 15 nm, surface area = 50 $m^2 g^{-1}$) were used for coating the activated samples.

PPNW were modified by plasma treatment in nitrogen atmosphere at atmospheric pressure.

After plasma activation PPNW were coated with nano-TiO_2 from water dispersion in concentration of 5 g l^{-1} at different time (30, 45, 60 and 90 minutes) under sonication.

The surface modifications were investigated by surface analysis technique. The polypropylene surfaces before and after plasma activation and TiO_2 coating were examined by scanning electron microdcopy (SEM) and atomic force microscopy (AFM) to characterize the substrate topography. For investigation of chemical changes on plasma treated PPNW surfaces X-ray photoelectron spectroscopy (XPS) was used. According to the standard STN EN 13758-1 were measured the solar UV protective properties of unmodified PPNW and PPNW with TiO_2 coating. Using this method the permeability of UV radiation was determined.

Results

The plasma treatment alters both the topographical and chemical states of the substrate surface. Fig. 1 shows noticeable differences between standard PPNW and plasma modified PPNW. While the surface of standard PPNW is smooth, the plasma treated PP NW surface has become rough.

For identification chemical changes on plasma treated surfaces the XPS is well suited tool as it is presented on Fig. 2.

It was found that plasma activation of PPNW in nitrogen atmosphere leds to built in oxygen and nitrogen.

This is evident from spectral features of the C_{1s} region between 286 and 290 eV and O_{1s} bond (~ 533 eV) which indicates the presence of oxygen-containig functional groups. N_{1s} peak was detected at about 400 eV pertaining to the reduced type nitrogen. An electron state of titanium ion in the titanium oxide is observed in the XPS spectrum by peak at a binding energy within the range from 458 eV to 460 eV.

Both these effects, the surface roughness and functionalization, or combination of these effects positively influenced the adhesion of TiO_2 nanoparticles to the fiber surface as it can be seen in Fig. 3.

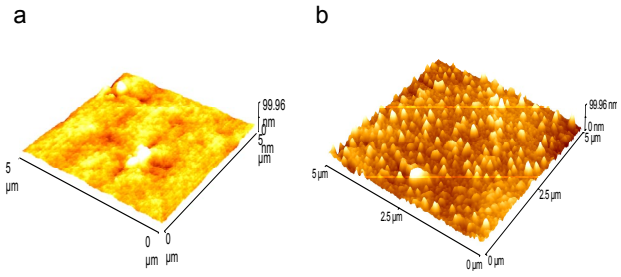

Fig. 1. **AFM images of a), standard PPNW and b), PPNW after plasma activation in nitrogen atmosphere**

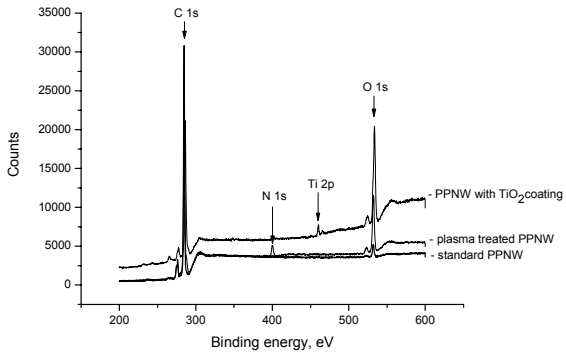

Fig. 2. **XPS spectrum of unmodified PP NW surface, PP NW after plasma modification and PP NW coated with TiO_2**

It is well known that without plasma treatment it is not possible to coat the polypropylene fiber surfaces by TiO_2.

The TiO_2 coated PP samples were washed 30 minutes in ultrasound in water to remove unlinked particles. It was found

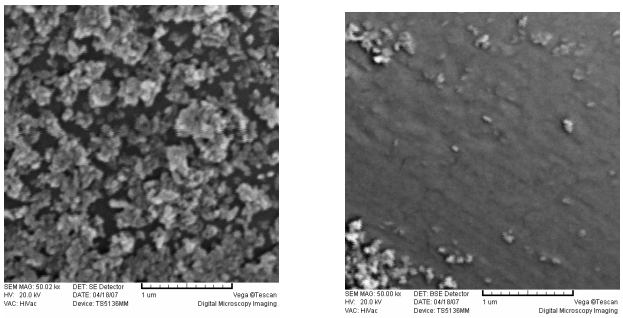

Fig. 3. **SEM images of TiO_2 coated polypropylene fibers A and polypropylene fibers coated with TiO_2 after washing in ultrasound**

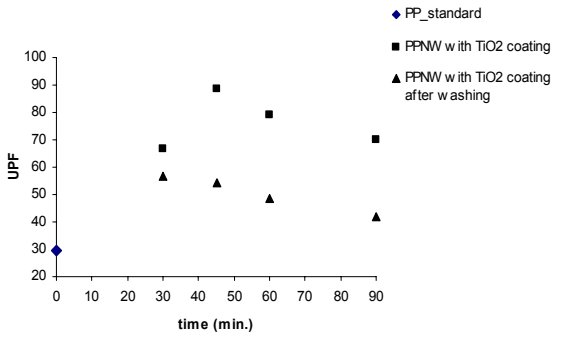

Fig. 4. **UV protective properties of standard PPNW and PPNW with TiO_2 coating subject to time of sonication during preparation of samples**

that about 40 % of TiO_2 were washed off.

Fig. 4 presents the comparison of ultraviolet protection factor (UPF) of the standard PPNW, PPNW with TiO_2 coating and PPNW with TiO_2 coating after washing in distilled water. In comparison with standard PPNW reached the UPF factor of modified textiles more than two times higher levels. Even after washing have some samples very good UV-protective properties and UPF was 50.

Conclusion

The plasma technique is an effective tool for surface modification of textile materials. The improvements in adhesion of polypropylene surfaces to nanoparticles of titanium oxides are correlated to the plasma induced chemical and physical changes on the surface. XPS surface analysis shows incorporation oxygen containing and nitrogen containing functional groups. The AFM measurements demonstrate the increasing in surface roughness after plasma activation in nitrogen.

The most part of TiO_2 are attached to the surface rather as micrometer-size aggregates. At the samples after washing out of unlinked particles, the nano TiO_2 particles were detected.

PPNW with TiO_2 coating demonstrated the very good UV protective properties.

This work was supported by Grant Agency of Slovak republic VEGA 1/4095/07, VEGA 1/ 0815/ 08 and Grant Agencyof Czech Republic KAN 101630651.
Author wishes to thank Martin-Luther University Halle-Wittenberg, Institute of Material Science, Merseburg, Germany for providing XPS measurements.

REFERENCES

1. http://www.reportbuyer.com/
2. http://www.root/cn.com/Knowledge/nano
3. Šimor M., Ráheľ J., Vojtek P., Brablec A., Černák M.: Appl. Phys. Lett. *81*, 2716 (2002).
4. Černáková Ľ., Szabová R., Wolfová M., Buček A., Černák M.: FIBRES&TEXTILES in Eastern Europe *15*, 121 (2007).

CL-06
COMPOSITION AND REDUCTION OF EMISSIONS OF PEROXIDE CROSSLINKED EPDM-ELASTOMERS*

ULRICH GIESE* and GERMAN LUCAS

Deutsches Institut für Kautschuktechnologie e. V., Eupener Str. 33, 30519 Hannover / Germany
Ulrich.Giese@DIKautschuk.de

Introduction

In order to keep the vehicle interior free of emissions and odors and to comply with the increasing environmental demands, the automotive industry and its suppliers are obliged to reduce volatile component emissions from parts used in the vehicle passenger compartment. This has resulted in high demands for high quality polymer based materials, including elastomers and thermoplastics elastomers (TPE). Alongside a high level of physicalmechanical properties and resistance to aging, a reduction in emission potential is also to be achieved[1]. This situation has been tightened by some regulations and directives[2–4]. Another problem is the so-called fogging effect, i.e. the formation of a greasy film on the inside of the windshield. Because of its light-diffusing effect it can hinder transparency and thus pose a safety risk. The fogging effect is due to the condensation of volatiles released from the polymer materials used, and is investigated for some thermoplastics and polyurethanes[5]. The emission potential of elastomers has been studied, especially under the aspect of "vulcanization fumes" in conjunction with manufacturing and processing[6,7]. A number of tests have been described for characterizing the cumulative emissions of volatile organic compounds (VOC`s). In these tests measurements are carried out on parts using elaborate test rig methods and test chambers[8–10]. These approaches, which are highly elaborate in technical terms, have the advantage of making it possible to simulate real-life situations in the passenger compartment[2,11,12]. Another approach is to use laboratory methods. The advantage of this over the test rig method is that the sample throughput is considerably higher and the cost per specimen much lower. Disadvantage is that the small specimen mass per analysis is not 100 % representative and the comparison to real article testing is less precise, on top "simulation testing" is hardly possible. The objective of the study described here is to obtain a detailed record and identification of the main constituents of the critical components of various peroxide crosslinked EPDM elastomers contributing to the fogging, odor and VOC values in comparison to a sulfur crosslinked analogue, with a trace-back to the formula constituents. The efficiency of applying a tempering processes is also investigated.

Crosslinking using Peroxides

Organic peroxides can be used for the crosslinking of rubber articles. These peroxides have, on one hand, sufficient thermal stability for the mixing process, while, on the other hand, decompose sufficiently fast within the usual vulcanization temperature range, thereby generating C-C crosslink's into the polymer matrix. As the crosslinking process commences more or less when the peroxide starts to decompose, a suitable decomposition temperature combined with the appropriate decomposition half lifetime is a key prerequisite if the rubber compound is to exhibit adequate processing reliability[13]. The general mechanism of peroxide crosslinking is

* Parts of this paper are published in. Kautsch. Gummi Kunstst. *180*, 61 (2008).

a radical mechanism[14]. The degree of crosslinking attainable with peroxides is geared primarily to the type and dosage of the peroxides and of the radical yield. The relevant radical yield for polymer crosslinking is reduced by all certain substances interfering with these formed radicals, such as, anti-aging agents or aromatic plasticizers[15,16]. On the other hand crosslinking degree can be considerably boosted by the use of so-called coagents. With a single peroxide excitation these polyvalent compounds make possible several crosslinking-effective follow-up reactions, and thus intervene in the occurrence of crosslinking[13,15,17]. On the whole the unsaturated groups of the coagent molecule make possible a star-shaped implantation into the network, by means of which the crosslinking yield is increased without releasing additional reaction products. Under the aspect of formation of low-molecular volatile reaction products, which contribute to emission, the neutralization of the peroxide radical occurring via a hydrogen abstraction from the polymer is of particular relevance. It gives rise to ketones or alcohols that can be subject to further secondary reactions. The use of multifunctional peroxides instead of coagent assisted monofunctional peroxides like dicumyl peroxide (DCP) provides good physical properties with reasonable crosslinking efficiency and comparable low emissions. The reason of this is, that multifunctional peroxides combine peroxide and coagent functionality in one molecule[23].

Experimental part

Compounds

For the assessment of the emission and fogging behavior of peroxide initiated crosslinking of EPDM materials, a sulfur-crosslinked EPDM compound was included in the study for the sake of comparison. The used compounds are listed in the following table. The peroxides are used alternatively in each case.

The products TBPC and DABT are to be classified as multifunctional peroxides[18].

The compounds are mixed in a two stage method and the vulcanization behavior was investigated by means of a torsional shear rheometer according to DIN 53529/2 at a vulcanization temperature of 180 °C.

Preparation of specimen

The 2 mm test plates were prepared by means of vulcanization in the press at 180 °C isotherm for a vulcanization time of t_{90}. The well-tempered specimens were left for two hours in a air circulating cabinet at 120 °C.

Methods for characterizing emissions behavior

The cumulative fogging value is established analogous to DIN 75201-B. The individual used temperatures are 80/100/120 ± 1 °C.

For detailed identification of individual substances thermodesorption analysis (TDS) to VDA 278 was used alongside GC-MS and FT-IR spectroscopic analysis of the condensates of the DIN-fogging test.

Table I
Composition of the EPDM compounds

components	sulfur phr	peroxide phr
EPDM, ENB-type	100	100
Paraffinic mineral oil	30	30
Carbon black (N550)	35	35
Zinc oxide	4,0	-
Stearic acid	2,0	-
Sulfur	0,7	-
TBBS	1,0	-
TBzTD	3,5	-
DHBP	-	3,3
TBPC	-	4,0
TBPTC	-	9,0
DCP	-	4,5
DABT	-	10,0

Abbreviations:

DHBP 2,5-dimethylhexane-2,5-di-tert. butyl peroxide
DIPP 1,4-bis (tert. butylperoxiisopropyl)-benzene
TBPC tert. butyl-3-isopropenylcumylperoxide [1]),
TBPTC 1,1-bis (tert.butylperoxy)-3,3,5-trimethylcyclohexane
DCP dicumylperoxide
DABT 2,4-diallyloxy-6-tert. butylperoxide-1,3,5-triazine[2]),
TBzTD tetrabenzyl thiuram disulfide
TBBS tert. butylamine benzthiazol sulphenamide

[1)]contains 80 % TBPC and 20 % DIPP as byproduct from processing, not available commercially, experimental product, multifunctional
[2)]contains 10 % triallylcyanurate (TAC) as byproduct, not available commercially, experimental product, multifunctional

As VOC value (VOC = volatile organic compounds) to VDA 278, the sum of the highly to moderately volatile substances in the boiling and elution range up to eicosane is given as toluene equivalent. The FOG value determined from the same sample is the sum of the not easily volatized substances eluting from the retention time of *n*-hexadecane onwards. This is calculated as a hexadecane equivalent.

Results

Fig. 1 plots the maximum torque values of the rheometer measurements in relation to molar concentrations of the added peroxides. As would be expected, all peroxides investigated

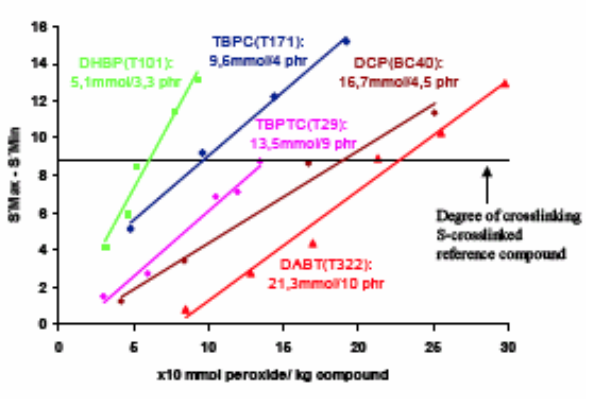

Fig. 1. **Crosslinking efficiency of the peroxide systems used**

show a linear rise in crosslinking density as peroxide concentration increases. The slopes of the lines represent the different crosslinking efficiencies of the peroxide systems used. The bifunctional peroxide DHBP shows the highest crosslinking efficiency, while DCP as monofunctional peroxide exhibits the lowest. The low efficiency of 1,1-Bis (*tert*. butylperoxy)-3,3,5-trimethylcyclohexane is possibly professed by the untypical high crosslink temperature for this peroxide. Recommended processing temperature is 145 °C only. The relatively high concentration needed in the case of the crosslinker DABT – 210 mmol kg^{-1} compound – is striking insofar as it contains a co-activator as byproduct.

The fogging values were determined according to DIN 75201/B at 80 °C, 100 °C and 120 °C. Specifications of approx. 1 mg condensate per 1 g vulcanizate at a test temperature of 100 °C serve generally as reference value for the evaluation of emissions as per the fogging test. In terms of low emission and simultaneously acceptable mechanical values for tensile strength and elongation at break, studies of the emission behavior of EPDM vulcanizates crosslinked with mono-, bi- and multifunctional peroxide systems in comparison to a typical sulfur system for EPDM profiles show that especially the systems TBPC (multifunctional) and DHBP (bifunctional) produce good results, even if they do not quite equal the VOC and FOG or mechanical values attained by the sulfur reference vulcanizate. In the case of TBPC most emissions originate from the byproduct DIPP and not from the main component TBPC. So this new developed product looks promising, but there is a necessity of optimization in purity! For the system crosslinked with DHBP in particular, some of the emission values measured were lower than for the sulfur reference vulcanizate, although DHBP has the highest permol emissions when compared to the other peroxides. However when the vulcanizates are standardized so as to have an approximately uniform crosslinking density, DHBP benefits from its high crosslinking efficiency, i. e. the molar concentration needed in the rubber compound is relatively low. Despite low crosslinking efficiency, the multifunctional system DABT containing small quantities of TAC as byproduct, which can react as co-activator displays good emissions behavior. This is due to its complex reaction mechanism with few cleavage products only.

Quantitative evaluations of the TDS-GC-MS analyses analogous to VDA 278 result in the cumulative values in the following figure. The VOC values are given as toluene equivalent corresponding to the retention times and calibration, the FOG values are given as hexadecane equivalent. With regard to the evaluation of results it is to be noted that the accepted industrial specifications are usually 100 µg/g for the VOC value and 250 µg/g for the FOG value.

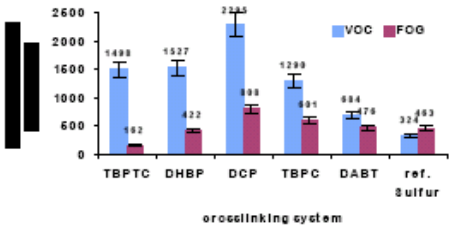

Fig. 2. **TDS analysis to VDA 278 for the vulcanizates optimized after rheometry with different peroxide**

In all emissions values, the mono-functional peroxide DCP shows comparatively high values, both in the fogging test to DIN 75201-B and in TDS-GC-MS analyses for determination of the FOG value and the VOC value analogous to VDA 278. Due to the high volatility of peroxide decomposition products in general, tempering is very effective in reducing the value to approx. 20 % of the level at outset.

The authors would like to thank the Deutsche Kautschuk Gesellschaft (DKG e.V.) for the project organization and the companies Akzo Nobel Polymer Chemicals, WOCO AVS GmbH, Daimler Chrys-ler AG, Paguag GmbH & Co., Dr. Ing. h.c. F. Porsche AG, Meteor Gummiwerke K. H. Bädje GmbH & Co., Opel GmbH for the financial support and for providing materials.

REFERENCES

1. Schmidt H.-J., Lüßmann-Geiger H.: Gefahrstoffe-Reinhaltung der Luft *43*, 56 (1996).
2. California Environmental Protection Agency Press Release 98−69, 5th November 1998.
3. Directive 70/156/EWG und 70/2220/EWG.
4. Geier M., Thiel W.: ATZ Automobiltechn. Zeitschrift *12*, 98 (1996).
5. Munz R., Fass U., Kurzmann P., Leitz R., Meister C.: Automobiltechn. Zeitschrift *238*, 96 (1994).
6. Zietlow J.: *Thesis Universität*. Hannover 1993.
7. Will T., Giese U.: Kautsch. Gummi Kunstst. *200*, 49 (1996).
8. Bauhof H., Zietlow J., in: *Emissionen im Kraftfahrzeuginnenraum*, BMBF-FAT, 51, (1998).
9. Meyer U., Möhle K., Eyerer P., Maresch L.: Staub-Reinhaltung der Luft *137*, 54 (1994).
10. Bauhof H., Wensing M., Zietlow J., Möhle K., Sonderausg. 25 Jahre FAT, Automobiltechn. Zeitschrift, 37.
11. Geier M., Thiel W.: Automobiltechn. Zeitschrift *678*, 98 (1996).
12. Research Project: BMBF, FKZ: 07 INR 27A8, FKZ: 07 INR 27 B0.

13. Hofmann W., Gupta H.: *Handbuch der Kautschuktechnologie*. Dr. Gupta Verlag, 44.
14. Keller R. C.: Rubber Chem. Technol. *240*, 61 (1988).
15. Dikland H. G., Maag L. R., Wommelsdorff R.: Kautsch. Gummi Kunstst. *176*, 52 (1999).
16. Loan L. D.: Rubber Chem. Technol. *140*, 40 (1967).
17. Dikland H. G., Hulskotte R. J. M., Does L. v. d., Bantjes A.: Kautsch. Gummi Kunstst. *608*, 46 (1993).
18. Naskar K., Noordermeer J. W. M.: Kautsch. Gummi Kunstst. *235*, 57 (2003).

CL-07
A LABORATORY UNIT FOR SCRAP TIRE PYROLYSIS

JUMA HAYDARY, ĽUDOVÍT JELEMENSKÝ, and JULIUS ANNUS

Institute of Chemical and Environmental Engineering, Faculty of Chemical and Food Technology, Slovak University of Technology, Radlinského 9, 812 37 Bratislava
juma.haydary@stuba.sk

Pyrolysis offers an environmentally and economically attractive method to transform waste tires into useful products and energy. In a pyrolysis reactor, shredded tyres are decomposed into pyrolysis products received in all three phases: solid char (30–40 wt.%), liquid oil (50–60 wt.%), and gases (3–20 wt.%) [1,2]. Distribution of material into the pyrolysis yields and composition of individual fractions depends not only on the composition of the rubber material, but also on the pyrolysis technique and process conditions applied. Temperature, heating rate, hydrodynamic conditions; catalyst and particle size are the main factors affecting the amount and composition of the pyrolysis yields.

A laboratory unit for pyrolysing shredded scrap tire was established; a scew type flow reactor being the main element of this unit. The system enables studying of the influence of various parameters on the amount and quality of pyrolysis products and provides a wide range of experimental arrangements.

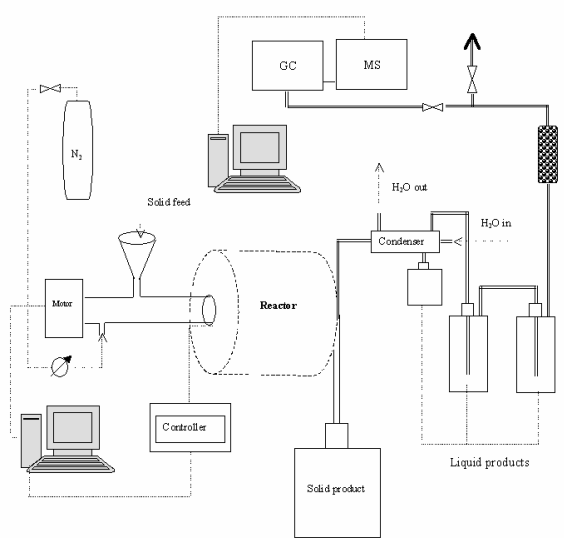

Fig. 1. **Laboratory pyrolysis unit**

The experimental set up shown in Fig. 1 aims at the maximization of the possibility of studying the influence of different factors on the pyrolysis process. The particles of scrap tires are fed into the system using a feeder. Then, the particles are passed through the reactor using a screw. The residence time of the particles in the reactor is controlled by the frequency cycle of the screw. The screw is moved by an electric stepping motor controlled by a regulator and a PC.

The reactor is heated electrically by a tube furnace. The reactor temperature is controlled by a PID controller and a software. Inert atmosphere in the reactor is achieved by nitrogen flowing trough the reactor in the same direction as the solid material. The flow of nitrogen is measured by a flowmeter. Passing through the reactor, rubber particles are decomposed. The volatiles are removed from the reactor at high temperature and they are led to a condenser. The solid residue is removed from the end of the reactor and collected in a jar.

Fields of application: The laboratory pyrolysis unit developed in the frame of our research project enables the realization of a number of different applications directly or indirectly after the treatment of pyrolysis products. The most important areas of its use are:

- Amount and composition of all pyrolysis products
- Influence of process conditions on the amount and quality of pyrolysis products
- Characterization of pyrolysis solid product; use of produced pyrolytic carbon black (CBp) for measurements of its specific surface area, pore structure and other characteristics; use of CBp in rubber compounds and measurement of mechanical properties of prepared rubber compounds; further treatment of produced carbon black by their activation to active carbon and measurement of adsorption parameters.
- Characterization of pyrolytic gases; amount, composition, energy value
- Characterization of pyrolytic liquid product; amount, composition, physical characteristics, characterization as liquid fuel, distribution range of molecular weight.
- Measurement of kinetic parameters of the release of individual components
- Experimental verification of the process mathematical model.

Optimization of the Ranges of operational parameters: One of the most important process parameter is pyrolysis temperature. As it is shown on Fig. 2, thermogravimetric (TG) analysis of scrap tire provided by us and also by various other authors[3–5] indicate that the thermal decomposition of rubber vulcanizates starts at a temperature of around 250 °C and finishes at temperatures around 550 °C. Based on these studies the non-catalytic pyrolysis of scrap tires at temperatures under 550 °C is not recommended.

At higher temperatures the residence time of the tire in the reactor can be reduced. At the same time the higher temperatures cause more development of the pore structure of pyrolytic carbon black which is an advantage for their using

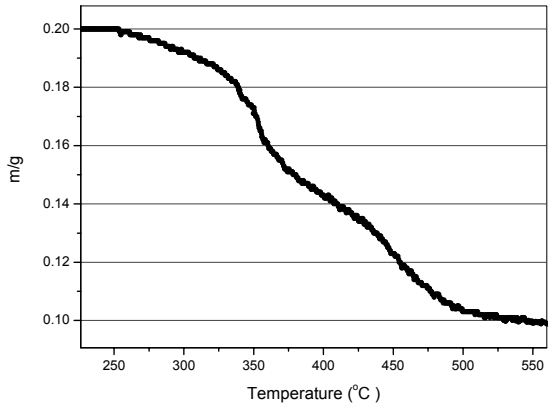

Fig. 2. **TG curve of scrap tire thermal degradation**

as reinforcement or adsorbents. However, pyrolysis at higher temperatures results into increasing of gas to liquid ratio, energy consumption and requirement for higher quality of equipment materials. The time needed for total conversion of the tire in the reactor depends on reactor temperature, residence time, particle sizes and heat and mass transfer conditions in the reactor.

The advantage of screw type flow reactor is in very good heat and mass transfer conditions. The tire particles with average sizes of 3 mm were pyrolyzed at isothermal conditions in the system described above. A residence time of only 3 min. was set. Different pyrolysis temperatures from 500°C to 800°C were used. The reaction conversion was tested by thermogravimetric analysis of the solid product. Figure 3 shows the TG curves of the pyrolytic chars that were received by tire pyrolysis at different temperatures.

At 500 °C and a residence time of 3 minutes (curve 1) the reaction was not finished. Around 12 % of the solid char that has created 35 % of the fed scrap tire was lost during the thermogravimetric analysis. The reaction conversion in pyrolytic reactor at this conditions was 93.5 %. However, at 600 °C the reaction conversion was 98 % and at 800 °C 99.5 %.

At a temperature of 550 °C a conversion of 100 % was achieved using a residence time of only 5 min. Fig. 4 shows the TG curve of the solid product produce at the mentioned conditions.

The developed pyrolytic unit enables working at pressures up to 100 kPa above the atmospheric. Usually the system works at a pressure slightly above the atmospheric, because of insuring the inert atmosphere in the reactor.

Particle size is another important parameter that can influence the amount and quality of pyrolytic products. The system enables the use of particles with sizes from 0.1 to 10 mm. Influence of particle size on reaction conversion was investigated. Naturally by increasing the size of particle the time needed for reaction increases.

The unit provides also the possibilities such as:

– partial oxidation or gasification of scrap tire,
– connection of a secondary gas pyrolysis reactor (catalytic or non catalytic),
– connection of other post pyrolytic treatment equipment.

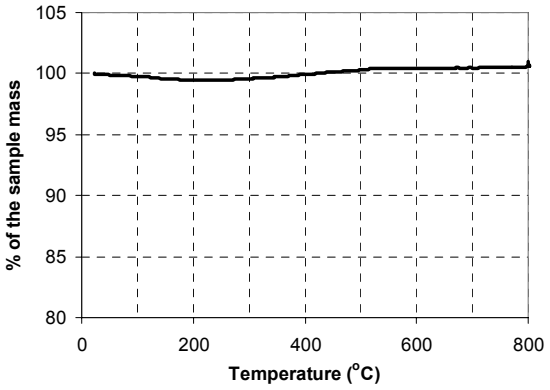

Fig. 4. **TG curve of the solid product produced at 550 °C and residence time 5 min**

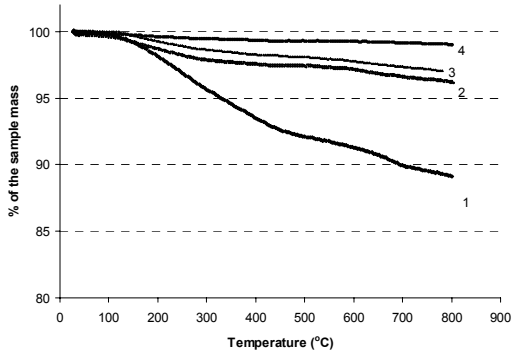

Fig. 3. **TG curves of solid products received by pyrolysis of scrap tire at different temperatures,** residence time: 3 min, 1 − 500 °C, 2 − 600 °C, 3 − 700 °C, 4 − 800 °C

This work was supported by the Grant VEGA No. 1/4446/07 from the Slovak Scientific grant Agency.

REFERENCES

1. Juma M., Koreňová Z., Markoš J., Annus J., Jelemenský Ľ.: Petroleum and Coal *48* (1), 2006.
2. Koreňová Z., Juma M., Annus J., Markoš J., Jelemenský Ľ.: Chemical Papers *60*, 422 (2006).
3. Leung D. Y. C., Wang C. L.: J. Anal. Appl. Pyrolysis 45, 153 (1998).
4. Berrueco C., Esperanza E., Mastral F. J., Ceamanos J., Garc ´a-Bacaicoa P.: J. Anal. Appl. Pyrolysis *73*, 65 (2005).
5. Chen K. S., Yeh R. Z., Chang, Y. R.: Combust Flame *108*, 408 (1997).

CL-08
DEVULCANIZATION AS AN OPPORTUNITY TO RECYCLE RUBBER

MAREIKE HESS, HARALD GEISLER, and ROBERT H. SCHUSTER

German Institute for Rubber Technology e.V., Eupenerstraße 33, 30519 Hannovert
Mareike.Hess@DIKautschuk.de

How to reduce rubber waste? There are several options to reduce rubber waste. A well known method is to burn the rubber waste to produce energy while producing cement. This kind of "recycling" has to be reduced in future. Due to its irreversible network, the different compounds and ingredients the recycling of rubber is not comparable with the recycling of plastics. In most cases the methods of recycling show unsatisfactory results for reuse. The "recycled" rubber crumb is typically used as an inactive filler for simple undemanding products. The aim of this research project is to produce recycled rubber which can be used without any additional ingredients.

Introduction

Devulcanization provides an opportunity to recycle rubber. It is the opposite of vulcanization. Thus, it is a process, which opens di- and polysulfidic bonds of sulphur-vulcanized rubber. Due to their high bonding energy it is impossible decomposing monosulfidic bonds yet. Ideally, it is possible to reuse a completely devulcanized elastomer without any other additionals.

There are several processes to devulcanize: mechanical, chemical, mechanic-chemical, biological and with the help of microwaves or ultrasonic. The chosen mechanic-chemical method has the advantage of being highly efficient, rapid and technically applicable.

The effectiveness of the devulcanizing chemicals is first investigated using squalene as a model compound, to replace polyisoprene rubber. Afterwards the chosen promising chemicals are tested in mechanic-chemical devulcanization of sulphur vulcanized polyisoprene rubber.

The mechanism of devulcanization of sulphur-vulcanized polyisoprene rubber with amines or disulphides can occur radical[1−3]or ionic[4].

After devulcanization the devulcanized rubber or mixtures which contain devulcanized rubber can be revulcanized. Physical properties of revulcanizates are measured and compared with those of the start-vulcanizates.

Experimental

The first step is to find a devulcanizing agent. Therefore networking and depolymerisation were accomplished with a model molecule used to mimick polyisoprene rubber. These molecules e.g. squalene

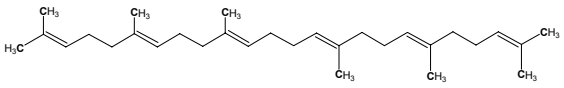

have a lower moleculare mass. Because of this attribute the substances are liquid and thus much easier to handle and analyse. With the aid of sulfur and an accelerator squalene was crosslinked. The curing in an autoclave (Fig. 1) took 60 minutes at 150 °C under nitrogen atmosphere and continuos stirring. The desulfuration was carried out through adding equimolare masses of different devulcanizing agents and again stirring for 60 minutes at 150 °C.

The best desulfurating agents were chosen to accomplish the rubber recycling by the mechanic-chemical method of devulcanization. Vulcanizated polyisoprene rubber was recycled using the internal mixer shown in Fig. 2 adding so-called devulcanizing agents.

Therefore the vulcanizate was reduced into small pieces. The internal mixer was filled with the rubber crumbs and the

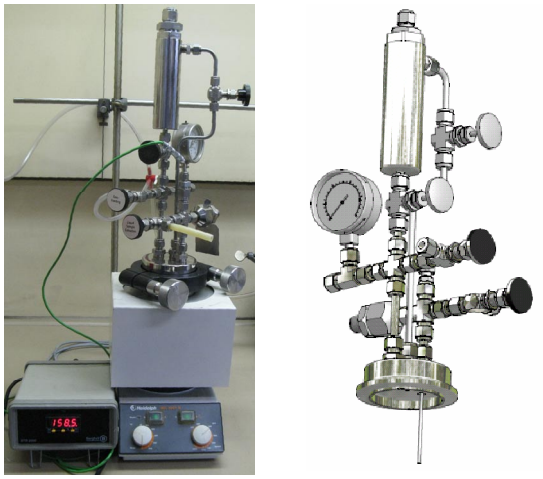

Fig. 1. **Autoclave, used to accomplish the model networking and desulfuration**

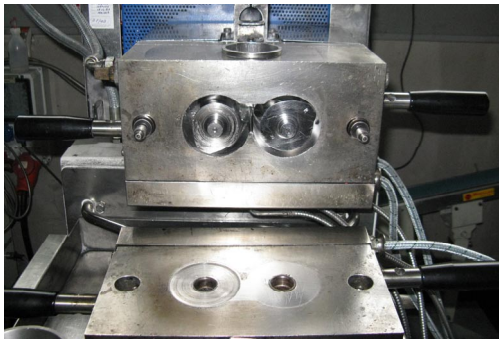

Fig. 2. **Internal mixer, used to accomplish the mechanic-chemical method of devulcanization**

devulcanizing agent. Through variation of temperature, mixing time, rotation speed, concentration of the devulcanizing agent, particle size and filling degree the rubber was going to be devulcanized[5].

Analytics and Results

During curing and desulfuration in the autoclave samples were taken to measure the distribution of their molar mass by GPC. Ideally after cross-linking the samples have multiple masses of squalene and after desulfuration again the mass of only one molecule of squalene. Fig. 3 shows the distribution of molar mass measured by GPC and with it the efficiency of different tested desulfuration agents.

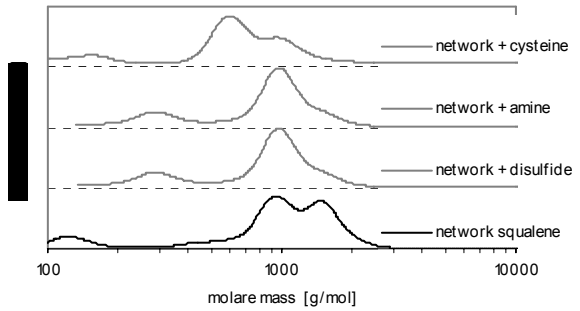

Fig. 3. **Distribution of molar mass measured by GPC to show the efficiency of different desulfuration agents**

Before desulfuration the samples had two, three and four times the molecular mass of squalene. After devulcanization with an amine or disulfide their molecular masses counted the twice mass of squalene. With the help of a cysteine the molecular mass of the desulfuration product almost had the molecular mass of only one molecule of squalene.

To compare the effectiveness of the three chemicals the following devulcanization experiments were done using these three chemicals.

After devulcanization in the internal mixer the viscosities of all samples were checked. To optimize the procedure the results are compared with the viscosity of the original polymer and the pure mechanical devulcanizates as can be seen in Fig. 4.

With the aid of IR measurements it was possible to confirm the preservation of the double bond character.

Furthermore GPC measurements followed to get informations about the distribution of the molar mass and with it also about the efficiency of tested devulcanizing agents.

Promising samples were mixed in different parts with the respective fresh polymer. Cross-linking agents were added and the mixtures were revulcanized. Their revulcanizing properties as well as their physical properties, i.e. stress-strain measurements, were measured and compared with the datas of the respective original vulcanizate.

In Fig. 5 the results of measuring the hardness Shore A and the swelling degree of the revulcanizates are shown. If the hardness is lower, the swelling degree increases because the

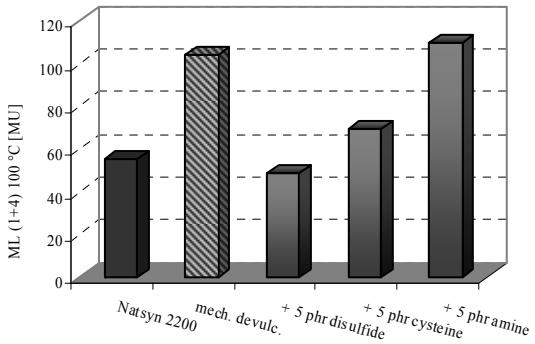

Fig. 4. **Mooney Viscosity after devulcanization at 150 °C in the internal mixer**

network density is lower as well. The results are compared with the original vulcanizate. The properties do not differ that much. Only the revulcanizate which contains devulcanizate decomposed with the help of a disulfide didn`t achieve the same properties.

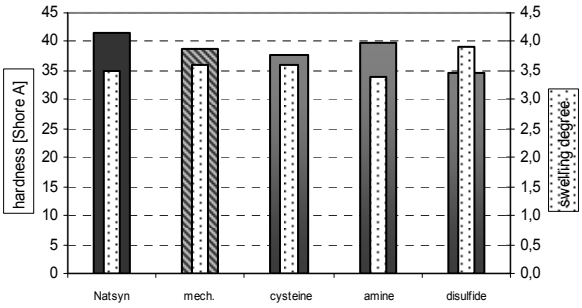

Fig. 5. **Hardness Shore A and swelling degree of some revulcanizates in comparison with the start-vulcanizate**

Stress-strain curves are graphical representations of the correlation between stress, derived from measuring the load applied on the sample, and strain, derived from measuring the deformation of the sample. The following diagram illustrates the stress-strain behaviour of the original vulcanizate and the revulcanizates.

Comparing the properties of the revulcanizates with the original vulcanizate and with it the effectiveness of the devulcanization and followed revulcanization, the use of a cysteine as a devulcanizing agent shows the best results. The following TEM pictures were used to see the distribution of the cysteindevulcanizate and the fresh polymer in the revulcanizate. To be able to distinguish between fresh polymer and devulcanizate, two phr carbon black were added the fresh polymer before mixing with the devulcanizate. The carbon black agglomerates show the parts with fresh polymer and the brighter parts with darker pieces inside show domains with cystein-

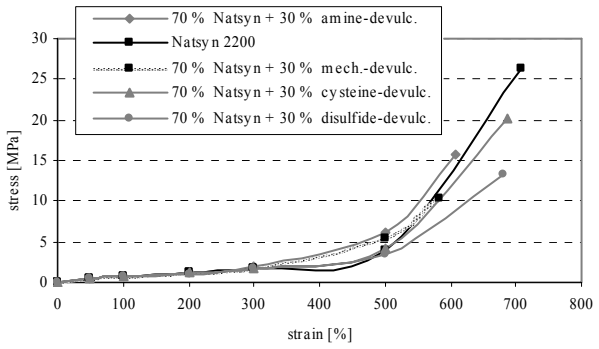

Fig. 6. **Stress-strain measurements of some selected revulcanizates what contain 30 % of different devulcanizates**

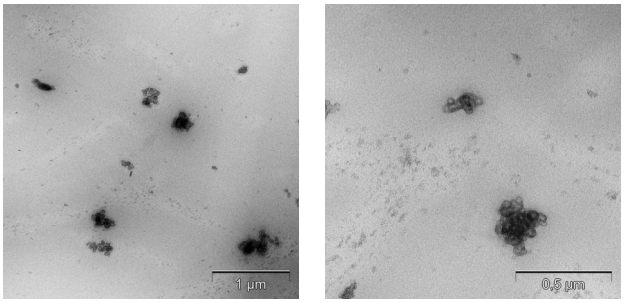

Fig. 7. **Transmission-Electron-Microscope (TEM) pictures of a revulcanizate which contains 30 % of cysteine-devulcanizate**

devulcanizate. The size of the domains are about one micrometer indicating a good intermixture.

Conclusions

Doing desulfuration measurements in an autoclave is a good opportunity to find out which chemicals are able to decompose a sulfur network and with it sulfidic bonds. Mechanic-chemical devulcanization is more effective than mechanical devulcanization. Revulcanizates including 30 % devulcanizate and 70 % polymere show promising results in physical properties.

Outlook

Ideally it will be possible to find out the mechanism of desulfuration and with it also the mechanism of devulcanization. Therefore it will be important to find out which products instead of the de-cross-linked network are produced during desulfuration / devulcanization. Furthermore it will be possible to clarify the kind of sulfidic bonds not only in (re-) vulcanizates by thiol-amine-methode also in liquid model-networks. Therefore de-cross-linked and re-cross-linked model molecules have to be analysed by means of NMR, HPLC[6], GCMS, IR and further GPC measurements.

The financial support of Schill & Seilacher, Oerlikon Accotex Texparts, Gummiwerk Kraiburg and Ellerbrock Runderneuerung is acknowledged.

REFERENCES

1. Kende I., Pickering T. L., Tobolsky A. V.: J. Am. Chem. Soc. *87*, 5582 (1965).
2. Pickering T. L., Saunders K. L., Tobolsky A. V.: J. Am. Chem. Soc. *89*, 2364 (1967).
3. Pickering T. L., Saunders K. J., Tobolsky A. V., in: *The Chemistry of Sulphides*, (Tobolsky A. V., ed.). pp 61. Interscience Publishers, New York 1968.
4. Milligan B.: Rubber Chem. Technol. *39*, 1115 (1966).
5. Kohler R., O, Neill J.: GAK *51*, 432 (1998).
6. Dierkes W., Rajan V., Noordermeer J. W. M.: KGK *58*, 312 (2005).

CL-09
IMPROVEMENT OF MECHANICAL AND TERMOMECHANICAL PROPERTIES OF POLYETHYLENE BY IRRADIATION CROSSLINKING

ZDENEK HOLIK[a], MIROSLAV MANAS[b], MICHAL DANEK[c], and JIŘÍ MACOUREK[a]

[a] Tomas Bata University in Zlin, Faculty of Technology, Department of Production Engineering, TGM 275, 762 72 Zlin, Czech Republic, [b] Tomas Bata University in Zlin, Faculty of Technology, Department of Production Engineering, TGM 275, 762 72 Zlin, Czech Republic, [c] BGS Beta – Gamma GmbH & Co.KG. – Service, Wiehl, Germany
holik@ft.utb.cz, manas@ft.utb.cz, danek@bgs.eu,

Abstract

The main objective of the study is investigation of mechanical and termomechanical properties of polyethylene. These properties were examined in dependence on the dosage of the ionizing electron beam (beta) radiation. Non-irradiated samples and those irradiated by dosage 15, 30, 45, 66, 99, 132, 165 and 198 kGy were compared.

Radiation cross-linking of polyolefin's results in increased mechanical strength, heat resistance, and breakdown voltage, and improved insulation properties, particularly at high temperatures.

Introduction

Radiation modification of materials refers to the production of beneficial changes by exposure to radiation. High-energy (ionizing) radiation is used most often to modify polymers. Irradiation crosslinking is the one of possible method how to get the required quality and it is a process

whereat it can be optimised properties of standard or engineering polymers and impart to them mechanical, thermal and chemical properties of high performance polymers. The main group presents standard polymers and it is the most considerable one and it is share in the production of all polymers is as high as 90 %. The engineering polymers offers much better properties in comparison with standard polymers. The production of these types of polymers takes less than 10 %. High performance polymers have the best mechanical and thermal properties but the share in production and use of all polymers is less than 1 %.

The most common forms of radiation employed are electromagnetic (gamma) radiation from the radioisotopes cobalt-60 and celsium-137, and electron beams (beta) generated by electron accelerators. Radiation processing covers use those beta or gamma radiations to break up bonds between atoms. Consequently, free radicals rise in materials that react with one another during chemical reactions (Fig. 1). The main difference between beta and gamma rays lies in their abilities of penetrating the irradiated material. Gamma rays have a high penetration capacity. The penetration capacity of electron rays depends on the energy of the accelerated electrons (Fig. 2 and Fig. 3)[1].

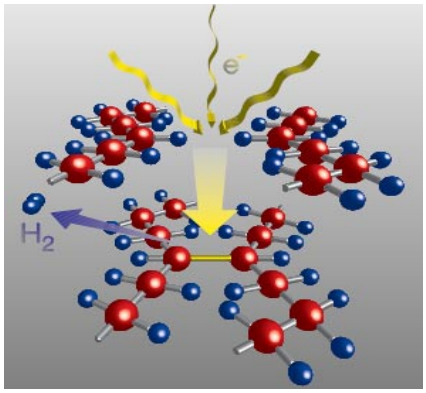

Fig. 1. **Scheme of irradiation crosslinking[2]**

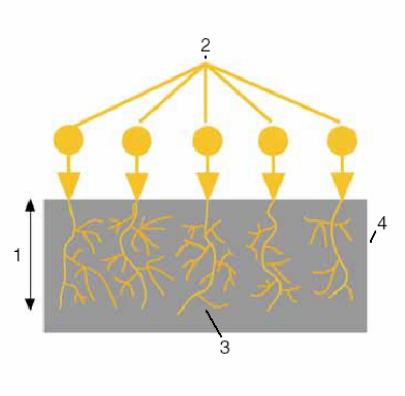

Fig. 2. **Design of Electron rays[2],** 1 – penetration depth of electron, 2 – primary electron, 3 – secondary electron, 4 – irradiated material

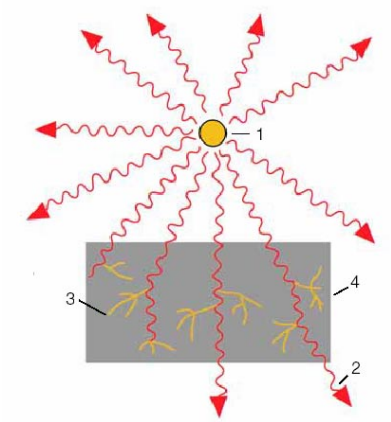

Fig. 3. **Design of Gamma rays[2],** 1 – encapsulated Co – 60 radiation source, 2 – Gamma ray 3 – secondary electrons, 4 – irradiated material

Experiment

The samples were prepared on the injection moulding machine (ARBURG ALLROUNDER 420 C 1000-350).

The materials of the all samples were polyethylene (PE), provided by The Dow Chemical Company:

– DOW HDPE 25055 E
– DOW LDPE 780 E

Processing conditions during the injection moulding were according to the recommendation of the producers.

All samples were irradiated with electron rays (electron energy 10 MeV, dosis: 15, 33, 45, 66, 99, 132, 165 and 198 kGy) in the firm BGS Beta Gamma Service GmbH & Co, Saal am Donau – Germany.

The following tests were carried out and equipment used:

– Tensile test, according to standard CSN EN ISO 527-1, 527-2 were carried out on tensile machine ZWICK 1456. Used rate: LDPE – 50 mm min^{-1}; HDPE – 50 mm min^{-1}. Test data was processed by Test Xpert Standard software and modulus (E [MPa]), tensile stress (σ_t [MPa]) were determined.
– TMA test (Thermal mechanical analysis) was carried out on Perkin – Elmer Thermal.

Results

Comparison of tensile strength and E – modulus (at 23 °C) of high-density polyethylene (HDPE) and low-density polyethylene (LDPE) before and after irradiation is given in the Fig. 3 and Fig. 4. It is evident that crosslinking improves the tensile strength (σ_t) and E – modulus of both PE.

The irradiation has a positive effect on tensile strength (σ_t) – both irradiated polyethylenes have reached higher value of tensile strength than non-irradiated polyethylene. After irradiation it is higher nearly by 10 % in case of LDPE and by 5 % in case of HDPE. However, as can be seen from Fig. 3, the highest value of doses does not mean a highest value of tensile strength.

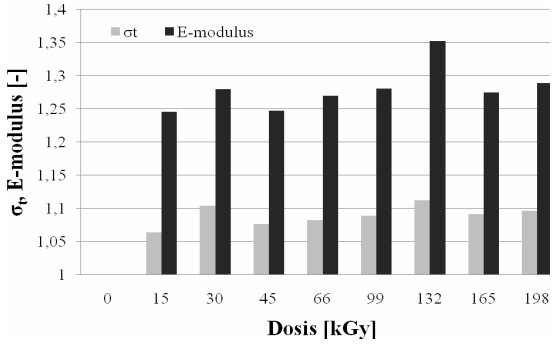

Fig. 3. **Comparisons of tensile strength and E – modulus of LDPE – 23 °C**

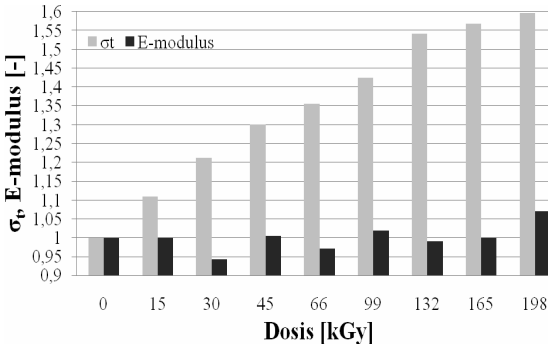

Fig. 5. **Comparisons of tensile strength and E – modulus of LDPE – 100 °C**

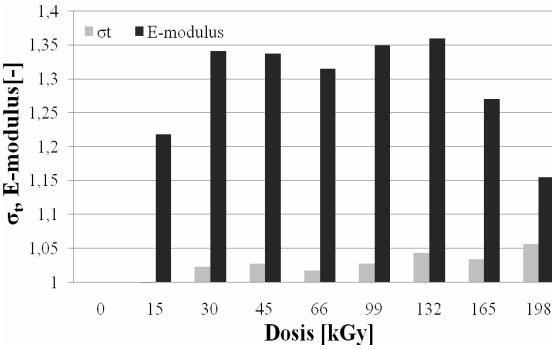

Fig. 4. **Comparisons of tensile strength and E – modulus of HDPE – 23 °C**

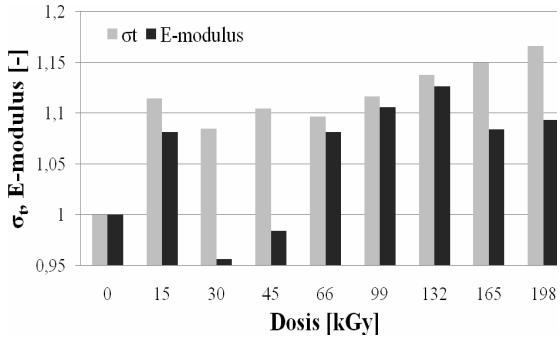

Fig. 6. **Comparisons of tensile strength and E – modulus of HDPE – 100 °C**

The irradiation has also a positive effect on E-modulus of both polyethylenes. After irradiation it is higher nearly by 30–35 % in case of LDPE and by 35 % in case of HDPE.

A positive effect of irradiation on tensile strength is much higher at 100 °C than at 23 °C but for LDPE only. After irradiation it is higher nearly by 60 % in case of LDPE irradiated by doses 198 kGy and by 10 % in case of HDPE. On the other hand, E – modulus does not increase significantly in case of both polyethylenes.

Finally, thermal stability of both irradiated polyethylenes increases with dosages. Fig. 7 and 8 show the thermal stability given as the position of a probe of irradiated LDPE and HDPE. The graph has eight curves. Each curve represents one dosage. The graph shows that the thermal stability of irradi-

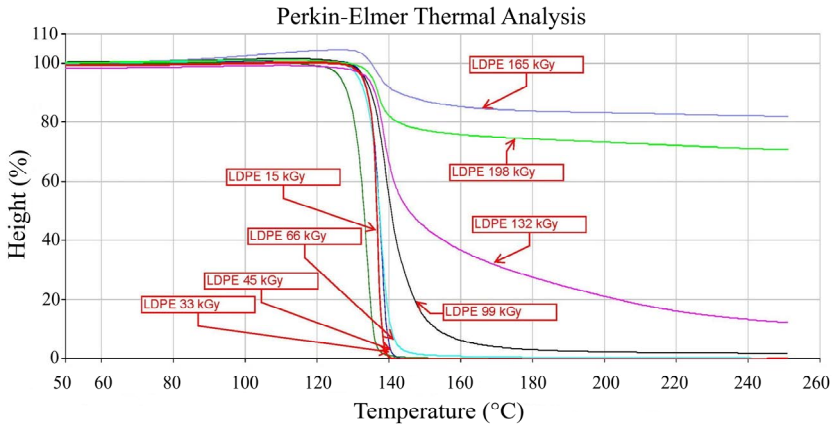

Fig. 7. **Results of thermal stability of LDPE**

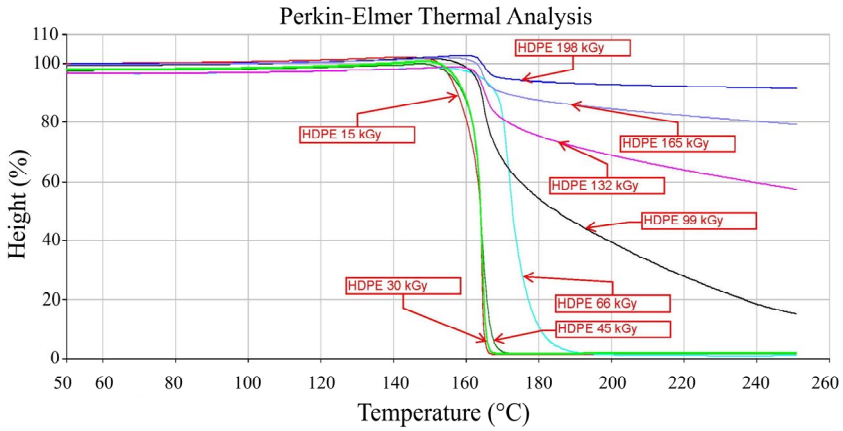

Fig. 8. **Results of thermal stability of HDPE**

ated LDPE (in case of dosage 165 kGy) and HDPE (in case of 198 kGy) are thermally stable up to 250 °C.

Conclusion

From the results of tests it is evident, that irradiation crosslinking improve the mechanical properties of each polyethylene. The improvement is more considerable in case of higher temperature (100 °C), in addition LDPE and HDPE show the greatest changes in thermomechanical properties.

That is a consequence of creation of cross-link (during irradiation crosslinking) and protraction of macromolecular string, which is than more flexible during thermal load than shorter macromolecular strings.

This article is financially supported by the Czech Ministry of Education, Youth and Sports in th R&D project under the title of 'Modelling and Control of Processing Procedures of Natural and Synthetic Polymers', No. MSM 7088352102.

REFERENCES

1. Woods R. J.: *Applied Radiation Chemistry: Radiation Processing*, 1994, ISBN 0-471-54452-3.
2. http://www.bgs.com/
3. http://www.pts-marketing.de/
4. Mańas D.: Improvement of Plastic Properties, Inter. Sci. J., www.archivesmse.org

CL-10

ARAMID REINFORCEMENT FOR LOW WEIGHT, LONG SERVICE LIFE AND FUEL SAVING

GERARD VAN DEN HONDEL

Elastomer Reinforcements, Teijin Aramid BV, Westervoortsedijk 73, NL-6827 AV Arnhem gerard.vandenhondel@teijinaramid.com

The automotive industry grew very rapidly in Central Europe, leading to large supply opportunities for local rubber parts producers. Aramids are para-crystalline materials for yarns with very high strength to weight ratio (tenacity):

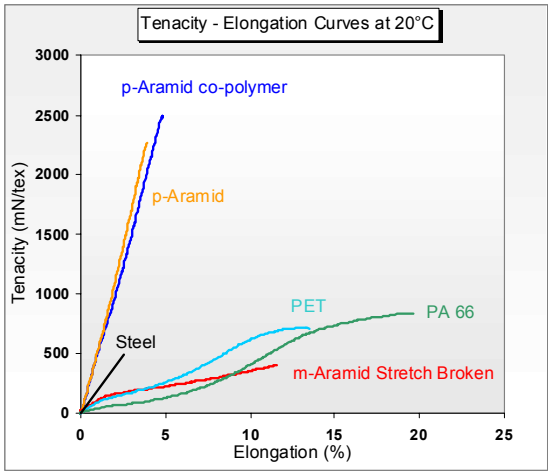

With aramid reinforcement it is possible to make many high performance automotive rubber parts:

1. radiator hoses – must withstand severe loads and conditions like heat, automotive fluids on the in- and outside, pressure and vibrations. Using aramid fibre reinforcement in knitted form gives large freedom of design for radiator hoses that withstand these severe conditions.
2. turbo hoses – these face even tougher conditions on tem-

perature, pressure and vibrations/dynamic loads. Aramids have an excellent track record in turbo hoses. They are especially suited for the next generation turbos with increased operating temperatures.

3. transmission-belts – these transfer strong, dynamic forces. Working life is much extended with aramid fibre as they have high modulus, strength and reduce belt abrasion. Belts and pulleys can be constructed smaller to save weight and space.
4. tires – need low weight reinforcement that is both flexible to withstand the continuous change of shape of rolling tires and strength and stiffness for predictable deformation and force transfer.
5. low rolling resistance tires – with chemically modified aramid short fibres, the heat build up in a filled rubber is significantly reduced, leading to substantially lower fuel consumption, longer life and lower wear.

The car industry in Central & Eastern Europe is looking for suppliers close to its plants. Using aramids to develop and manufacture high performance rubber products offers superb chances for local producers to supply to the automotive industry.

CL-11
STRUCTURE AND PROPERTIES OF POLYESTER FIBERS FROM DMT AND TEREPHTHALIC ACID FOR RUBBER INDUSTRY

M. JAMBRICH[a], J. ROSA[b], O. JAČANIN[b], K. ŠČASNÍKOVÁ[a], and M. BEČAVEROVÁ[a]

[a] *Faculty of Industrial Technologies, TnU AD Púchov,*
[b] *Kordtrade, s.r.o. Senica*

The work is aimed at preparation and evaluation of structure and basic utility properties of high-modulus, low-shrinkage polyester technical fibers prepared from different initial raw materials, DMT and terephthalic acid (PTA), produced by continuous spin-draw process. The evaluation of PET technical fibers was centered on physical-mechanical properties and on supramolecular, morphological, and macromorphological structure parameters. The results of the comparison of properties and structure of fibers have confirmed that fibers made from terephthalic acid represent a more favorable type of technical polyester fibers.

Introduction

High-tenacity polyester fibers have been marketed since the 1960s and have become the dominant construction material for various technical applications. PES technical fibers include conventional high-tenacity types (HT), as well as high-modulus low-shrinkage types (HMLS). HMLS fibers have higher dimensional stability and are preferentially used for the production of tires. The development of HMLS fibers was influenced mostly by increased requirements of the rubber industry. Main suppliers of PES fibers include global corporations, such as AKZO (now ACORDIS) KoSa (former Hoechst Celanese), Honeywell (as a part of General Electric), and Kordtrade[1].

Polyester technical fibers are used in a wide range of applications in automotive and rubber industry and for the production of various composite construction materials. Today's advanced technologies of preparation importantly increase the level of usage of PES technical fibers[2–4,7].

In the future, the automotive industry, as well as other sectors will need to develop newer fibrous materials with better utility properties. Today, the world production of PES cord is more than 300,000 t/y.

Leading production companies have developed special technologies of its preparation based on production of high-molecular PES polymers spinned at high speeds. HMLS PES fibers differ from conventional types by their supramolecular and morphological structure and corresponding thermodynamic-mechanical properties.

Experimental part

Experimental works were focused on the preparation of PES technical fibers type HMLS from DMT and terephthalic acid with linear density of 1,500 dtex by means of continuous process, and on the evaluation of their structure and utility properties. In polymers used to produce HMLS fibers from DMT and terephthalic acid, the viscosity limit number LVČ was > 100 mL g^{-1}. The preparation of fibers was carried out on a continuous equipment at Vn > 6,000 m min^{-1} (Fig. 1).

Prepared technical polyester fibers were evaluated for their supramolecular structure parameters (Δn, speed of sound – C, crystalline portion – β), mechanical properties (tenacity, elongation, E, shrinkage), and thermodynamic-mechanical properties (tg δ = E“/E’) at temperatures from −50 to 250 °C (ref.[5,8]).

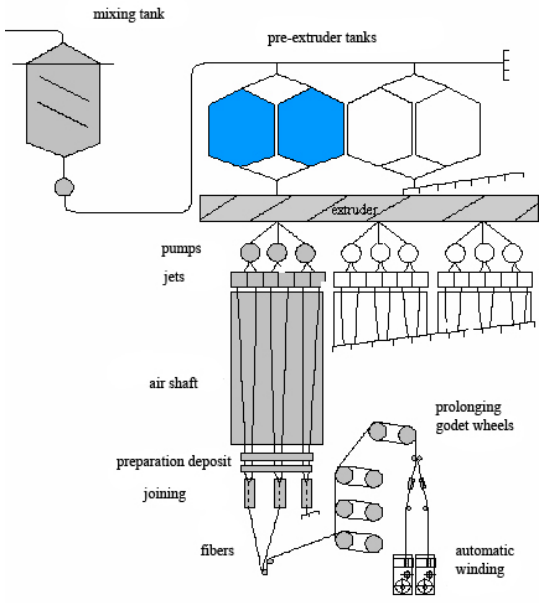

Fig. 1. **Diagram of the equipment for continuous preparation of PET fibers**

Thermodynamic properties parameter tg δ (E“/E’ = level of mechanical losses) is displayed on Fig. 2, 3.

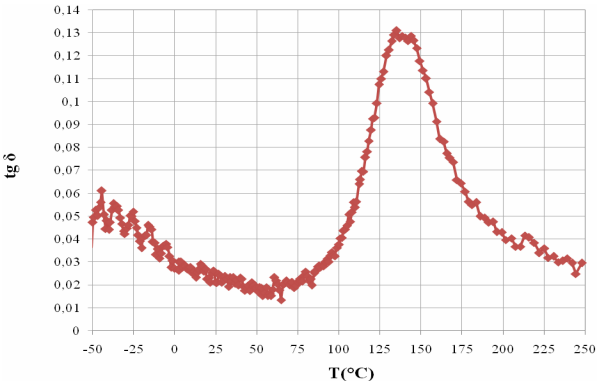

Fig. 2. **Loss factor tg δ of fibers from DMT fibers**

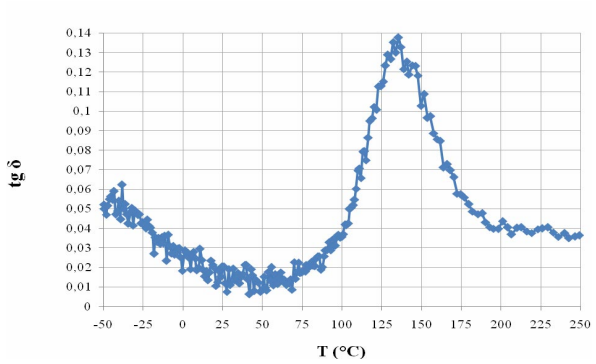

Fig. 3. **Loss factor tg δ of fibers from PTA fibers**

Discussion and conclusion

Our work was aimed at preparation and evaluation of physical-mechanical properties, supramolecular, morphological, and macromorphological structure parameters, and dynamic-mechanical properties of PET technical fibers from dimethyl terephthalate and terephthalic acid. Fibers were prepared using a spin-draw equipment. Based on obtained results from the evaluation of physical-mechanical properties, thermodynamic properties and structure parameters, we suggest the following conclusions:

Physical-mechanical properties (tenacity, elongation) and shrinkage of polyester HMLS fibers prepared from DMT and terephthalic acid (PTA) are comparable, but the tenacity is partly higher in fibers from terephthalic acid.

The comparison of module LASE, thermodynamic-mechanical properties and loss angle tg δ showed that the fibers prepared from terephthalic acid are more suitable.

Morphological and macromorphological structure of polyester fibers prepared from DMT and terephthalic acid are essentially on the same level, with high homogeneity and uniformity of inner structure and transversal geometry.

Supramolecular structure parameters (orientation and crystalline portion) suggest that the polyester fiber prepared from terephthalic acid has partly higher average orientation and crystalline portion, which results in more favorable physical-mechanical properties.

We can state that the properties of polyester HMLS fibers prepared from DMT and PTA are in accordance with the criteria for PET fibers applied in technical textiles.

REFERENCES

1. Wiliams L. Q.: International Fiber Journal. Polyester for Technical Textiles: Meeting Demands of Chalenging Market. *16*, 24 (2001).
2. Fourné F.: *Synthetic Fibers*. Hanser Publisherrs, Munich 1999.
3. Horrocks A. R., Anand S. C.: *The Textile Institute*. Woodhedsd Publishing Limited, Cambridge 2000.
4. Jambrich M., Budzák D., Kochan.J., in: prednáška na *59. Zjazde chemikov, 2.-6. september 2007, Vysoké Tatry, Tatranské Matliare* CD, Zborník, ChemZi 1/3, pp. 256−257 (2007).
5. Jambrich M., Pikler A., Diačik J.: *Fyzika vlákien*, Alfa, Bratislava 1987.
6. Jambrich M., Starigazda J., Sýkorová J., Cuninková J., Lániová A., in: prednáška na medzinárodnej konferencii *Slovak Rubber Conference, máj 2006, Púchov*, zborník.
7. Horrocks A. R.: *Handbook of Technical Textiles*. Woodhead Publishing Ltd, Cambridge 2000.
8. Bečaverová M.: *Diplomová práca*. FPT TnUAD, Púchov 2008.

CL-12
APPLICATION OF POLYMER NANOCOMPOSITES IN AUTOMOTIVE: THE PRESENT STATE AND PERSPECTIVES

VIERA KHUNOVÁ[a], IVAN KELNAR[b], and JÁNOS KRISTOF[c]

[a] The Slovak University of Technology, Faculty of Chemical and Food Technology, Institute of Polymer Materials, Radlinského 9, 812 37 Bratislava, SK, [b] Institute of Macromolecular Chemistry, Academy of Sciences of the Czech Republic, Heyrovsky Sq. 2, 162 06 Prague, CR, [c] University of Pannonia, Department of Analytical Chemistry, Egyetem 10, H-8200 Veszprém, HU

From point of view of application of polymer nanocomposites in automotive industry, the most significant fact is that together with remarkable improvement of end-use properties, the density of nanocomposites is virtually the same as that of the unfilled polymer. This means that substantial reduction of fuel consumption and air pollution, better performance and energy saving can also be made. According to a recent prognoses, widespread utilization of polymer nanocomposites in automotive would save annually over 1.5 billion liters of gasoline and would reduce carbon dioxide emissions by nearly 10 billion pounds[1].

Polymer nanocomposites often exhibit remarkable improvement in a wide range of physical and engineering properties:

- improved mechanical properties,
- reduced weight at the same performance,
- increased dimensional stability,
- improved barrier properties,
- increased heat distortion temperature,
- flame retardant properties (safety),
- high chemical resistance,
- high scratch resistance, smooth surface,
- electroconductivity,
- transparency (better visual impact).

The most stimulating for further development of polymer nanocomposites is the fact, that above property improvements are accessible in filler content which is about 10 times lower than currently used traditional fiber reinforced composites.

Althought the idea behind nanotechnology originated from Nobel Prize Laureate Richard Feynman 50 years ago, it took nearly 25 years, before the first polymer nanocomposite was prepared. The history of commercially used polymer nanocomposites has been written in 1989, when Toyota Motors introduced the first nanocomposites based on nylon 6 and clay (exfoliated montmorillonite). By replacing existing timing-belt cover material with PA6 nanocomposites they achieved together with high rigidity, no wrap, excellent thermal stability and the weight saving up to 25 %.

In spite of very optimistic prognoses, it took fairly long time untill other automotive companies followed Toyota and integrated polymer nanocomposites in their cars. The most recognized examples are summarized in the Table I.

It is now suggested that polymer/clay nanocomposites can be successfully applied in a range of vehicles for external and internal parts such as engine cover, oil reservoir tank, fuel hose, mirror housings, door handles and under-the-hood parts. Examples of current applications of polymer nanocomposites are given in Table II. It is believed that the weight advantage could bring except of significant environmental advantages also improvement in material recycling of used cars. That is why automotive is expected to be the second-largest application of polymer nanocomposites.

According the data[3] the volume of nanocomposites is expected to grow from $75 million globally market (in 2005) to $250 million in 2010[3]. Even more optimistic prognoses are given by Freedonia analyses[4]. They expext that by 2010, nanocomposites demand will grow to over $ 273 million, will further rise to over $3,8 billion in 2015 and $15 billion by 2020.

However, current economic crisis will certainly have its impact on the long term prognoses. For a while, automotive industry will very likely become reluctant to do major investments in innovative materials, thus certain delay in commercialization of new materials can be expected. On the other hand, the present situation in car industry may also be an opportunity for breakthrough innovations.

In spite the attractive properties and optimistic prognoses polymer nanocomposites applications are still far from to compete the market of high performance glass and carbon fibre reinforced composites. There are several reasons why commercialization of polymer nanocomposites is below the previous expectations.

Expect of difficulties connected with production of polymer nanocomposites in melt (only industrially acceptable mode), the second important reason is also lack of commercially available organoclays with acceptable thermal stability. This is because of most commercially available organoclays and nanocomposites (Table III, IV) are produced by the exchange of metal cations in clay galleries with thermally unstable organic ammonium salts[4]. Manufacturing costs also remain a significant factor restricting the growth of polymer–nanocomposite applications[4].

Table I
Concise history of polymer nanocomposites in car industry

Year	Company	Application
1989	Toyota Motors	Timing belt cover
	Mitsubishi´sGDI	engine cover
2004	General Motors	step assistant in GMC Safari and Chevrolet Astro vans, heavy-duty electrical enclosure
2006	Noble Polymer Forte PP	seat backs of Acura TL and center console of light truck.
2007	Yamaha Motor Corporation	light, smooth finish, nimble watercraft hulls made from NanoXcel

Table II
Current applications of polymer nanocomposites in automotives

Nanocomposite	Application
PA/clay	timing belt cover, car interior under hood
PP/clay	variety of applications replacing PP/talc and PP/glass fibres composites
TPO/clay	exterior car parts
PU/clay	car tyres
PP/clay	car body parts

Table III
Selected commercial nanoclays

Product	Producer
Nanomers	Nanocor
Closite	Southern Clay Products
Bentone	Elementis Specialties
Masterbatches	PolyOne, Clariant, RTP
Nanofil	Sud-Chemie
Planomers	TNO

Our research in polymer nanocomposites is related to

- Polypropylene composites based on natural nanofibres. The main research effort is oriented on study of potential application of natural nanotube in polypropylene nano-

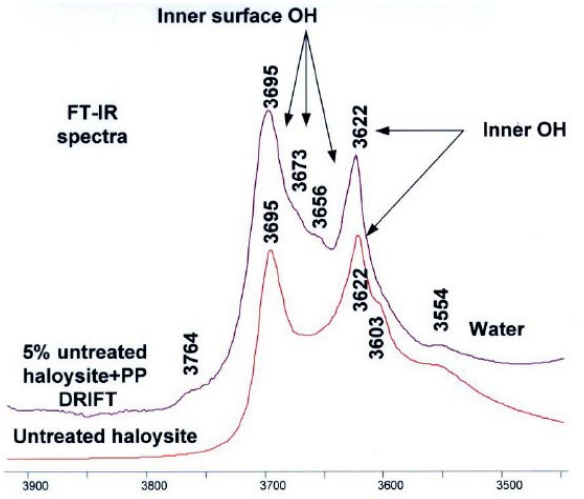

Fig. 1. **FT-IR spectra of hallosite and PP/halloysite composites**

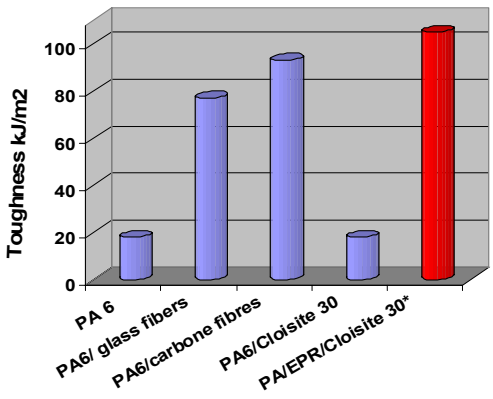

Fig. 3. **Comparison of toughness of short fibre (20 % w/w) and clay (5 % w/w) polyamide 6 composites**

composites

– Development of polyamide composites based on commercial organoclay and polyamide with improved toughness.

Comprehensive analyse of halloysite from source Michalovce Biela Hora, Slovakia has revealed that studied type of clay is favourable from both chemical structure (Fig. 1) and tubular particles (Fig. 2) for application in polymer nanocomposites. Our present work is focused on the development of effective and thermally stable modifiers as well as modification technologies enable to develop nanocomposites with improved end-use properties. The very first results indicate that an intensive intercalation of halloysite was achieved by mechanochemical treatment.

The impact of the intercalated structure of halloysite was confirmed by improving of mechanical properties, as well as reduction of flammability PP/halloysite nanocomposites. The investigation of structure of polymer nanocomposites based on intercalated halloysite confirmed considerable reduction of particle size and high degree of filler exfoliation.

Results related to our investigations concerning to polyamide nanocomposites are summarized in Fig. 3 and Table IV. It was found that by favorable combination of polyamide with EPR and two commercial organoclays with different polarity it is possible to prepare nanocomposites with highly (up to 400 %) improved toughness compared to neat polyamide without loosing stress, modulus and elongation.

This best balanced mechanical behaviour of PA6 nanocomposite was achieved by pre-blending of less polarity organoclay (Coisite 15A) into elastomer (EPR) followed by subsequent blending with PA and high polarity clay (Cloisite 30B). By this method a high degree of matrix reinforcement (exfoliation of clay with more polar treatment) was combined with favorable size and structure of dispersed EPR phase.

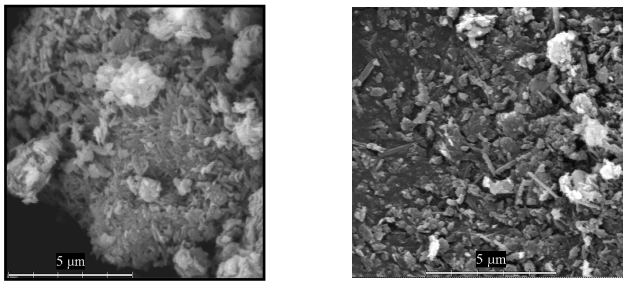

Fig. 2. **SEM analyse of Hallosite-Biela Hora, SK**

Table IV
Influence of glass fibres (GF), carbon fibres (CF) and organoclay (Cloisite 15, Cloisite 30) on toughness of PA6 composites

Sample	Filler content [% w/w]	Stress at break [MPa]	Elong [%]	E [MPa]
PA 6	0	74	150	1620
PA6/GF	20	138	7	3875
PA6/CF	20	151	5	7000
PA6/C30	5	94	90	2610
PA/EPR/C30	5	87	183	2560

The localization of less polarity organoclay in the interfacial area brought an important new effect consisting of enhancement of toughness by formation of “core-shell” particles. Detailed explanation of toughening effect is given in our papers[5,6].

Summary

In spite optimistic prognoses polymer nanocomposites applications present only negligible part and they are far from

to compete the market of currently used high performance fibre reinforced and particulate composites.

There are several reasons why commercialization of polymer nanocomposites in automotive is lower than the earlier prognoses. Among the key obstacles are:

- lack of commercial organoclay with acceptable thermal properties,
- difficulties related to structure of melt prepared nanocomposites,
- the extremely high price of carbon nanotubes.

Investigations related to polypropylene based on natural nanofibres underline the potential for future utilisation of halloysite from source Biela Hora, Slovakia, for production of polymer nanocomposites with outstanding end use properties.

It was found that by favorable combination of EPR and organoclays with different polarity it is possible to prepare nanocomposites with highly (up to 400 %) improved toughness compared to neat polyamide without loosing stress, modulus and elongation.

The project N°. 1/0662/08 was supported by Slovak Scientific Grant Agency (VEGA).

REFERENCES

1. MRS Report, 2003.
2. Zeng Q. H., Yu A. B., Lu G. Q. (Max), Paul D. R.: J. Nanosci. Nanotech. *5*, 1574 (2005). Markarian J.: Plastics *7*, 18 (2005).
3. *The Fredonia Group, Nanomaterials Demand in Composites*, Nanocomposites, Industry Study with Forecasts to 2010, 2015 & 2020, 2006
4. Pavlidoua S., Papaspyridesb C. D.: A review on polymer–layered silicate nanocomposites Progress in Polymer Science *33*, 1119 (2008).
5. Kelnar I., Khunová V., Kotek J., Kaprálková L.: Polymer *48*, 5332 (2007).
6. Khunová V., Kelnar I., Lehocký P.: The influence of interphase modifier on strucutre and properties of particulate and fibers polypropylene and polyamide composites, in proceedings of conference *Theplac, Brindisi, 2007*.

CL-13
WASTE OF POLYAMIDE 6.6 FLOCK FROM AUTOMOTIVE INDUSTRY AS A FILLER OF POLYAMIDE 6 COMPOSITE

KORNIEJENKO KINGA and KUCIEL STANISLAV

Cracow University of Technology (Poitechnika Krakowska), Al. Jana Pawła II 37, Kraków, Poland
kkorniej@wp.pl

Polyamide 6.6 flock is used as a material for aluminum gaskets during their production. The powder is atomized on gaskets and covers the surface, the rest of the powder is treated as a waste. Every month several tones were created and the company had to pay for their utilization.

In order to appraise the potential possibilities of use there were made some tests on the powder from the waste production. The possibility of material recycling was evaluated.

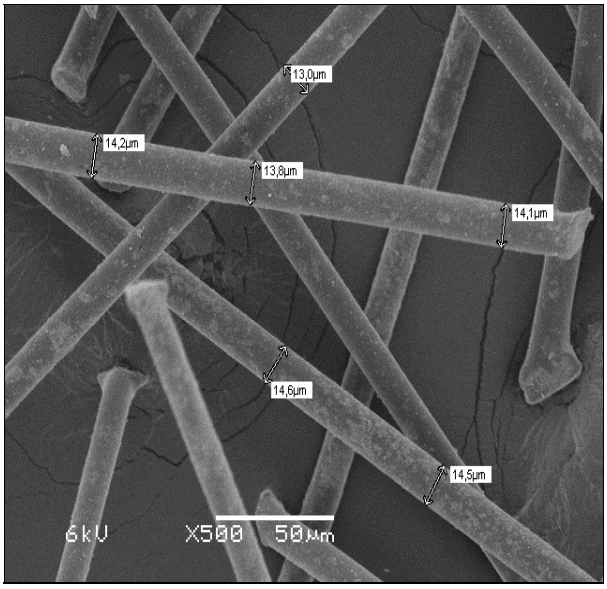

Fig. **Photography 1. SEM** – waste of flock

The waste of flock is for the most part homogeneous and little dirty or glutted. Flock, in its physical form, is fibers of polyamide 6.6 a length of 500 μm and the average diameter of 14–15 μm.

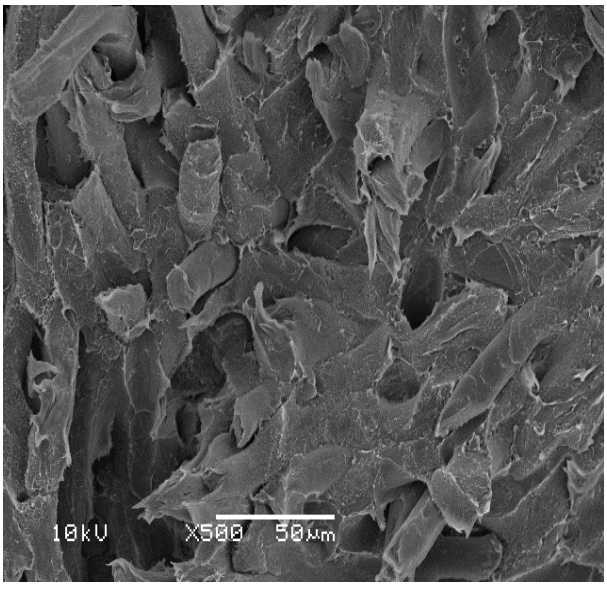

Fig. **SEM image of cross section after elongation test** - composite 4PA – polyamide 6 filled by 40% of waste flock

It is possible to use a flock as a filler to composite – by mixing it with the standard granuled Polyamide 6. After the preliminary trials rejected the possibility of direct injection flock, because of the difficulty in collecting the material, and

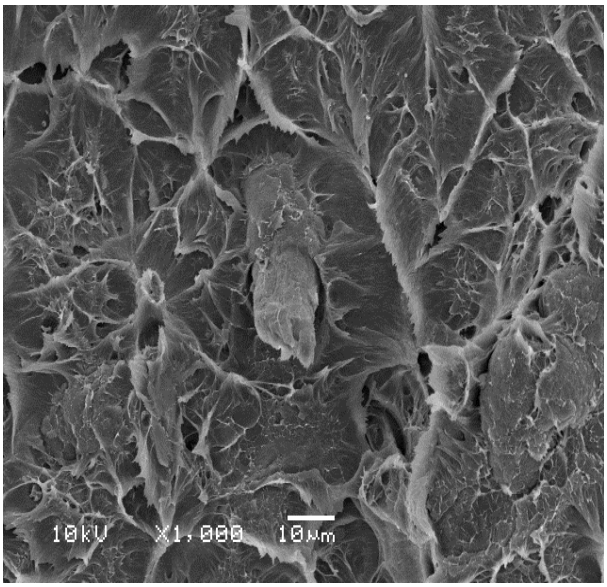

Fig. **SEM image of cross section after elongation test** - composite 2PA polyamide 6 filled by 20% of waste flock – simple flock fiber on the base of PA6 matrix

performed the test sample from two types of composition, from the compare used a samples from Polyamide 6.

Marker the samples used for testing:

PA6	–	Polyamide 6 – Tarnamide T27
2PA	–	20 % flock and 80 % T27
4PA	–	40 % flock and 60 % T27
PA6D	–	Polyamide 6 – Tarnamide T27 after 1 day washed a samples
2PAD	–	20 % flock and 80 % T27 after 1 day washed a samples
4PAD	–	40 % flock and 60 % T27 after 1 day washed a samples
PA6M	–	Polyamide 6 – Tarnamide T27 after 1 month washed a samples
2PAM	–	20 % flock and 80 % T27 po 30 after 1 month washed a samples
4PAM	–	40 % flock and 60 % T27 after 1 month washed a samples

Tested properties of tensile strength in the sample on a strength machine INSTRON: tensile strength, modulus of elasticity, strain at break for these 3 compositions and 3 states – dry samples in two weeks after injection, drenched samples after 1 day and 1 month. We can see a reduction in absorbance of water after adding the flock to pure PA6.

Results for determining the mechanical properties were compared which is reveal below:

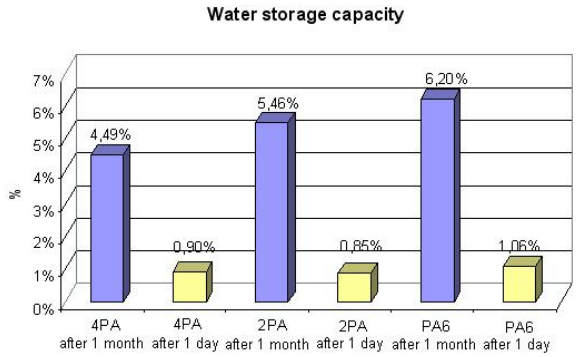

Chart 1. **Compare a water absorption samples with different additive material waste**

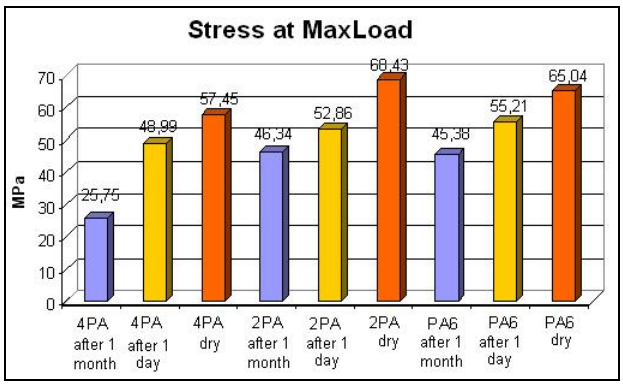

Chart 2. **Stress at MaxLoad**

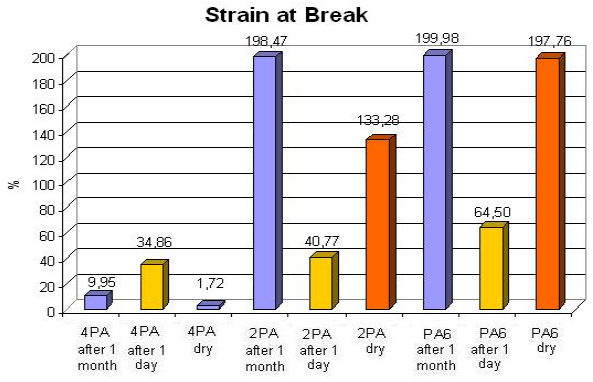

Chart 3. **Strain at Break**

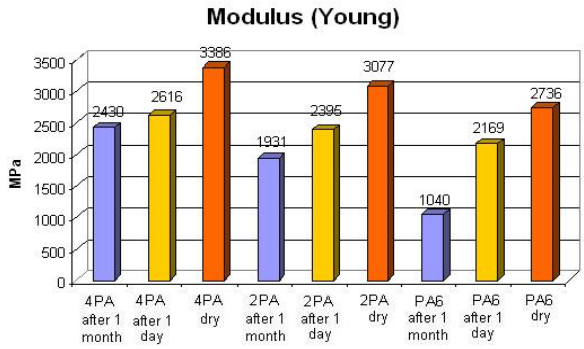

Chart 4. **Modulus (Young)**

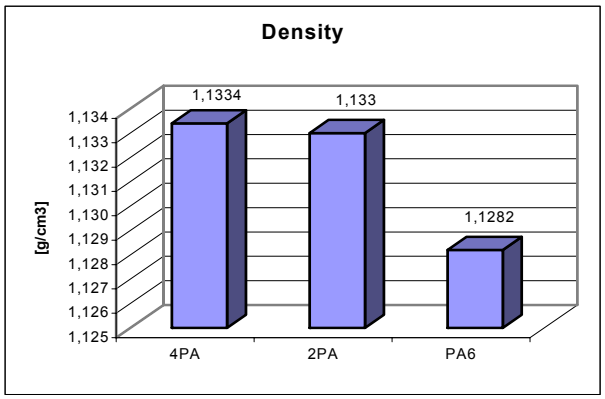

Chart 5. **Density**

Summing up the possibility of using flock by recycling material we can say that it appears to be the optimal use of the flock as a 20 % addition to polyamide 6 (for example Tarnamide T27). 20 % additional waste of flock can develop an increase of about 20 MPa modules of elasticity and slight decrease in strain at break. In this case it is also important to reduce absorbance of water in this composition.

Conclusion

The flock can be used as a supplement to original polyamides (black colored) or others materials.

It appears to be the optimal use of the flock as a 20 % addition to polyamide 6.

CL-14
EXPERIMENTAL RESULTS IN STABILIZATION OF STYRENE- BUTADIENE RUBBER

K. KOSÁR[a], P. LEHOCKÝ[a], P. ŠIMON[b], J. UHLÁR[a], and M. ĎURAČKA[a]

[a] VUCHT a.s. , Nobelova 34, 836 03 Bratislava, Slovakia,
[b] Slovak Technical University, Faculty of and Food Chemical Technology,Departmen of Physical Chemistry, Radlinského 10, 812 37 Bratislava, Slovakia
kkosar@vucht.sk; peter.simon@stuba.sk

The presentation deals with the stabilization of synthetic rubbers before their processing by the consumers. It shows the used methods of evaluation of the stability of rubbers during thermo-oxidative and thermo-mechanical duration and also gives real results from comparing measurements of efficiency of different types of stabilizers during stabilization of emulsion type SBR.

CL-15
MAGNETIC ELASTOMERIC MATERIALS FOR INTELLIGENT TYRES

J. KRUŽELÁK, R. SZABOVÁ, D. BELLUŠOVÁ, G. KYSELÁ, and I. HUDEC

Slovak University of Technology in Bratislava, Faculty of Chemical and Food Technology, Institute of Polymer Materials, Department of Plastics and Rubber, Radlinského 9, 812 37 Bratislava, jan.kruzelak@stuba.sk

Tyres are one of the most extensive and economic effective products of rubber industry. The demands on their driving properties increase with increasing of running speed and transport safety of modern vehicles. The progress in this sphere is also aimed at intelligent tyres that are able to respond to changes of driving conditions. One of possibilities of their construction is application of magnetic materials. They can be applied as permanent magnets able to communicate with external sensors[1,2]. The rubber compounds filled with powdery magnetic fillers are possible to include among these materials. They can be used to produce tyre sidewalls or treads, eventually small rubber components incorporated in tyres. The study of the change of elastomeric magnetic material properties in model and real rubber systems is focus of this work as well.

In this work the two different types of rubber compounds were used. Model rubber compounds A based on natural rubber NR, besides rubber and fillers, contained only ingredients which support curing process. Strontium ferrite $SrFe_{12}O_{19}$ (F) type FD 8/24 together with carbon black (CB) type N-660 were applied as fillers. The total content of fillers was kept constant (60 phr), only the weight fraction of ferrite in the combination of both fillers (w_f = F/(F+CB)) was changed. In case of rubber compounds B, real rubber compound which is generally used for producing passenger tyre sidewalls was used. These rubber compounds based on three diene rubbers

of general purpose (SIR20-NR, SBR, SKD20-BR) contained combination of ferrite and carbon black as fillers as well.

The results of study of physical – mechanical properties of vulcanizates A showed that the combination of applied fillers affects especially moduli. From Fig. 1 is evident significant decrease of modulus M300 with increasing of ferrite loading in fillers combinations. The decrease of modulus value of vulcanizate filled only with ferrite represents at about 260 % in comparison with modulus value of vulcanizate filled only with carbon black. The tensile strength of vulcanizates gently increases in whole examined ferrite concentration range in contrast to moduli.

The character of dependences of all evaluated physical-mechanical properties of vulcanizates filled with combinations of ferrite and carbon black points out its additive effect in model compounds of natural rubber.

The magnetic characteristics, namely remanent magnetic induction B_r, maximum magnetic induction B_m and maximum magnetic polarization J_m show significant non-linear increasing tendency with increasing of ferrite content in fillers combinations.

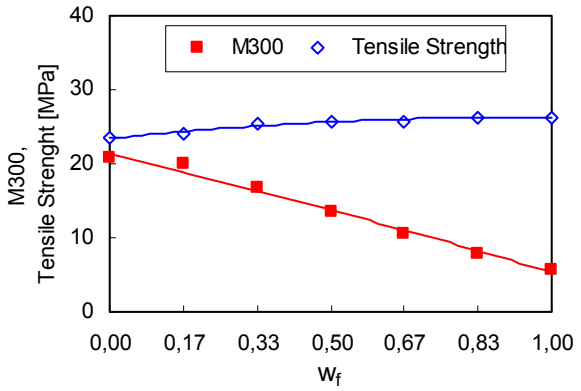

Fig. 1. **Influence of ferrite weight fraction w_f on modulus M300 and tensile strength of vulcanizates A**

Together, with the study of properties of elastomeric composites, the cross-link density and the sulfur cross-link structure were analysed. The highest total cross-link density ν_c exhibits vulcanizate filled with carbon black only and the lowest density ν_c vulcanizate filled with ferrite only. Therefore the increase of ferrite content in fillers combinations leads to consistent linear decrease of density ν_c. The chemical cross-link density ν_{ch} of all evaluated vulcanizates is lower than total cross-link density, but the differences between both densities become less with w_f increasing, above the $w_f > 0.5$ their values become nearly the same. The content of physical cross-links is low. With w_f increasing the next decrease of density ν_f was shown (Fig. 2). In the cross-link structure only polysulfidic and disulfidic cross-links were experimentally found with dominance of polysulfidic cross-links.

The study of influence of magnetic filler content on properties of real rubber compounds B was based on two-factor five-level planning experiment. As independent variables the weight ratio of ferrite and carbon black – x_1 (x_1=F/CB) and the total content of applied fillers in rubber compounds – x_2 (x_2=F+CB) were chosen. The content of carbon black was changed from around 15 phr to 54 phr and the total content of ferrite was changed from about 11 phr to 54 phr.

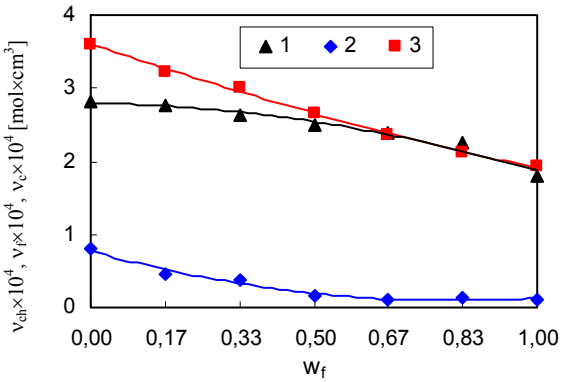

Fig. 2. **Influence of ferrite weight fraction w_f on chemical ν_{ch} (1), physical ν_f (2) and total cross-link density ν_c (3) of vulcanizates A**

The values of modulus M300 are relatively low and the differences between the modulus of vulcanizates filled with various ferrite content and various total content of both fillers are low as well. With increasing of weight ratio of both fillers F/CB the evaluated modulus non-linearly decreases. The increasing of total content of fillers F+CB has almost no influence on modulus M300 (Fig. 3).

The remanent magnetic induction shows a slight maximum with increasing of weight ratio of ferrite and carbon black. With increasing of total fillers content non-linear increasing tendency of observed magnetic property was detected. The increase becomes more evident with increasing of ferrite in combination of used fillers (Fig. 4).

The influence of magnetic filler content on cross-link density was evaluated on the chosen samples with different content of ferrite and carbon black. The results of measure-

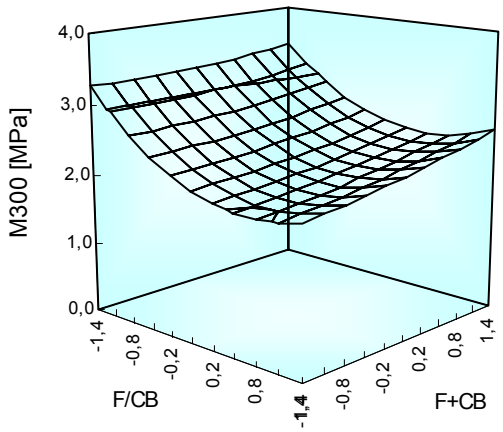

Fig. 3. **Influence of weight ratio of ferrite and carbon black (F/CB) and total content of fillers (F+CB) on M300 of vulcanizates B**

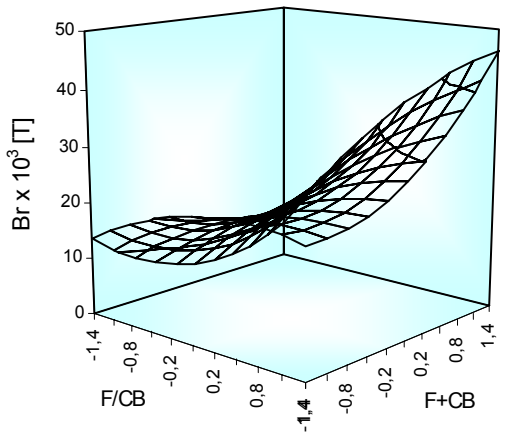

Fig. 4. **Influence of weight ratio of ferrite and carbon black (F/CB) and total content of fillers (F+CB) on remanent magnetic induction Br of vulcanizates B**

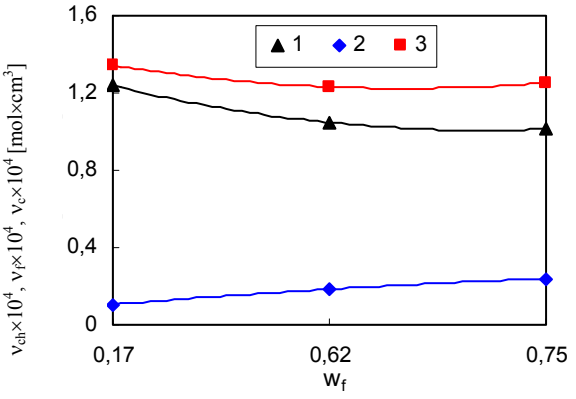

Fig. 5. **Influence of ferrite weight fraction w_f on chemical ν_{ch} (1), physical ν_f (2) and total cross-link density ν_c (3) of vulcanizates B**

ments showed, that the total cross-link density ν_c and the chemical cross-link density ν_{ch} gently decrease with increasing of ferrite loading in combination of both fillers. Despite of that the physical cross-link density ν_f is low as well as in case of vulcanizates A with w_f increasing slight increase of ν_f was observable (Fig. 5).

All types of sulfidic cross-links are present in prepared rubber compounds B with dominance of polysulfidic cross-links. The content of polysulfidic cross-links gently decreases with increasing of ferrite loading, while the content of dissulfidic cross-links gently increases with the same observed parameter.

REFERENCES

1. US Patent, US6550320 B1, April 22, 2003
2. Grönefeld M.: *Encyclopedia of Materials Science and Technology*, Permanent Magnets-Sensor applications, p. 6822–6825, 2003.

CL-16
WEAR OF MULTIPURPOSE TIRE TREADS

DAVID MANAS, MIROSLAV MANAS, MICHAL STANEK, MILAN ZALUDEK, STEPAN SANDA, JAKUB JAVORIK, and VLADIMIR PATA

Tomas Bata University, Faculty of Technology, Department of Production Engineering, TGM 275, 762 72 Zlin, Czech Republic
dmanas@ft.utb.cz

Abstract

Wear of tire treads at roads surfaces is measured as abrasion resistance. Off – road behavior of tire treads on surfaces with sharp stones is not well characterized by abrasion resistance as the mechanism of rubber damage is here rather different. The sharp edges of stones can cut a rubber tread surfaces and gradually tear off bigger pieces of rubber (chip – chunk).The aim of this article is evaluation of chip – chunk behaviour of different rubber compounds The process of the damage of multipurpose tire treads is described in this article as well.

Introduction

In rubber practice we often meet the problem of wear of the rubber parts. Some types of wear, especially the wear of tire treads, are very similar to machining. The tire tread (Fig. 1) is a part of tire that which in direct contact of the vehicle with the road and is thus is responsible for the driving force transfer. The wear of the tire tread of passenger and trucks cars travelling on common roads is characterized by its abrasion. The tread of a tire of a car is disposed to the abrasive effect of the road.

However, the mechanism of wear of tires working in very hard terrain conditions is absolutely different. Sharp stone edges and terrain irregularities gradually cut (tear off) parts of the rubber tread surface, which can be understood as a way of working – e.g. milling or turning, although under very specific conditions. The mechanism of tire tread wear working in hard terrain conditions is technically called Chip-Chunk effect and it can be considered as “workability” of

Fig. 1. **Cross section of radial tread of a passenger tire**, 1 – Inner-Liner, 2 - Carcass material, 3 – Bead wire (Core), 4 – Apex, 5 – Tire strip, 6 – Rim (Bead) strip, 7 – Sidewall, 8 – Breaker strip, 9 – PA Breaker strip, 10 – Tread

rubber surface.

The tire wear is usually tested under running conditions, these times demanding tests are very expensive. It would be very useful in practice to find a quick test of wear which could be carried out on small samples. Creating a model predicting the behavior of tire tread compounds would improve the development in wear research.

Experiment

Used materials (compounds)

Thirteen kinds of tire tread compounds used for motorcycle treads subjected to high stress, treads for technical, agricultural and multipurpose vehicles were experimented. All compounds represent real products and are produced and machined:

- Motorcycle tread cross (compounds number 183, 185, 186),
- Motorcycle tread enduro (compound 290),
- Technical vehicle treads (compound 188),
- Agricultural tire (104, 110, 114, 116),
- Gear tire (161),
- Tire for high-lift (162),
- Farm-tractor tire (165),
- MPT/R (168).

Test of wear

The tests of tire (tread) wear are time and money consuming. They are carried out using real tires in testing rooms or directly in the terrain during driving tests. That is one of the reasons for searching a method that would in a very short time (in minutes) and on small samples test the wear for a comparison of the different kinds of compounds.

Based on these requirements an equipment seen on Fig. 2 was designed. The Chip – Chunk wear testing machine (J. R. Beatty and B. J. Miksch in RCHT, vol. 55, p. 1531) was used for basal measurements. A new machine enabling changing the tested parameters and true simulations of the process conditions was designed, see Fig. 2.

Arm 1 pivotable around the neck is lifted by lifting part (piston of the pneumatic cylinder) 2. The arm that has a special ceramic edge tool is lifted and dropped 3 on the perimeter of the revolving wheel 4 (testing sample) driven by the electric motor 5. When it drops on the revolving wheel, the ceramic tool gradually chips the material and creates a groove on the wheel. The size of the groove chipped by the ceramic tool in a given time is the scale of wear. The following requirements had to be taken into consideration during the design:

- The rotations of the wheel (testing sample) must be adjustable in a wide range. To fulfill this requirement, an electro motor with adjustable revolutions using a static converter of frequency was chosen. This eliminated reduction of the revolutions by a transmitter enabling the frequency to be regulated from 0 to the maximum value. An electro motor 4AP80 – 6s and a static converter of frequency Alitivar 08 were used.
- For an adjustable arm lift a pneumatic mechanism composed of piston with adjustable lift was designed and machined. The cylinder is supplied directly from the regulated valve EVK 3120 by SMC and the process is controlled by a control unit FESTO type FEC – FC20/10W.
- Secure the constant parameters of the edge tool. First, a steel tool was designed, which however lead to a very fast wear changing the conditions of the experiment. For this reason a ceramic tool was tested – a treated edge for cutting tools (type TNGN 220608, Saint Gobein). Cutting edges with 60° angle were ground (Fig. 2).

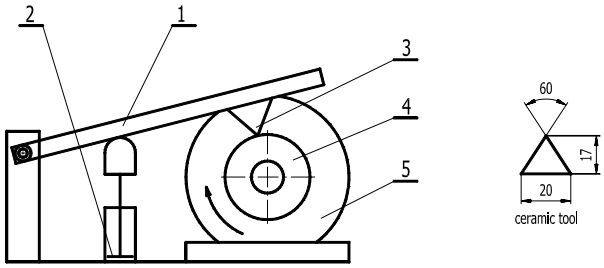

Fig. 2. **Design of testing equipment;** 1 – Arm, 2 – Pneumatic cylinder, 3 – Ceramic tool, 4 – Rubber sample, 5 – Electric motor

The ceramic edges proved a perfect resistance to wear. If the tool was well manipulated there was no difference between original and "worn" plate.

Dimensions of the testing sample

For easier preparation of testing samples the form seen on Fig. 3 was designed (the outer dimensions correspond to the testing sample of test Luepke).

A groove was made (chipped) by the ceramic tool into the testing sample during the experiment. It was expected

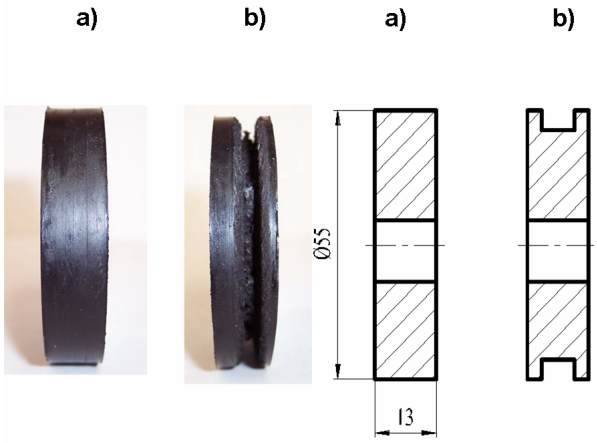

Fig. 3. **Testing sample for fast wear test a) before the test, b) after the test**

from experience with tooling other materials, esp. metals, wood or plastic, that the groove would be regular. Due to the properties of machined rubber – which demonstrated its elasticity – the moment the rotating ceramic tool dropped on the rotating wheel, pieces of material were torn off. For this reason, the initial intension of wear evaluation by measuring the groove diameter was changed to gravimetric evaluation.

Wear analysis

The influence of drop of the ceramic tool on the surface of the testing sample is crucial. If the sample were rigid, the evaluation of the impact of dropping force would be quite easy. The elastic properties of the testing sample however cause a series of other effects of smaller intensity (jumping on the surface) apart from the main effect (the first drop of the ceramic tool on the testing sample). The main effects of the ceramic tool have only partial influence on the total wear. It turned out that evaluating total work needed for wear (i.e. creating a groove on the testing sample) only by the energy of the drop would be biased. After the first testing of the experiment equipment, it was clear that the results in a given series of measurements would be comparable if the experiments ran under the same conditions. The construction of the main body with a key fitting the groove on the shaft and clamping basement with teeth prevent skidding of the testing sample while running and the control system of the testing machine will secure constant conditions for testing.

Test conditions

The conditions for experimental testing of fast wear were kept:

– Sample revolution 500 min^{-1}, 750 min^{-1}, 910 min^{-1}
– Impact frequency 1 Hz
– Ceramic tool stroke 60 mm
– Temperature 21 °C
– Test period 270s

The testing sample was clamped in the jaws of the machine to prevent is skidding and was rotated. The lifting mechanism for lifting the arm with ceramic tool was started. The time was measured from the first contact of the ceramic tool with the testing sample. Ten samples from each compound were used for the measurements. The mass loss was investigated by weighing on analytical balances after the experiment. Measured values were statistically evaluated.

The greatest wear was observed with compounds 183, 186 and 116. The best properties according to the wear were reported with testing samples prepared from compounds 168, 110 a 162 (Fig. 4).

Dependence on running conditions

The vehicles move in a different speed in the terrain in running conditions which can be characterised by the circumferencial speed of the tire tread. For this reason, other experiments were carried out to characterise the wear during different conditions. The wear test was done during the frequencies of testing samples of $n_1 = 910$ revolutions/min, $n_2 = 500$ revolutions/min, $n_3 = 250$ revolutions/min. The other conditions of the experiment remained unchanged. Fig. 5 shows the expected increasing tendency of the wear.

Wear procedure

The aim of the experiment was also to observe the mass difference of the testing sample (wear) during the test.

The mass of the samples was measured in regular inter-

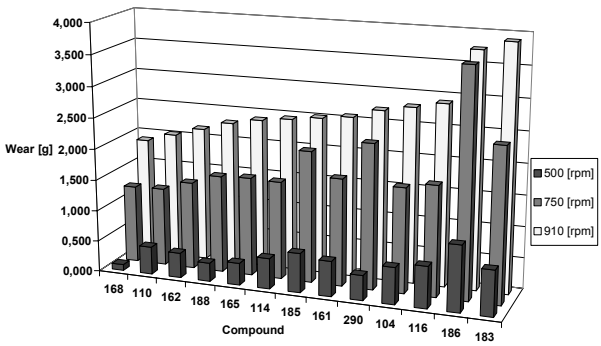

Fig. 5. **Comparison of mass loss at different frequencies**

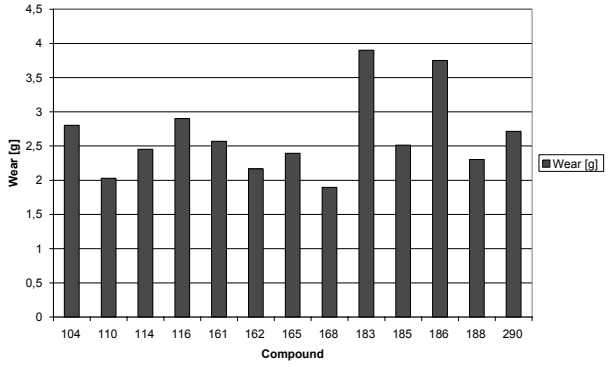

Fig. 4. **Comparison of the mass loss**

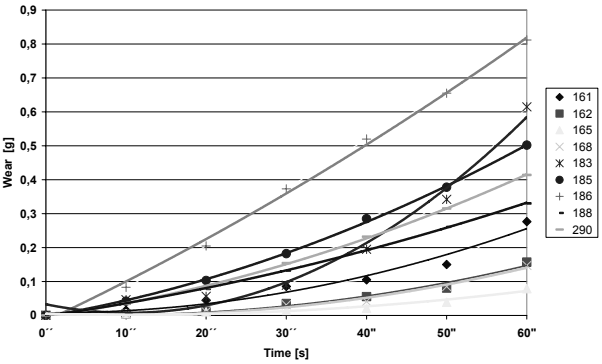

Fig. 6. **Gradual mass loss in all compounds in time 0–60 s**

vals (30 s) during the whole time of the experiment (270 s). Attention was paid to the interval 0–60 s due to the different behaviour of the tested compounds and the mass of the tested sample in this interval was measured every 10 s (Fig. 6, 7, 8).

Fig. 7. **Gradual mass loss in all compounds in time 0–60 s**

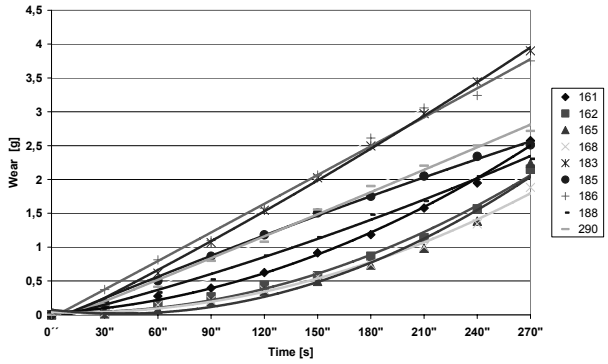

Fig. 8. **Gradual mass loss in all compounds in time 0–270 s**

Study of wear procedure using high speed camera

To be able to learn and understand much more the wear procedure the study using high speed camera was carried out. Observation of wear mechanisms showed that the wear mechanism itself happens in the area between the "splinter" and testing sample, which is found between already deformed and not yet deformed material. This is usually determined by the proportion between the layer thickness of the chipped rubber material and the thickness of the deformed "splinter". Considerable part of exerted energy (kinetic energy of the ceramic tool during drop) is – during the wear – concentrated to the place where the rubber material touches the ceramic tool and where parts of rubber material are detached.

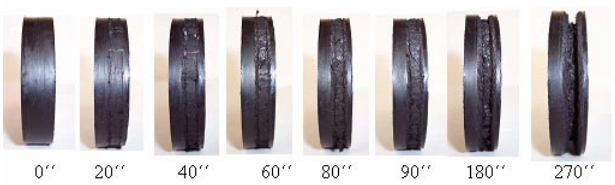

Fig. 9. **Wear of tested samples in time 0–270 s**

When investigating properties of the testing samples, high-speed video camera system Olympus i-SPEED 2 was used. The camera system was intended to visualize the behavior of the tested sample during the ceramic tool drop. The path of the ceramic tool when falling on the tested sample and the course of speed in a certain time were observed (Fig. 10, 11).

Discussion

The amount of the deforming force is closely related to the angle front (rake) of the ceramic tool (terrain roughness and sharp stone edges). In practice, this means that the angle front (rake) and the speed of motion on terrain roughness and sharp stone edges dramatically influence the conditions of created distortional deformation. The area between the splinter and rubber sample represents the crucial moment of the wear process during which material is taken away and splinter created. However, this is also a moment where shear stress and shear force, which have a substantial importance on the process happening on the ceramic tool area, are generated. Friction also plays a very important role, as the rubber material is during the ceramic tool drop exposed to high pressures. The rubber splinter is moving due to the deformation process on the front area of the ceramic tool and affects the temperature slightly by its activity and movement. There is a wide range of rubber mixtures with different properties. For that reason, it is necessary to pay attention to their behaviour and

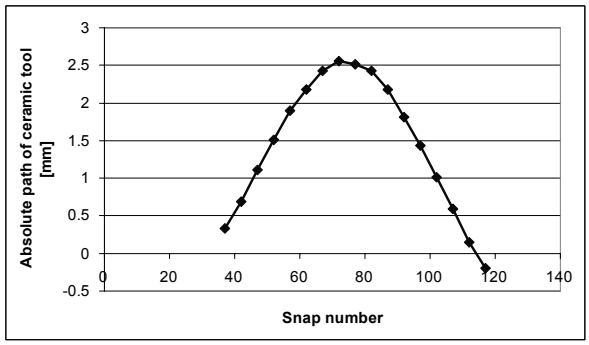

Fig. 10. **The absolute path of ceramic tool movement after dropping on the testing sample**

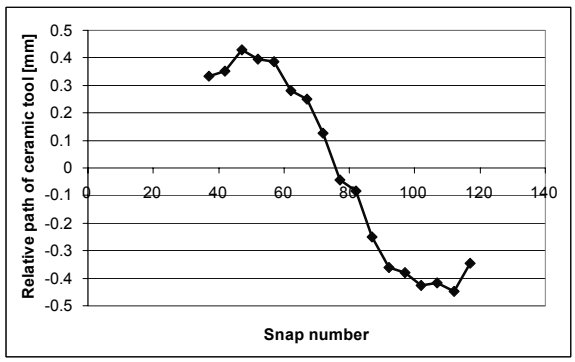

Fig. 11. **The relative path of ceramic tool movement after dropping on the testing sample**

bear in mind that the force ratio distribution during the wear is different with each mixture.

Conclusion

The presented test method shows the possibility of the evaluation of wear (chip – chunk) resistance of tire treads on small samples. This method makes possible to compare various types of compound with a standard and to observe the wear progress during the test period. The wear of the sample during the test period depends on the properties of rubber compounds and on test conditions.

The evaluation of the wear test using a high-speed video camera system Olympus i-SPEED 2 enables very detailed analysis of the wear process of heavily strained rubber parts, tire treads in particular. The visualisation of the ceramic tool drop on the testing samples can determine the path of tool penetration, as well as its speed (Fig. 10, 11). Simultaneously, the deformation of the testing sample can be observed. The path and speed ratio can determine the moment when the surface is damaged and first rips created.

This article is financially supported by the Czech Ministry of Education, Youth and Sports in the R&D project under the title 'Modelling and Control of Processing Procedures of Natural and Synthetic Polymers', No. MSM 7088352102.

REFERENCES

1. Batty J. R., Miksh B. J.: Rubber Chem. Technol. *55* (1989).
2. Johnson S. J.: *Rubber processing*, Hanser Publishers, Munich 2001.
3. Manas D.: *Rubber Workability and Wear of Rubber Parts*, VUT FSI, Brno 2005.
4. Manas D., Stanek M., Manas M., Dvorak Z.: *Off – Road Tires Behavior*, IRC 2005, Yokohama, Japan (2005).
6. ČSN ISO 37 Curred rubber or thermoplastic rubber – Tensile properties, Prague.

CL-17

SURFACE PROPERTIES OF POLY (IMIDE-CO-SILOXANE) BLOCK COPOLYMERS

IGOR NOVÁK[a]*, PETR SYSEL[b], IVAN CHODÁK[a], MILENA ŠPÍRKOVÁ[c], and IVICA JANIGOVÁ[a]

[a] *Polymer Institute, Slovak Academy of Sciences, 842 36 Bratislava, Slovakia,* [b] *Institute of Chemical Technology, Faculty of Chemical Technology, Dept Polymers, 166 28 Praha, Czech Republic,* [c] *Institute of Macromolecular Compounds of the Czech Academy of Sciences, 162 06 Praha, Czech Republic*
upolnovi@savba.sk

Abstract

Poly(imide-siloxane) (PIS) block copolymers have been studied with respect to their structure and surface properties relationship. The relatively small amount of siloxane in PIS block copolymer, 10–20 wt.%, increased significantly the contact angle of water due to the surface hydrophobization of the copolymer. The significant decrease of the surface energy of the PIS copolymer due to growth of the siloxane content was observed. The polar component of surface energy shows an intense decrease, whereas its dispersive component increases. The study of the morphology of PIS copolymers characterized by The X-ray Photoelectron Spectroscopy (XPS) analysis showed an excessive increase of Si on the polymeric surface. Scanning electron microscopy (SEM) shows a growth of the surface roughness by increase of the content of siloxane.

Introduction

Polyimides present a class of polymers, necessary in microelectronics, printed circuits construction, and aerospace investigation, mainly because their high thermal stability and good dielectric properties[1,2]. In the last years, several sorts of block polyimide based copolymers, namely poly(imide-siloxane) (PIS) block copolymers containing siloxane blocks in their polymer backbone have been investigated[3,4]. In comparison with homopolymer polyimides the PIS block copolymers possess some improvements, e.g. enhanced solubility, low moisture sorption, and their surface reaches the higher degree of hydrophobicity already at low content of polysiloxane in PIS copolymer. This kind of the block copolymers are used as high-performance adhesives and coatings. The surface properties of PIS block copolymers are strongly influenced by enrichment of the surface with siloxane segments. Micro phase separation of PIS block copolymers occurs due to the dissimilarity between the chemical structures of siloxane, and imide blocks even at relatively low lengths of the blocks. The imide segments at room temperature are below their glassy temperature and their mobility is reduced. The glassy temperature of siloxane segments is below the room temperature, thus these segments enable to migrate to the copolymer surface area.

Experimental

Synthesis of PIS block copolymers

2-Aminoterminated polyimides with controlled molecular weight were synthesized by solution imidization. The number-average molecular weights of products were in the range M_n = 2000–18,000 g mol^{-1} (by ^{1}H NMR spectroscopy). α,ω-bis(3-aminopropyl) polydimethylsiloxanes were prepared by anionic ring-opening equilibrium polymerization initiated with potassium siloxanolate. Their molecular weights were in the range M_n = 1000–5000 g mol^{-1}. Polyimide–polysiloxane copolymers were prepared via transimidization route[5].

Measurement methods

Surface energy

The surface energy of PIS block copolymer was determined via measurements of contact angles of a set of testing

liquids (i.e. re-distilled water, ethylene glycol, formamide, methylene iodide, 1-bromo naphthalene using SEE (Surface Energy Evaluation) system completed with a web camera (Masaryk University, Czech Republic). The surface energies of the polymer were evaluated by Owens-Wendt-Rabel-Kaelble (OWRK) equation modified by the least squares method[6].

XPS

The XPS spectra were recorded with an angle-resolved photoelectron spectrometer ADES 400 (VG Scientific) equipped with Mg Ka and Al Ka excitation sources, and a movable hemispherical electron energy analyzer. The analyzer was operated in the FAT mode at pass energy of 100 eV.

SEM

Morphology of the samples was studied by methods of electron microscopy – SEM and TEM. The surfaces of prepared block copolymers were observed using JSM 6400 (Jeol, Japan) microscope. The samples were sputter-coated by a thin layer of carbon due to better contrast of materials.

Results and discussion

Fig. 1 shows the surface energy ant its polar component of PIS block copolymer versus content of siloxane in copolymer. The surface energy of PIS decreases significantly with the concentration of siloxane from 46.0 mJ m^{-2} (net polyimide) to 34.2 mJ m^{-2} (PIS with 10 wt.% of siloxane), and to 30.2 mJ m^{-2} (PIS with 30 wt.% of siloxane). The polar component of the surface energy reached the value 22.4 mJ m^{-2} [net polyimide], which decreases with content of siloxane in PIS copolymer to 0.8 mJ m^{-2} (30 wt.% of siloxane) The decline of the surface energy, and its polar component of PIS block copolymer with raising siloxane content are very intense mainly between 0 and 10 wt.% of siloxane in copolymer. In the case of further increase of siloxane concentration (above 20 wt.% of siloxane), the surface energy of PIS copolymer, and its polar component is leveled off.

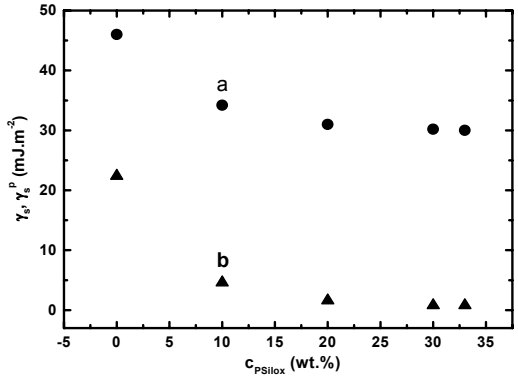

Fig. 1. **Surface energy (a) and its polar component (b) of PSI block copolymer *vs*. siloxane content**

XPS

Table I shows the element concentrations on the surface of the PSI block copolymer. For larger content of siloxane component, atomic concentration of Si increased, and atomic concentration of nitrogen decreased, as expected. XPS measurement was carried out at take-off angle of the emission 60˚ measured from the surface normal. The relation between Si and N reflecting the concentration of siloxane in PIS block copolymers is introduced to the last column of the Table I. The XPS results indicate the surface segregation of the siloxane component in the copolymer. The net polyimide contains by XPS analysis no Si atoms. XPS analysis at take-off angle 60° of PSI block copolymer shows an increase of the relation Si/N to: 6.8 (10 % copolymer); 19.6 (20 % copolymer). Only 2.8 of Si/N have been determined in the case of 30 % copolymer. The concentration of Si in 30 % copolymer is significantly lower than in the case of 20 % copolymers and might be caused by the changes in the chemical matrix of PIS block copolymer during its preparation. The above-summarized XPS results suggest significant enrichment of the surface layer of PSI block copolymer by Si and/or by siloxane segments most probably due to micro phase segregation the polar polyimide matrix.

SEM

Table I
Content of the element (at. %) at the surface of PSI block copolymers measured by XPS

	C	O	N	Si	Si/N
net PI	85.3	12.1	2.5	--	0
10 % silox.	73.5	14.9	1.5	10.2	6.8
20 % silox.	65.2	18.3	0.8	15.7	19.6
30 % silox.	81.9	12.2	1.6	4.4	2.8

SEM micrographs of net polyimide and PSI block copolymer with 30 wt.% of siloxane are shown in Fig. 2. The changes on the surface of the PSI block copolymers in comparison with net polyimide reflects the micro phase separation

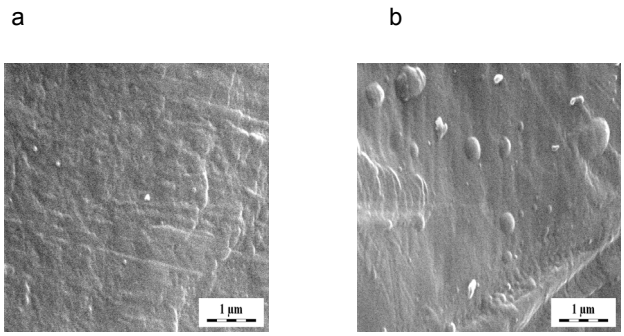

Fig. 2. **SEM micro photos of polymeric film containing net polyimide (a), and PSI block copolymer with 30 wt.% of siloxane (b)**

of the siloxane blocks forming a siloxane enriched circle places on the surface of the copolymer. SEM micrograph shows the surface of net polyimide (Fig. 2a) containing very fine roughness. In the case of 30 wt.% of siloxane in PSI copolymer (Fig. 2b) the roughness is higher comparing to net polyimide due to creation of the micro phase separated structure.

Conclusion

(i) the content of siloxane in copolymer increased, the surface energy, and its polar component of PSI copolymer diminished,
(ii) the morphology of PIS block copolymer has been changed due segregation of siloxane segments; constitution of polyimide continuous phase in copolymer was affirmed,
(iii) XPS analysis affirmed the surface segregation of the siloxane component in PIS copolymer.

The research was supported by Slovak Scientific Agency project VEGA, No. 2/7103/27 and by projects of the Grant Agency of the Academy of Sciences of the Czech Republic (A400500505, IAA100100622). and by Institutional Research Plan No. AV0Z10100521 is acknowledged as well.

REFERENCES

1. Chan-Park M. B., Tan S. S.: Int. J. Adhes**.** Adhesives *22*, 471 (2002).
2. Liaw W. C., Chen K. P.: J. Appl. Polym. Sci. *105*, 809 (2007).
3. Lu C., Wang Z., Liu F., Yan J., Gao L.: J. Appl. Polym. Sci. *100*, 124 (2006).
4. McGrath J. E., Dunson D. L., Mecham S. J., Hedrick J. L.: Adv. Polym. Sci. *140*, 61 (1999).
5. Sysel P., Hobzova R., Sindelar V., Brus J.: Polymer *42*, 10079 (2001).
6. Novák I., Števiar M., Chodák I., Krupa I., Nedelčev T., Špírková M., Chehimi M. M., Mosnáček J., Kleinová A.: Polym. Adv. Technol. *18*, 97 (2007).

CL-18
INVESTIGATION OF HIGH FREQUENCY DYNAMICS OF POLYMERS AND POLYMER BLENDS

CRISTIAN A. OPRISONI, THOMAS ALSHUTH, and ROBERT H. SCHUSTER

Deutsches Institut für Kautschuktechnologie e. V., Eupener Str. 33, 30519 Hannover, Germany
Cristian.Oprisoni@dikautschuk.de

A detailed knowledge of the dynamic – mechanical properties of elastomers on a frequency range that spans from 0,1–1 Hz to the high MHz region is highly awarded for modern product design. Currently, predictive testing of rubber parts at frequencies up to 1000 Hz can be performed with a reasonable accuracy by a wide array of testing equipments as for instance dynamic mechanical analyzers (DMA). Meanwhile, the behavior at higher frequencies, up to the MHz region, is affected by a scarcity of direct measuring techniques. The knowledge of the dynamic properties in this frequency range is crucially important for the prediction of grip phenomena.

The aim of this contribution is to study the influence different microstructures and fillers have on the high frequency dynamics of different rubbers. As a more global aim it is of great interest to predict the behavior of a rubber part during service when exposed to high frequency excitations.

The knowledge of the acoustic* properties of polymers, longitudinal and shear sound velocities and damping, contributes to a better understanding of the material properties at high frequencies especially of the structural characteristics of these polymers. The main characteristics of an acoustic wave are sound velocity and sound absorption or damping. The latter is a measure of the energy removed from the sound wave by conversion to heat during its propagation through a certain medium and it is a material property, different from attenuation, which also includes energy loss due to scattering and reflection and depends on sample size and experimental configuration.

Ivey et al. measured the longitudinal wave velocity and damping using the pulse transmission technique on IIR, SBR and NR at frequencies between 0.04 and 10 MHz in a temperature range from –60 °C to 40 °C. The rotating plate method was employed by Kono to measure transverse and longitudinal wave propagation on polystyrene and polymethyl methacrylate (PMMA) at frequencies of 0.5, 1 and 2.25 MHz in a temperature range from 20 °C to 210 °C and drew some conclusions with regard to the effect of large side groups on the positions of the longitudinal and shear maxima on the temperature scale and the effect of frequency on the maxima shift. Also Yee and Takemori calculated the dynamic compression modulus and the shear modulus from the simultaneous measurement of the dynamic Young's modulus and Poisson's ratio on PMMA at frequencies of 0.01, 0.1, 1 and 11 Hz between 0 °C and 40 °C.

Theoretical aspects

In an unbound, isotropic solid, two types of waves can be propagated. In one case the chain segments vibrate along the direction of propagation producing a longitudinal wave. In the other case the motion is perpendicular to the direction of propagation and is called a shear wave. The latter type of wave cannot be measured with the current experimental setup and will not be discussed here.

The current construction of the ultrasonic spectrometer allows the measurement of the longitudinal waves due to the positioning of the samples at a 90° angle to the incident wave.

* The term *acoustic* refers to a periodic pressure wave and it includes both audible and inaudible (infrasound and ultrasound) sound waves.

This position is critical since any variation of the angle would induce shear waves in the sample and reduce the precision of the measurement.

When longitudinal waves are propagated along thin strips and the wavelength is large compared to the sample thickness but small compared to its length the deformation is a simple extension and the complex Young's modulus is measured. At the other extreme, when the wavelength is small compared to the sample dimensions the wave propagation is governed by the complex longitudinal wave modulus:

$$M^* = M' + iM'' = \frac{4}{3}G^* + K^* \qquad (1)$$

where M* – complex longitudinal wave modulus, M' – storage part, M'' – loss part, G* – complex shear modulus, K* – compression modulus.
In the above equation the components of the complex longitudinal modulus are calculated as follows:

$$M' = \frac{\rho c_{rubber}^2 (1-\beta^2)}{(1+\beta^2)^2} \qquad (2)$$

$$M'' = \frac{2\rho c_{rubber}^2 \beta}{(1+\beta^2)^2} \qquad (3)$$

where

$$\beta = \frac{\alpha_{rubber} c_{rubber}}{2\pi f}$$

ρ – rubber density, c – sound velocity, α – damping coefficient, f – frequency

As can be seen from equations (*2*) and (*3*), the unknown terms are c_{rubber} and α, the sound velocity in the rubber and the attenuation coefficient, respectively. Both these terms are measured by the ultrasonic spectrometer (Fig. 1) and they give the first insight on the polymer behavior at high frequency.

As seen above calculating the components of the complex longitudinal wave modulus is not a difficult task, however comparing it with the complex shear modulus is quite tricky due to the composition of the first:

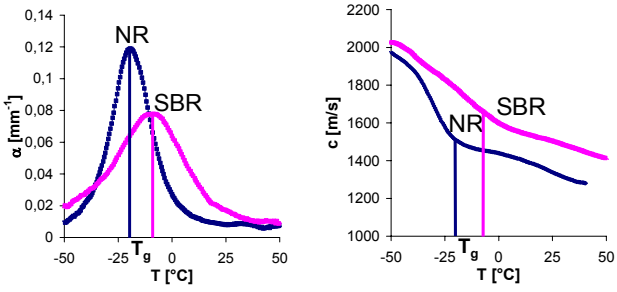

Fig. 1. **Sound attenuation (left) and velocity (right)**

$$M^* = \frac{4}{3}G^* + K^* \qquad (4)$$

$$K^* = K_0 + K_1^* \qquad (5)$$

$$K_1^* = K_1' + iK_1'' \qquad (6)$$

In the above equations K_1^* is the frequency dependent component and K_0 is the temperature dependent static compression modulus.

Experimental

The polymers used were, alongside the SBRs with varying styrene and vinyl content (Table I), SBR 2525, NR CV50 and 3 NBRs with different acrylonitrile (ACN) content (18, 28, 34 and 44 % ACN, respectively).

Table I
Solution SBR systems – styrene and vinyl variation

Material	SSBR 20/60	SSBR 20/45	SSBR 30/30	SSBR 20/30	SSBR 10/30
Styrene, %	21	21	30	21	10
Vinyl, %	62	46	33	31	33
T_g (DSC), °C	–21	–38	–38	–50	–60

The polymers were mixed and crosslinked to the rheometer optimum (160 °C) using a common vulcanizing system (sulfur – 2 phr, TBBS – 2 phr, stearic acid – 1 phr and zinc oxide – 3 phr) and an anti aging agent (6PPD) – 4 phr. Carbon black (N347) and silanized silica were incorporated at loadings of 20, 40 and 60 phr in an one step mixing process by using an internal mixer (Haake Rheomix 3000E) at 50 rpm.

Dynamic-mechanical analysis were carried out on samples of 2×10×35 mm^3 in size, on an RDA (Rheometrics Data Analyzer) apparatus, in torsion, at an amplitude of 0,5 %. The temperature increase rate for the temperature sweeps (–60 °C – +60 °C) was 1 °C min^{-1} and the testing frequency was 1 Hz.

High frequency measurements were performed in a prototype ultrasonic analyzer at 0,5 MHz using the wave transmission technique.

Results

Unfilled polymers

The increase of the styrene and vinyl content determines higher values of the loss moduli (Fig. 2).

The glass transition is shifted to higher temperatures with increasing styrene and vinyl content. This increase is

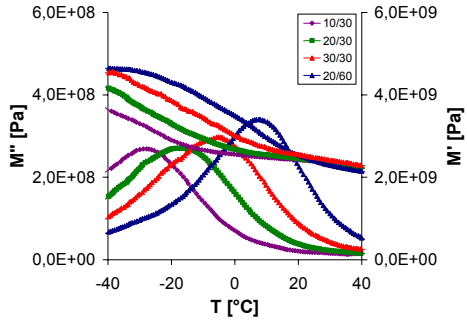

Fig. 2. **Real (M') and imaginary (M") part of the longitudinal wave modulus for unfilled polymers**

expected since the presence of side groups on a macromolecular chain induces steric hindrances that reduce its capability of free motion. Furthermore, the more side groups the more energy is needed for the chain to move and, hence, the higher the maximum of the M" peak.

It's worth noticing that the styrene influence, in the case of the SBRs, is lower than that of the vinyl due, probably, to an increased molecular friction induced by the latter.

A similar behavior is observed for NBR when increasing the ACN content. It brings about a shift of the glass transition to higher temperatures as well as an increase of the magnitude of the loss modulus. The NBR with the highest content of ACN also displays the smallest half width.

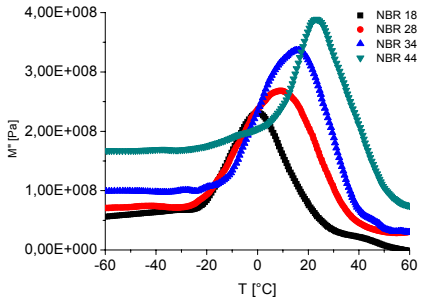

Fig. 3. **Loss component of the longitudinal wave modulus for unfilled NBRs with increasing ACN content**

Polymer blends (SBR:NR)

The discussion sets forth with the low frequency analysis. A first glimpse at the shear data ascertains that the two polymers are immiscible but for the SBR:NR 20:80.

A simple estimation shows that about 17 percent of the SBR is apparently soluble in the NR forming a single phase. Over this quantity, more SBR phase separation occurs with one pase composed of NR and SBR and a distinct second phase containing SBR only.

Table II
Glass transition temperature (G"max) of the SBR/NR blends

SBR/NR	0/100	20/80	40/60	50/50	60/40	80/20	100/0
Tg SBR, °C	n. a.	n. a.	–39	–41	–42	–42	–42
Tg NR, °C	–60	–58	–58	–58	–57	–57	n. a.

When one considers the glass transition temperatures of the different mixes, the addition of 20 percent of SBR induces a 2–3 °C shift in the transition temperature which does not change any further when adding more SBR. This shift compared to the 18 °C difference between the two raw polymers indicates an approximate amount of 15 percent of SBR in the mixed phase.

The 0,5 MHz measurements show the same ranking of the blends according to their different concentrations.

The difference between the transition temperatures of the 2 peaks is reduced from 18 °C at 1 Hz to only 14 °C at 0,5 MHz. The highest energy dissipation is shown by the unblended NR. With the addition of SBR the height decreases while the broadness of the peaks increases slightly. The glass transition temperature (due to the high frequency only one

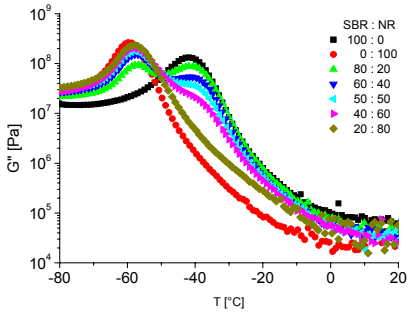

Fig. 4. **Shear modulus of the SBR/NR blends at 1 Hz**

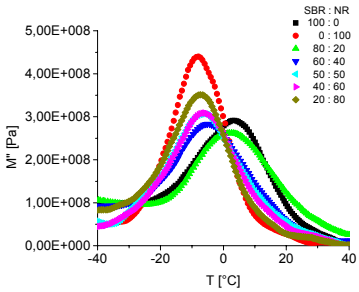

Fig. 5. **Energy dissipation of the SBR/NR blends at** 0,5 MHz

** The difference between the solubility parameters of NR (δ = ~1,7 $Pa^{-1/2}$) and SBR (δ = ~17 $MPa^{-1/2}$)[6] means that the two polymers are insoluble. However, the dynamic – mechanical measurement at 1 Hz does not distinguish 2 phases below 17 % of SBR

Table III
Glass transition temperature (maximum attenuation) of the SBR/NR blends

SBR/NR	0/ 100	20/ 80	40/ 60	50/ 50	60/ 40	80/ 20	100/ 0
Tg SBR, °C	n. a.	n. a.	n. a.	n. a.	3	4	6
Tg NR, °C	–8	–5	–5	–5	–4	–5	n. a.

peak is seen for all mixes) does not change significantly until 80 parts of SBR are added when it shifts close to the SBR temperature at 0,5 MHz. Seen from the right to the left, the addition of 20 parts of NR into SBR determines, similar to the addition of SBR in NR, a decrease in the maximum dissipated energy and a broadening of the peak. The joining closer together and the higher broadness of the peaks is a well known effect of the increase in frequency.

As a result the different peaks of the polymers can no longer be distinguished and the NR seems to dominate at this frequency.

Filled polymers

The addition of carbon black to the SBR mixes determines an overall increase of the moduli and a widening of the loss peaks due to the noticeable filler – polymer interaction.

As was to be expected the glass transition temperature does not vary significantly with the filler concentration.

Silica was also used in the experiments presented in this contribution. Because pure silica is seldom used nowadays, a surface treatment was applied using silan Si69. The silanization lead to important changes in its reinforcing characteristics. If one considers the surface energies of carbon black and (unsilanized) silica, the main difference resides in the fact that, due to its high dispersive component, carbon black achieves reinforcement by strong rubber-filler interactions while its filler-filler network is weak whereas silica reveals a weak interaction with the rubber (by comparison with carbon black) but a good interaction with itself forming a strong filler-filler network.

After the silanization, the dispersive component of the surface energies drops even compared to the unmodified silica, and the polar component (which gives a hint on the strength of the filler-filler interaction) becomes insignificant thus the formation of the filler network is prevented.

The result of this effect is shown in Fig. 7, where the maxima of the loss longitudinal modulus is plotted against the styrene fraction for unfilled rubber and filled with carbon black and silanized silica. The silica filled material displays lower energy dissipation than its carbon black filled counterpart.

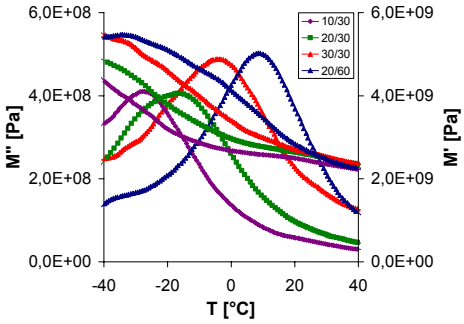

Fig. 6. **Real (M') and imaginary (M") part of the longitudinal wave modulus for filled polymers (60 phr carbon black)**

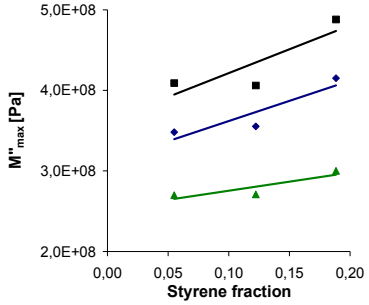

Fig. 7. **Filler and styrene content influence on the maxima of the longitudinal wave modulus**

Conclusions

A clear and accurate picture of the high frequency behavior of rubber materials is difficult to asses and ultrasound is one of the few methods able to directly measure dynamic properties in the MHz region.

The discrete influence of the polymer microstructure (vinyl, styrene and acrylonitrile content) as well as that of nanoscaled fillers on the chain dynamics is analyzed at 0,5 MHz.

Ultrasound spectroscopy proves to be a valuable tool in determining energy dissipation at high frequency for polymeric blends; the shifting procedure associated with the WLF equation cannot be applied to most blends.

The authors would like to express their gratitude to the Deutsche Kautschuk – Gesellschaft e. V. for providing the financial means to carry out this research and to Lanxess Deutschland GmbH and DOW Olefinverbund GmbH for supplying the polymers.

REFERENCES

1. Sinha M., Buckley D.: *Acoustic Properties of Polymers in Physical Properties of Polymers Handbook*, 2nd Edition, (J. E. Mark, ed.) *60*, 1021, 2007.
2. Ivey D. S., Mrowca B. A., Guth E.: J. Appl. Phys. *20*, 486, (1949).
3. Kono R.: J. Phys. Soc. Jpn. *15*, 718 (1960).
4. Yee A. F., Takemori M. T.: J. Pol. Sci., Part B: Polym. Phys. *20*, 205 (1982).
5. *Science and Technology of Rubber*, 2nd ed., Academic Press, 1994.
6. *Polymer Handbook*, Second Edition, J. Wiley & Sons, New York 1975.

CL-19
THERMAL DESORPTION –
PROGRESSIVE WAY OF ANALYTICAL CHEMISTRY ON PLASTICS AND RUBBERS

FRANKY PUYPE and JIŘÍ SAMSONEK

Institute for Testing and Certification – Zlín, Třida T. Bati 299,CZ-764 21 Zlín-Louky
fpuype@itczlin.cz

1. Introduction

Thermal desorption (TD) is the last decade a sampling technology in evolution. The main applications are supporting the automotive and building material industry as well the environmental sector.

This evolution goes simultaneously with the complaints about odors and emissions of volatile organic compounds from plastic/rubber material causing a major problem for indoor air quality. This paper describes briefly the analytical approach of analyzing a broad range of plastic/rubber materials with thermal desorption gas chromatography coupled with mass spectrometry (TD-GC-MS).

Thermal desorption is defined as a sampling technology that utilizes heat to increase the volatility of analytes such that they can be removed (separated) from the solid matrix (plastics, wood, textile, extracts, foam, hair, gel, paint, etc.). Thermal desorption allows analysis of almost all sorts of materials including insoluble materials and complex materials at trace levels without any pretreatment of samples.

TD-GC-MS is used since short time in many applications due to the many advantages compared to conventional solvent-based sample preparation methods like solvent extraction, solvent exchange and steam distillation. Advantages of thermal desorption are mainly:

- 1000 fold improvement of the sensitivity because there is no solvent needed which is diluting the interested analyte. A good sensitivity is needed when looking for ultra-trace compounds
- Automation: vapours or test materials are collected/ weighted into sample tubes or cups and directly introduced on the thermal desorber unit.
- There is no additional sample preparation required. This is saving time and costs. Conventional analytical methods like gas chromatography, thin layer chromatography (TLC) and liquid chromatography (HPLC) require a time consuming liquid extraction.
- Nearly no sample contamination is possible due to reduced manual preparation.
- There is selective focus on compounds of interests without interferences like water.
- There is no contamination from solvent peaks. The chromatographical data is coming from the sample itself.
- The adsorbent tubes are reusable, the solvent consumption is lead to a minimum. It eliminates the envirionmental health and safety issues.

There are 2 basic possibilities for sampling. The first possibility is the easiest. The sample is direct desorbed as it was placed into a sample tube or cup used for TD-GC-MS. The second possibility is the purge and trapping of air or vapours from a solid sample on sorbent tubes followed by TD-GC-MS.

This purge and trapping process is mostly done by off-line process (emission chamber technique and on-site air quality measurement). The on-line trapping process is practically done by refocusing thermal desorption instruments (chapter 2.2). The sorbent has to be chosen according to the analyte which is required. There are on the market lots of sorbent materials available that for each application there exists a sorbent however nowadays there are more universal trapping materials used like carbon absorbent material (carbotrap) and polymeric adsorbents (TENAX TA). They can according to the application be used as mixed combinations (TENAX GR). All of them have a low affinity for water and methanol.

The thermal desorption range varies from very volatiles (Bp 0 °C) till the "heavies" from the semi-volatile class (Bp 400 °C, MW approx. 1000 g mol^{-1}). The use of temperatures higher than 400 °C will lead to a C-C bound cleavage. This is not favored due to the pyrolysis process of the analyte and the polymer matrix as well.

2. Available systems

Below are given the commercial systems available for thermal desorption at this moment. They are devided according the injection technique however all are based on the same processes: desorbing, separating and detecting.

2.1. Direct thermal desorption

The easiest commercial thermal desorption systems are direct thermal desorption systems. The sample is transported to a furnace and at certain temperature heated. The evolved gasses are going immediately to the beginning of the analytical column and the analysis starts. Direct thermal desorption is mainly used for fast screening or quantitative analysis of high mol weight compounds (up till 1000 g mol^{-1}). The main application with direct thermal desorption are the identification of antioxidants/brominated flame retardants in plastic materials and accelerators/stabilisers in rubbers. Fig. 1 shows a schematic presentation of direct thermal desorption system.

There are a number of considerations to be made for this analysis. Firstly the sample needs to be very small (max. 10 mg) and therefore the sample should be sufficiently homogeneous. The sample needs to have a relatively high surface area. This surface area is needed to have an optimum diffusion process from inside the polymer/rubber to the gas stream.

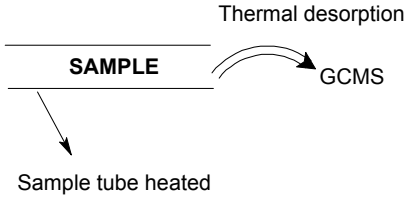

Fig. 1. **Schematic presentation of direct thermal desorption system**

2.2. Refocusing thermal desorption (cold trap)

A more complex thermal desorption system is refocussing thermal desorption. The sample is transported into a furnace and the evolved gasses are refocussed on a cooled adsorption tube with TENAX TA. Refocusing is a collection technique. A volume of several liters of gas is pulled over an adsorption tube. Permanent gasses pass the tube while molecules with higher molecular weight remains on the absorbent in the sample tube. Refocusing is done by cooling. The injection exists of fast heating of this TENAX TA trap and evaporating the analytes towards the analytical column.

Refocusing thermal desoption has the advantage that the analytical peaks are far sharper and the sensitivity is bigger. The TENAX TA trapping material has a high capacity and it is possible to refocus the analytes for a longer time. This longer trapping time is required for quantitative analysis.

The thermal desorption unit used for this paper was a TD-20 system (Shimadzu) with Peltier cooling/programable tempearture vaporising injector. The advantage of the TD-20 systems is that they have a reverse sample path. The sample leaves the TENAX TA tube in opposite direction than it was trapped (Fig. 2).

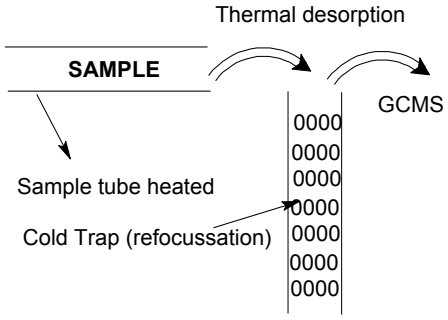

Fig. 2. **Schematic presentation of a refocusing thermal desorption system**

2.3. Emission chamber-TD-GC-MS

The test chamber method followed by thermal desorption is an analysis which is associated with the "sick building syndrome" for building materials but can also applied for testing of car materials and air quality measurements. Sick building syndrome (SBS) is a combination of ailments associated with an individual's place of work (office building) or residence. A 1984 World Health Organization report into the syndrome suggested up to 30 % of new and remodelled buildings worldwide may be linked to symptoms of SBS. Most of the sick building syndrome is related to poor indoor air quality.

The principle of the emission chamber can be explained that the sample is staying at certain conditions (temperature and humidity) in an emission chamber. The most influencing factor is the air exchange rate. It is possible to regulate the flow and change the air by continue stream. The air can flow over an adsorbent tube filled with an appropriate trapping material (Fig. 3). The emissions can be measured by performing refocusing TD-GC-MS analysis of the adsorbent tube. The main application with this chamber is the ISO 16000 emission chamber test for building material. However the automotive industry needs a similar testing for characterizing air quality in car interiors.

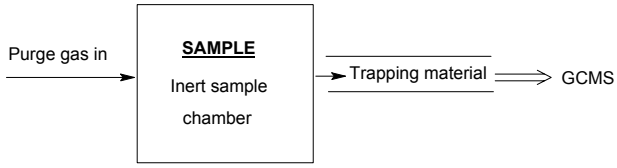

Fig. 3. **Schematic presentation of a test chamber system**

The emission chamber can predict long term emissions for real areas like car interior or rooms. The mass spectrometry detection can not only detect the real emissions and odor but also give understanding of the reaction mechanism between emissions. It is known that carpets and water based adhesives might cause a reaction between the hydrolysed phenoxypropanol and the inorganic bromine from the latex textile covering. This is resulting in formation of smelling bromophenols.

2.4. Evolved-Gas-Analysis (EGA)

Evolved gas analysis is a thermal analysis which determinates evolved products at certain temperature. The polymer sample is placed in a desorption unit and the evolved gasses are immediately detected by GC-MS. This analysis doesn`t need chromatographical separation due to the quick gas flow in the system. The analysis result is a graph with in abscissa the desorption temperatures and in ordinate the identified volatile and its intensity. Evolved gas analysis is comparable with thermal gravimetrical analysis but has the advantage to give the exact compound identification due to the mass spectrometrical detection (Fig. 4).

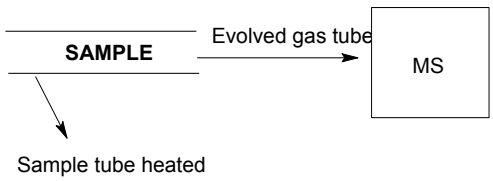

Fig. 4. **Schematic presentation of a the EGA analysis**

This method is mostly used to optimize the production process temperatures. Sometimes during polymer preparing processes some unexpected thermal reactions might occur or component loss. A sim ulation of the production process can learn a lot about the behavior of the blended compounds. This is applicable for rubber blends as well for polyolefin/ condensed polymers.

3. Potential applications for automotive industry

3.1. Additives from plastic material and rubber

The trend observed in plastic technology is that the additives are far higher mol weight molecules. This is needed to get them more stable and slow down the migration in the plastic material. To get an identification report of the additives classical liquid extraction might be applied. The quick thermal desorption is again a great alternative. This method can be used to check the raw materials or defects from the supplier. The automotive business requires certain quick analytical methods like this.

In Fig. 5 is seen that all the additives are separated from the matrix peaks. The polycarbonate was stabilized against oxidation by irgafos 168 and irganox 1076. While the sample also was stabilized against UV by tinuvin 350 and uvinul 3027.

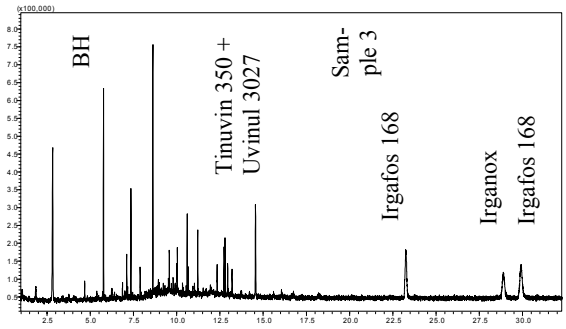

Fig. 5. **Additive screening by TD-GC-MS of polycarbonate based coating**

3.2. Volatile organic compounds (VOC/SVOC)

VDA is the German Quality Management System (QMS) for the automobile industry (Verband der Automobilindustrie). Their VDA 278 norm describes the emission from plastic materials intended to use in automotive industry. This analysis exists into two parts:

– The first part describes the volatile organic compound analysis (VOC) with thermal desorption at 90 ºC for 30 minutes. The peaks are calibrated with and compared to a toluene standard.
– The second part describes the semi-volatile organic compound analysis (FOG) with thermal desorption at 120 ºC for 60 minutes. The peaks are calibrated with and compared to a hexadecane standard.

The example in Fig. 6 shows a chromatogram overlay of VOC analysis. 3 polyethylene samples were measured and were taken from different batches. This method proved that the lowest 2 chromatograms (sample 1 and 2) have a VOC value of 360 μg g^{-1} toluene equivalent. The sample 3 (highest chromatogram) gives the highest VOC emission of 500 μg g^{-1}

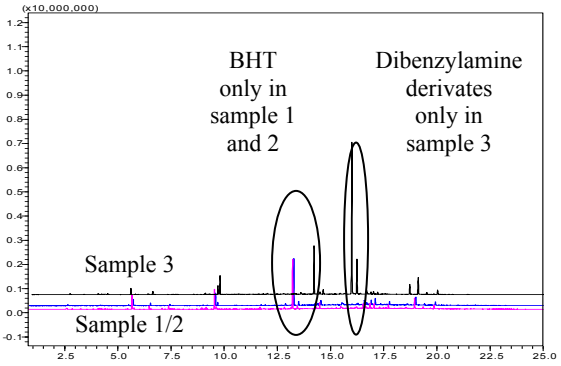

Fig. 6. **VOC analysis of 3 polyethylene samples by refocusing GC-MS**

toluene equivalent. The VOC analysis shows that the material is based on the same due to the presence of similar matrix releated emissions. The used additives are different. Sample 1 and 2 contains butylated hydroxyl toluene (BHT) at retention time 13,2 min while sample 3 contains dibenzylamine derivates at retention time 16 minutes.

This VDA 278 analysis gives information about the additives and their emission value. The power of this method is that the emission of a single compound can be calculated and the formulation can be adjusted by reverse engineering.

3.3. Defect analysis

Thermal desorption is a perfect tool for the explanation of many defects on surfaces and raw materials for automotive industry. Defects can either be surface defects like blooming, cracking, discoloring or smelling but also physical defects like cracking, weakening, etc.

The rubber production process is one by complex handlings after each other like mixing, extrusion, calandering, vulcanization but also storage. This happens all under certain conditions like temperature and mixing speed but also by adding a complex mixture of chemicals. Not only the rubber industry but the automotive polymer industry in common is more and more faced by short delivery times and high production speed. This all can lead to defects in production and storage due to the lack of good storage conditions. Rubber for instance is still vulcanising during storage. As the rubber product arrives to the customer it sometimes happens that the defect is noticed after selling the final product.

The chromatogram below in Fig. 7 shows a defect from a polypropylene production plant. The lower chromatogram gives the reference sample which has no defect at all. The paint was adhesive to the polypropylene profile. The upper chromatogram shows the defect sample where the paint could not stay on the polypropylene profile. A simple screening by direct thermal desorption proved the presence of wax in the defect sample.

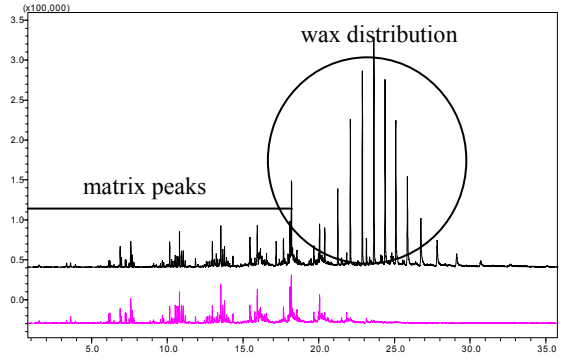

Fig. 7. **Determination of differences between polypropylene samples can lead to a solution for defects in the production**

3.4. Liquid injections/extracts/washes

To omit the large volume injections in liquid chromatography large volume injections can also be done easily by thermal desorption. An amount of 100 µl can be added to a tenax tube if the solvent is methanol. Other solvents can be used if the analyte is much heavier than the solvent. The solvent can evaporate and the analyte remains in the sample cup or tube. This residue can be oil or a thin film which is excellent for using thermal desorption.

Applications are mainly surface related problems of car parts like dashboards, rubber, leather, tires, driving wheel, carpets, paint, adhesives, etc.

Blooming is a recently more and more appearing defect which implements the migration of additives, accelerators towards the surface or a synthetic polymer. The surface gets affected by a flower field shaped structure and even a snow white layer can be seen if the sample is blooming for long time.

This blooming process is depending on the polarity of the analyte, its volatility, concentration, migration time and storage conditions. The following example is the analysis of a blooming door panel. The white smear on the surface is making a flowerfield structure on the surface of the sample (Fig. 8).

Fig. 8. **Detailed picture of a blooming defect on a car door panel**

Thermal desorption after surface washing proved that the bloom was caused by the toxic hexabromocyclododecane (Fig. 9). This is a commonly used flame retardant for automotive applications. On the surface of the blooming panel was seen such a high concentration of hexabromocyclododecane that there was surely a mistake in the production line of the manufacturer.

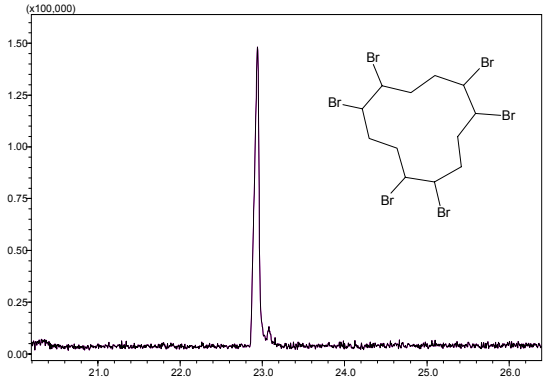

Fig. 9. **Chromatogram after TD-GC-MS of a surface wash for blooming analysis**

4. Conclusion

The new trends in modern analytical chemistry are based on quickness, trueness and quality. The automotive/rubber sector requires the same assessments and both sections are fully cooperating with labs nearby. To fulfill the needs of the industry thermal desorption can save lots of time and money compared to the classical wet chemistry or instrumental chemistry.

Its applications range from quality control to defect analysis. The importance of this technique is still not well understood by customers from analytical laboratories. However the huge number applications with this technique are proving their need.

REFERENCES

1. Burt T.: Indoor and Built Environment, Vol. 5, No. 1, 44-59 (1996) DOI: 10.1177/1420326X9600500107
2. Hinshaw. John V.: LCGC *18*, 940 (2008).
3. Baier HU: Shimadzu news 2 (2007).
4. Markes international limited, Thermal desorption and air monitoring products, 2006.
5. Supelco, air monitoring – a complete line of products for air monitoring, 2008.

CL-20
EMISSION BEHAVIOUR OF NON-METALLIC PARTS, INTENDED INTO A CAR INTERIOR

JIRI SAMSONEK and FRANKY PUYPE

Institute for testing and certification, a.s. Tř. T. Bati 299, 764 72 Zlín, Czech Republic
analyt@itczlin.cz

Introduction

Almost all car manufacturers take care about environment inside the car having regards the passenger's health, comfort or protection. Modern car interiors are loaded by many non-metallic components (plastics, rubbers, textiles, varnishes, lubricants or adhesives) so the study of their influence on the car environment is vital. The approach of each car manufacturer varies, but generally they are based on similar principles. Material is tested under the conditions that simulate real conditions in a car environment.

Testing is based on establishing of the balance between solid phase (tested sample) and vapour phase (ambient air or generally gaseous phase). Then the vapour phase (or substances, that are emitted to the gaseous phase) are subjected to the analysis. Standards are aimed on testing of odour, total organic compounds, selective organic substance emission and transport behaviour of certain substances.

Examples[1] of volatile organic substance (VOCs) and semi-volatile organic substances (SVOCs) are:
VOCs – alkans, alkens, aromatic hydrocarbons, carbonyl compounds, alcohols, esters, ethers, aldehydes, halogenated hydrocarbons, terpenes, nitrogen and sulphur compounds
SVOCs – high boiling point substances such as paraffins, glycols, higher fatty acid and their esters, phenols, phthalates, adipates (generally plasticisers), organophosphorous substances, organobromine substances (flame retardants), organosilicon substances (silicon oil), amines (catalysts from PU foams) etc.

Emission kinetics

The process of vaporisation of volatile or semi-volatile organic substance (low molecular substances) from solid material (plastic, rubber, textile) can be described from thermodynamical point of view by many equations. The basic is vapour pressure equilibrium. All liquids and solids have a tendency to evaporate to a gaseous form, and all gases have a tendency to condense back into their original form (either liquid or solid). The equilibrium is dependent on the temperature, molecular weight, interaction between substance and the solid matrix and interactions between each volatile substance.

Presence of volatile and semivolatile compounds in the car environment can be described by following balance diagram:

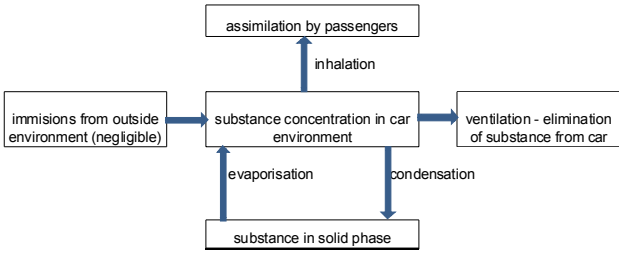

Fig. 1. **Emission diagram**

The main process that occurs is vaporisation and subsequent condensation. The imisions from outside are source of different substances (like exhaust fumes, dust etc.). They have no relation to the emission behaviour of car material. Comparing to the concentration levels of organic pollutants inside the car it can be named as a "diluting or clean" air. Over a long period of non-usage of a car the vaporisation and condensation reach equilibrium so the air is saturated by volatile and semi-volatile substances. All the process depends on a temperature, the higher the quicker the equilibrium is reached and higher is the final concentration level of each substance. Passengers are exposed to this equilibrium emission concentration immediately after they sit into the car. As they run a car and the air exchange dilutes the ambient environment the concentration of chemicals start to decrease. The opposite process can be increasing the emission flow by heating of interior caused by car-heating system. Transport of the pollutant inside the car is complex process. Evaporation and condensation can occur on different surfaces so one material can emit semi-volatile substance and on another material the condensation can occur. A typical phenomenon is fogging of phthalic acid esters. This plasticisers can be emitted to the car environment mainly when it is heated and then strong condensation on the cold front glass result in light scattering thin film on the inside of the windshield[1,2] fogging.

Typical tests of emission behaviour

There are several very often used tests for evaluation of emission behaviour of non-metallic materials in far interiours. Some of them are non-selective, describing complex behaviour of sample, others are selective, focusing on certain substance.

Emissions of total organic carbon

This test evaluates total amount of organic substances emitted under certain temperature and time (typically 120 °C, 5 hours) from the material. The quantification is done by recalculation of all quantifiable substances expressed as an acetone organic carbon. This test can characterise samples capability to emit mainly volatile substances that remains in the sample like residual solvents, monomers, dimmers, volatile and semivolatile additives etc. Semivolatile substances con-

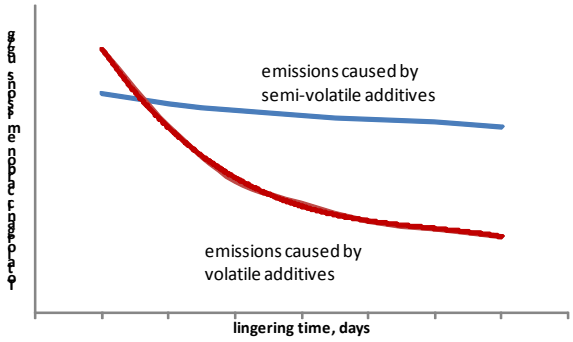

Fig. 2. **Decreasing of TVOC on the lingering time**

tribute to the total emission lower than those of lower boiling point. Excessive results of total organic carbon can be caused by many factors, like high residual monomer content, high dosing of volatile or semi-volatile additives, like plasticisers, lubricants, stabilisers, or residual solvents in the surface treatments. Total organic carbon emissions (TVOC) arising from polymer additives are difficult to omit as even after leaving the part to linger after manufacturing for a longer time almost the same vapour phase equilibrium during the test is reached again. Excessive organic carbon emissions caused by residual high volatile substances like varnish solvents, monomers etc. have a tendency to decrease easily (approximately 20 % per week, with the stabilisation after 6 month[1]) so the total TVOC in the time fall depends mainly on the ratio between high volatile and semivolatile substances in the sample. Higher emission of organic substance does not necessary lead to the worse odour of the material as many of the organics are not sensorial important than others.

Special care is placed on the emission of formaldehyde. Although its emission is included into a total organic carbon these substance is controlled separately[5] due to its enormous influence on the human health. Formaldehyde is classified as a positional carcinogenic substance class 2A.

Fogging behaviour

Mainly presence of semi-volatile substances in the non-metallic car interior parts can lead to the phenomena, named "fogging". Substances with higher boiling point that have vapour pressure which enable them to vaporise during heating can condensate on colder parts of car interiors (windshield). Typical substance that can concern in fogging are phthalic acid esters (phthalates), commonly used as a plasticiser. Also flame retardants of plastics and rubbers can increase the fogging[1] as they show similar behaviour as phthalates because molecular weight and the boiling point of both groups of chemicals are comparable. Fogging-supporting chemicals are generally those that have similar physical/chemical properties like plasticisers or flame retardants. They can be residual catalysts[3], by-products of polymerisation, carriers of colour batches, oils, waxes etc.

Lingering of sample in the storage before testing or assembling cannot decrease significantly fogging characteristics. High loading of car parts by fogging-supporting chemicals supports the fogging effect for a long period of time regardless the number of heating/cooling cycles. To avoid fogging of non-metallic parts the manufacturer has to change the composition of the whole materials.

Special tests are concerning to the direct measurement of light beam reflection[6]. The sample is heated on 100 °C and above it the glass plate, cooled on 20 °C is kept. Then the light beam reflection is measured and compared the clean glass surface reflection.

Odour

Sensorial perception of car interior air is heavily influence by non-metallic parts properties. Regardless the other parameters human smell can detect certain substances on the levels difficult to quantify by common analytical techniques. Samples are tested under defined conditions and raised odour evaluated by group of trained evaluators by use of rating scale. Some car manufacturers have set more detailed standards for describing of the smell[7]. Main substances that can influence the final smell are amine or sulphur-based organics, aldehydes, ketons, organic acids, esters, phenolic substances, products of microbiological proceses etc.

The whole car testing

Another approach can be also applied to the evaluation of emission behaviour. While above mentioned tests are describing each material the summary test of final car can be also applied. Either sensorial tests or analysis of ambient car can be performed or testing of ambient air quality by adsorbing of the air on the sorbents (charcoal tubes, TENAX® sorbents). with this type of analysis we can better understand the real behaviour of VOCs in the real car interior an. Also analysis of fogging film on the windows can give information about real transport of SVOCs in the car interior.

REFERENCES

1. Henneuse C., Catherine Henneuse-Boxus, Pacary T.: *Emissions from Plastics*, Rapra Technology Limited, 2003.
2. Loock F., Lampe T., Bahadir M.: Fresenius' J. Anal. Chem. *347*, (1993).
3. Standard PV 3015, DIN 75201-B.
4. Bradford L., Pinzoni E. and Wuestenenk J.: *Proceedings of the Polyurethane Foam Association, October 17 & 18, 1996*.
5. Standard PV 3900.
6. Standard DIN 75201.
7. Standard TSM0505G.

CL-21
PLASTICS PARTS DESIGN SUPPORTED BY REVERSE ENGINEERING AND RAPID PROTOTYPING

MICHAL STANEK, MIROSLAV MANAS, DAVID MANAS, and STEPAN SANDA

Tomas Bata University in Zlin, Faculty of Technology, Department of Production Engineering, TGM 275, 762 72 Zlin, Czech Republic, stanek@ft.tub.cz

Abstract

Rapid prototyping technologies for easy production of prototype, parts and tools are new methods which are developing unbelievably quickly. The main objective of this article is to give the basic introduction to this problem.

1. Introduction

Successful product development means developing a product of high quality, at lowest cost, in the shortest time, in at a reasonable price[1]. The development of the part and its introduction to market is time consumption process. But „time is money“ and therefore could be said that money saving is greatest when time to market is minimalized utmost.

On principle, the conventional model making processes based on two-dimensional (2D) drawings. The rapid prototyping process is based on complete 3D models. The 3D geometric information from the CAD is split into layer information and the layers are gradually build directly with the aid of the computer. The advantage of the rapid prototyping technologies is the part building possibility using 3D CAD data only.

All process by which 3D models and components are produced additively, that is, by fitting or mounting volume elements together (voxels or layers) are called generative production process. Rapid prototyping describes the technology of generative production processes. The application of rapid prototyping technology lays in solid imagining and functional prototyping. Prototypes are made from plastics (mainly ABS, PVC or special resins, metals or other materials that simulate one or more mechanical or technological functionalities of the final serial component.

Often use word Rapid tooling describes a principles and technologies for tools and molds preparation. This prototypes are used for production of prototypes and preseries products. The rapid tooling uses the same processes as those used in rapid prototyping. Rapid manufacturing represent such a rapid prototyping applications that produce products with serial character. For these purposes can be used most of rapid prototyping methods. But the mechanical and other properties of materials used for the rapid prototyping do not reach mostly the characteristics of the serial products.

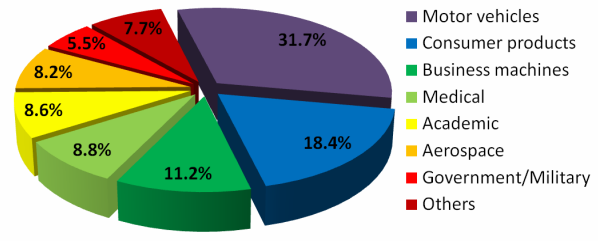

Fig. 1. **Percentage use of rapid prototyping worldwide**

2. Principles of Rapid prototyping

Rapid prototyping belong to the additive production processes. In contrast to abrasive processes such a milling, drilling, grinding eroding etc. in which the form is shaped by material removing, in rapid prototyping the part is formed by joining volume elements. Most of used rapid prototyping processes work with layers where single layers are produced and joined to a final geometry. On principle, rapid prototyping processes are two and half D processes, that is tacked up 2D contours with constant thickness. But for layer creation 3D model is necessary. Rapid prototyping as the generative manufacturing processes are divided among two fundamental process steps:

- generation of the mathematical layer information,
- generation of the physical layer model.

The principle is given in the Fig. 2.

Industrially are used many types of rapid prototyping systems working on different physical principles:

- solidification of liquid materials (polymerization process),
- generation from the solid phase:
  - cutting from foils or paper (LOM),
  - binder of powder or granules,
  - powder sintering,
- generation form the pasty phase.

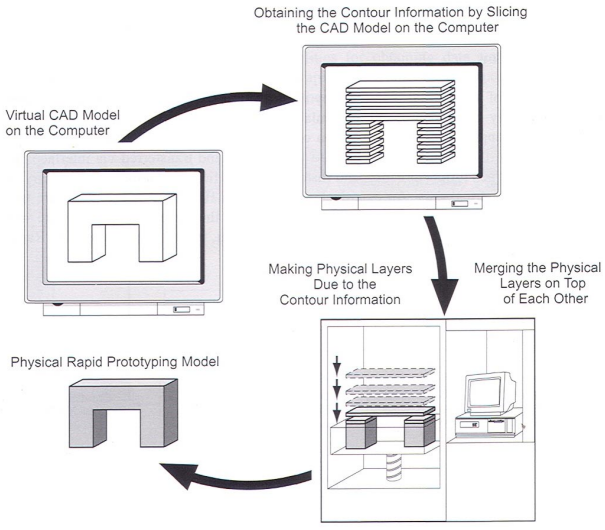

Fig. 2. **Rapid prototyping principle**

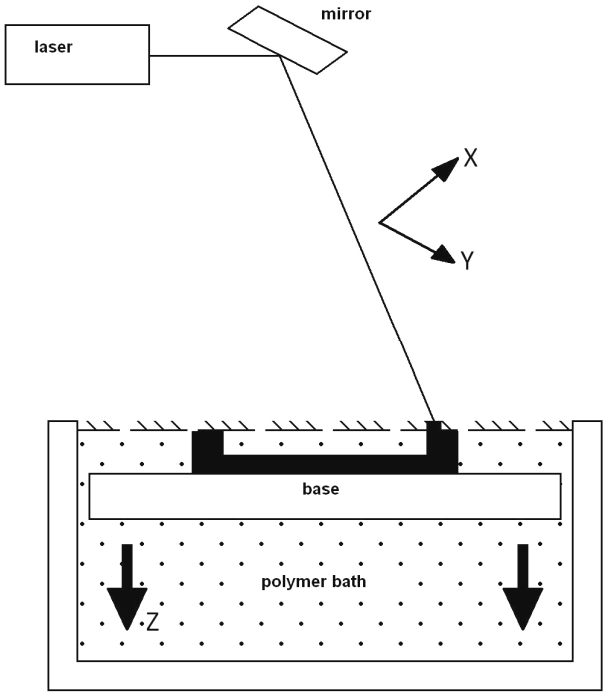

Fig. 3. **Principle of Stereolythography**

Solidification of liquid materials (Photopolymerization) represents stereolithography. Stereolythography use a viscous monomer. Exposed to ultraviolet radiation or laser beam set off a spontaneous polymerization and the liquid monomer changes to solid polymer (Fig. 3).

Laser sintering (LS) is most important principle from the group of RP technologies which use the product generation from the solid phase.LS works with the powder (polymers, metals,tec) which is sintered by he laser beam and form a layer usually in the thickness of the powder particles size (Fig. 4).

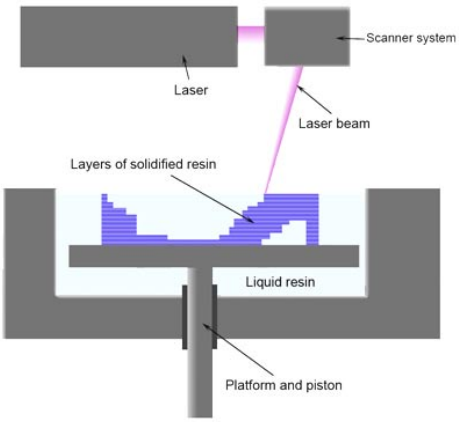

Fig. 4. **Principle of Laser Synthering**

Laminated Object Manufacturing is the most simple method producing 3D models Models are produced from 2D countered layers cutted out from the foils or paper by the help of knife or laser beam and than to assembled them into 3D models (Fig. 5).

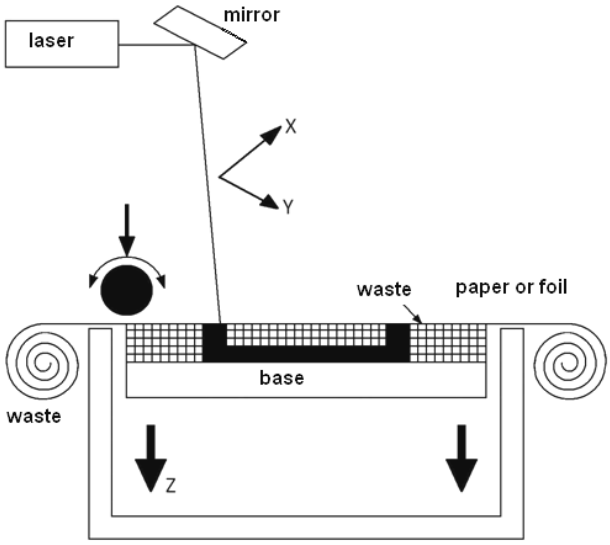

Fig. 5. **Principle of Laminated Object Manufacturing**

Extrusion process is based on molted polymer which is extruded from nozzle system (extrusion die) and deposited geometrically defined onto a structure. As building materials are used different types of polymers (Fig. 6).

3D printing is very often used rapid prototyping method.The principle is very similar to 2D printing proces sof inkjet pointer.The injected materiál is a polymer which after cooling form the required layer or binder which bonds

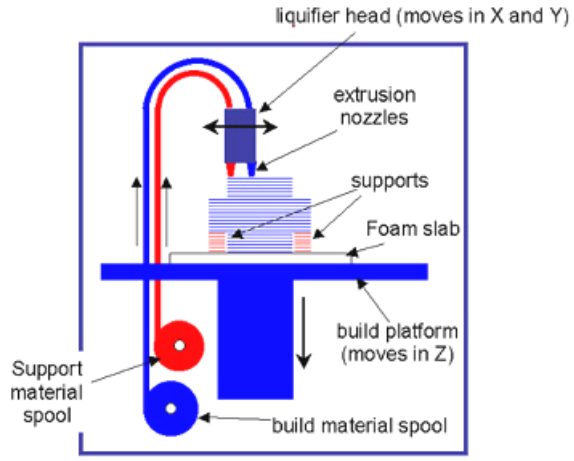

Fig. 6. **Principle of Fused Deposition Modeling**

Fig. 7. **Examples of parts from FDM**

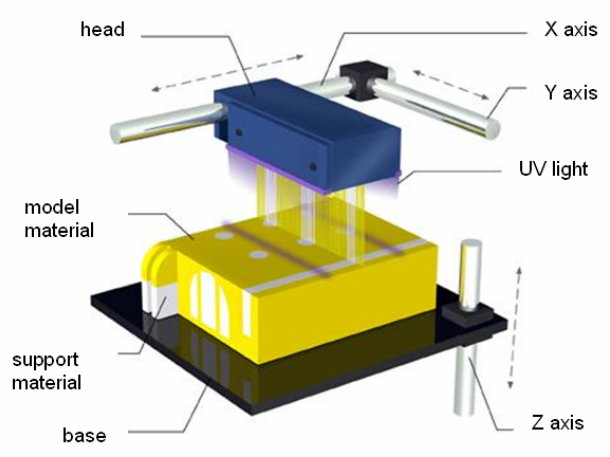

Fig. 8. **Principle of 3D printing**

a powder particles.As in case of the inject printer, also 3D printer makes print the multicolor parts possible (Fig. 8).

Fig. 9. **Examples of printed parts**

3. Reverse engineering

Reverse Engineering allows stacking already existing product. For this reason the entire surface needs to be able measured and recorded and returned to the CAD system.

The measurement produces an enormous number of data that are also known as clouds of points. Reverse engineering enables these clouds of points to be defined as surface elements, thereby facilitate their further processing in the CAD system.

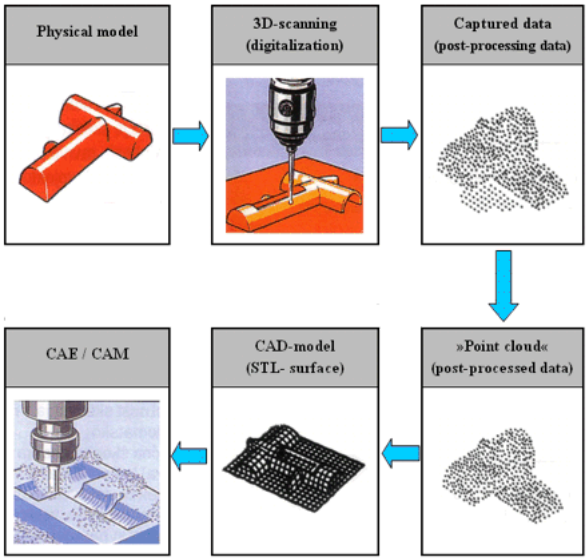

Fig. 10. **Principle of Reverse Engineering**

Fig. 11. **Reverse engineering system with the laser scanner Copy Mate**

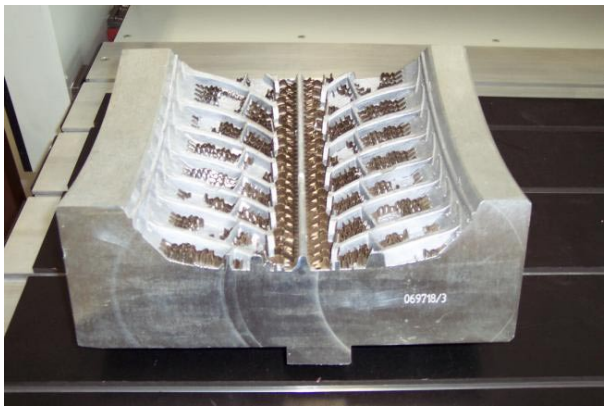

Fig. 12. **Part before scanning**

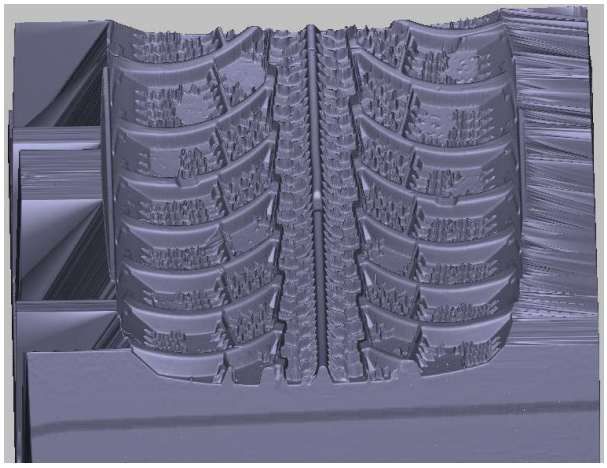

Fig. 13. **Scanned part**

4. Conclusion

Rapid prototyping and reverse engineering are very useful tools which can accelerate the way of product from the idea to market. Generative principle of rapid prototyping methods enables to produce parts of any geometry. These processes are practically unlimited in their ability to form complex shapes, they can produce both positives (parts) and negatives (dies and molds).

This article is financially supported by the Czech Ministry of Education, Youth and Sports in the R&D project under the title 'Modelling and Control of Processing Procedures of Natural and Synthetic Polymers', No. MSM 7088352102.

REFERENCES

1. Objet Geometries. Polyjet Technology developed by Objet Geometries [online]. c2008 [cit. 2008-12-12]. Dostupný z WWW: http://www.objet.com/Products / PolyJetTechnologyAnimationMovie/tabid/83/ Default.aspx
2. Wikipedia contributors. Rapid prototyping : Wikipedia, The free encyklopedia [online]. 3 December 2008 [cit. 2008-12-12]. Dostupný z WWW: < http:// en.wikipedia.org/wiki/Rapid_prototyping>
3. http://www.emag.cz
4. *Percentage use of rapid prototyping worldwide as of year 2000*. Data based on: D. T. Pham, S. S. Dimov, Rapid manufacturing, p. 6. Springer-Verlag, 2001.

CL-22
INFLUENCE OF SURFACE ROUGHNESS ON FLUIDITY OF THERMOPLASTICS MATERIALS

MICHAL STANEK, MIROSLAV MANAS, DAVID MANAS, and STEPAN SANDA

Tomas Bata University in Zlin, Faculty of Technology, Department of Production Engineering, TGM 275, 762 72 Zlin, Czech Republic
stanek@ft.tub.cz

Introduction

Polymer injection molding is the most used technology of polymer processing nowadays. It enables the manufacture of final products, which do not require any further operations. The tools used for their production – the injection molds – are very complicated machines that are made using several technologies. Working of shaping cavities is the major problem involving not only the cavity of the mold itself, giving the shape and dimensions of the future product, but also the runners leading the polymer melt to the separate cavities. The runners may be very complex and in most cases takes up to 40 % volume of the product itself (shape cavity). In practice, high quality of runner surface is still very often required. Hence surface polishing for perfect conditions for melt flow is demanded. The stated finishing operations are very time and money consuming leading to high costs of the tool production. This work gives the results of studying the influence of the quality of flow pathway surface and influences of other technological parameters on the polymer melt flow.

Results of the experiments carried out with selected types of thermoplastics proved a minimal influence of surface roughness of the flow channels on the polymer melt flow. This considers excluding (if the conditions allow it) the very complex and expensive finishing operations from the technological process as the influence of the surface roughness on the flow characteristics does not seem to play as important role as was previously thought.

Regressive models created on the basis of experiment results enable to predict the flow behaviour of the polymers quite precisely with regard to the surface quality and the parameters of the process injection molding itself. Application of the measurement results may have significant influence on the production of shaping parts of the injection molds especially in changing the so far used processes and substituting them by less costly production processes which might increase the competitiveness of the tool producers and shorten the time between product plan and its implementation.

Injection molding

Injection molding is one of the most used and the most popular manufacturing technologies. The main phase of injection molding is the transport of polymer melt to the mold, where the polymer solidifies and shapes into the required product. Injection proceeds at non-isothermal conditions, when the process of melt solidifying gets influenced by a number of rheological polymeric properties.

Process of polymer material injection

Injection molding is a way of shaping polymeric materials, during which the molded material is filled at high rate (injected) into a closed cavity of a tempered mold. It produces high quality and precise products (shots) from a wide range of plastics. Injection molding has some other advantages. For instance, precise mold design might eliminate other working. Cold runner molds in case of thermoplastics can be crushed and reused, decreasing the polymer waste to minimum. The injection molding process is quite fast and can be well automated. In order to get a shot with good physical properties and good surface, the filling of the mold must be controlled so that the melt would not flow into the form in one flow front but gradually. A plastic nucleus is formed by this way of laminar flow, which enables the compression of the melt in the mold and consecutive creeping. A constant flowing rate given by the axial movement of the screw is chosen for most of the flows. During filling the mold cavity the plastic material does not slide along the mold surface but it is rolled over. This type of laminar flow is usually described as a "fountain flow" (Fig. 1).

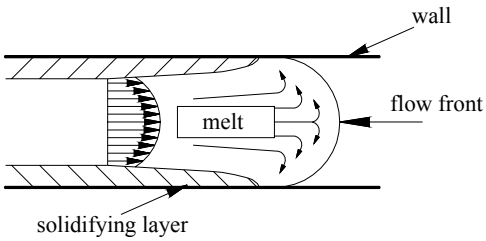

Fig. 1. **Fountain flow**

Injection mold for samples

The injection mold was designed for the easiest possible manipulation both with the mold itself and during injection while changing the testing plates, size of the mold gate etc. The injection mold is inserted into a universal frame. Its description and reasons for use are stated bellow.

Universal frame

The frame was designed for use with many different injection molds that fit the size of the frame. This makes the change of the separate injection molds easier, because the frame remains clamped to the injection molding machine and only the shaping and ejection parts of the molds are changed. Attaching right and left sides of the frame to fixed and moving plates of the injection machine is done using four clamps on each side.

Cavity parts of the injection mold for thermoplastics

The shaping part of the injection mold is composed of right and left sides, see Fig. 2. The most important parts of the injection mold concerning the measurements are: testing plate 2, cavity plate 3 and a special sprue puller insert 8.

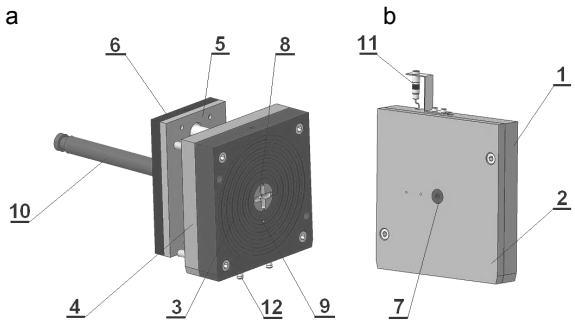

Fig. 2. **Cavity parts of the injection mold for thermoplastics a) left side, b) right side;** 1 – clamping plate, 2 – testing plate, 3 – cavity plate, 4 – plate, 5 – anchor plate, 6 – ejector plate, 7 – sprue puller insert, 8 – special sprue puller, 9 – ejector, 10 – ejector rod, 11 – pressure sensor, 12 – cooling end

Special sprue puller insert

The sprue puller insert is used for changing the gate size. It is composed of four different gates (1, 2, 4 a 6 mm). Turning the sprue puller changes the size of the gate, the position of the sprue puller is secured by a stopping bushing.

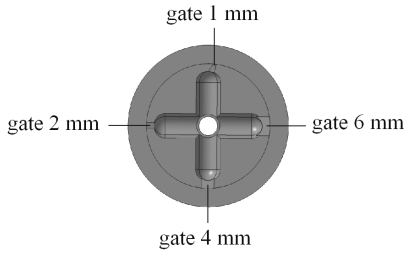

Fig. 3. **Special sprue puller**

Cavity plate

The cavity of injection mold is in a shape of a spiral with the length of 2000 mm. The cavity is created when the injection mold is closed, i.e. when shaping plate seals the testing plate. The dimensions of cavity are indicated on Fig. 4.

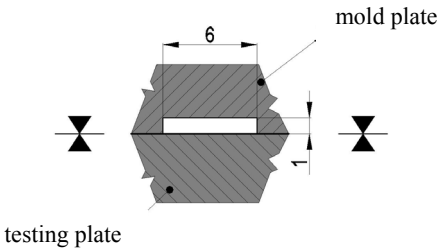

Fig. 4. **Cross section of mold cavity**

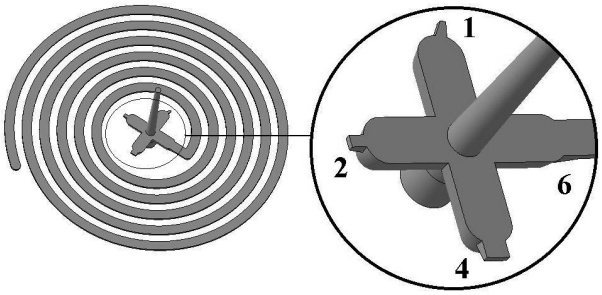

Fig. 5. **Testing sample**

Testing plates

The injection mold can operate with 5 exchangeable testing plates with different surface roughness. The surface of the plates was machined by four different technologies, which are most commonly used to work down the cavities of molds and runners. These technologies are polishing, grinding, milling and electro-spark erosion. The testing plates are used for changing the surface of the mold cavity.

Injected materials

Representatives of thermoplastics with varying flow properties were chosen for the experiment with the other decisive criteria being representation of almost all kinds of materials that are commonly used in injection molding. These are: LDPE (Bralen VA 20-60), ABS (Polylac PA 757), PP (Mosten GB 003), PP filled by 10 % talk (Keltan TP 7603), PP filled by 20 % talk (Taboren PH 89 T20).

Table I
Surface of testing plates

Technology	Photo	Surface roughness
Polishing		Ra = 0,102 μm
Grinding		Ra = 0,172 μm
Electro – spark machining (fine design)		Ra = 4,055 μm
Milling		Ra = 4,499 μm
Electro – spark machining (rough design)	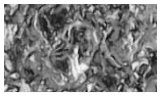	Ra = 9,566 μm

Injection molding machine DEMAG ERGOtech 50-200 with oil tempering unit Regloplas 250 KL were used to prepare samples (Fig. 6).

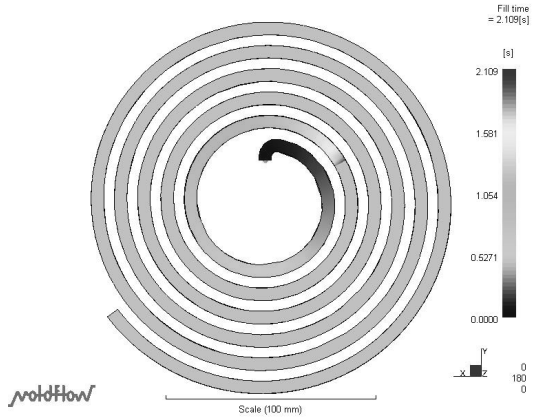

Fig. 6. **Simulation of the flow length**

Injection molding process simulation

A simulation of the injection molding process in SW Mouldflow 6.1 was carried out for comparison with the reality. The same conditions were set as during the actual injection molding. The flow length in the mould cavity of the polymers was observed.

Discussion

The effect of material and surface roughness of the plate on the flow length

The aim of the measurements was to find out the influence of separate technological parameters, especially the quality of the injection mold cavity surface, on the flow length of the injected materials.

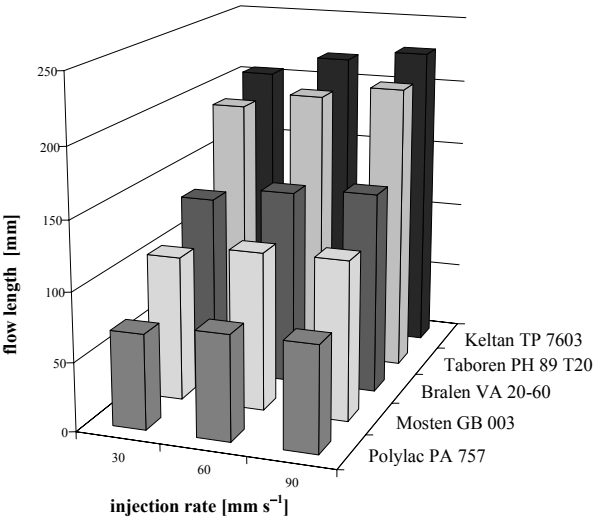

Fig. 7. **Dependence of the flow length on the injected material and injection rate;** plate with fine design, injection rate 30 mm s^{-1}, size of gate 2 mm

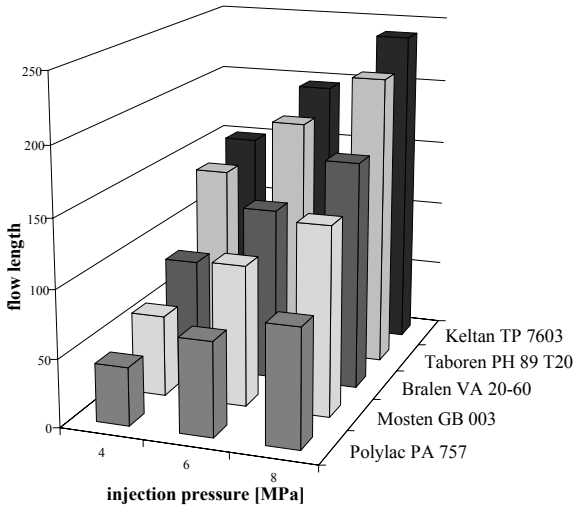

Fig. 9. **Dependence of the flow length on the injected material and injection pressure;** plate with rough design, injection pressure 6 MPa, size of gate 2 mm

The observed influences on filling the injection mold cavity (the flow length respectively) in the thermoplastics were injection pressure, injection rate, size of the gate and the surface roughness of the testing plates.

Statistical evaluation of the measured data

The final statistical evaluation of the measured data was done by SW STATISTICA 7. The aim of the statistical evaluation was to determine the influence of separate parameters on filling the mold cavity by material. Due to the influence of more factors (some independent variables) on the change of the observed feature (dependent variables), multiple

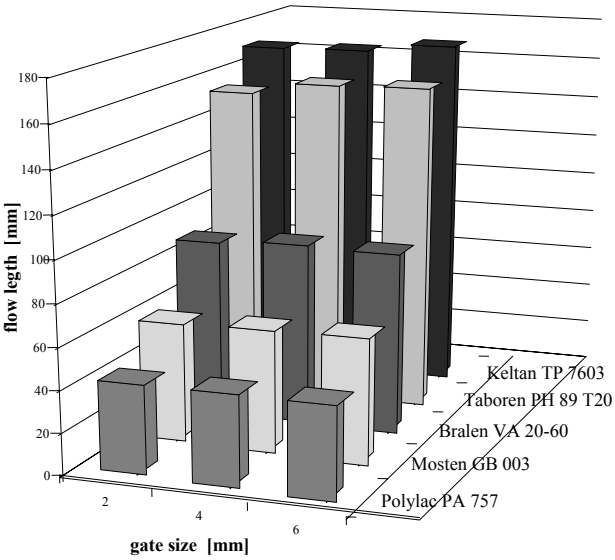

Fig. 10. **Dependence of the flow length on the injected material and gate size;** polished plate, injection rate 90 mm s^{-1}, injection pressure 4 MPa

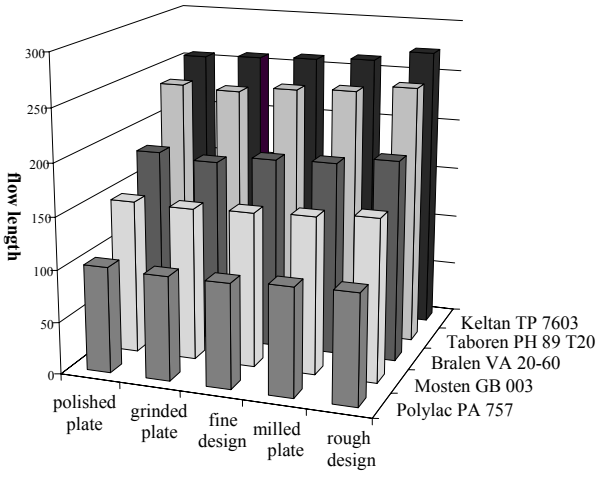

Fig. 8. **Dependence of the flow length on the injected material;** injection rate 60 mm s^{-1}, injection pressure 8 MPa, size of gate 6 mm

regression was chosen for the description. The result of the regressive analysis is the regressive model used to predict the value of dependent variable at a given value of independent variable. The dependent variable is the flow length. We observe the influence of five independent variables (injection pressure, injection rate, size of the gate, surface roughness of the testing plates and Melt Flow Index of the materials) on the flow length. To find out the impact of the factors on flow length, the dispersion analysis was carried out. The resulting

p-values are stated in Table II. The values under $p < 0,05$ are statistically relevant.
The following regressive model was found out using the multiple regression.

Table II
p-values of observed factors

Factor	p-value
Injection rate	0,000001
Injection pressure	0,000000
Size of gate	0,000000
Surface roughness of testing plate	0,291675
Melt flow index	0,000000

$R^2 = 0,943915$

$$y_t = 0,025286X_1 + 0,692656X_2 - 0,041169X_3 - 0,003387X_4 + 0,351107X_5 + \varepsilon_i$$

where y_t – flow length, X_1 – injection rate, X_2 – injection, pressure, X_3 – size of gate, X_4 – surface roughness of testing plate, X_5 – melt flow index, ε_i – incidental values

Conclusion

This research looked into the influence of technological parameters on filling the injection mold cavity and the flow length respectively. The parameters observed during the experiments were injection pressure, injection rate, size of the gate, surface roughness of the testing plates and injected material. All stated parameters, especially injection pressure and injection rate, showed influence on the flow length of all three groups of materials; the influence of surface roughness on the flow length of thermoplastic materials was not so significant. The differences in flow lengths at the plates were very small, rather higher in case of rougher surfaces. The measurement shows that surface roughness of the injection mold cavity or runners have no substantial influence on the length of flow. This can be directly put into practice. It also suggests that working and machining (e.g. grinding and polishing) of some parts of the mold, especially the runers, are not necessary.

This article is financially supported by the Czech Ministry of Education, Youth and Sports in the R&D project under the title 'Modelling and Control of Processing Procedures of Natural and Synthetic Polymers', No. MSM 7088352102.

REFERENCES

1. Stanek M.: *Modelling of polymers forming process inc. tools design*. VUT FSI Brno, Brno Res. *304*, 81 (2005).
2. Beaumont J. P.: *Runner and gating design handbook*. Hanser Publishers, Munich 2004.
3. Manas M., Vlcek J.: *Applied rheology*. UTB Zlin, Zlin 2001.
4. Kazmer L.: *Injection mold design engineering*. Hanser Publishers, Munich 2007.
5. Rees H.: *Mold engineering,* Hanser Publishers, Munich 2002.

CL-23

STRUCTURE AND PROPERTIES OF FIBRES PREPARED FROM METALLOCENE AND ZIEGLER-NATTA POLYPROPYLENE

ANNA UJHELYIOVÁ[a], PETER MICHLÍK[b], and JOZEF RYBA[a]

[a] Department of Fibres and Textile Chemistry, Institute of Polymer Materials, Faculty of Chemical and Food Technolog, Slovak University of Technology in Bratislava, Radlinského 9, 812 37 Bratislava, [b] Research Institute for Man-Made Fibres, a.s., Šturova 2, 059 21 Svit, Slovak Republica
anna.ujhelyiova@stuba.sk

The fiber-forming properties of polypropylene (PP) prepared by Ziegler-Natta (ZN) catalysts for over five decades had started an interest in its application in all areas of fibre and textile industries. The high molecular weight as well as wide molecular distribution caused the problems at the fibre preparation.

The introduction of chemical degradation enabled to prepare the PP with the lower molecular weight and narrower molecular distribution, what had led to an improvement of processability and increase of evenness of PP fibres. Today, the fibres prepared from ZN-PP are applied in the many engineering areas such as human and household goods, various electronic, building and medical products, automotive parts, etc.[1].

After several years since the industrial application of ZN-PP there were generated the metallocene catalysts for the polymerisation of polyolefine polymers with narrower molecular weight distribution, lower melting temperature, tacticity etc.[2–5].

mPP has the narrower molecular weight distribution $M_w/M_n \approx 2–2.5$, lower portion of high molecular fraction, lower rheological index polydispersity PI ≈ 2.0 (ref.[7]), lower elasticity of melt, low atacticity portion (< 0.5 %) and index isotacticity above 99 % (ref.[1,6]), lower melting temperature about 15 °C, crystallization temperature about 2–3 °C and melting enthalpy about 3–11 J g^{-1} (ref.[10,11]). These properties of m-PP provide to use the higher take-up speed at the spinning with the lower rate of PP melt in the wide range of sheared rates. The application of direct deformation at the spinning and drawing of fibres from m-PP with the presented properties leads to their better drawingability, higher orientation and tenacity in comparison with the fibres prepared from ZN-PP. It is able to prepare the fibres from mPP with the lower linear density, higher tenacity, lower elongation and higher Young's modulus[1,8,9].

This paper deals with the evaluation of structure, thermal and mechanical properties of drawn fibres formed from mPP and ZN-PP at the same prepared conditions.

The undrawn mPP and ZN-PP fibres prepared from the metallocene polypropylene HM562N (mPP, Lyondell Basell Co., Italy) and Ziegler-Natta polyprolyne Tatren HG1007 (ZN-PP, Slovnaft, a.s. Bratislava, Slovak Republic) with MFI = 27 g/10 min of the both polymers by classical procedure using laboratory pilot plant with the twin screw $\phi = 16$ mm with the take-up speed at the spinning from 8.33 to 18.33 m s^{-1}. The prepared undrawn fibres were drawn on the drawn ratio of 3.0

with the final linear density from 4.7 to 2.3 dtex.

Melting (ΔH_m) enthalpies of mPP and ZN-PP fibres were measured using DSC 7 Perkin Elmer and evaluated from thermograms of 1st heating. All measurements were curried out under nitrogen.

The birefringence represents the anisotropy of oriented polymer system and expresses the full orientation of macromolecular chains in fibres. The full orientation of m-PP and ZN-PP fibres was estimated on the basis of measurements of birefringence using polarization microscope DNP 714BI.

The average orientation of macromolecular chains in the surface layers of fibre has been estimated on the basis the different speed sound between particles of variously oriented systems. The supermolecular structure of drawn mPP and ZN-PP fibres was determined on the basic of the measurement of sound speed in fibres using equipment of PND 129-126-06.

The Instron equipment was used for evaluation of the mechanical properties (tenacity and elongation at break, Young's modulus) of the mPP and ZN-PP fibres.

The mainly aim of this work is the comparison of the supermolecular structure and properties of fibres prepared from mPP and ZN-PP at the same spinning and drawing conditions. There were observed the effects the take-up of spinning on parameters of the supermolecular structure, thermal and mechanical properties of these fibres.

The melting enthalpies were estimated for the drawn mPP and ZNPP fibres from the endotherms measured at the 1st heating (Fig. 1). The conditions used at the spinning and drawing of fibres from polymers induce the form of their supermolecular structure which is different than the supermolecular structure of un-oriented polymers. The melting temperatures of fibres from both m-PP and ZN-PP are different and the melting temperatures of mPP fibres are lower about 8−10° than the ZN-PP fibres.

The melting enthalpies of drawn ZN-PP fibres are higher than the drawn mPP fibres in the full observed area of take-up spinning (Fig. 1). The mPP has the lower ability of crystallization, which go out from their molecular structure[11].

The direct deformation of undrawn fibres in process of their preparation on the drawn ratio = 3.0, excepted the fibres from mPP at the take-up spinning used of 15.83 and 18.83 m s^{-1}, where the drawn ratios were of 2.7 and 2.5 increases the orientation of their macromolecular chains. It is represented by the growing of average orientation estimated on basis of the measured birefringence (Fig. 2). The birefringence of fibres from mPP as well as ZN-PP increases with the growing of take-up speeds at the spinning at the same drawn ratio, but the increase of berifringence of mPP is lower than the increase of fibre birefringe from ZN-PP. But, the absolutely values of birefringence of m-PP fibres are higher than the values of ZN-PP fibres. The both dependencies have the direct proportional in the observed areas of take-up speeds at the spinning without achievement of equilibrium state.

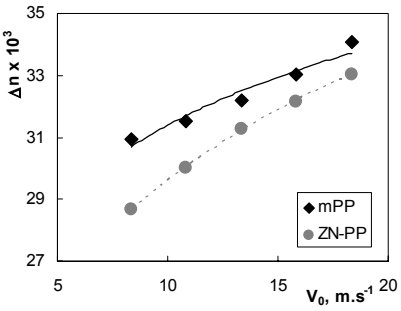

Fig. 2. **The dependencies of birefringence on the take-up speed of drawn mPP and ZN-PP fibres**

The similar dependence was obtained at the evaluation of average orientation estimated on the basis of measurements of sound speed of drawn m-PP and ZN-PP fibres (Fig. 3).

The better ability of deformation can support also the improvement of mechanical properties, mainly higher tenacity at break and Young's modulus and lower elongation at the break.

The previous positive results of structured parameters of mPP as well as ZN-PP fibres confirm the results obtained at the evaluation of the mechanical properties (tenacity at the break) (Fig. 4). The higher take-up speeds used at the spinning at the same drawn ratio of mPP and ZN-PP fibres induce proportionally the higher tenacity. But the tenacity of m-PP fibres is higher than the ZN-PP one (Fig. 4) and the increase of tenacity and Young's modulus is more rapid and elongation is slower than the increase of ZN-PP fibres. It is in the accordance with the formed supermolecular structure of drawn mPP.

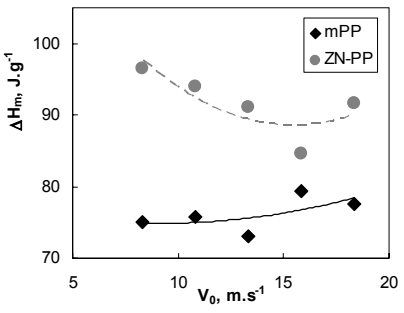

Fig. 1. **The dependencies of melting enthalpy obtained from 1st heating of drawn mPP and ZN-PP fibres on take-up speed used**

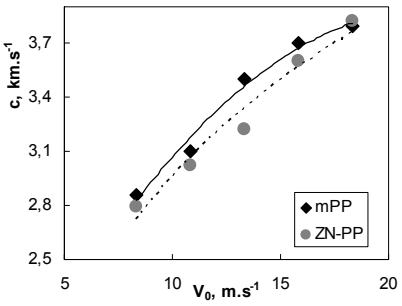

Fig. 3. **The dependencies of sound speed on the take-up speed of drawn mPP and ZN-PP fibres**

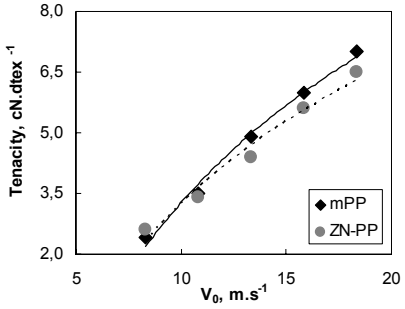

Fig. 4. **The dependencies of tenacity on the take-up speed of drawn mPP and ZN-PP fibres**

Conclussion

- The melting enthalpies of mPP fibres are lower than the ZN-PP fibres prepared at the same spinning and drawing conditions.
- The lower level structural arrangement of undrawn mPP fibres ensures their better deformation at the same deformation (the same drawn ratio) with the improvement of structured parameters (the better orientation of macromolecular chains estimated on the basis of measurements of berifringence) of drawn mPP fibres.
- The better orientation of mPP fibres induces the improved mechanical properties in comparison with ZNPP fibres.

This work was supported by the Slovak Research and Development Agency under the contract No. APVV-0226-06.

REFERENCES

1. Folvarcikova K. et al: *Book of Proceedings of the International conference "Polymer Materials", 29.-30. October 2003, Bratislava*.
2. Arranz-Andres J. et al: Eur. Polymer J. *43*, 2357 (2007).
3. Bubeck R. A.: Mater. Sci. Eng., R *39*, 1 (2002).
4. Gomez-Elvira J. M. et al: Polym. Degrad. Stab. *85*, 873 (2004)
5. Choon K. Chai et al: Polymer *44*, 773 (2003)
6. Schmenk B. et al: Chem. Fibers Int. *50*, 233 (2000)
7. Herben P., Lonardo A.: Chem. Fibers Int. *52*, 318 (2002)
8. Kamath M. G., Dahiya A., Hegde R. R.: Development of metallocene based polypropylene. Available from http://www.engr.utk.edu/mse/pages/Textiles/Olefin%20fibers.htm
9. Jambrich M. et al: *Book of Proceedings of the conference STRUTEX, TU v Liberci, December 1999, Liberec*, pp. 33-38.
10. Bond E. B., Spruiell J. E.: Published online 9. October 2001, DOI 10.1002/app.2181, pp. 3223-3247.
11. Elvira M., Tiemblo P., Gomez-Elvira J. M.: Polym. Degrad. Stab. *83*, 509 (2004).

CL-24

CRYSTAL STRUCTURE OF A 4,4'-BIPHENYLENE BASED POLYKETONE WITHOUT ETHER LINKAGES

ZULKIFLI AHMAD[a] and HOWARD M.COLQUHOUN[b]

[a] *School of Material and Mineral Resources, Universiti Sains Malaysia, Transkrian, 14300, Pulau Pinang Malaysia,* [b] *The University of Reading, Whiteknight, Reading, Berkshire, RG6 6AH, UK*
zulkifli@eng.usm.my

Abstract

A wholly aromatic ketone polymer and its crystalline structure of the polymer was elucidated using powder XRD and electron diffraction method and interfaced with molecular mechanic force-field computational modeling. It was found that the polymer adopted an orthorhombic system in Pbcn having 2 chains per unit cell of dimensions a = 7.55, b = 6.28 and c = 17.88 Å. The biaryl unit of the aromatic ring is coplanar with the ketone bridge torsin angle of ca. 30o. Reitveld refinement of final structure yield an agreement factor (Rwp) of 9.16 %. The simulated electron diffraction of the proposed structure corresponded well with that of the experimental.

Introduction

Aromatic polyketone is a high performance polymer widely used in automotive industry due to their ability to withstand high pressures, chemical resistant and high temperatures. This is due mostly to their highly crystalline nature. Several efforts were geared in elucidating and understanding the polymer crystal system. However, it is this very nature which hinder the production of high molecular weight polyketone which is indispensable for a good x-ray diffraction data. Numerous structural studies have been reported for aromatic polyketone series, mostly containing ether bond[1–10]. They display a consistent basic crystal structure with minor dimensional changes[1–5]. by adopting a space group of Pbcn with two chain orthorhombic cell. It has also been shown that the ether and ketone groups are crystallographically equivalent. Similarly, the substitution of biphenylene unit at each alternate phenyl position found in a homologous PEEK result in a crystal structure closely related to that of parent PEK and PEEK[8]. Interestingly, the simulated biphenylene unit displayed co-palnarity despite this being an unfavorable conformation in gas phase[9,10]. To the best of authors knowledge, no structural study has previously been reported for wholly aromatic polyketones without ether linkages.

In the present work, poly(4,4'-biphenyleneketone), a biphenylene polyketone without ether linkages, were synthesized. It crystal structure was elucidated using XRD powder data followed by computer modeling and simulation of its crystal structure whose structural parameters were based on synthesized six-ring all-ketone analogous oligomer, 4,4'-bis (4"-biphenylcarbonyl)biphenyl and other analogous oligomers previously studied.

Experimental Section

A six rings aromatic polyektone 4,4'-bis(4"-biphenylcarbonyl)biphenyl was firstly synthesized based on the reaction scheme 1 as shown below.

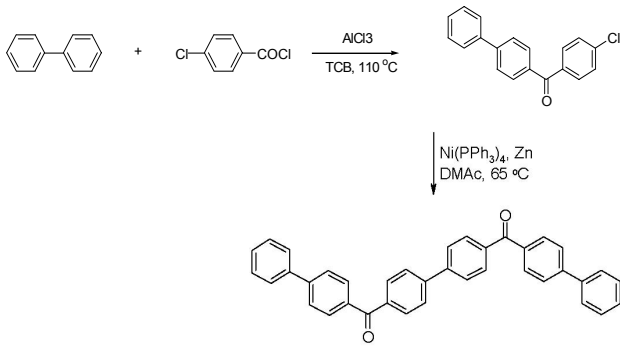

Scheme 1.

The polyketone, poly(4,4'-biphenyleneketone) was then synthesized based on the reaction scheme 2 as shown below

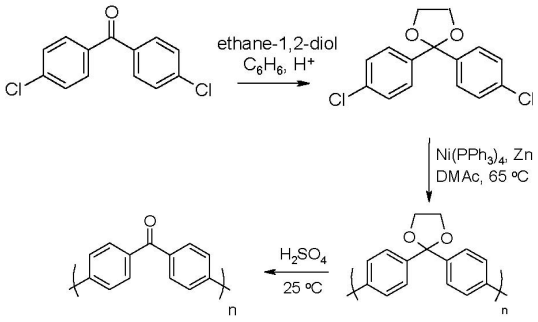

Scheme 2.

Crystallographic and modeling method

X-ray powder difraction data were collected on a Bruker D5000 X-Ray powder diffractometer (The University of Reading). Computational modeling was performed using software package *Cerius2 (v.3.5)*. The model-building and energy-minimisation was derived from molecular mechanics Dreiding 2.21 Force-field. Rietveld refinement was performed in Rietveld Refinement module of *Material Studio (v.2.0)*.

Result and discussion

FTIR, H-NMR, C-NMR, DSC, elemental analysis and GCMS analysis confirm the right six ring oligomer as synthesized. It shows a melting point of 355 °CC (DSC) and a molar mass of 514.19 (*MS-CI*). The polyketone polymer was successfully synthesized by polycondensation of a ketal-protected monomer to give an amorphous polyketal, followed by hydrolysis to reform the ketone function (Scheme 2). FTIR spectrum corresponded well with the anticipated structure of the polymer. It is insoluble in most solvents which precluded NMR analysis. It showed a glass transition temperature of 322 °C and crystal melting range of 440–480 °C, the first ever reported thermal properties for this polymer. No other thermal transitions occurred up to 500 °C.

Modelling was initially performed by constructing a repeat unit of the polymer whose structural parameters were derived from the analogous six rings oligomers as well other related structures from past works[11,12,13]. This structure was energy minimized using Dreiding Force Field resulting an almost linear zig-zag chain conformation. An arbitrary unit cell of dimension 20.0 × 20.0 × 18.0 Å was created comprising of 2 minimised chains structurse, one along the centre of the unit cell and the other passing through the origin with both parallel to c–axis. Successive optimization of the system was performed so as to give a simulated x-ray diffraction pattern comparable with the experimental. This operation finally led to a final structure with two diagonally-related chains, generated by *b*-glide symmetry, one passing along the *c*-axis and

Table I
Selected bond, angles and torsion angles for 1,4-polybiphenyleneketone

Bond	Distance(Å)	Bond	Angle(°)	Bond	Angle(°)
O-C9	1.240	C3-C8-C7	118.5	C7-C6-C5-C4	1.4
C1-C2	1.394	C1-C2-C3	120.6	C3-C4-C5-C6	-178.0
C6-C9	1.470	C3-C4-C5	118.0	C1-C2-C3-C4	0.1
C2-C3	1.492	O-C9-C10	119.6	C5-C6-C9-C10	-29.7
		C6-C9-C10	120.0		

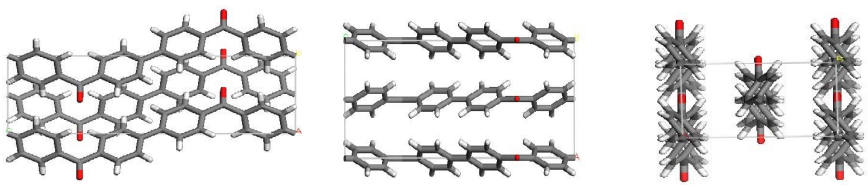

Fig. 1. **Crystal structure of poly(4,4'-biphenyleneketone) in various;** projections:(a) *bc* plane, (b) *ac* plane, (c) *ab* plane

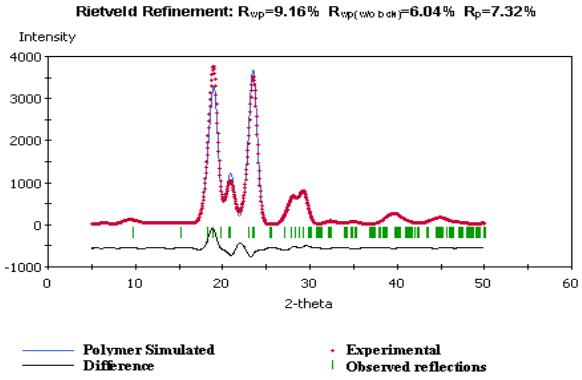

Fig. 2. **Rietveld Refinement plot for poly(4,4'-biphenyleneketone)**

the other, parallel to this, at the centre of the unit cell, with the carbonyl groups in register between the chains. The unit cell was orthorhombic in space group *Pbcn* with dimensions a = 7.56, b = 6.384 and c = 18.000 Å Rietveld Refinement was performed on the minimized crystal system which finally led to a R_{wp} value of 0.092.. Selected chain conformation was given in Table I and the crystal structures viewed from various projection were shown in Fig. 1. Rietveld refinement plot was shown in Fig. 2. The aromatic rings in the biaryl unit are co-planar, with the C–C bond connecting the two rings set at 1.48 Å, whilst the C-$O_{carbonyl}$ distance is 1.23 Å. The space group of the polyketone found here is similar to the analogous polymer, poly(4,4'-biphenylene ether)[14] substantiating further the proposal that aromatic carbonyl and ether groups are crystallographically interchangeable.

Conclusion

An aromatic polyletone without ether linkage was successfully synthesized and its crystal structure elucidated. The polymer adopt space group of Pbcn with unit cell dimension a = 7.56, b = 6.384 and c = 18.000 Å. The biphenylene unit adopted a coplanar conformation with the carbonyl linkage torsional angle of ca. 37°. This work substantiate further that ether and carbonyl linkages are crystallogaphically equivalent.

The first author would like to acknowledge the sponsorship from Public Service Department and Universiti Sains Malaysia for the support of this study.

REFERENCES

1. Blundell D. J., Newton A. B.: Polymer *32*, 308 (1991).
2. Rong-Ming Ho, Stephen Z. D. Cheng, Howard P. Fisher, Ronald K. Eby, Benjamin S. Hsiao, Kenncorwin H. Gardner: Macromolecules *27*, 5787 (1994).
3. Waddon A. J., Keller A., Blundell D. J.: Polymer *33*, 27 (1992).
4. Dawson P. C., Blundell D. J.: Polymer *21*, 577 (1980).
5. Fratini A. V., Cross E. M., Whitaker R. B., Adams W. W.: Polymer *27*, 861 (1986).
6. Blundell D. J., Liggat J. J., Flory A.: Polymer *33*, 2475 (1992).
7. Baxter I., Colquhoun H. M., Kohnke F. H., Lewis D. F., Williams D. J.: Polymer *40*, 607 (1990).
8. Blundell D. J., Bayon V.: Polymer *34*, 1354 (1993).
9. Rabias I., Langlois C., Provata A. B., Howlin J., Theodoru D. N.: Polymer *43*, 185 (2002).
10. Aldred P. L., Colquhoun H. M., Williams D. J., Blundell D. J.: Macromolecules *35*, 9420 (2002).
11. Kendrick J .J.: J. Chem. Soc. Faraday Trans. *86*, 3995 (1990).
12. William D. J., Colquhoun H. M., O'Mahoney C. A.: J. Chem. Soc. Commun. *1994*, 1643.
13. Colquhoun H. M., William D. J.: Macromolecules *29*, 3311 (1996).
14. Simcock M. N.: *Final Year Project B.Sc* (Hons) *Thesis*, University of Salford 1998.

POSTERS

P-01
SURFACE MODIFICATION OF TEXTILE REINFORCING MATERIAL BY PLASMA TREATMENT AND PLASMA POLYMERIZATION

IHSSAN AMIR, IVAN HUDEC, and MILAN VOLOVIČ

Slovak University of Technology in Bratislava, Faculty of Chemical and Food Technology, Institute of Polymer Materials, Department of Plastics and Rubber, Radlinského 9, 812 37 Bratislava
ihssan.amir@stuba.sk

Polyester cords play an important role in the modern tyre industry as a reinforcing materials because of their extraordinary mechanical and physical properties. Many problems concerning to the adhesion between polyester cords an tyre rubber come from the relatively low surface energy of polyethyleneterephtalate (PET) and also its chemical inertness. The standard method for the improvement of adhesion strength between polyester cord yarns and the rubber matrix are based on RFL system – the fibre surfaces are treated with a solution or emulsion consisting of resorcinol-formaldehyde resin and vinyl-pyridine latex[1,2]. The next change of improvement of adhesion cords to rubber is surface modification of cords by plasma treatment, where is a change to creation new group, eventually new polymeric layer at the surface cords when reactive monomer are applied as working gas in plasma polymerization process[3–5].

The aim of this work is presentation of some results obtained by the studying of the influence of plasma treatment conditions on the static adhesion strength and adhesion strength after dynamic stress of polyester high modulus low shrinkage cord yarn (HMLS – Slovkord 1440 Dtex 1x2, twists 380/380 produced by SH Senica, Slovakia) to rubber. The rubber compounds contained natural rubber, SBR and polybutadiene rubber was used for fabric coating. The static adhesion strength to rubber and adhesion strength after dynamic stress (the sample was exposed to a cyclic flexural stress with frequency = 7.5 Hz for 12 h in a chamber at 80 ± 1.5 °C) to rubber was studied by means of Henley test method according to STN 62 01464.

Polyester cords were treated by Difusion Coplanar Surface Barrier Discharge (DCSBD) at atmospheric pressure. A sinusoidal high-frequency high-voltage (~ 1–15 kHz, up to 10 kV peak to peak) was applied between the electrodes. Such a discharge electrode arrangement and energization were found to generate visually almost uniform plasmas in nitrogen and ambient air at atmospheric pressure. DCSBD was powered by the high voltage harmonic source with the frequency of 10 kHz (LIFETECH, Ltd., Brno, Czech Republik). The polyester cords were modified by plasma treatment in ambient air, technical air or nitrogene and by plasma polymerization process in gas of propane-butane with nitrogen admixture in flow rate ratio 0.5 to 3 liters per minute. The power of discharge was set to 350W and time of treatment varies in the range from 1 to 20 seconds. Cords were treated from both sides between electrodes.

The results of the influence of plasma treatment time and plasma polymerization time on the static adhesion strength and adhesion strength after dynamic stress of polyester cord to rubber in the case of distance of electrodes 0,5 mm are summarized in Fig. 1 and Fig. 2.

The results of the influence of plasma treatment time and plasma polymerization time on the static adhesion strength and adhesion strength after dynamic stress of polyester cord to rubber in the case distance of electrodes 1,0 mm are summarized in Fig. 3 and Fig. 4.

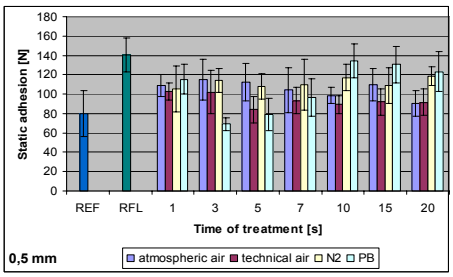

Fig. 1. **Graphical comparison of static adhesion strength of plasma modified PET cords to rubber compound**

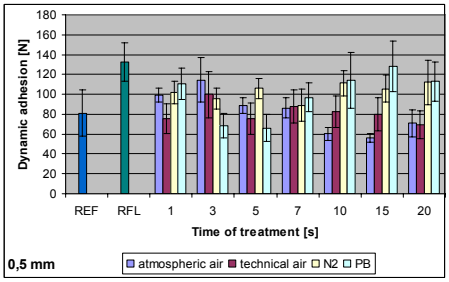

Fig. 2. **Graphical comparison of adhesion strength after dynamic stress of plasma modified PET cords to rubber**

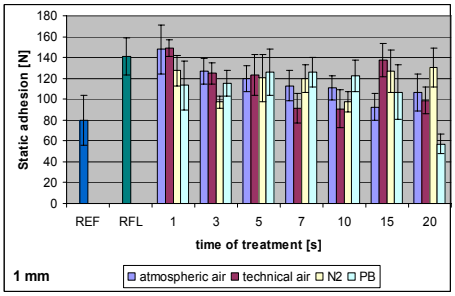

Fig. 3. **Graphical comparison of static adhesion strength of plasma modified PET cords to rubber compound**

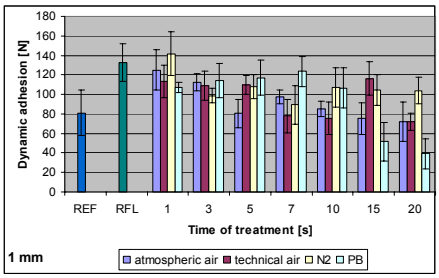

Fig. 4. **Graphical comparison of adhesion strength after dynamic stress of plasma modified PET cords to rubber compound**

Static adhesion strength of cords to rubber and adhesion strength after dynamic stress (dynamic adhesion) of plasma treated cords were compared with adhesion strength of cords treated with resorcinol-formaldehyde latex (RFL) system. From Fig. 1 and 3 is evident that the maximum static adhesion strength of polyester cords modified in technical air and ambient air plasma (difference is only in humidity content) was observed in very short time of plasma treatment (1second) when distance of electrodes was 1mm. In both type of plasma treatment obtained level of static adhesion were comparable with the static adhesion when resorcinol formaldehyde (RFL) system was used for surface modification of polyester cord (Fig. 3). As Krump[3] mentioned before, under sufficient conditions, the relatively short contact between the PET cords and plasma is sufficient for incresing of surface energy and adhesion to rubber. Higher exposure by plasma treatment caused decrease of static adhesion strength.

From results of the influence of activation time on adhesion strenght after dynamic stress obtained from plasma treatment in technical air and ambient air plasma (Fig. 2 and 4) is clear that the higher exposure time by plasma treatment decrease of adhesion strenght after dynamic stress too.

From the experimental data of adhesion testing it is clear, that with plasma polymerization technique is possible to obtain adhesion strength comparable with nitrogene plasma treatment process. In comparison with untreated virgin cords it is possible to obtain more than 30 % increasing in static and 50 % increasing in dynamic adhesion strength.

Conclusion

From measured data it is evident that plasma treatment and plasma polymerization has strong influence on the adhesion strength of polyester cords to rubber. From the results it is clear that adhesion strength of plasma treated cord achieved the adhesion level of RFL system treated cords. Plasma treatment process can lead to the chemical changes on the surface layer of polyester cords yarn.

As a result of plasma polymerization a new non-polar layer with different chemical structure as well as higher roughness has been create on the surface of polyester cords. In the deposited layer – rubber interface several mechanisms can occur that can result in increasing of adhesion to rubber. The polymer chain of deposited layer and the rubber matrix can form a diffusive layer due to chain diffusion and mechanical interlocking of the rubber matrix on the roughness surface can form too. These changes can contribute into increasing of adhesion of polyester cords modified by plasma polymerization to rubber compound.

REFERENCES

1. Sheu M. S., et all.: Tenaciously bound hydrophilic coatings on polymer surfaces, *Polymer Surfaces and Interfaces: Characterization, Modification and Application,* (1997), pp. 83–91.
2. Luo S., et all.: J. Adhes. Sci.Technol. *16*, 1715 (2002).
3. Krump H., Hudec I., Luyt A. S.: Int. J. Adhesion Adhesives *25*, 269 (2005).
4. Jasso M. et all.: Surf. Coating Technol. *201*, 57 (2006).
5. Amir I., Hudec I., Široký J.: Chem. Listy *101*, 41 (2007).

P-02
MAGNETIC FIELD SENSITIVE RUBBER NANOCOMPOSITES

DENISA BELLUŠOVÁ, TIMO STEINKE, THOMAS ALSHUTH, and ROBERT H. SCHUSTER*

German Institute of Rubber Technology, Eupener Strasse 33, 305 19 Hannover, Germany
denisa.bellusova@dikautschuk.de

A particular group of magnetic materials, for which the interest have been regained in the last few years are the composites consisting of magnetic particles dispersed in a non-magnetic, elastomeric matrix during the cross-linking process. Composites made of ferromagnetic particles and a soft matrix belong to specific class of smart materials where the mechanical properties can be changed under different magnetic environments. The one of the aims of this work is investigate dispersion of ferrite magnetic particles in butadiene rubber. Various types of ferrites (Ba, Sr) prepared in laboratory using co-precipitation and auto-combustion method and for the comparison wet milled commercial ferrite (Sr) were used as a magnetic fillers for magnetoactive elastomers. The morphology of the ferrite particles was observed. The atomic force microscopy and stress-strain measurements were used to obtain the results displaying the homogeneity of the magnetoactive elastomers. The change in the stiffness, elasticity on the content and particle size dependence in the presence and without the presence of the magnetic field is shown in this work.

Introduction

The magnetic particles (which may be aligned during the composite production by means of an external magnetizing field) within the non-magnetic, elastic matrix exhibit unique properties, which are not characteristic of the monolithic magnetic materials, such as strong dependence of the magnetic permeability on stress, together with good mechanical characteristics[1,2]. Due to the above mentioned magnetoelastic characteristics, as well due to their ability to be: manufactured into complex shapes (using for example the mold injection methods) and easily machined, these composites have already found many applications as sensors, high strain actuators, converters, controlled vibration dampers, variable stiffness components, etc [3–5].

Experimental

Ferrites (4-11vol.%) were embedded in 1.4-cis butadiene as a magnetic filler. The M-type barium ferrite was synthesized from iron and barium chlorides using a chemically reliable co-precipitation method. The comercial strontium ferrite was prepared using wet milling with the addition of polyvinylalcohol on the surface. The morphology of magnetic powders was studied using a combined field-emission (scanning) transmission electron microscope LIBRAÒ 120, Zeiss. Characterized ferrites powders were incorporated into 1.4-cis butadiene rubber in internal mixer Haake Rheocord System 90 under the following conditions: temperature: 50 °C, rotation speed: 50 min^{-1} and mixing time: 10 min. The dispersion of the magnetic particles in isotropic and anisotropic magnetoactive composites was observed using high-resolution type of scanning probe microscopy - atomic force microscopy. Stress-strain measurements of the samples were carried out using an universal testing instrument (Zwick Typ 1445). The measurements were carried out according to DIN 53504 with 5 specimens (S3A) per material with a deformation velocity of 200 mm min^{-1} at temperature of 23 °C. Dynamic-mechanical properties of the samples were studied using a Servohydraulic 1000 Hz Elastomer test System MTS 831.50. Testing was carried out at 10Hz with and without an external magnetic field of 0.35T.

Results and discussion

Fig. 1 represents the transmission electron microscope image (a) and optical microscope image (b) of the ferrites morphology used for magnetoactive elastomers. TEM image (Fig. 1a) shows the co-precipitated barium ferrite consisting of hexagonal platelet crystallites mostly in the 300-400 nm size. Commercial strontium ferrite for the comparison was chosen. Commercial strontium ferrite (Fig. 1b) is microsized in the range from 30 to 200 micrometer and the particles are in spherical shape.

In the absence of an applied magnetic field the magnetic moments are randomly oriented and thus the composites has no magnetization. In an external field, two distinct types of interactions can be identified, field-particle interaction as well as particle-particle interaction.

From the AFM image (Fig. 2a) it is evident the vulcanization without the presence of the magnetic field results in magnetoactive elastomer with isotropic properties. The particles are dispersed randomly in elastomer matrix. On the other side the application of the magnetic field during the vulcanization leads to the formation of the columnar structure of the magnetic particles in elastomer matrix. Particles are aligned and fixed to the direction of the applied magnetic field. The anisotropic magnetoactive elastomer was obtained (Fig. 2b).

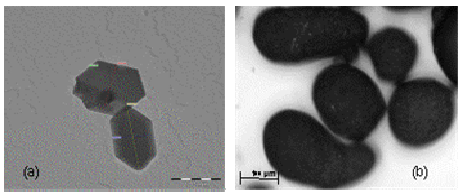

Fig. 1. **The morphology of (a) barium ferrite (b) strontium ferrite**

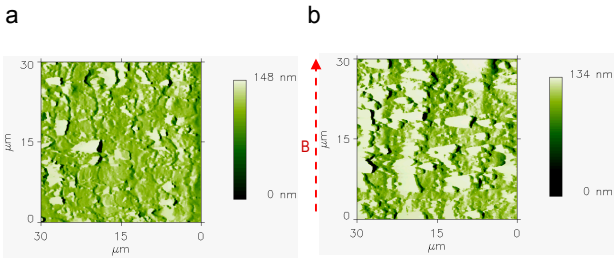

Fig. 2. **AFM images of barium ferrite magnetoactive elastomers vulcanized (a) without the presence of the magnetic field, (b) in the presence of the magnetic field**

The effect of the alignment of the ferrite particles to the direction of the applied magnetic field during vulcanization on the mechanical properties is shown (Fig. 3). The results show that the higher content of strontium ferrite causes the higher tensile strength at break and this increase is even better if the ferrite magnetoactive elastomers are vulcanized while applying magnetic field.

From the dependencies it is evident that the particle size has an influence on the tensile strength at break, also. It is clear observed the higher tensile strength at break thus better particle dispersion and homogeneity of the sample by the application of ferrite nanosized particles in comparison with microsized commercial strontium ferrite. The tensile strength at break is influenced to a high degree of +70 % to +100 %.

The application of the magnetic field gives rise to a magnetic dipole-dipole interaction between the ferrite particles causing the apparent changes in stiffness and damping. The strong magneto-sensitivity can be viewed in both Fig. 4a, b for the magnitude of the storage modulus. For the case of barium nanoferrite +15 % increase is observed, while for the second case strontium microferrite it is a little less, yet strong. Furthermore, it will subsequently be shown that the increase

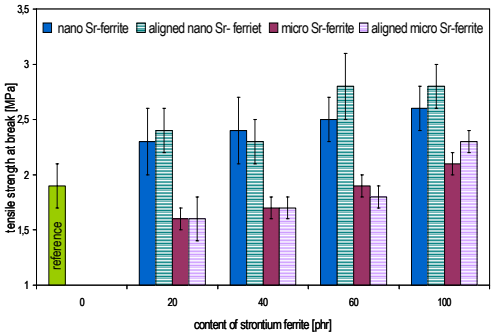

Fig. 3. **The dependence of the tensile strength at break on the content of the nanosized and microsized strontium ferrite in isotropic and anisotropic magnetoactive elastomers**

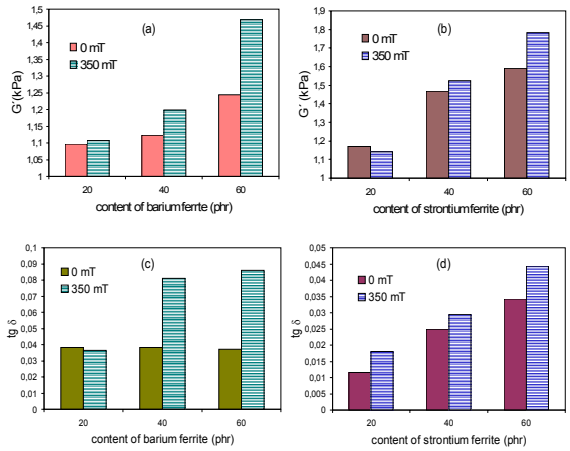

Fig. 4. **The dependence of (a), (c) the storage modulus and (b), (d) the loss modulus of the magnetoactive elastomers on the content of barium and strontium ferrite in the absence and presence of magnetic field (0.35T) at 10Hz frequency**

in storage modulus magnitude with magnetic field grows with the concentration of the ferrite particles. The small amount of ferrite filler influences the change of storage modulus on the magnetic field dependency too small. The higher content of ferrite filler indicates that the change of storage modulus in the presence of magnetic field become much larger. Subsequently, the intensity of magnetic field was switched of and the magnitude of storage modulus decreases to origin magnitude of storage modulus and it means the rheological change is entirely reversible. The loss factor (Fig. 4c, d) displays an ferrite content dependence in the presence of magnetic field that is very large (110 %) for relatively small content of 40 phr (7.5 vol.%) of barium nanoferrite.

Conclusions

Analysis of the results leads to the following: under the influence of the magnetic field a characteristic structuring of magnetic particles within the composite during curing takes place. Particles can move under the influence of the field to form magnetic structures of chains and it leads to the change of the physical-mechanical properties. The columnar structure of the particles in the elastomer matrix gives rise to tensile strength at break. An increasing content of ferrite gives rise to an increasing storage modulus and loss factor while applying magnetic field. The effect grows stronger with the smaller ferrite nanoparticles then with the microsized strontium ferrite. Thus it can roughly be said that the stronger the magnetorheological effect, the higher content of magnetic particle with smaller particle size.

The financial support of Deutsche Kautschuk -Gesellschaft is gratefully acknowledged.

REFERENCES

1. Bednarek S.: Appl. Phys. *A 66*, 643 (1998).
2. Jin S., Tiefel T. H., Wolfe R., et al.: Science *225*, 446 (1992).
3. Zaltsgendler E. A., Kolomentsev A. V., Kordonskii V. I., et al.: Mag. Hydr. *4*, 105(1985).
4. Ginder J. M., Nichols M. E., Elie L. D., Clark S. M.: *Smart Structures and Materials*, Proceedings of SPIE, Norman M. Weseley (2000).
5. Ginder J. M., Schlotter W. F., Nichols M. E.: *Smart Structures and Materials*, Proceedings of SPIE, *4331*, 103-110 (2001).

P-03
ANALYSIS OF RUBBER-FILLER GEL FOR CHARACTERIZATION OF SILICA LOCALIZATION IN RUBBER BLENDS

DANIEL HEIDENREICH, HAI HONG LE, SYBILL ILISCH, ANDRÉ WUTZLER, and HANS-JOACHIM RADUSCH

Center of Engineering Sciences, Martin Luther University Halle-Wittenberg, D-06099 Halle (Saale) Germany
hans-joachim.radusch@iw.uni- halle.de

Silica as a filler for rubber has a great reinforcing capability. It leads to improved abrasion resistance, tear strength, aging resistance and adhesion properties. In tire treads silica yields a lower rolling resistance by maintaining a high wear resistance and wet grip. Currently, a number of rubber blends filled with silica are commercially used. The distribution of filler in rubber blends is one of the most important factors affecting the physical properties of rubber final products. Generally, it can be assumed that the main factors controlling the filler distribution into each phase of the blends are the nature of rubber, filler–rubber interaction and the mixing sequence. Several techniques have been developed for determining the filler distribution in blends[1–5]. However, the most of the methods are time consuming and need a complicated sample preparation. The other common problem for the determination of the filler distribution is related to the fact, that along the mixing process the filler undergoes a large change in their size. There is a broad spectrum of large agglomerates and aggregates at short mixing time, and a narrow spectrum of small aggregates at longer mixing time. The analysis of the phase specific filler distribution could be done only for the finished compounds containing only small aggregates. At shorter mixing time, when the agglomerates themselves are larger than the blend phase, the available methods failed. Thus, the kinetics of the filler distribution in binary blends along the mixing process has not been investigated so far.

In our previous works[6,7] a new method – the so-called wetting concept – was proposed for determination of the selective wetting behavior of filler by the blend phases. Based on the thermogravimetric analysis (TGA) of the rubber-filler gel the phase selective carbon black (CB) distribution in rubber blends could be quantified. Using the wetting concept it became possible to characterize the free CB fraction and the fraction of CB in separated blend phases as function of mixing time regardless of the agglomerate size. However, the

TGA technique is usable only when the two rubber components demonstrate distinctly different degradation temperatures. In order to overcome this problem in the present work we have used the Fourier transform infrared (FTIR) spectroscopy for evaluation of the rubber-filler gel of silica filled SBR/NR blends. The effects of the material and technological parameters on the wetting behavior of rubber and the kinetics of the phase selective distribution of silica in NR/SBR blends were investigated in detail. The results received from FTIR method will be compared with those received from TGA method.

REFERENCES

1. Sirisinha C., Prayoonchatphan N.: J. Appl. Polym. Sci. *81*, 3198 (2001).
2. Jeon I. H., Kim H., Kim S. G.: Rubber Chem. Technol. *76*, 1 (2003).
3. Cotton G. R., Murphy L. J.: Kautsch Gummi. Kunstst. *41*, 54 (1988).
4. Maiti S., De S. K., Bhowmick A. K.: Rubber Chem. Technol. *65*, 293 (1992).
5. Klüppel M., Schuster R. H., Schaper J.: Rubber Chem. Technol. *72*, 91 (1999).
6. Le H. H., Ilisch S., Kasaliwal G. R., Radusch H.-J.: Kautsch Gummi. Kunstst. *60*, 241 (2007).
7. Le H. H., Ilisch S., Kasaliwal G. R., Radusch H.-J.: Rubber Chem. Technol. *2008*, 81.

P-04

STRUCTURE AND PROPERTIES OF THE POLYPROPYLENE/CARBON NANOTUBES COMPOSITES AND COMPOSITE FIBRES

MARCELA HRICOVÁ*, ANTON MARCINČIN, and ALENA HOFERÍKOVÁ

Slovak University of Technology in Bratislava, FCHFT, IPM, Department of Fibres and Textile Chemistry, Radlinského 9, 812 37 Bratislava, SK
marcela.hricova@stuba.sk

The carbon nanotubes (CNT) with regard of their unique properties (mainly electrical and mechanical properties) are attractive fillers for electroconductive polymer composites and composite fibres[1]. The multiwall carbon nanotube (MWCNT) have been used for reinforcing and enhancement of electrical conductivity of the engineering polymers and polymer fibres such as polypropylene (PP), polyamide (PA6), polyethylene terephthalate (PET) and others[2–4]. The low concentration of the CNT is sufficient for improvement of the tensile properties of composite fibres. The essentially higher concentration of the fibrous particles is needed for formation of the electroconductive composite fibres with electrical conductivity higher than 10^{-2} S cm^{-1}. However, higher concentration of CNT affects negatively processing of composites at spinning and drawing. Therefore, the combination of CNT with others suitable additives, such as carbon black pigments (CBP) or organoclays, was used to get electrical conductivity of fibres at lower concentration of CNT[5].

In this paper, the spinning and electrical properties of the PP/MWCNT composites and composite fibres, as well as their supermolecular structure, thermal and mechanical properties are presented. The laboratory twin-screw extruder Φ = 28 mm was used for preparation of PP/MWCNT composites before spinning. PP composite fibres were prepared using laboratory spinning plant with extruder Φ = 16 mm and drawn at maximal draw ratio. The supermolecular structure and thermal properties of fibres have been investigated by DSC analysis. Electrical conductivity of PP composites and fibres was evaluated using two methods: four-contact method (FCM) and method of resistivity of the linear textiles (RLT). The mechanical and electrical properties of the PP composites and fibres in dependence on concentration of electroconductive fillers and compatibilisers-dispersants were evaluated.

The results show that melt viscosity of the PP/MWCNT composites increases gradually with content of the MWCNT (1−8 wt.%) in PP matrix (Fig. 1). The worsening of spinning of the composite melt containing concentration of MWCNT above 6 wt.% was observed and only low spinning speed was possible.

Similarly, the low deformation gradient and temperature 140 °C in drawing process for PP fibres with MWCNT content above 1 wt.% was used. The fibres were drawn on relative high drawing ratio in this case (Table II). To improve spinability of the PP/MWCNT composites the series of the PP composites containing 3.0 wt.% of MWCNT and 3.0 wt.% of CBP PL6 with polar oligomers-dispersants based on polyglycols was prepared. Total content of electro-conductive carbon particles in the composite was 6.0 wt.%. The positive effect of MWCNT on tensile properties of PP fibres was found for low content of nano filler in PP fibres up to 1.0 wt.%. Some selected compatibilisers also contribute to mechanical properties of composite fibres (Table I).

Tenacity and Young's modulus of PP/MWCNT composite fibres decrease gradually with content of the fibrous particles in PP fibres. The low elongation at break (about 15 %) and high non-uniformity of the mechanical properties are characteristic for the fibres (Table II). The compatibilisers-dispersants (PEG and NOV) have significantly improved spinability and deformation of the fibres in drawing. In addition, they have improved the non-uniformity of the composite

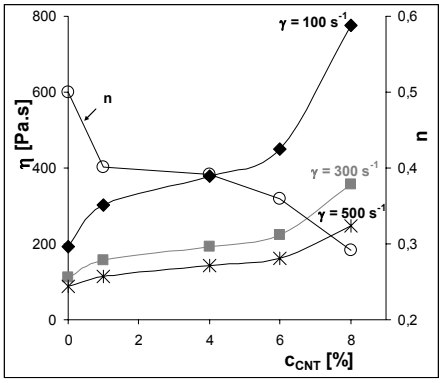

Fig. 1. **Dependence of viscosity η and power law exponent n on concentration of MWCNT in PP500R/MWCNT composites at 250 °C**

Table I
Tenacity T, elongation E and Young's modulus YM of the PP500R/MWCNT composite fibres (λ_{max}). Content of MWCNT in fibres 0.1 wt.%

Additive in PP fibres	Draw ratio λ_{max}	T [cN/tex]	E [%]	YM [N/tex]
PP standard	7.0	64.8	22.6	7.2
MWCNT	7.0	65.1	22.6	7.3
MWCNT+Boehmite D40	7.2	76.1	20.7	8.7
MWCNT+layered silicate C15A	7.5	72.8	21.6	7.9
MWCNT+C15A+der. siloxane	7.5	81.2	21.7	9.5
MWCNT+PP-g-MA+der. silox.	7.2	76.6	22.0	8.9
MWCNT+der. oxazoline	7.5	74.0	20.0	8.8

fibres expressed by lower CV_T and CV_E in comparison with PP/MWCNT fibres without compatibilisers-dispersants.

Thermal analysis of the PP/MWCNT fibres showed on double melting endotherm of the fibres with higher content of filler (1–6 wt.%) and the same shape of the endotherms for PP fibres modified by mixture of MWCNT and CBP PL6 with dispersant. Double melting endotherm of the PP/MWCNT composite fibres shows on heterogeneity in the supermolecular structure of fibres and can corresponds with worsening of their spinability and drawability. The MWCNT act as nucleating agent with high efficiency and shifts the crystallisation temperature about 10–20 °C higher, gradually with concentration of MWCNT.

Electrical properties of the PP/MWCNT composites and composite fibres were measured using two methods: standard four contact method (FCM) and resistivity of the linear textile method (RLT). Both methods show that electrical conductivity increases with the content of MWCNT. The percolation threshold is dependent on shape of sample measured and shifted from the PP composites to PP composite drawn fibres within the nanofiller concentration of 4.0–8.0 wt.%. The electrically conductive composites were obtained already at 4.0 wt.% of conductive particles, but 8.0 wt.% was insufficient for conductive drawn fibres (Fig. 2). Improvement of the rheological properties and spinability of the PP/MWCNT/CBP PL6 composite fibres by polar additives (PEG and

Table II
Tenacity T, elongation E and Young's modulus YM of the PP500R/MWCNT composite fibres, drawn at low gradient of deformation

Content of MWCNT [%]	Draw ratio λ_{max}	T [cN/tex]	E [%]	YM [N/tex]
1.0	7.6	47.5	15.7	4.36
4.0	6.8	38.4	14.8	4.24
6.0	9.3	35.0	13.1	4.27
8.0	7.0	33.3	14.3	4.14

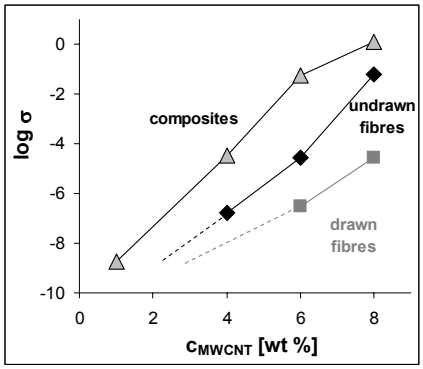

Fig. 2. **Dependence of the log of conductivity σ on concentration of MWCNT in the fibres**

NOV) led to decrease their electrical conductivity compared to PP/MWCNT fibres. This phenomena can be explained by separation and flocculation of the fibrous nanofiller in the PP matrix what shifts the percolation threshold to higher concentration of electrically conductive additives.

The experimental work was supported by EC, FP6 Project: NMP3-CT-2005-516972 and Grant Agency VEGA: 1/4456/07 and 1/0444/09.

REFERENCES

1. Thostenson E. T., Li Ch., Chou T. W.: Compos. Sci. Technol. *65*, 491 (2005).
2. Seo M. K., Lee J. R., Park S. J.: Material Sci. Eng., A *404*, 79 (2005).
3. Xushan G., Yan T., Shuangyan H., Zhenfu G.: Chem. Fib. Int. *55*, 170 (2005).
4. Li Z., Luo G., Wei F., Huang Y.: Compos. Sci. Technol. *66*, 1022 (2006).
5. Konishi Y., Cakmak M.: Polymer *47*, 5371 (2006).

P-05
DETERNINATION OF ALKOXYAMINE CONCENTRATION IN POLSTYRENES PREPARED BY NITROXIDE MEDIATED POLYMERIZATION

ĽUDMILA HRČKOVÁ, ŠTEFAN CHMELA, JOZEF KOLLÁR, and MAREK STACH

Polymer Institute, Slovak Academy of Sciences, Dubravska cesta 9, 842 36 Bratislava, Slovakia
upollud@savba.sk

Over the past several years attempts to moderate the reactivity of the propagating species in radical polymerization have been multifold. Nitroxide mediated radical polymerization (NMP) offers simple method for preparation of polymers with programmable construction of macromolecules[1–4]. This method permits molar mass regulation, offers polymers with rather low molar mass distribution, allows polymer preparation with desirable choice of end groups and allows preparation of block copolymers. Contrary to the anionic polymeriza-

tion it does not require precise purity of monomers and is not sensitive to the moisture. NMP is based on the ability of nitroxide to trap growing radical under the production of an alkoxyamine dormant end-functionality. Alkoxyamine at higher temperature (90−130 °C) decomposes into nitroxide and growing radical which is able to admit a part of monomer according to the following scheme:

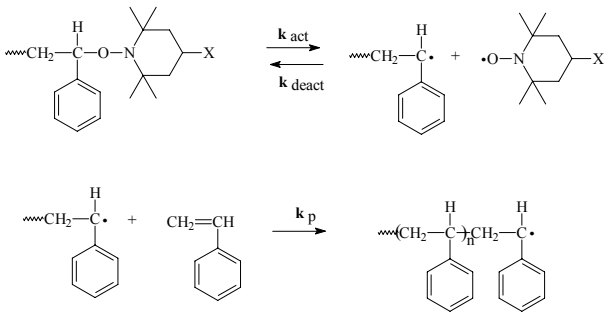

Steady-state concentration of growing radicals is markedly lower than at common radical polymerization. Reversible reaction of macro radicals with nitroxides eliminates non-reversible termination reactions of macro radicals (recombination, disproportionation and transfer on monomer). Polymerization can be terminated at the consumption of monomer or by decreasing of temperature. Resulted polymer contains at the chain end nitroxyl radical in the form of alkoxyamine, which is able of additional growing reaction. Quantification of active chain ends represents serious problem. Up to now used approaches are problematical. NMR spectroscopy is not sufficiently precise and post-polymerization is indirect way. The last approach required substitution reaction of chain-end nitroxyl radical by another radical, which could be detectable by spectrophotometry.

In this work we prepared polystyrenes by NMP using combined molar mass regulators containing besides alkoxyamine part the structure of fluorescence mark. Stable nitroxyl radical represented 2,2,6,6-tetramethylpiperidine-*N*-oxyl and covalently bonded fluorescence mark is 1,8-naphthylimide – Scheme 1. Concentration of marked polystyrene chain ends in polymers was measured directly by UV-absorption or emission spectroscopy. Theoretical molar masses of polystyrenes were calculated from these concentrations on the assumption that all polystyrene chains are terminated by alkoxyamine dormant end-functionality bearing fluorescence probe. Comparisons of these data with the molar masses from GPC gave us the range of the marked active polymer chain ends. Fractions of active polymer chain ends depended on the conversion. With increased conversion the fraction of alkoxyamines was decreased. At lower conversion (10 %) roughly 90 % of polymer chain ends contained alkoxylamine while at higher conversion (60 %) this value represented just 50 %. In this case just each second polymer chain is terminated by alkoxyamine. From this follows that the „livingness“ of polymerization process was decreased with the increasing of conversion. It should result in the increase of polydispersity with increased conversion. Despite this polydispersity was the same for all conversions and reached value ca. 1.3.

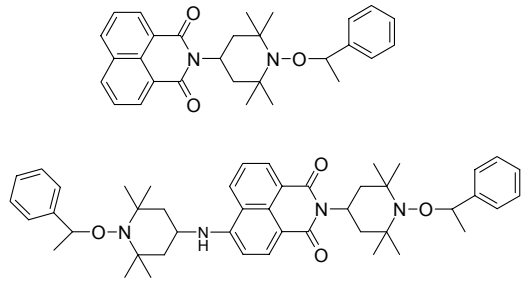

Scheme 1. **Structures of unimolecular initiators**

The authors thank Grant Agency VEGA for financial support through grant 2/0082/08 and through APVV project 0562-07.

REFERENCES

1. Solomon D. H., Rizzardo E., Cacioli P.: U.S. Patent 4,581,429; 1985.
2. Georges M. K., Veregin R. P. N., Kazmair P. M., Hamer G. K.: Macromolecules *26*, 2983 (1993).
3. Hawker C. J., Bosman A. W., Harth E.: Chem. Rev. *101*, 3661 (2001).
4. Benoit D., Chaplinski V., Braslau R., Hawker C. J.: J. Am. Chem. Soc. *121*, 3904 (1999).

P-06
THE SYNTHESES AND ELECTRONIC STRUCTURE OF OLIGOTHIOPHENES TERMINATED WITH (10H-ANTHRACENE-9-ONE)METHYLENE CHROMOPHORES

VLADIMIR LUKEŠ[a], IVAN HRABLAY[a], ROLAND ŠTOLC[a], DANIEL VÉGH[b], PAVOL HRDLOVIČ[c], and VILIAM LAURINC[a]

[a] Department of Chemical Physics, Slovak University of Technology, Radlinského 9,SK-812 37 Bratislava, [b] Department of Organic Chemistry, Slovak University of Technology, Radlinského 9, SK-812 37 Bratislava, [c] Polymer Institute, Slovak Academy of Science, Dúbravská cesta 9, SK-842 36 Bratislava, Slovak Republic
upolhrdl@savba.sk

The automotive industry is a material intensive industry. A wide variety of metal, fillers, plastics, pigments and dyes are required to meet specific applications. The synthetic polymers represent the growing fraction of materials used for different parts of the car. Conducting polymers and oligomers find special applications in this automotive and electronic industry. There is the strong drive to develop and apply new conducting oligomers which can be applied as such or doped in polymers.

In this study the synthesis, spectral measurements and theoretical study of simple model oligothiophenes terminated symmetrically or a symetrically by (10H-anthracen-9-one) methylene chromophores according the Scheme are presented[1].

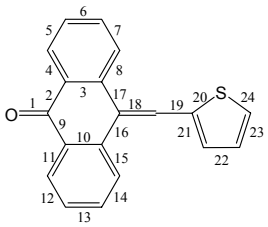

AT

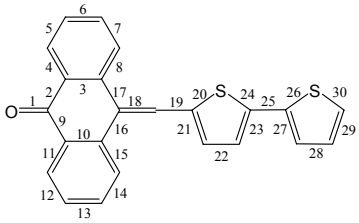

ATT

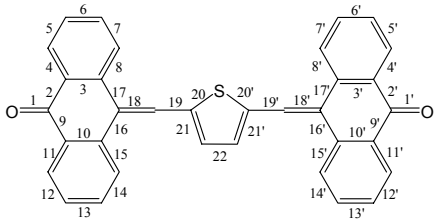

ATA

Scheme 1

The electron absorption spectra of prepared molecules were measured in polymer matrices and chloroform solution. The absorption spectra of the investigated systems are represented by broad band without vibrational structure. The maxima of the compounds under investigation are given in the Table.

S[a]	$\lambda_A(\log\varepsilon)$[b] [nm]	$\lambda_A(\log\varepsilon)$[b] [nm]	λ_F[c] [nm]	Φ_r[d]	$\Delta\nu$[f] [cm^{-1}]
Ia, AT	322(3.60)				
Ib, ATT	328(3.95)	445(3.07)	520	0.39	3241
IIa, ATA	323(3.55)	450(2.80)	467	0.97	810

[a] Substrates according to Scheme 1. [b] Wavelength of the maximum of absorption band at long wavelength edge (log of decadic extinction coefficient in $dm^3\,mol^{-1}\,cm^{-1}$). [c] Wavelength of the maximum of fluorescence. [d] Quantum yield relative to anthracene in the given medium. [f] Stoke's shift

Theoretical calculations of the electronic ground state structures have been performed at the density functional theory (DFT) level of the theory. The vertical excitations energies were calculated using the time dependent version of DFT and semiempirical Zerner´s Intermediate Neglect of Differential Overlap (ZINDO).

The evaluated DFT HOMO orbitals are dominantly localized on the thiophene oligomers where as LUMO is spread into the anthrone chromophore. Excitation to the S_1 state corresponds exclusively to the significant promotion of an electron from HOMO to LUMO as it is clearly demonstrated on ATA.

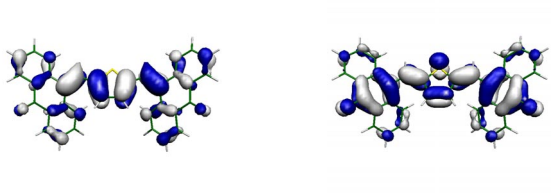

HOMO ……. → LUMO

In conclusion it can be stated that the studied systems exhibit interesting spectral properties namely fluorescence depending on the molecular architecture and the medium. Therefore these materials might serve as the basis for the spectroelectrochemical characterisation with repect to their potential usage in various optical devices, e.g. plastic solar cells or organic light emitting devices.

This work has been supported by Slovak Grant Agency VEGA (Projects No. 1/3036/06, 2/0097/09, 1/0774/08 and 1/4453/07).

REFERENCE

1. Lukeš V., Hrablay I., Šolc R., Végh D., Hrdlovič P., Laurinc V.: Synth. Metal, doi: 10.1016synthmetal.2008.12.002.

P-07
PYROLYSIS OF USED TYRES

IVAN HUDEC[a], JOZEF FERANC[a], JUMA HAYDARY[b], and I. ŠURINA[a]

[a] Slovak University of Technology in Bratislava, Faculty of Chemical and Food Technology, Institute of Polymer Materials, Department of Plastics and Rubber, [b] Institute of Chemical and Environmental Engineering, Radlinského 9, 812 37 Bratislava
ivan.hudec@stuba.sk

In generally, the scrap tyres recycling methods can be divided into:

– Mechanical recycling – re-processing of tyres into new rubber products,
– Feedstock recycling – processing of tyres into raw materials,
– Energy recovery – recovery of energy from waste through incineration.

A promising recycling rote for used tyres is their transformation into useful products by pyrolysis[1]. Pyrolysis can be defined as the thermal decomposition of organic material in the absence of air. Upon heating, shredded tyres are decomposed and converted into oils, gases and pyrolytic residue. The liquid oil product consists of a very complex mixture of organic components. The gaseous fraction is composed of non-condensable gases, such as H_2, H_2S, CO, CO_2, CH_4,

C_2H_4, C_3H_6, etc. The gas fraction can be used as fuel in the pyrolysis process. By using the gas fraction as fuel the consumption of external energy source is minimized. This is an advantage of pyrolysis compared to other recycling methods in which the consumption of energy is very high. From the ecological point of view, pyrolysis has practically no impact on the environment due to the closed pyrolysis system. The pyrolysis residue consists of the recovered carbon black filler, inorganic materials and varying proportions of carbonaceous materials formed from the rubber decomposition products.

A literature review[2–4] shows a large variety of results depending on the technology and process conditions used in pyrolysis process. All parameters, temperature, heating rate, hydrodynamic conditions, catalyst and particle size are the main factors affecting the amount and composition of the pyrolysis products.

The aim of this work is presentation of some results obtained by the studying of the isothermal pyrolysis of rubber granulate of scrap tyre under nitrogene was investigated in the temperature range from 400 °C to 800 °C. The laboratory unit with srew type flow reactor for isothermal pyrolysis process of rubber granulate was used. The composition and properties of pyrolysis products were studied in relation to the temperature and time of pyrolysis process.

Rubber granulate from pasenger tyres with different particle size distribution produced by V.O.D.S. Košice, Slovakia was used in all experiments. The laboratory pyrolysis unit was used in the study. The rubber granulat was fed into the system using a feeder and the particles are passed through the reactor using a rotation of screw. The residence time of pyrolysis process of the particles in the reactor was controlled by the rate of the screw rotation. Inert atmosphere in the reactor is achieved by nitrogen flowing trough the reactor in the same direction as the solid material. Passing through the reactor, rubber particles are decomposed. The volatilly products are removed from the reactor at high temperature and they are led to a condenser. The solid residue is removed from the end of the reactor and collected. The volatile fraction after partial condensation is cooled in two scrubber type coolers. Composition of the gas and liquid fraction was measured by GC/MS spectroscopy.

Solid pyrolytic residues were characterized by specific surface area (measured by nitrogene adsorbtion method) and mercury porosimetry for pore size distribution. Table I shows comparison between basic structural properties of solid residue from laboratory screw pyrolytic reactor, pilot batch reactor and two types of industrial carbon black products.

From comparison is evident, that pyrolytic carbon black from laboratory srew reactor has the similar surface activity as that of low-surface commercial carbon black. In Table II the influence of temperature of pyrolysis in laboratory reactor on pyrolysis products content and surface area of carbon residue are shown.

From data is eviddent that by changing of basic technological parameters it is possible to change quantity of pyrolysis products and properties of carbon residue in wide range.

Table I
Comparison of different types of carbon black

Sample	CBp, srew flow reactor	CBp, batch reactor	CBp, batch reactor, cyclon	Carbon black N550	Carbon black N660
Specific surface area, $m^2\ g^{-1}$	46	18	25	40	38

Table II
The influence of temperature on content and properties of pyrolysis products

Temperature, °C	500	600	700	800
CBp content, wt.%	39,3	37,4	38,9	41,9
Specific surface aream, $m^2\ g^{-1}$	58,2	71,5	68,1	57,7
Pyrolytic oils content, wt.%	25,2	13,9	7,0	4,95

This work has been supported by APVV Grant Agency (project EURB-0013-06).

REFERENCES

1. De S. K., Isayev A. I., Khait K.: *Rubber Recycling*, Taylor&Francis Group, 2005.
2. Juma M., Korenova Z., Markos J., Annus J., Jelemensky L.: Petroleum and Coal *48*, 1 (2006).
3. Rodriguez I. M., Lagersgoiti M. F., Cabrero M. A., Torres A, Chomon M. J., Caballero B.: Fuel Processing Technology *72*, 9 (2001).
4. Berrueco C., Esperanza E., Mastral F. J.,Ceamanos J., Garcia-Bacaicoa P.: J. Anal. Appl. Pyrolysis *73*, 65 (2005).
5. Olayar M., Aguado R., San Jose M. J., Alvarez S., Bilbao J.: Powder Technology *165*, 128 (2006).

P-08

PROPERTIES OF CONDUCTIVE NANOCOMPOSITES BASED ON EVA COPOLYMER AND EXPANDED GRAPHITE

IGOR KRUPA[a*], VOLKAN CECEN[b], ABDEL BOUDENNE[c], LAURENT IBOS[c], RADHOUAN TLILI[c], IGOR NOVÁK[a], MÁRIA OMASTOVÁ[a], JAN PROKEŠ[d], JÜRGEN PIONTECK[e], ZUZANA KRIŽANOVÁ[f], and IVO VÁVRA[f]

[a] Polymer Institute, Slovak Academy of Sciences, Dúbravská cesta 9, 842 36 Bratislava, Slovakia; [b] Dokuz Eylul University Mechanical Eng. Department 35100 Bornova/Izmir, Turkey; [c] CERTES EA 3481 - Centre d'Etude et de Recherche en Thermique, Environnement et Systèmes, Université Paris 12 Val de Marne, 61 Av. du Général de Gaulle, 94010 Créteil cedex, France; [d] Charles University Prague, Faculty of Mathematics and Physics, V Holešovičkách 2, 182 00 Prague 8, Czech Republic; [e] Leibniz Institute of Polymer Research Dresden, Hohe Str. 6, 01069 Dresden, Germany; [f] Institute of Electrical Engineering, Slovak Academy of Sciences, Dúbravská cesta 9, 841 04 Bratislava, Slovakia
upolkrup@savba.sk

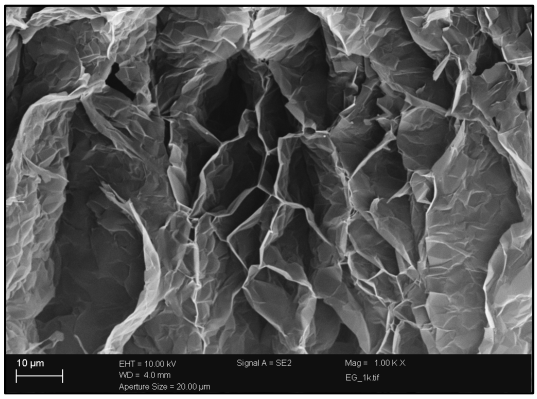

Fig. 1. **SEM image of EG**

Carbon additives are used in polymer composites as fillers, reinforcing agents and pigments. For some applications it is necessary that polymers exhibit a certain degree of conductivity, which can be reached by mixing conventional isolating polymers with electrically conductive fillers. One promising carbon based filler is graphite, especially in its expanded form (Fig. 1).

Polymeric nanocomposites prepared from high aspect ratio layered graphite nanofillers achieve significant improvements in mechanical, thermal, electrical and barrier properties at very low filler concentrations[1], compared to conventional composites, without a significant increase in density. This is caused by the sheet-like structure of natural graphite where the atoms are strongly bonded on a hexagonal plane but weakly bonded normal to that plane. If these graphene layers are separated down to a nanometer thickness through intercalation and exfoliation, they are able to form graphite nanosheets, which possess a huge surface area and high aspect ratio (200−1500) what results in a formation of percolating network at very low filler content. Moreover, such materials have a high strength due to a strong reinforcing effect of the nanosheets[2,3]. The exfoliation of expanded graphite is demonstrated in Fig. 2. It is seen that the exfoliation process starts on the edges of EG grains.

Various aspects of electrical, structural, thermal and mechanical behavior of nanocomposites based on the ethylene-vinylacetate (EVA) matrix filled with nanostructuralized expanded graphite and standard, micro-sized graphite were investigated. The influence of micro and nano sized fillers on the final physical properties were also studied. It was found that the electrical conductivity of composites strongly depends not only on the filler content but also on the graphite structure. If micro-sized graphite was used, the percolation concentration of the filler was found to be 15−17 vol.%, whereas the percolation concentration of the filler in nanocomposites filled with expanded graphite was significantly lower – its value was at about 5−6 vol.%. Electrical conductivity of nanocomposites was also much higher than electrical conductivity of composites filled with micro-sized filer at comparable concentrations. Similarly, the strength and Young's modulus of nanocomposites filled with expanded graphite was significantly higher than the strength and Young's modulus of composites filled with micrographite.

Fig. 2. **TEM micrograph of the EVA/EG nanocomposite**

The research was supported by the Scientific Grant Agency of the Ministry of Education of Slovak Republic and the Slovak Academy of Sciences (project No. 2/0063/09) and by Science and Technology Assistance Agency contract No. APVV-0478-07. This work is also a part of the research plan MSM0021620834 that is financed by the Ministry of Education, Youth and Sports of the Czech Republic. The authors appreciate the financial support by the DAAD within the program PPP Slovakia, D/07/01261. The Scientific and Technological Research Council of Turkey is acknowledged for granting of V. Cecen postdoctoral study in the framework of TUBITAK-BIDEB 2219-International Postdoctoral Research Scholarship Program. This research was also supported by the Scientific Support of the bilateral Project No. 107 M 227 of TUBITAK and Slovak Academy of Sciences.

REFERENCES

1. Fukushima H., Drzal L. T., Rook B. P., Rich M. J.: J. Therm. Anal. Calor. *85*, 235 (2006).
2. Kalaitzidou K., Fukushima H., Drzal L. T.: Carbon *45*, 1446 (2007).
3. Xie S. H., Liu Y. Y., Li J. Y.: Appl. Phys. Let. *92*, Article No. 243121 (2008).

P-09

THERMAL STABILITY AND COMBUSTIBILITY OF CHLOROSULPHONATED POLYETHYLENE AND ITS BLENDS WITH STYRENE-BUTADIENE RUBBER

AGNIESZKA KUCHARSKA-JASTRZĄBEK, GRAŻYNA JANOWSKA, and JAKUB KAWAŁEK

Technical University of Lodz, Intitute of Polymer and Dye Technology
janowska@p.lodz.pl

Introduction

Thermodynamic miscibility of polymers, which depends greatly on their solubility parameters, is a rather rare phenomenon. Polymer blends offer a possibility for their physical modification which can result in the formation of

new polymer materials characterized by interesting and sometimes specific properties, including thermal ones with good mechanical features. This is very often a consequence of co-curing processes, i.e. an interpolymer bonding of macromolecules which form polymer blend in a common network structure[1]. It follows from the literature survey that the methods of production of polymer blends and their properties are investigated in many research centers, in that number also in the Institute of Polymer and Dye Technology, Lodz Technical University[2]. However, there has been no information on systematic studies of thermal properties and flammability of cross-linked polymer blends. The present study is dedicated to this subject.

Experimental

Studies were focused on two chlorosulphonated polyethylene with different content of chlorine: CSM24 (24 % of combined Cl) and CSM43 (43 % of combined Cl) – commercial products of Du Pont Dow Elastomers. Under investigation was also styrene-butadiene rubber, SBR, containing 23,5 % of styrene mers, product of Synthos S. A. Elastomer blends containing 85 phr of SBR and 15 phr of CSM were cross-linked by 2 phr of ZnO (product of Huta Oława) and 1 phr of nano ZnO (product of Nanostructured&Amorphous Materials Inc.) .

The thermal analysis of elastomers and elastomer blends were carried out in inert gas atmosphere by means of differential scanning calorimetry (DSC) of Netzsch, DSC-204, using portions of about 5mg at heating rate of 10 °C min^{-1} within temperature range −100 to 500 °C and in air atmosphere by means of Derivatograph; Paulik-Paulik-Erdey system (MOM, Hungary) using weighed portions of 90 mg at heating rate of 7,9 °C min^{-1} within the temperature range from 20 to 800 °C.

The combustibility of elastomers and elastomer blends were determined by the method of oxygene index, using the apparatus of our own construction, according to the standard PN-ISO 4589-2. The flammability was also tested on the base of combustion rate measurements in air, using the same specimens as in case of oxygen index.

Discussion

Under the inert atmosphere styrene-butadiene rubber, SBR, preserves elastic properties from the temperature –52.2 °C in which it turns from the glassy to the elastic state, to the initial temperature of thermal cross-linking process 259 °C.

In case of researched chlorosulphonated polyethylenes their glassy transition takes place at higher temperature when compared with SBR rubber (Table I). Simultaneously the chlorine content in CSM influences the increase of glass transition temperature, T_g (ref.[3,4]). The thermal stability range of the researched CSM is much narrower when compared with SBR as a result of thermal transitions connected with the process of macromolecule dehydrochlorination at the temperature over 190 °C. The dehydrochlorination process causes thermal modification of polymer chains which results in creation of double bonds, even conjugated ~CH=CH-CH=CH~, as in the case of polyvinyl chloride, PVC[3–5].

Researched elastomer blends CSM/SBR cross-linked by zinc and nanozinc oxide are characterized by singular temperature of the transition from the glassy to the elastic state, higher than T_g of SBR and lower than T_g of CSM. It confirms good comiscibility of examined elastomers[3]. The initial temperature of cross-linking process, T_C, of SBR is significantly higher than T_C of researched elastomer blends. As is shown in Table I, the application of nano ZnO in the cross-linking process of examined blends influences the increase of their T_C when compared with ZnO. It proves that changing zinc oxide to nanozinc oxide causes an increase of thermal stability range.

Table I
Thermal properties of elastomers and their blends

Atmosphere	Nitrogen		Air				
Sample	T_g [°C]	T_C [°C]	T_5 [°C]	T_{50} [°C]	dm/dt [mm]	Pe [%]	P_{800} [%]
SBR	–52,5	259,5	270	410	65	16,1	5,0
CSM24	–24,2	193,5*	250	420	60	15,0	5,5
CSM43	10,0	198,0*	230	375	30	21,1	2,2
CSM24/SBR_{Zno}	–49,7	130,3	240	420	57	25,9	7,8
CSM24/SBR_{nZno}	–48,2	149,3	240	415	50	24,0	5,5
CSM43/SBR_{Zno}	–38,8	141,1	195	415	47	35,9	12,8
CSM43/SBR_{nZno}	–44,1	179,1	200	415	48	29,0	7,8

* – initial temperature of dehydrochlorination process, T_g – glass transition temperature, T_C – initial temperature of cross-linking process,T_5 – temperature of elastomer/blend 5% mass loss, T_{50} – temperature of elastomer/blend 50 % mass loss, dm/dt – maksimum rate of elastomer/blend thermal decomposition, Pe – residue after thermal decomposition, P_{800} – residue after heating upto 800 °C, SBR – styrene-butadiene rubber, CSM24 – chlosulphonated polyethylen containing 24 % of combined Cl, CSM43 – chlosulphonated polyethylen containing 43 % of combined Cl,CSM24/SBR_{Zno} – elastomer blend of CSM24 and SBR cross-linked by ZnO, CSM24/SBR_{nZno} – elastomer blend of CSM24 and SBR cross-linked by nZnO, CSM43/SBR_{Zno} – elastomer blend of CSM43 and SBR cross-linked by ZnO, CSM43/SBR_{nZno} – elastomer blend of CSM43 and SBR cross-linked by nZnO

The increase of chlorine content in CSM influences the thermal stability indicates under the air atmosphere[5]. The higher content of chlorine in CSM is, the lower is the thermal stability defined by value of T_5 of examined polymer and its blend with SBR (Table I). From among examined blends only CSM24/SBR is characterized by the highest thermal stability indicated irrespective of zinc oxide applied.

The rate of SBR thermal decomposition, dm/dt, is significantly higher than the destruction rate of examined polyethylene, because HCl which is emitted in this reaction favours ionic decomposition of polymer and its blends with SBR. Therefore higher content of chlorine in CSM causes a decrease of thermal decomposition rate in air, whereas the residue after thermal decomposition, Pe, increases.

We observed a distinct influence of the applied CSM type on the residue after thermal decomposition, Pe, of the examined blends (Table I). Higher content of chlorine and as a result higher emission of HCl, favours elastomer blend CSM43/SBR carbonization.

In case of researched chlorosulphonated polyethylenes their glassy transition takes place at higher temperature when compared with SBR rubber (Table I). Simultaneously the chlorine content in CSM influences the increase of glass transition temperature, T_g (ref.[3,4]). The thermal stability range of the researched CSM is much narrower when compared with SBR as a result of thermal transitions connected with the process of macromolecule dehydrochlorination at the temperature over 190 °C. The dehydrochlorination process causes thermal modification of polymer chains which results in creation of double bonds, even conjugated ~CH=CH-CH=CH~, as in the case of polyvinyl chloride, PVC[3−5].

Researched elastomer blends CSM/SBR cross-linked by zinc and nanozinc oxide are characterized by singular temperature of the transition from the glassy to the elastic state, higher than T_g of SBR and lower than T_g of CSM. It confirms good comiscibility of examined elastomers[3]. The initial temperature of cross-linking process, T_C, of SBR is significantly higher than T_C of researched elastomer blends. As is shown in Table I, the application of nano ZnO in the cross-linking process of examined blends influences the increase of their T_C when compared with ZnO. It proves that changing zinc oxide to nanozinc oxide causes an increase of thermal stability range.

The increase of chlorine content in CSM influences the thermal stability indicates under the air atmosphere[5]. The higher content of chlorine in CSM is, the lower is the thermal stability defined by value of T_5 of examined polymer and its blend with SBR (Table I). From among examined blends only CSM24/SBR is characterized by the highest thermal stability indicated irrespective of zinc oxide applied.

The rate of SBR thermal decomposition, dm/dt, is significantly higher than the destruction rate of examined polyethylene, because HCl which is emitted in this reaction favours ionic decomposition of polymer and its blends with SBR. Therefore higher content of chlorine in CSM causes a decrease of thermal decomposition rate in air, whereas the residue after thermal decomposition, Pe, increases.

Table II
Combustibility of elastomers and their blends

Sample	t [s]	OI
SBR	206	0,293
CSM24	18*	>0,375
CSM43	incombustible	>0,375
$CSM24/SBR_{Zno}$	252	>0,375
$CSM24/SBR_{nZno}$	246	>0,375
$CSM43/SBR_{Zno}$	290	0,375
$CSM43/SBR_{nZno}$	270	0,375

***** – próbka samogasnąca, **t** – time of burning in air, **OI** – oxygene index

We observed a distinct influence of the applied CSM type on the residue after thermal decomposition, Pe, of the examined blends (Table I). Higher content of chlorine and as a result higher emission of HCl, favours elastomer blend CSM43/SBR carbonization.

High-molecular components of researched blend are differentiated in respect of their flammability (Table II). SBR is a flammable polymer and flammability of CSM depends on their chlorine content, CSM belong to self-extinguishing or non-flammable polymers. So, addition of 15 phr of chlorosulphonated polyethylene to SBR causes a substantial decrease of its flammability.

The research proved that changing zinc oxide to nanozinc oxide caused inconsiderable reduction of crosslinked elastomer blend CSM/SBR burning time in air regardless of chlorine content in CSM.

Changing of CSM24 to CSM43 caused elongation of burning time of crosslinked blends, however, contrary to expectations, we did not receive samples self-extinguishing in air.

REFERENCES

1. Indian Rubber Institute: *Rubber Engineering*, McGraw – Hill, New York 2000.
2. Rzymski W. M., Wolska B., Wawrzecka A. M.: Patent PL 198304/2007.
3. Janowska G., Kucharska A., Kawałek J., Rzymski W. M.: Paper accepted for publication in Polimery.
4. Janowska G., Rzymski W. M., Kmiotek M., Kucharska A., Kasiczak A.: Paper accepted for publication in J. Therm. Anal. Calorimetry.
5. Janowska G., Rzymski W. M., Kucharska A., Kmiotek M., Kasiczak A.: Paper accepted for publication in Polimery.

P-10
IMPROVEMENT OF DYE ADSORPTION ON REGENERATED CELLULOSE FIBERS BY RF PLASMA PRE-TREATMENT

MARIÁN LEHOCKÝ[a*], MUSA SOWE[b], and PETR SÁHA[b]

[a] Tomas Bata University in Zlín, T.G.M. Square 5555, 760 01 Zlín, [b] Polymer Centre, Faculty of Technology, Tomas Bata University in Zlín, T.G.M. Square 275, 762 72 Zlín, Czech Republic
lehocky@post.cz

Adsorption of the dyes on the surface of the natural or synthetic polymer fibers, or weaved fabrics is created due to the effect of the intermolecular forces between fiber surface and the dye. Such forces are causing relatively strong bonding interaction between dye dipoles and the stained matrix. In the case of polymer and biopolymer materials the number of the dipoles is directly proportional to the number of polar groups in macromolecular side chains. The latter number of present dipoles is possible to be increased by several physico-chemical methods, e.g. fire treatment, chemical etching by strong acid, UV irradiation, corona discharge or low-temperature plasma treatments etc. In this communication the effect of low-temperature plasma treatment of regenerated cellulose weaved fabric on dye adsorption to the surface of the studied substrate is discussed. Obtained increased dye selectivity to the stained matrix results in improved tinctorial strength, better economical effectiveness as well as to the improved ecology of the process.

Radiofrequency (RF) plasma treatments can advantageously replace thermal, radiative or chemical processes of surface modification of fibres or weaved fabrics. In fact, these treatments can be easily controlled and are environmental-friendly. Moreover, plasma modifies the surface layer at a depth of few nanometres, depending on power and time, and leaves the bulk characteristics unaffected. Due to this fact, in some cases, plasma provides the only acceptable solution to common surface treatment problems[1–5]. A cold plasma process, also referred as to as a low-temperature, low-pressure or glow discharge plasma process, is a vacuum process utilizing interactions of reactive species created in a low-temperature plasma with solid surfaces. Cold plasma is an ionized or partially ionized fluid that, as whole, is electrically neutral. The reactive species include electrons, ions, free radicals, various neutral molecules and photons of wide range of energies. The change of surface behaviour with regards to its hydrophilic modification is often useful and it allows using in different areas of temporary technologies (printing and packaging industry). It is possible to provide the necessary biocompatibility by modification of surface, for example by fixing of active organic or biopolymer thin film[6]. Fixing of metal particles for improvement especially mechanical or electromagnetic properties and design of the commercial product is also helpful[7,8]. In this communication the measured quantity of the adsorption was the reflectance, which is directly proportional to the dye adsorption. Reflectance is the quantity characterizing ability of the materials body to reflect electromagnetic radiation falling onto it. With increasing dye adsorption, the higher is the amount of the dye adsorbed what is reflected also in the higher sample reflectance. There was used contact angle measurement to evaluate surface hydrophilicity/ hydrophobicity of the used plasma treatment. Chemical composition of viscose surface was studied by means of XPS analysis. Topography of virgin and treated fabrics was visualized using SEM.

Air plasma surface treatment was used as an effective tool to increase surface hydrophilicity and roughness of viscose surface. The level of incorporated nitrogen and oxygen was investigated to describe the kinetics of the process and to confirm wettability studies showing decrease of contact angle with treatment time. The SEM was used for surface morphology visualization observing change from relatively smooth for virgin viscose to rough one for treated substrate. Dyeing of weaved fabrics was proceeding in much better way. A new recipe for dyeing bath without any use of sodium sulphate was found with the same result of reflectance of final dyed fabrics. Thus, due to the effect of plasma treatment we could eliminate sodium sulphate in dyeing bath to obtain the same intensity of colour after dyeing what is very important from both ecological and economical point of view.

Authors would like to express their gratitude for financing of this research to the Ministry of Education, Youth and Sport of the Czech Republic (grant VZ MSM 7088352101).

REFERENCES

1. Strobel M., Lyons C. S., Mittal K. L., in.: *Plasma Surface Modification of Polymers: Relevance to Adhesion*, VSP, Utrecht 1994.
2. Šíra M., Trunec D., Sťahel P., Buršíková V., Navrátil Z., Buršík J.: J. Phys. D: Appl. Phys. *38*, 621 (2005).
3. Novák I., Pollák V., Chodák I.: Plasma Process. Polym. *3*, 355 (2006).
4. Novák I., Števiar M., Chodák I.: Monatshefte für Chemie *137*, 943 (2006).
5. Šíra M., Sťahel P., Buršíková V., Vohánka V., Trunec D.: Czech. J. Phys. *54*, C835 (2004).
6. Trunec D., Navrátil Z., Sťahel P., Zajíčková L., Buršíková V.: J. Phys. D: Appl. Phys. *37*, 2112 (2004).
7. Kotál V., Švorčík V., Slepička P., Sajdl P., Bláhová O., Šutta P. Hnatowicz V: Plasma Process. Polym. *4*, 69 (2007).
8. Švorčík V., Kotál V., Slepička P., Bláhová O., Šutta P.: Polym. Eng. Sci. *46*, 1236 (2006).

P-11
PLASMA-MODIFICATION OF THERMOPLASTIC FOR IMPROVE BONDING PROPERTIES

ANNA MISIUN,* S. SCHMID, H. GEISLER, and R. H. SCHUSTER

Deutsches Institut für Kautschuktechnologie e.V., Eupener Straße 33, 30519 Hannover, Germany
Anna.Misiun@dikautschuk.de

In this work the influence of atmospheric pressure plasma activation and plasma polymerization processes on the

rubberthermoplastics bonding was investigated. Chemical and physical properties of the modified surfaces were confirmed through contact angle measurements, infrared spectroscopy and atomic force microscopy. It was shown, that plasma activation and polymerization affect the surface properties and were able to improve the bonding between the investigated materials.

Introduction

The industrial use of plasma processing has been known since late 1960. Most of the progress was done by the use of low pressure plasma. The disadvantage here is, that this is not suitable for the commercial technology. A new entry in this field is given by the non-thermal atmospheric pressure plasma process. From begin it was clear, that this new technique will have a favorable affect in improving material properties in the bonding technology.

The focus of this research is the influence of atmospheric pressure plasma discharge on the properties of rubberthermoplastic bonding.

Experimental

Commercial thermoplasts like PP, PBT and PA6 were used as a substrate for plasma treatment. The materials were cleaned in acetone and modified through atmospheric pressure plasma (open air plasma reactor, model PFW 20, Plasma-Treat, Germany). The samples were treated using various process gases (nitrogen, air or argon). Plasma polymerization experiments were performed with various precursors suitable for this process. Experiment conditions like modification time, power or sample to plasma outlet distance were varied during the work.

After plasma treatment PBT and PA6 were bond with nitrile-butadiene-rubber (NBR) via vulcanization with a 1-component and 2-component adhesive system. After the treatment polypropylene was glued via an adhesive based on CR with a styrene-butadiene-rubber (SBR).

The effectiveness of experiments was measured using the contact angle method. The treated thermoplastic surfaces were also examined using atomic force microscopy (AFM) to characterize the substrate topography and the thickness of the polymer films after treatment. The chemically properties of the plasma polymers were confirmed using infrared spectroscopy.

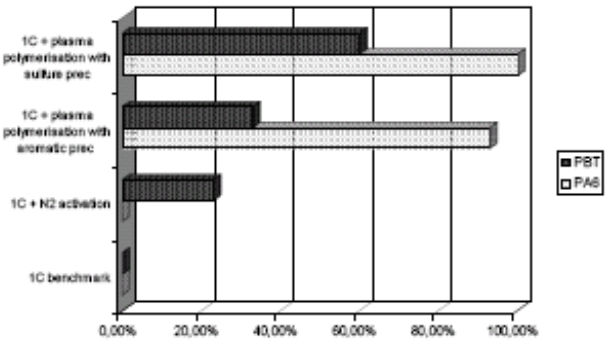

Scheme 2. **Application on plasma activation and plasma polymerization as a replacement of adhesives primer**

Results

The plasma processes lead to the following effects: cleaning, activation and functionalization of the thermoplastic surfaces. All this factors have a genuinely influence during the composite preparation via gluing or vulcanization.

Practical adhesion of SBR on polypropylene by use of CR adhesive equal to zero. The activation alone of the material in air or nitrogen plasma induce the adhesion forces between the bonded surfaces. However, the best effects are observed after plasma polymerization process using fluor- or aliphatic precursor (Scheme 1).

The vulcanization of NBR on thermoplastic materials can be realized by using a 2-components adhesive system, where one of the components is the primer. Without the primer the bonding can not occur. The latest experiments with various plasma polymerization precursors showed, that plasma give the opportunity to successfully replace the primer (Scheme 2) leading to a 1-component (1C) system.

The surface analysis confirms the chemical and physical changes of the treated materials. Wetability measurements are

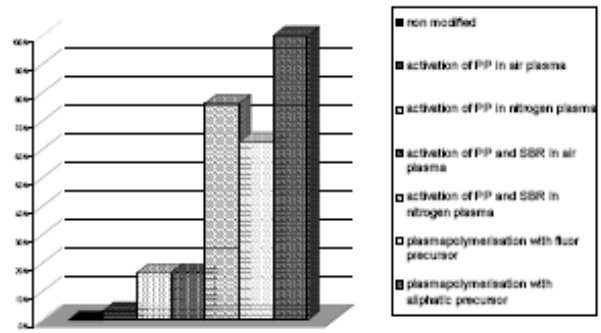

Scheme 1. **The gluing of polypropylene with SBR with a contact adhesive based on CR**

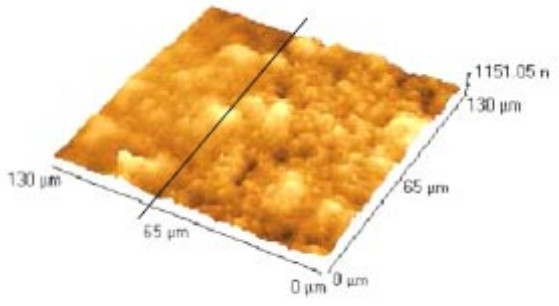

Scheme 3. **AFM picture of deposited plasmapolymer based on aliphatic precursor (right) and untreated sample (left)**

showing a correlation between the experiment conditions and surface energy. This gives an ability to control the process outcome and to "adjust" the surface energies of partners, what have a relevant influence during bonding process.

Morphological images from atomic force microscopy showed a different thickness and shape of deposited layers as a function of precursor flow rate and the type of precursor itself. Scheme 3 shows the polypropylene surface with a typical layer of plasmapolymer based on an aliphatic precursor.

Conclusions

It has been confirmed, that the plasma technique can be an effective surface treatment for promoting adhesion between thermoplastic and rubber. The most successful results were obtained during the plasma polymerization process with aliphatic substances as precursors for the bonding of NBR and SBR on PP, PBT and PA6.

However, at the moment this technique can not substitute the complete adhesive system.

We thank the following companies for financial support:REMA TIP TOP GmbH, Artemis Kautschuk- und Kunststofftechnik GmbH, SKF Sealing Solution GmbH, Maschinenfabrik Herwarth Reich GmbH, Vulkan Kupplungsund Getriebebau GmbH & Co. KG, Stromag AG, helsacomp GmbH, Berleburger Schaumstoffwerke GmbH, Plasmatreat GmbH.

REFERENCES

1. Poncin-Epaillard F., Chevet B., Brosse J., in: *Plasma Surface Modification of Polymers*, pp. 168-180, VSP BV, Utrecht 1994.
2. Yasuda H., Plasma Process. Polym. *2*, 293 (2005).
3. Wang J., Liu X., Choi H.: J. Polym. Sci. *46*, 1594 (2008).
4. Thurston R., Clay J., Schulte M.: J. Plast. Film Sheeting *23*, 63 (2007).

P-12
STRUCTURAL EVOLUTION IN LAYERED SILICATES NANOCOMPOSITES

DANIELA JOCHEC MOŠKOVÁ*, IVICA JANIGOVÁ, and IVAN CHODÁK

Polymer Institute of the Slovak Academy of Sciences, Dúbravská cesta 9,842 36 Bratislava, Slovakia
upoldamo@savba.sk

Polymer/layered silicate nanocomposites have attracted great interest because they often exhibit remarkable improvement in materials properties when compared virgin polymer or conventional micro- and macro-composites. Nanocomposites based on biodegradable polycaprolactone (PCL) and native or organically modified layered silicates (Cloisite with different organophilisation) were prepared by melt mixing and using co-rotating twin screw extruder for comparison of the influence of mixing rate on the structure of composites. The structure and properties of prepared materials were characterized by SEM, TEM, wide-angle X-ray diffraction and rheological measurements which provides additional information about structure.

The experiments revealed that various fillers differ in their effect and different method of homogenization strongly influenced structure. The increase of layer spacing depends on the clay concentration. Intercalation and/or exfoliation of PCL/C20A is achieved by homogenization at igher shear rate.

In the TEM images for the PCL/C20A it is clearly seen that nanoclay sheets are homogeneously dispersed in the PCL matrix. Although exfoliated individual layers can be detected by TEM, the method can not be used to draw general conclusions about the structure. TEM images for the PCL/CNa show several large dark domains and clay aggregates at a micrometer level. Exfoliated nanoclay sheets for the PCL/CNa are observed only in composites prepared via extrusion process. In order to obtain indications about the differencies in composite structure in quantitative terms, SEM analysis was performed.

The melt rheological properties were analyzed using viscoelastic properties obtained from oscillatory rheological measurements. The nanocomposites showed a much higher complex viscosity than the neat PCL and significant shear-thinning behavior in the low frequency range. The storage modulus and loss modulus of the nanocomposites were also found to be less frequency dependent in the low frequency range than the virgin PCL. The reason is seen in the strong interactions between the organoclay layers and PCL molecules and in good dispersion of organoclay platelets in the polymer matrix.

Acknowledgement. APVV-51-050505.

P-13
EFFECT OF PLASMA TREATMENT ON THE PRINTABILITY OF MEDICAL GRADE PVC

MUSA SOWE[a*], IGOR NOVÁK[b], MARIÁN LEHOCKÝ[c], PETR SÁHA[a], and IVAN CHODÁK[b]

[a] Polymer Center, Tomas Bata University in Zlin, T.G.M Square 275, 762 72 Zlin, Czech Republic, [b] Department of Composite Thermoplastics, Polymer Institute, Slovak Academy of Sciences, Dúbravská cesta 9, 842 36 Bratislava, Slovakia, [c] Tomas Bata University in Zlin, T.G.M Square 5555, 760 01 Zlin, Czech Republic
musa_sowe2002@yahoo.com

Introduction

Polymers are applied widely in modern industry and act in very important roles for many obvious advantages[1]. However, bonding and finishing of many polymers present a problem due to the low hydrophilicity of their surfaces. Hydrophlicity affects the wettability, paintability, colorability, printability, biocompatibility, anti-electrostatic properties, adhesion, etc. Many methods have been devised and are commercially available to modify the polymer surfaces. Among them, plasma treatment has emerged as a convenient and versatile surface modification and coating technique and it is

now a common method in industry because it is a very effective way to give hydrophilicity to a polymer surface[2].

Poly (vinyl chloride), PVC, is a particularly important commodity polymer that accounts for an annual world-wide production of about 26 million tons. Medical grade PVC continues to be extensively used in the medical field as a biomaterial to produce catheters (intravenous and urological), blood storage bags and dialysis tubing despite public scrutiny for some of the plasticizers used in PVC[3]. And, in that regard extensive research on surface cross linking and surface coating have addressed some of the problems of plasticizer migration or biocompatibility of PVC[4].

Although PVC has many applications due to its attractive characteristics such as flexibility, softness, transparency, and low production cost, the required surface properties, such as, adhesive ability, biocompatibility, antibacterial ability and printability, are often different from those of the bulk in many applications[5,6]. For example, its surface inertness creates challenges for adhesion of ink on its surface, and therefore affects its printability[6]. In order for an ink to adhere to a substrate, it must have adhesion properties that make it capable of wetting the material. And, upon drying, it should remain adhered to the surface and not peel or chip. If this is to occur, the surface tension of the ink must be lower than the surface energy of the substrate[7].

It has been shown that surface characteristics including surface chemistry, charge, wettability and roughness all affect biocompatibility and adhesion capability on surfaces[8–10]. Surface plasma treatment of polymers has been shown to be a viable method in enhancing adhesion properties in that it does not affect the bulk characteristics of the material. In this regard, plasma-surface modification (PSM) is an effective and economical surface treatment technique for many materials and continues to be of growing interest in medical devices technology.

And so the purpose of this work is to investigate the effect of cold plasma treatment on the printability of medical grade PVC. The scope of the work is limited to correlating printability on PVC virgin and plasma treated samples.

Experimental method

Commercially available medical grade PVC of material RB1/T3M for extrusion, in pellet form, from Moden Plast S.P.A, Hungary, was used in this study. The additives included stabilizers and lubricants. Films of 5 cm × 5 cm × 1 cm size were produced using a hot press at 160 ºC.

Experiments were performed on PVC film pieces of 4 cm × 5 cm × 1 cm. Prior to plasma treatment the samples were washed using triton and de-ionized water, sonicated, oven dried and individually stored. The coplanar discharger was used for the PVC modification. The plasma treatment was conducted in air under atmospheric pressure at room temperature for 15 seconds using 200 W power.

Wettability of the plasma treated PVC surface was evaluated by making contact angle measurements immediately after the treatment. For this purpose, 3 liquids were used, namely, deionized water, ethylene glycol, and diiodomethane. Measurement of contact angles for virgin and plasma treated PVC was made using the Surface Energy Evaluation (See) System (Brno, Czech Republic).

Absorbance by the samples was evaluated using a FT-IR spectroscopy. Measurements were performed on a Nicollet model 730 FT-IR spectrometer.

The morphology of the surface of the virgin and plasma modified PVC was evaluated using the Tescan Vega II LMU machine at 20.0 kV and 30.00 magnifications. Samples were sliced to 1 cm x 2 cm sizes for the purpose.

After plasma treatment GPX ink series (GPX 90) from Lemmaco Ltd Company of Hungary was used for printing the PVC films at 130 °C using a Baier Gmbh & Co machine. For this purpose, samples of the virgin and plasma treated PVC were cut to 4 cm by 5 cm sizes. Printing was done on one side of the sample only.

The printed PVC films were then evaluated using the Helios Thermo Scientific spectroscopy machine. Spectral images were recorded from 400−700 nm for each set of peels of both samples with intervals of 5 peels, 10 peels, 20 peels and 40 peels until no further change was registered.

Results and discussion

Water contact angle measurements showed a decrease from 85.86 for virgin PVC to 64.85 for plasma treated, which corresponds to a higher hydrophilicity for the plasma treated. This result is consistent with SEM measurements which suggest that the plasma treatment effectively changed the surface morphology and the surface becomes rough after treatment signaling higher hydrophilicity. Also, absorbance measurements by FTIR showed higher intensity for plasma treated samples although absorbance occurred at similar locations for both virgin and treated samples. This fact again points to higher hydrophilicity after treatment correlating well with contact angle and SEM results. The “Tape test” and visible spectroscopy measurements of the printed virgin and plasma treated samples indicated that plasma modification improved adhesion of the ink to the PVC, probably because of its higher hydrophilicity. This suggests that plasma treatment has enhanced the printability of PVC.

The authors would like to express their gratitude for financing of this research to the Ministry of Education, Youth and Sport of the Czech Republic (grant VZ MSM 7088352101). Grant (MPO 2A-1TP1/126) and Scientific Grant Agency of the Ministry of Education and Slovak Academy of Science (grant VEGA 2/7103/27) is also acknowledged.

REFERENCES

1. Mandl S., Rauschenbach B.: Biomed. Technik *45*, 193 (2000).
2. Schroder K., Meyer-Plath A., Keller D., Ohl A.: Plasmas Polym. *7*, 103 (2002).
3. Yunchuan xie., Qingfang Yang.: J. Appl. Polymer Sci. *85*, 1013 (2002).
4. Rahman M., Brazel C.: Prog. Polym. Sci. *29*, 1223 (2004).
5. Novak I., Florian S.: J. Mater. Sci. Lett. *18*, 1055 (1999).
6. Schroder K., Meyer-Plath A., Keller D., Ohl A.: Plasmas Polym. *7*, 103 (2002).
7. Chua P., Chena J., Wanga B.: Huang Mater. Sci. Eng. *36*,

143 (2002).
8. Schroder K., Meyer-Plath A., Keller D., Ohl A.: Plasmas Polym. *7*, 103 (2002).
9. Jiangnan Lai., Sunderland B., Jianming Xue., Sha Yan., Weijiang Zhao., Melvyn Folkard., Barry D., Michael B., Yugang Wang.: Appl. Surf. Sci. *252*, 3375 (2006).
10. Morent R., De Geyter N., Leys C.: Nucl. Instrum. Mmethods Phys. Res. *266*, 3081 (2008).
11. Deshmukh R R., Shetty A R.: J. Appl. Polymer Sci. *104*, 449 (2007).
12. Yun Chung M., Min Jung J., Jeon Han G., Min Lee W., Yong Kim M.: Thin Solid Films *447*, 354 (2004).

P-14
COMPARISON OF THE EFFECT OF VARIOUS NANOFILLERS IN COMPOSITES BASED ON THERMOPLASTIC AND ELASTOMERIC MATRIX

ZUZANA NÓGELLOVÁ[a], PETER KOMADEL[b], JANA HRACHOVÁ[b], and IVAN CHODÁK[a]

[a] *Polymer Institute, Slovak Academy of Sciences, Dúbravská cesta 9, SK-842 36 Bratislava,* [b] *Institute of Inorganic Chemistry, Slovak Academy of Sciences, Dúbravská cesta 9, SK-845 36 Bratislava, Slovakia*
Zuzana.Nogellova@savba.sk

Layered silicates are often used as fillers for improving mechanical properties of composites based on plastics or rubbers. Their effectivity consists in their ability to create intercalated or exfoliated structures. Thus, presence of small amount of clay in plastic or rubber should result in substantial changes in properties of the composite. The effect depends significantly on the appropriate surface modification of the filler, since usually the polymer is hydrophobic while the filler is hydrophilic. The properties of composites should depend on a particle size of the filler as well.

In this work three types of unmodified fillers and one organically modified filler were used. Inorganic fillers included two types of bentonite from Jelšový potok deposit, Slovakia, with different particle size (Ca-bentonite J10 – below 10 μm and Na-bentonite BJ40 – below 40 μm) and a Japanese Na-montmorillonite Kunipia-F (Kunimine Industries Co., Ltd.). Nanofil 15 (particle size 15 μm) (Süd-Chemie, Germany) with hydrophobic modification of surface was chosen as the organically modified filler. The fillers were added in concentration range up to 10 wt.%. The effectivity of these nanofillers were studied in three various polymeric matrices: low density polyethylene LDPE (Bralen RA 2-19, MFI = 2 g/10 min, Slovnaft, Slovakia) as an apolar thermoplastic polymer, ionomeric copolymer polyethylene-co-acrylic acid (Nucrel HC 1202, DuPont) as polar thermoplastic polymer and elastomeric polymer SBR rubber (Kralex 1500, Kaučuk Kralupy, Czech Republic).

The effect of the fillers was evaluated regarding to mechanical properties of the respective nanocomposites. Examples of the results are shown for tensile strength and for two matrices, namely LDPE and SBR rubber in Fig. 1 and 2. In both thermoplastic matrices tensile strength and elongation at break slightly decreased with the concentration of the bentonites and Nanofil. Small differences between the fillers were observed. The addition of Kunipia-F resulted in more significant decrease of mechanical parameters considered. In elastomeric matrix (SBR rubber) tensile strength and elongation at break increased with increasing filler concentration, except for Kunipia-F, where only slight effect was observed with rising amount of the filler.

Comparison of relative values of mechanical parameters (values for composites divided by values for matrix without filler) was made. Changes of tensile strength and elongation at break were very similar for both thermoplastic polymers containing all fillers except for nanocomposites filled with Kunipia-F, where relative elongation at break for composites with ionomeric Nucrel showed higher values in comparison with apolar LDPE. Regarding the behaviour in elastomeric matrix (SBR rubber), relative mechanical properties were improved with rising concentration of nanofiller. The best

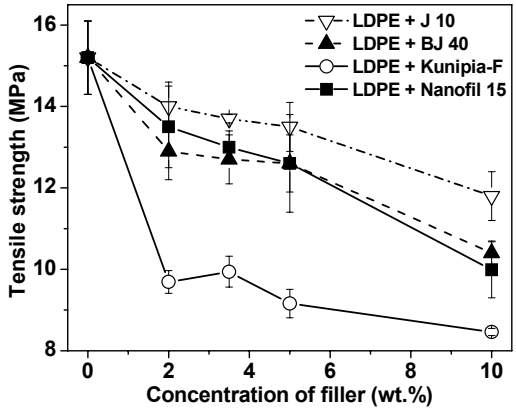

Fig. 1. **Tensile strength of composites of LPDE and clay *vs.* concentration of the filler**

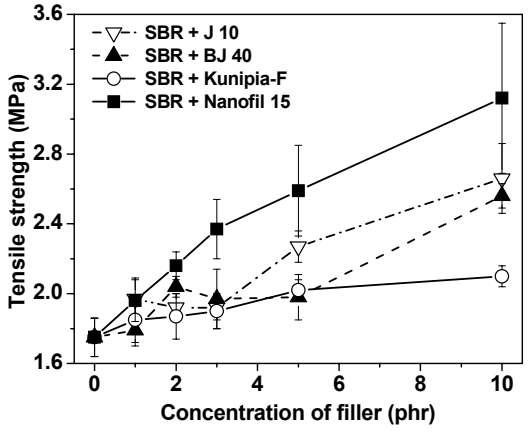

Fig. 2. **Tensile strength of composites of SBR and clay *vs.* concentration of the filler**

appeared to be the filler with smaller particle size (10 μm and 15 μm), medium increase of mechanical parameters was achieved for bentonite with particle size below 40 μm and marginal changes were observed in composites filled with Kunipia-F.

The authors acknowledge financial support of the Slovak Research and Development Agency (Grant APVV 51-050505).

P-15
POLYETHYLENE POROUS FILM FUNCTIONALIZED BY ELECTRICAL DISCHARGE PLASMA

IGOR NOVÁK*[a], GALINA ELYASHEVICH[b], IVAN CHODÁK[a], and MILENA ŠPÍRKOVÁ[c]

[a] Polymer Institute, Slovak Academy of Sciences, 842 36 Bratislava, Slovakia, [b] Institute of Macromolecular Compounds, Russian Academy of Sciences, 199 004 St. Petersburg, Russian Federation, [c] Institute of Macromolecular Chemistry AS CR, v. v. i., 162 06 Prague, Czech Republic
upolnovi@savba.sk

The polyethylene porous films (PEPF) were treated by dielectric surface barrier discharge (DSBD) plasma at atmospheric pressure in oxygen (O_2), air or nitrogen (N_2) (ref.[1–4]). The surface energy of films was carried out by direct measurements of contact angles of six testing liquids. The strength of adhesive joints in the system modified polyethylene porous films – polyacrylate was measured by peeling of the joints under the angle of 90°. The significant increase of the surface energy and its polar component of PEPF modified by all types of plasma were observed. The modification of PEPF was performed in static conditions by DSBD plasma in a laboratory reactor. The modification of polymer was carried out in static conditions at atmospheric pressure in N_2 or O_2 of a technical purity.

Measurement of the surface energy of polymer was carried out by direct measurements of contact angles of testing liquids set[4] (re-distilled water, ethylene glycol, thiodiglycol, formamide, methylene iodide, and 1-bromonaphthalene using SEE (Surface Energy Evaluation) system (Masaryk Univ, Czech Republik).

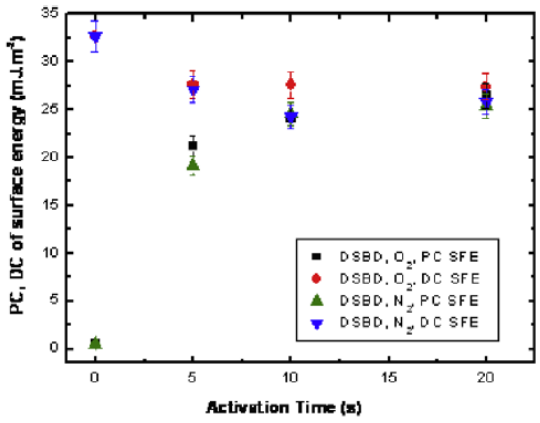

Fig. 1. **Polar and dispersive component of the surface energy of PEPF modified by DSBD (50 W) plasma in O_2, and N_2 *vs.* time of activation**

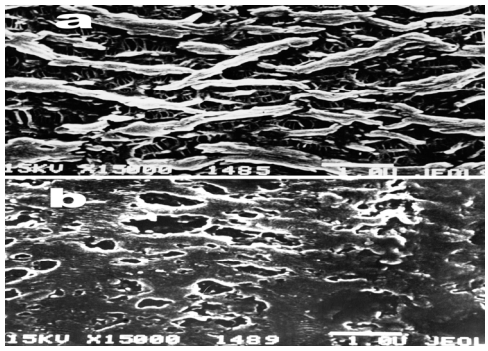

Fig. 2. **SEM photographs of the untreated PEPF (a) and this sample after plasma treatment (b)**

The surface energy and its polar component of PEPF modified by DSBD (Fig. 1) plasma increased markedly in comparison with unmodified polymer. The total surface energy of DSBD plasma modified PEPF increased from 33.2 mJ m^{-2} (unmodified sample) up to 51.8 mJ m^{-2} (DSBD, O_2, 10s) and 53.9 mJ m^{-2} (DSBD, O_2, 20 s), or 48.9 mJ m^{-2} (DSBD, N_2, 10 s) and 51.3 mJ m^{-2} (DSBD, N_2, 20 s), respectively.

As it is seen at Fig. 2 the morphology of the film surface is changed after plasma irradiation. First of all, the stresses ties between crystalline regions disappeared, and as a result the shape of pores became more symmetric, more close to round. The pore sizes and number of the pores sharply decreases, and the portion of dense material on the surface increases due to coalescence of crystalline regions.

The significant increase of the surface energy and its polar component of PEPF modified by DSBD plasma in O_2, N_2, and in air at atmospheric pressure was observed. This increase was important yet for short times of polymer modification. The morphology of the PEPF film surface was substantially changed due to plasma irradiation, and sizes and number of the pores sharply decreased.

The research was supported by the Slovak Scientific Agency project VEGA, No. 2/7103/27, by the Grant Agency of the Academy of Sciences of the Czech Republic (grant A400500505) and the Russian Foundation for Basic Research (Grant № 07-03-00177).

REFERENCES

1. Mirabedini S. M., Rahimi H., Hamedifar S., Mohseni M.: Intern. J. Adhes. Adhesives *24*, 163 (2004).
2. Novák I., Pollák V., Chodák I.: Plasma Proc. Polyms. *3*, 355 (2006).
3. Novák I., Chodák I.: Angew. Makromol. Chem. *260*, 47 (1998).
4. Novák I., Števiar M., Chodák I., Krupa I., Nedelčev T., Špírková M., Chehimi M. M., Mosnáček J., Kleinová A.: Polym. Adv. Technol. *18*, 97 (2007).

P-16

MICROHARDNESS OF POLYPROPYLENE BASED ELECTROCONDUCTIVE NANOCOMPOSITES

LILIYA MINKOVA[a], MARIA VALCHEVA[a], JÜRGEN PIONTECK[b], MATEJ MIČUŠÍK[c], and MÁRIA OMASTOVÁ[c*]

[a] *Institute of Polymers, Bulgarian Academy of Sciences, Acad. G. Bontchev str. bl. 103A, Sofia 1113, Bulgaria;* [b] *Leibniz Institute of Polymer Research Dresden, Hohe Str. 6, 01069 Dresden, Germany;* [c] *Polymer Institute, Slovak Academy of Sciences, Dúbravská cesta 9, 842 36 Bratislava, Slovakia upolmaom@savba.sk*

The nanocomposites with polymeric matrices are being considered for a large variety of commercial applications because of the wide range of properties which comes from the presence of these highly anisometric nanofillers: heat distortion temperature, fire resistance, mechanical properties, permeability, biodegradability, etc. Nanocomposites of montmorillonite and isotactic polypropylene have been obtained and studied because of the industrial importance of this polymer and possible using also in automotive industry. The materials demonstrate an enhancement of moduli and improvement of the thermal stability. A significant increase in mechanical properties and specifically in electric conductivity were reported for PP/carbon nanotubes (CNT) nanocomposites at low content levels of the nanotubes.

Previous investigations reported the preparation of nanocomposites of a new type, containing different amounts of montmorillonite (MMT) and of conducting polypyrrole (PPy) in a polypropylene (PP) matrix. The new nanocomposites turned to possess very good conductivity and thermal stability[1,2].

In the present study the Vickers microhardness and the creep rate of two types of PP based nanocomposites have been determined: PP/MMT/PPy nanocomposites with different content of filler and PP/CNT nanocomposites with different CNT concentration. The aim was to establish the influence of the microstructure of the materials and their composition on the microhardness and the creep rate.

Preparation of PP/MMT/PPy composites. 10 g PP were added to 100 ml water containing dodecylbenzenesulfonic acid (DBSA, in molar ratio pyrrole/DBSA = 5) for the preparation of a PP suspension. MMT was added to the suspension of PP in a weight ratio of PP/MMT = 20/1. The suspension was treated with ultrasound for 10 min for MMT exfoliation. Subsequently the oxidant, 2.3 mol $FeCl_3$ per mol pyrrole dissolved in water, was added under continuous vigorous stirring. After 15 min 4.8–17 wt.% pyrrole related to the combined amount of PP and MMT were introduced dropwise. The oxidative polymerization of pyrrole proceeded for 1 h under stirring. After 24 hours at room temperature the product was filtered off, washed with distilled water, and dried at 60 °C. For comparison PP/PPy devoid of MMT composites with the same amount of conductive PPy were prepared by the same procedure. PP/MMT composites containing 4.8 wt.% of MMT were prepared by mixing the components in a Brabender internal mixer (PLE 330, Brabender, Germany) with 75 rpm at 190 °C for 10 min. Subsequently the homogenized mixture was compression moulded into plates. These composites are named PP/PPyX_B and PP/MMT/PPyX_B, respectively, where X indicates the amount of pyrrole in weight % related to PP or PP and MMT, respectively.

Preparation of PP/CNT nanocomposites. For the preparation of PP/CNT nanocomposites the masterbatch MB3020-01 consisting of PP Hyperion, MFI = 11.8 g/10 min. (at 230°C; 2.16 kg), and 20 wt.% of multi-walled carbon nanotubes, in a granular form from Hyperion Catalysis, USA, was used. A maleic anhydride modified polypropylene, OREVAC 18732, MFI = 8 g/10 min, density = 0.89 g cm^{-3}, from Arkema Inc., France, and unmodified polypropylene HD214CF, MFI = 8 g/10 min, density = 0.9 g cm^{-3}, from Borealis A/S, Denmark were used for composite preparation. The amount of maleic anhydride in OREVAC 18732 was determined by a titration method; it was 0.13 wt.%.

The composites were prepared by mixing of maleinated PP OREVAC 18732 (PP 18732), or unmodified HD214CF (PP HD214CF) with various amounts of MB3020-01 in the 30 ml mixing chamber of a Plasti-corder kneading machine PLE 331 (Brabender, Germany) at 190 °C for 10 min at a mixing speed of 35 rpm. For comparison, a series of composites was prepared by diluting the original masterbatch with the same PP (PP Hyperion). Specimens for further testing were prepared in the form of 1 mm thick slabs by compression moulding of the mixed composites using a laboratory hydraulic press SRA 100 (Fontijne, Netherlands) at 2.4 MPa and 190 °C for 2 min.

Microhardness of the materials was measured on a standard Vickers microhardness tester mhp-160 for a light microscope NU-2 (Germany). The indenter was a square shaped diamond pyramid, with top angle of 136°. Loads of 0.4, 0.6, 0.8 and 1.0 N to correct the instant elastic recovery were employed. A loading cycle of 0.5 min was used. The standard Vickers microhardness (H) was determined by the equation:

$$H = k\,P / d^2 \qquad (1)$$

where P is the applied load, k is a geometric factor equal to 1.854 and d is the mean diagonal length of the imprint after removing the indenter. At least 10 imprints were made under each load. The H value was determined within $\Delta H/H = 0.05$. Under the loads applied the mean diagonal length of the imprints varies in the range 100–200 μm.

For the determination of the creep constant, experiments using different loading times under the indenter were performed.

The microhardness values of neat PP_B and nanocomposites PP/MMT/PPy_B are depicted in Fig. 1. The experimental hardness values of the composites are higher than that of the neat PP, which is 97 MPa. Both types of fillers, MMT particles and PPy, are reinforcing agents for the ternary composites. The microhardness increases with the increase of PPy content for the material with equal MMT content of 4.8 wt.% related to the PP amount (Fig. 1a) and with the increase of the content of MMT for the materials with equal pyrrole content (13 wt.%) as shown in Fig. 1b.

The results show that the presence of MMT and PPy leads to the increase in microhardness of the PP/MMT/PPy materials. The final microhardness values have been determined by the influence that both kinds of fillers, MMT and

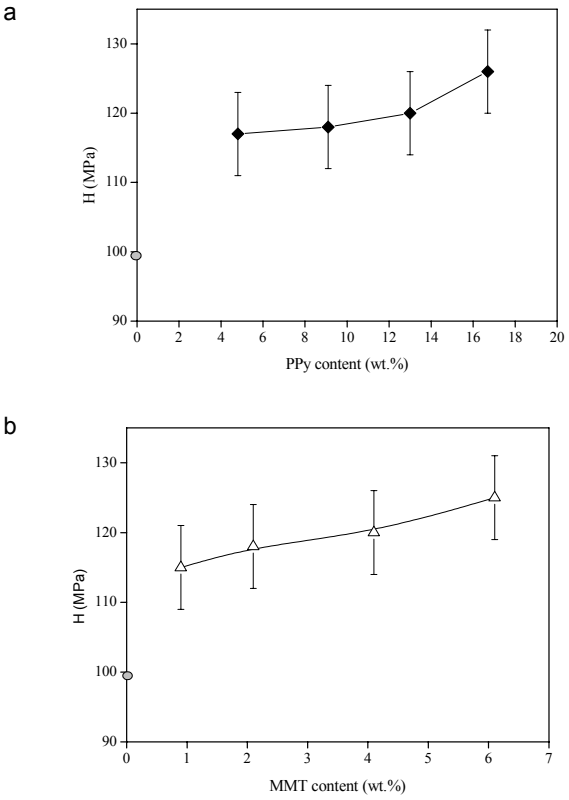

Fig. 1. **Dependence of microhardness on (a) PPy concentration for PP/MMT/PPy_B composites with constant MMT content of 4.8 wt.% related to PP and (b) on MMT concentration for composites containing 13 wt.% of PPy.** The value of pure PP_B (o) as reference. The solid lines are to guide the eyes

PPy increased the microhardness of the composites[3]. Concerning PP/CNT nanocomposites, it has been established that the microhardness increases with increasing the filler content and then remains constant at certain filler content[4].

It is well known that the microhardness values are in close relation with the macro-mechanical properties of the materials. In particular, the microhardness has a linear dependence with the modulus of elasticity. Consequently, a strong increase in the modulus of elasticity should be expected for the PP/CNT nanocomposites.

The creep constants for both types of nanocomposites decrease with the increasing the content of fillers in the composites. However, the decrease of the creep constant with the fillers addition is not significant as should be expected when inorganic filler has been added into a polymer matrix. This is due to the very fine dispersion of the fillers in the when inorganic filler has been added into a polymer matrix. This is due to the very fine dispersion of the fillers in the polymer matrix at nanoscale level. The results show that the new materials possess several valuable characteristics.

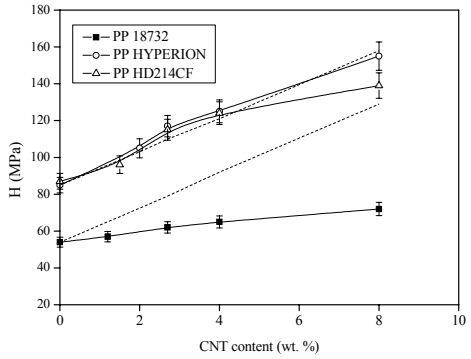

Fig. 2. **Dependence of the microhardness on the concentration of CNT in the nanocomposites**

The research was supported by Bulgarian-Slovak bilateral project "Multicomponent polymer systems with improved properties", by project of the Bulgarian Science Fund, contract TK01/0110, and by project of the Scientific Grant Agency of the Ministry of Education of Slovakia and the Slovak Academy of Sciences (VEGA 2/7103/27).

REFERENCES

1. Mravčáková M., Omastová M., Pötschke P., Pozsgay A., Pukánszky B., Pionteck J.: Polym. Adv. Technol. *17*, 715 (2006).
2. Omastová M., Mravčáková M., Pionteck J., Häussler L., Chodák I.: Polym. Eng. Sci. *46*, 1169 (2006).
3. Pandis C, Logakis E., Peoglos V., Pissis P., Omastová M., Mravčáková M., Janke A., Pionteck J., Peneva Y., Minkova L.: J. Polym. Sci., B: Polym. Phys. *47*, 407 (2009).
4. Peneva Y., Valcheva M., Minkova L., Mičušík M., Omastová M.: J. Macromol. Sci., B: Phys. *47*, 1197 (2008).

P-17
PROPERTIES OF RUBBER COMPOUNDS WITH ZEOLITE NANOADDITIVES

DARINA ONDRUŠOVÁ* , TATIANA BAZYLÁKOVÁ, MARIANA PAJTÁŠOVÁ , SLÁVKA ĽALÍKOVÁ, MICHAELA MASÁROVÁ, MILAN OLŠOVSKÝ, and EUGEN JÓNA

Faculty of Industrial Technologies, TnU AD, I. Krasku 491/30, 020 01 Púchov, Slovakia
ondrusova@fpt.tnuni.sk

Abstract

Natural zeolites form a group of hydrated aluminosilicates with the porous structure (Fig. 1). The best known type of zeolites is clinoptilolite. Its structure is based on threedimensional framework composed of tetrahedral SiO_4 and AlO_4

units, which are connected by shared oxygen atoms. The special porous structure of zeolite has lots of practical applications as an ion-exchange, adsorbent, material for reversible hydratation and dehydratation and also as a nanofiller in polymer materials[1].

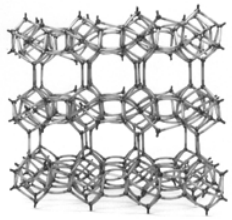

Fig. 1. **Structure of zeolite**

The application of inorganic materials in organic polymers is one of the usual ways to improve up of physical-mechanical properties of polymer. Compozite materials show generally better properties than pure and homogeneous materials. The changes is possible to observe at very low concentration of inorganic component in polymers[2,3].

Present paper deals with the preparation of modified rubber compounds with the addition of nanofillers on the base of natural zeolite – clinoptilolite and give the information about their thermal properties, rheology, vulcanization performance and physical-mechanical properties.

Samples of newprepared modified rubber compounds with zeolite filler were studied by methods of thermal analysis – DTA and TG in the temperature range of 40–900 °C (Fig. 2 and 3) and DSC method in the temperature range 30–250 °C.

Rheology and vulcanization performances (M_L, M_H, t_S, t_{90}, R_V) of prepared rubber compounds were tested and physical-mechanical properties (tensile strength, modulus 300, tensibility, hardness) of vulkanized rubber was studied[4,5]. The values of prepared modified rubber compounds was compared with the standard (comercial rubber compound).

From study of properties of modified rubber compounds with the addition of natural zeolite nanofiller follow that natural zeolite – clinoptilolite may be used for the application in the rubber compounds improving the properties studied.

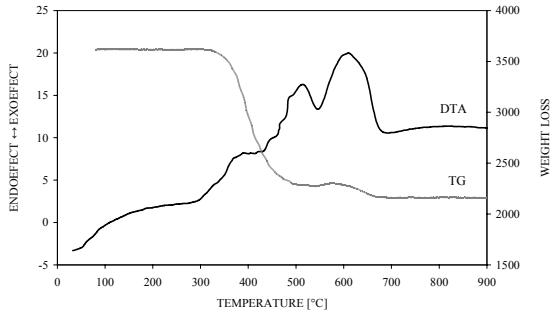

Fig. 2. **DTA-TG of standard rubber compound**

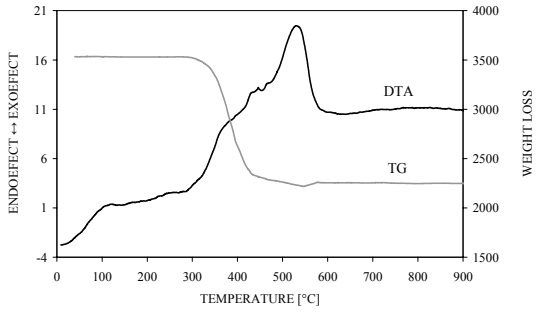

Fig. 3. **DTA-TG of rubber compound with zeolite**

The authors sincerely thank the Slovak Grant Agency AV 4/2014/08 for the financial support.

REFERENCES

1. Šamajová E.: Z histórie výskumu zeolitových surovín Slovenska, *Seminár Prírodné a syntetické zeolity, FCHPT STU Bratislava, 2003.*
2. Jesenák K.: Chem. Listy *101*, 657 (2007).
3. Olšovský H., in: *Proceedings of the International Conference on Geomembranes. 1984, Denver, CO, USA*. Industrial Fabrics Association International, 181.
4. Prekop Š. et al.: *Gumárenská technológia l.*, Žilinská univerzita, Žilina 1998.
5. Kovářová M.: *Pomocné zpracovatelské přísady v gumárenském průmyslu*, SPUR a.s., Zlín 1999.

P-18
DMA ANALYSIS OF ORIENTED POLYPROPYLENE FIBERS

SILVIA PODHRADSKÁ[a], IVAN CHODÁK[a], and ANNA UJHELYIOVÁ[b]

[a] Polymer Institute Slovak Academy of Sciences, Dúbravská cesta 9, 842 36 Bratislava, [b] Institute of Polymer Materials, Department of Fibres and Textile Chemistry, Faculty of Chemical and Food Technology, STU, Bratislava, Radlinského 9, 812 37 Bratislava, Slovakia
anna.ujhelyiova@stuba.sk, upolpodh@savba.sk

Synthetic fibers have a lot of properties which natural fibers miss such as high tenacity and high modulus, dimensional stability, etc. On the other side they have a lot of insufficiences: low hydrophility, worse dyeability, etc. However, development of synthetic fibers is still in progress. Recently a new progress started for PP fibres made from metallocene – made polypropylene. Therefore it is if utmost importance to compare the metallocene PP fibres with the conventional PP fibres made by Ziegler-Natta catalyzed process.

Dynamic mechanical analysis (DMA) yields information about the mechanical properties of a specimen deformed sinusoidally (strain) while the sinusoidally varying responding force (stress) is measured. Oriented fibers have a specific

structure which comes into existence on the definite degree of orientation of macromolecular chains and it is closely associated with orientation speed. This phase transition can be seen on the DMA spectra characterized by glass transition, Tg.

This work presents comparison of dynamic-mechanical properties of two types of oriented model polypropylene fibers, Ziegler-Natta polypropylene (ZN-PP) as well as metallocene polypropylene (m-PP). Model fibres were prepared by LOY technology. Changes of relaxation spectra were identified in dependence on take-up speed (V0) and as a function of melt flow index (MFI). It was found that method of polymerization as well as MFI have an influence to the shift of relaxation peak. Glass transitions of used fibers were located at temperature interval between +50 °C and +110 °C.

This work was supported by the Slovak Research and Development Agency under the contract No. APVV-0226-06.

P-19
POLYETHYLENE SURFACE MODIFIED BY POLY(OXAZOLINES) AND BY COPLANAR BARRIER DISCHARGE PLASMA

ANTON POPELKA, IGOR NOVÁK, JURAJ KRONEK, ANGELA KLEINOVÁ, and IVAN CHODÁK

Polymer Institute, Slovak Academy of Sciences, Dúbravská cesta 9, 842 36 Bratislava, Slovakia
upoltopo@savba.sk

Polyethylene (PE) has widely application in the industry. PE is frequently construction material in the automotive industry, for example PE is often using in the bumpers manufacture. In this work, surface properties of thin foil low density polyethylene (LDPE) were studied. The hydrophobic character of LDPE causes that its surface properties are unsuitable in bonding, printing and laminating processes[1].

The increase of the hydrophilicity of LDPE films can be achieved grafting by 2-oxazoline polymers using various methods of LDPE modification by coplanar surface barrier discharge plasma. The surface treatment of polymers by coplanar barrier discharge is magnificent mean to modify polymers. Treated surface of polymers is homogenous without the bulk changes. The surface of LDPE film can be modified by oxygen, nitrogen, argon, carbon dioxide plasma treatment[2]. Polymers poly(2-ethyl-2-oxazoline) (PETOX) was prepared by cationic polymerization of 2-ethyl-2-oxazoline with the degree of polymerization equals to 100 (Scheme 1)[3]. Prepared polymer contains polar amide groups on the backbone. Moreover, PETOX belong to groups of biocompatible materials, hence they are of an interest in biomedical applications[4].

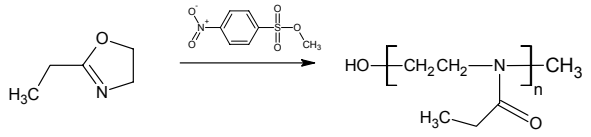

Scheme 1. **Preparation poly(2-ethyl-2-oxazoline)**

Following treatment conditions were used in our experiments: solutions of PETOX in dichloromethane with concentration 0,01, 0,03, 0,05, 0,07, 0,1 g cm^{-3}, dynamic treatments by coplanar barrier discharge plasma in oxygen at atmospheric pressure, power = 200 W and treatment time = 20 s.

The surface properties of polymer were investigated by Surface Energy Evaluation System (SEE system) and by Fourier Transform Infrared Spectroscopy-Attenuated Total Reflectance (FTIR-ATR). The hydrophilicity of modified surface was estimated by contact angles measurements using a set of 5 testing liquids (redistilled water, ethylene glycol, diiodomethane, formamide, and glycerol).

The plasma treatment and grafting by PETOX onto LDPE led to the decrease of the contact angle of water droplet from 99° up to 31° and the surface free energy increased at 66 %. The polar component of the polymer surface energy increased from 0,2 up to 25,6 mJ m^{-2}.

The appearance of amide group's signal at 1625 cm^{-1} was observed in FTIR-ATR spectra and its intensity increased with concentration of PETOX.

Authors are grateful to Slovak Grant Agency VEGA (grant No. 2/7103/27), and Slovak Research and Development Agency - APVV (grants No. 0044-07 and No. 0032-06).

REFERENCES

1. Novák I., Chodák I.: Angew. Makromol. Chem. *260*, 47 (1998).
2. Novák I., Pollák V., Chodák I.: Plasma Proc. Polyms. *3*, 355 (2006).
3. Kobayashi S.: Prog. Polym. Sci. *15*, 751 (1990).
4. Adams N., Schubert U. S.:Adv. Drug Delivery Rev. *59*, 1504 (2007).

P-20
PREPARATION OF THE VULCANIZING AGENTS BASED ON THE COPOLYMERIC SULPHUR WITH AUXILIARIES SUBSTANCES

MARTIN PREKOP, VENDELÍN MACHO, MILAN OLŠOVSKÝ, and IVA SROKOVÁ

Faculty of Industrial Technologies TnUAD in Púchov, Ivana Krasku 491/30, 020 01 SK - Púchov
prekop@fpt.tnuni.sk

This contribution is focused on preparation of copolymeric sulphur prepared by addition or polyaddition of cyclooctameric sulphur to low molecular weight polybutadiene (Krasol LB) and to polybutadiene with average of molecular weight 10 059 g mol^{-1}. The most appropriate content of organic fraction in copolymeric sulphur was 10–20 wt.%. The temperature of copolymerization was in range 125–150 °C, with optimal one at 140 °C.

Vulcanizing characteristics of rubber mixtures and physical-mechanical properties of cured rubbers prepared with above mentioned ternary or multicomponent copolymers of sulfur were evaluated and compared to the results with commercial sulfur (Síra N). In this study was monitored the influence of selected samples of sulfur vulcanizing agent in

real rubber mixtures on vulcanization characteristics, processing and physical – mechanical properties (strength, elongation, hardness and modulus 300).

Was evaluated hight effect of auxiliaries substances by the preparation of copolymeric sulphur. Prepared samples of rubber mixtures with copolymeric sulphur had better compatibility than mixtures with polymeric sulphur. Time of „blooming" vulcanizing agents prepared with auxiliaries substances were 7–8 days and time of "blooming" under assistance of polymeric sulphur (Síra N) was 6 days.

REFERENCES

1. Fan R., Zhang Y., Huang Y., Gong P.: Rubber Chem. Technol. 75, 287 (2002).
2. Akiba M., Hashim A. S.: Prog. Polym. Sci. 22, 475 (1997).
3. Tomita K., Mukoyama N., Yamamoto Y. [Sanshin Kagaku]: JP 2 003 268 240 (2003).
4. Hahn J., Runk M.., Weidenhaupt H. J., Buding H.: [Bayer AG]: EP 1 277 732 (2003).
5. Olšovský M., Štubňa M., Macho V.: *Nové vulkanizačné činidlo na báze multikomponentnej kopolymérnej síry. 14. medzinárodná konferencia APROCHEM 2005. Milovy, 24. – 26. 10. 2005.*
6. Macho V., Olšovský M., Špirk E., Michálek J., Karvaš A., Klabník M., Cíbik B., Komora L.: *Vulkanizačné činidlo gumárenských zmesí.* UV 4589 (16. 8. 2006).

P-21
QUANTIFICATION OF RESIDUAL AMINE CATALYSTS IN POLYURETHANE FOAMS BY THERMAL DESORPTION GAS CHROMATOGRAPHY MASS SPECTROMETRY

FRANKY PUYPE and JIŘÍ SAMSONEK

Institute for Testing and Certification – Zlín, Třida T. Bati 299, CZ-764 21 Zlín-Louky
fpuype@itczlin.cz

Introduction

Polyurethanes are widely used polymers for automotive and building industry. Car seats, sealants, adhesives (glue) and synthetic leather are its most used applications. Tertiary amines are common chemicals for catalysis of the reaction between isocyanate and hydroxyl groups to form cellular and solid polyurethanes (PU). In PU foams tertiary amine catalysts are able to control the blowing of the raising foam (blowing catalysts) and speed up the polymerization reactions (gelling catalysts). The blowing catalysts promote the blowing reaction between the isocyanate and water. These amine catalysts have mainly ethylene groups between the active centers (oxygen and nitrogen atoms) forming hydrogen bridges with the hydrogen atoms from the water (Fig. 1). This conjugation system is able to bring the water closer to the isocyanate group and forms polyurea and carbondioxide which act as a blowing agent.

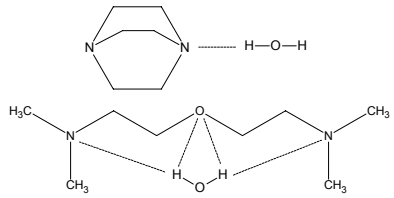

Fig. 1. **Interaction of water with gel catalysts triethylenediamine (TEDA, upper) and bis(2-dimethylaminoethyl)ether (BDMAEE, lower)**

Gelling catalysts make use of the free non-sterically hindered electron pair (e.g. triethylenediamine) on the nitrogen atom to influence the active hydrogen from the polyol and speed up the reaction with the isocyanate by forming a complex between the nucleophilic reagent and the tertiary amine (quaternary ammonium). This reaction is known as the Otto Bayer mechanism (Fig. 2).

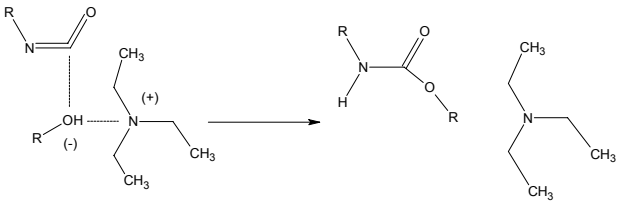

Fig. 2. **Principle of gelling catalysts**

Beside the gelling and blowing catalysis, amine catalysts can influence also the decreasing of the reaction speed. These delayed action catalysts helps operators by giving them time to fill the molds especially for large and complicated mold shapes. Other catalysts are able to cure the skin of the PU foams by providing an additional isocyanate reaction at the surface avoiding fingerprints. These catalysts are very volatile and need to migrate upwards to give more reactivity at the mold surface (e.g. triethylamine) or are not incompatible with the developing foam (e.g. *N*-ethylmorpholine) to migrate to the mold surface and create also a local higher activity.

The last group of amine catalysts is able to react with the isocyanate (reactive catalysts) due to the presence of a hydroxyl group. The meaning for use is the capturing of the catalysts in the PU foam to avoid migration and discoloring on the surface. This is important for the automotive industry because these catalysts cannot bloom (e.g. *N*,*N*`-dimethylethanolamine).

Due to the more strictly quality/emission limits for use of PU material in automotive and building industries, the PU industry needs to develop amine catalysts that give high activity and low-emissions. Some amine catalysts have a strong odor and can influence the VOC/FOG results dramatically from emissions of the organic compounds of non metallic automobile materials (VDA 278 or PV 3341). It is known that amine catalysts like TEDA are responsible for condensation on cold spots in automotive applications. The residual concentrations of amine catalysts in polyurethane can vary from a few mg kg^{-1} till a few percents.

The main advantage to use thermal desorption as an injection technique is the speed of analysis. A time consuming liquid extraction is not needed.

Experimental

Analytical method

All measurements were performed on a refocussation thermal desorption unit (TD-20, Shimadzu, Japan) coupled to a gas chromatograph with mass spectrometrical detection (GCMS 2010, Shimadzu, Japan). The thermal desorption technique is a sampling technology that utilizes heat to increase the volatility of analytes such that they can be removed (separated) from the solid matrix (PU foam, wood, etc.). Thermal desorption allows analysis of almost all sorts of materials including insoluble materials and complex materials at trace levels without any pretreatment of samples.

The thermal desorption of the PU samples was done at 200 °C for 5 min. Due to the volatility of many amine catalysts the evolved products after thermal desorption are once more trapped on a TENAX TA trapping material at –20 °C in the injector. A quick heating of the injector evolves the analytes of interest towards the analytical column (SLB-5 ms, 30 m × 0,25 mm × 0,25 μm) for separation. The detection was done by electron impact ionization in full scan mode however a mass separation is possible for some overlay peaks.

Chemicals

All amine catalysts were purchased from Huntsman Corporation (Everberg, Belgium) and are most commonly used in PU applications. A sample was spiked with the amine catalysts to get the recovery. All used solvents were HPLC grade.

Results and discussion

Separation/calibration

The separation of all peaks from tertiary amines is good and mostly a base peak separation (Fig. 3).

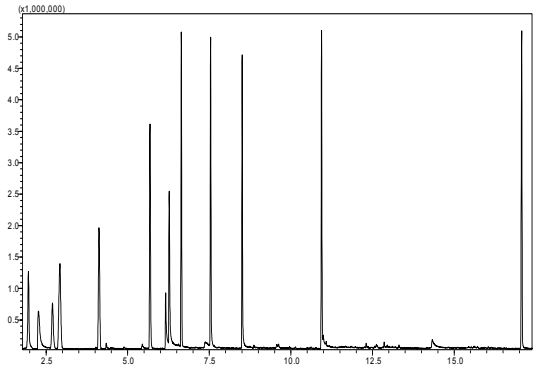

Fig. 3. **Chromatogram of a calibration mixture amine catalysts** (1: DMEA, 2: NEM, 3: NMM, 4: DMCHA, 5: TEDA, 6: BDMA, 7: ZF-20, 8: PMDETA, 9: ZR40, 10: DMDEE)

Calibrations were done for all amine catalysts showing a linear abundance between 5 mg kg^{-1} and 100 mg kg^{-1} amine catalyst in foam (Fig. 4).

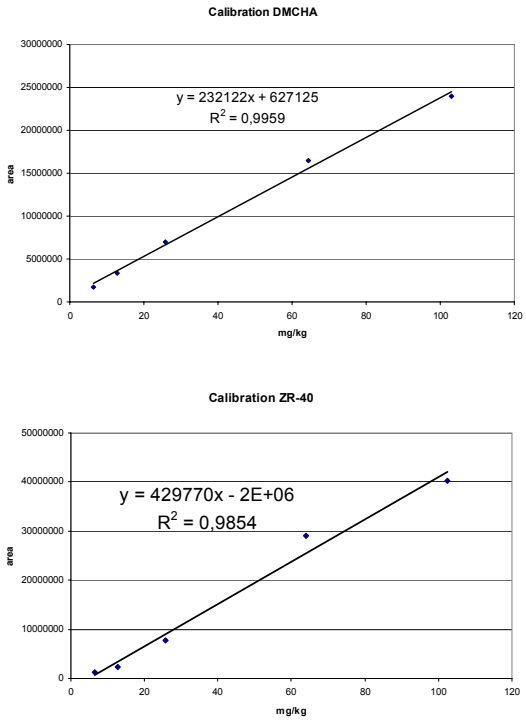

Fig. 4. **Calibration curve for *N*,*N*-dimethylcyclohexylamine (DMCHA) and *N*,*N*,*N*',*N*'',*N*''-pentamethyldipropylenetriamine (ZR-40)**

Recovery

A sample was spiked with the amine catalysts to get the recovery. The average amine concentration for each amine catalyst was 25 mg kg^{-1}. The recovery for all catalysts was varying between 80 % and 121 %. The specific recovery for amine catalysts is given in the figure below (Fig. 5).

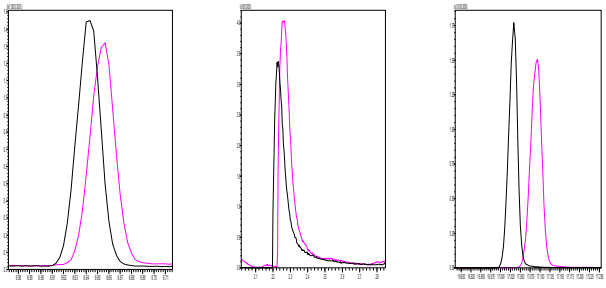

Fig. 5. **Specific recovery for PU sample spiked with a calibration mixture at a level of 25 mg kg^{-1}** (from left to right BDMA, 91 % recovery; DMEA, 121 % recovery ; DMDEE, 85% recovery)

Applications

The emission analysis like VDA 278 and PV 3341 give emission quantities according to external standards like acetone, toluene and *n*-hexadecane. To get an idea of the real emission, the quantity of the analyte itself need to be measured. This is the only possibility to get to know the real amount of amine catalysts in the actual sample. After this analysis the operator will be able to adjust the formulation and correct the PU composition in case of too high emission values.

Many defects in polyurethanes might be related to amine catalysts like cracking, blooming, collapse, breaking, high fogging, smelling etc. This method can support automotive and building material industry to get an idea of the residual/ actual amine catalyst composition.

Conclusions

Analytical parameters like recovery, separation, linearity and mass separation are well performing. The main advantage to use thermal desorption as an injection technique is the speed of analysis. A time consuming liquid extraction is not needed.

The analysis of residual amine catalysts in polyurethane shows its essence in defect analysis, emission analysis and competitive analysis for the automotive and building material industry. This method can give real quantities of amine catalyst emissions/concentrations from PU foam.

REFERENCES

1. Huntsman polyurethanes Europe application list amine catalysts. 2004
2. J. Chromatography *321*, 295 (1985).

P-22
HYDROLYSIS OF POLYURETHANES FOR THE RAPID DETERMINATION OF SAMPLE COMPOSITION

FRANKY PUYPE and JIŘÍ SAMSONEK

Institute for Testing and Certification – Zlín
Třida T. Bati 299, CZ-764 21 Zlín-Louky
fpuype@itczlin.cz

Introduction

Polyurethanes (PU) are widely used in automotive applications for automobile seats, varnish, sealants, electronical compounds and adhesives. To understand their chemistry and behave their composition is needed to characterize before selling them on the market. PU is very different from the polyolefin based polymers because PU exist from different monomers (condensed polymers) and its composition might be difficult to analyse. Condensed polymers are commonly characterized by reactive pyrolysis and direct pyrolysis. An alternative method for polyurethanes is alkali fusion of the urethane groups. Alkali fusion or hydrolysis of polyurethanes is an analytical procedure for the qualitative and quantitative analysis of polyurethanes. It is based on the high temperature/ pressure alkali reaction of the condensed polyurethane polymer forming amines, glycols and esters. All this has to occur in the presence of methanol. The PU application for this method can be either polyester based or polyether based. The principle of the polyether/MDI PU hydrolysis reaction is shown in Fig. 1 below.

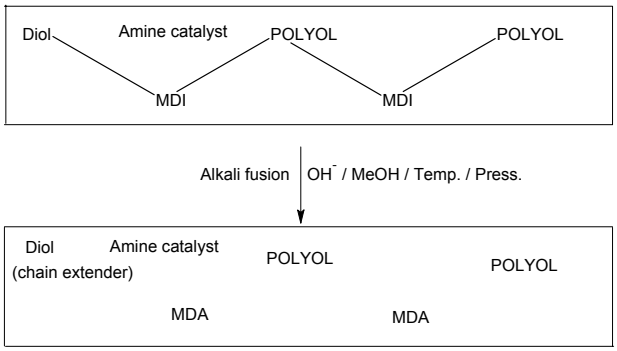

Fig. 1. **Principle of hydrolysis of polyether/MDI polyurethane**

The polyurethanes are cleaved into the corresponding diamine which is the fingerprint of the isocyanate group (methylene diphenyl diisocyanate reacts to methylene diphenyl amine, toluene diisocyanate reacts to toluene diamine, etc.). Free short diols can be determined as chain extender (f=2) and dicarboxylic acids can suspect the presence of a polyester based polyol. The ether bounds from a polyether cannot be broken by hydrolysis. The ether (PO/EO) polyols are seen completely like they were added before.

Experimental

The hydrolysis reaction was done on some commercial polyurethanes. The samples were mixed with a methanol/ KOH mixture and reacting at high temperature and pressure for 8 hours. The results were yellow/brown liquids which were extracted and collected in 2 phases. The first phase contained the polyol fraction (ether or ester based). The second fraction contained all amine based molecules. These fractions were measured by GC-MS. The mass spectrometrical detection is required to get a real identification report of the PU sample.

Results and discussion

Phase 1 – polyol composition

The phase 1 after hydrolysis contains mainly polyols and additives. This fraction explains the type of polyol used (ester/ether based) in the formulation. A flexible PU foam was hydrolysed and a propylene oxide polyol distribution was seen (Fig. 2) with average mol weight 200.

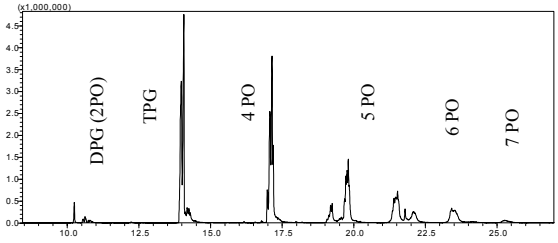

Fig. 2. **Distribution of PO polyether (MW 200) detected in flexible polyurethane foam after hydrolysis**

Phase 2 – Amine composition

An isocyanate finger print can be done by screening the amine composition in one extract (phase 2). Fig. 3 shows the isocyanate composition of flexible foam. These are not the MDI (isocyanate) peaks but the MDA (amine) peaks. The area percent ratio can characterize the type of MDI used (Table I).

The presence of the polymeric MDA for approx. 8 % proves that the used isocyanate was polymeric MDI (PMDI). The ratio between the pure MDI and the polymeric MDI is important. The high amount of pure MDI proves that the sample was used for flexible molded and microcellular foam. For some applications it is necessary to know the ratio between the 2,4'-MDA and 4,4'MDA because the isocyanate goup in position 4 is about 4 times more reactive than the isocyanate group on position 2.

Other isocyanates like toluene diisocyanate can be characterized. The detection of the 2 toluene diamine isomers (2,4-TDA and 2,6-TDA) can lead to great conclusions. There

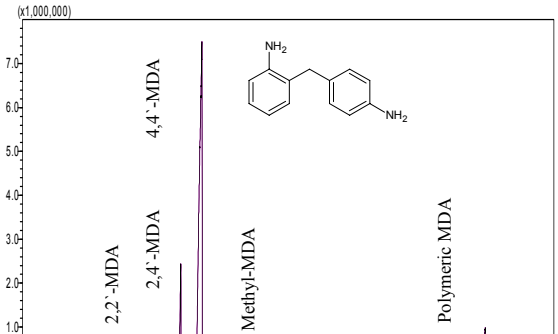

Fig. 3. **MDA distribution after hydrolysis of flexible PU foam.**

Table I
MDA ratio after hydrolysis of flexible PU foam

Compound name	Area [%]
2,2'-MDA	0,8
2,4'-MDA	11,7
4,4'MDA	78,7
Methyl-MDA	0,8
2,4'-4,4'-Polymeric MDA	1,0
2,4'-2,4'- Polymeric MDA	0,6
2,4'-4,4'- Polymeric MDA	6,3

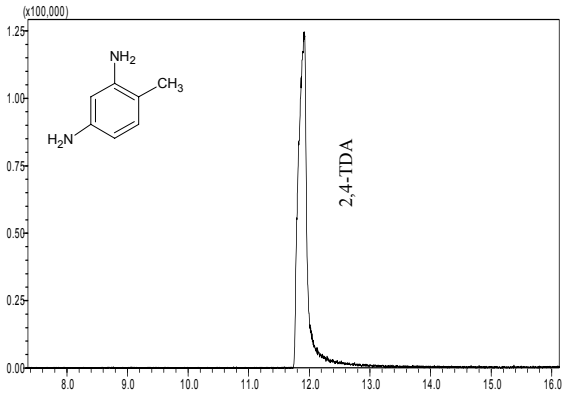

Fig. 4. **2,4-TDA after hydrolysis of rigid PU foam**

are on the TDI market 3 combinations possible. These are the 80/20 and 65/35 mixtures of the 2,4 and 2,6 isomers but also the pure 2,4 product. In Fig. 4 is shown the chromatogram of a pure 2,4-TDI type of isocyanate detected in rigid foam.

Phase 1 and 2 – full PU composition

The power of this method is mainly seen by the separation between the amine phase and polyol phase. The combination of the 2 phases can lead to full composition analysis of the PU sample. Some PU systems can be understood better and defects might be detected.

The following example shows a hydrolysis of an elastomer sample. The first fraction gave a big peak of caprolactone and a small peak of 4-ethylmorpholine (NEM). The caprolactone is a monomer which can react with itself to form polyester. The second fraction gives hexamethylenediamine

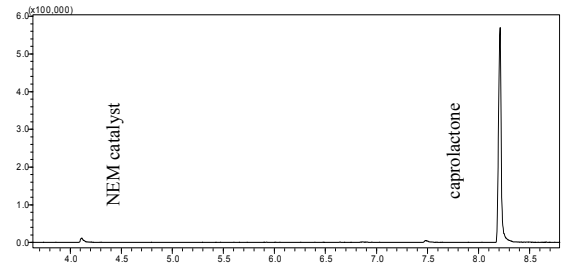

Fig. 5. **First fraction of elastomer (polyol fraction)**

and *N*,*N*-dimethylcyclohexylamine (DMCHA) catalyst. The hexamethylenediamine is the amine product from hexamethylene diisocyanate (HDI) which is an aliphatic isocyanate produced for < 3 % of the isocyanate market. The Fig. 5 and 6 give the chromatograms of first fraction and second fraction of these samples.

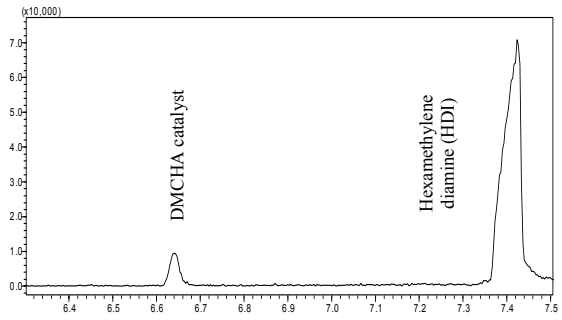

Fig. 6. **Second fraction of elastomer (amine fraction)**

The results from Fig. 5 and 6 shows us that the PU sample is based on a polycaprolactone/HDI system catalysed by DMCHA and NEM.

Conclusions

Hydrolysis as analytical technique is a powerful method for the full characterization of PU material. This method is suitable for automotive applications in the field of quality control, research and competitive analysis.

Hydrolysis of PU makes it possible to determine isocyanate ratio, iso/poyol identification as well chain extenders, amine catalysts, stabilizers, plasticizers and flame retardants charcterisation. This method allows analysis of complex PU matrixes and heavily crosslinked PU networks.

REFERENCES

1. Huntsman polyurethanes Europe application list amine catalysts. 2004
2. J. Chromatography *321*, 295 (1985)
3. Polymer *48*, 3477 (2007).

P-23

CHARACTERISATION OF SYNTHETIC POLYMERS BY PYROLYSIS GAS CHROMATOGRAPHY MASS SPECTROMETRY

FRANKY PUYPE and JIŘÍ SAMSONEK

Institute for Testing and Certification – Zlín
Třida T. Bati 299, CZ-764 21 Zlín-Louky
fpuype@itczlin.cz

Introduction

Pyrolysis coupled with gas chromatography and mass spectrometry (Py-GC-MS) is an instrumental method that enables a reproducible characterisation of (co-)polymers. The method allows identification of monomers and pyrolysis degradation products to get a full composition overview of the polymer matrix. Pyrolysis is a sampling technology that utilizes heat to create thermally induced chemical reactions. The model of pyrolytic reactions in plastics is depending on the kind of polymer. Each single reaction step is representative for a complex network of reactions. The thermal degradation is initially a matter of intrinsic kinetics. The polymer is heated up till it reaches a certain kinetic limit which is depending on molecular weight, presence of a weak link, additives, type of (co)-polymer and experimental conditions (temperature, heating rate, oxygen level, etc.). The physical properties are changing and the polymer become more liquid. The radical chain pyrolysis reactions take place mainly in the liquid phase. In a second stage several reactions can occure. The thermally induced chemical reactions can be:

– Depolymerisation: A radical is formed and induces a homolytic cleavage with the carbon in α-position. (e.g. ethene in polyethylene). Many authors call this process "unzipping"`.
  R-C-C-C-C-C. + .C-C-R → R-C-C-C. + C=C + .C-C-R
– Intramolecular radical transfer: This is a change of the polymer chain followed by β-scission forming a dimer. This happens in natural rubber forming

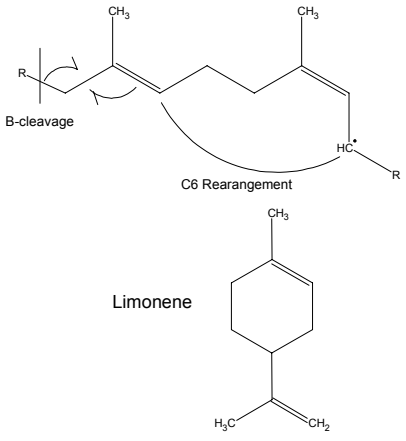

Fig. 1. **Intramolecular radical transfer in natural rubber (NR) forming limonene**

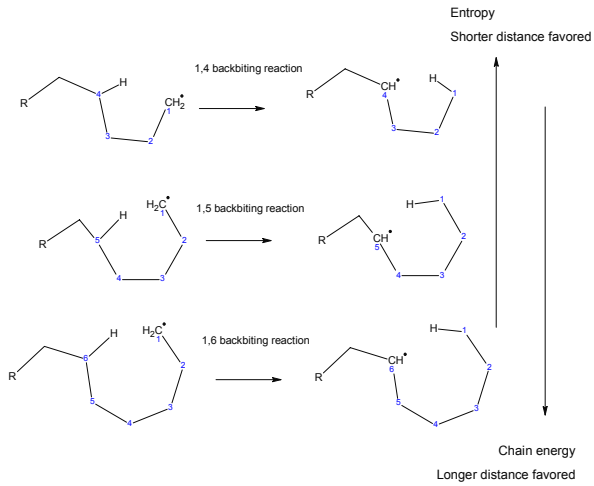

Fig. 2. **Possible proton transfer positions in polyethylene**

a cyclic dimer (Fig. 1).

– Intramolecular and intermolecular H-transfer followed by unzipping. A typical example is the 1,5-hydrogen transfer in PE which is the most favorable transfer due to the balance between entropy and chain energy (Fig. 2). This process can continue and the proton can transfer further from position 5 to position 9, from position 9 to position 13, etc.

The remaining radicals are unzipping till a termination process occurs and 2 radical-ending molecules have reacted together. Unsaturated and saturated structures remain. The evolved analytes are swept onto the analytical column of the GC and GC-MS proceeds as normal.

In classical pyrolysis of polymers like polyesters and polycarbonates peaks of terminal groups or cross linking products are masked by the large peaks arising from polar material from the polymer. For some macromolecules it is desireable to introduce a chemical reagent that, upon heating, will react with the macromolecule in a more directed manner, e.g. the preferential cleavage of ester domains, to produce a mixture of derivatized low molecular weight products in a process known as thermally assisted chemolysis. A derivatisation with tetramethyl amonium hydroxide (TMAH)/methanol is commonly used (Fig. 3). This pyrolysis technique is known as reactive pyrolysis and forms on polar groups methylethers.

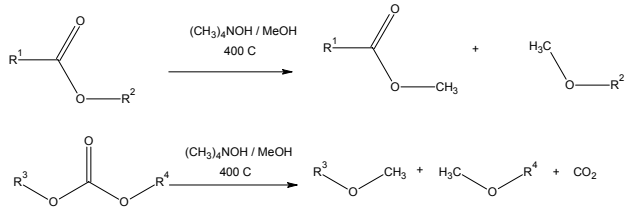

Fig. 3. **Mechanism of reactive pyrolysis**

Experimental

Sampling

The sample is cut in small pieces (1 mg) and placed in a sample cup. In case the sample contains lots of additives (e.g. plastisizers, flame retardants) which interfere the pyrogram, the sample needs to be extracted by a soxhled extraction with acetone. The sample cup is placed in an autosampler on top of the furnace.

Analytical method

According to the TGA data from different kind of polymers a pyrolysis temperature of 650 °C has been chosen. The pyrolyzer used is a pyrolysis unit PY-2020iD (Frontier lab) with a 48 position auto sampler connected to a GC-MS-QP2010plus (Shimadzu). The pyrolysis is performed for a very short time (20 seconds). The separation is done on a special metal capillary separation column (Frontier Lab, Ultra ALLOY-PBDE; 0.25 mm i.d. × 15 m) coated with a very thin (0,05 µm) film of immobilized-polydimethylsiloxane. The ultra alloy columns are used for their stability at high temperature. For reactive pyrolysis a pyrolysis temperature of 400 °C was applied.

Results and discussion

Direct pyrolysis-GC-MS

Direct pyrolysis gives for every polymer specific reactions. The direct pyrolysis process is able to get information about the co-polymer ratio, structure (head-tail, head-head, tail-tail) and cross linking agents. Even the simulation of the resin network can be visualized. The program of polypropylene shows mainly dimer and trimer (Fig. 4). Higher mol weight fragments (from C14) give nice repeating structures due to the formed branched oligomers.

Copolymers like NR/PI-SBR rubber can be identified by pyrolysis-GC-MS (Fig. 5). This due to the identification of the monomers after unzipping process or the cyclic dimers after the intramolecular radical transfer (4-ethenyl-cyclobenzene and limonene). The method allows also to get information about the ratio between the nonomers. This method has another dimention than the classical pyrolysis-

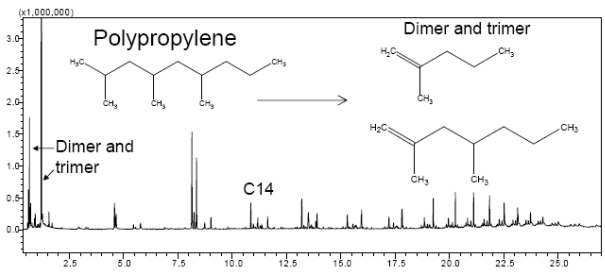

Fig. 4. **Pyrogram of polypropylene**

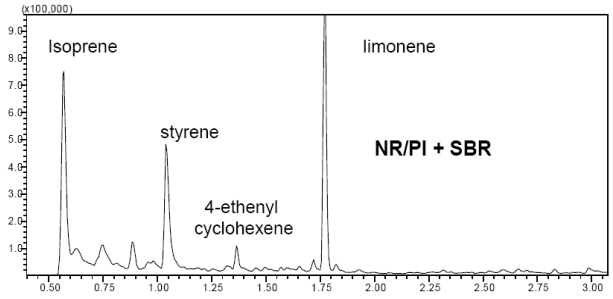

Fig. 5. **Pyrogram of NR/PI + SBR**

FTIR due to its separation (GC) and mass separation/ identification (MS).

Reactive pyrolysis-GC-MS

The polymers which reactive pyrolysis is able to characterize (PC, PET, PU, PBT etc.) are mostly polar compounds. The reaction with THMA/MeOH makes them more non-polar. This results in a cleaner chromatogram. The reaction give mainly reacted monomer but cross-linking agents, additives and en-capping products as well. Due to the relative low temperature this technique can visualize the additives. In Fig. 6 is shown the reactive pyrolysis chromatogram of polycarbonate. There is seen the monomer biphenol A in its dimethylether form but also the end group tert.butylphenol in its methylether form. This tert.butylphenol is strongly limited for food contact material.

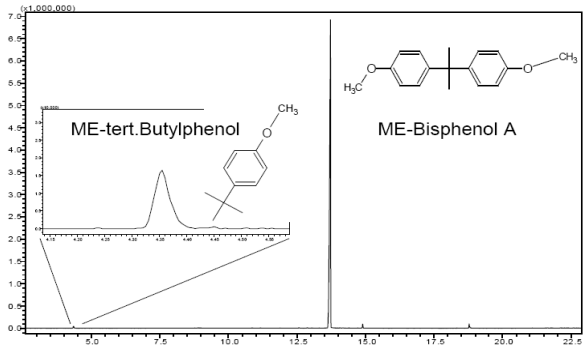

Fig. 6. **Reactive pyrogram of polycarbonate with detection of the monomer and initiator/encapping group**

Conclusions

Both pyrolysis techniques can improve the quality of the full characterization of polymers used in the automotive industry. The power is the ability to compare batch to batch and gives more information about the polymer structure/ratio and its production process. This information is mostly not known by the automotive dealers itself but in-house knowledge from the production/manufacturer.

REFERENCES

1. European norm: *Rubber Analysis*, 7270 part 1 (2003).
2. Pinto F. et al.: J. Anal. Appl. Pyrolysis *51*, 39 (1999).
3. Gonzales F. J.: J. Anal. Appl. Pyrolysis *58-59*, 315 (2001).
4. Reimert R.: Chem. Eng. Proc. *41*, 289 (2002).

P-24
STUDY OF THERMAL BEHAVIOR OF METALLOCENE POLYOLEFINS IN BLENDED FIBERS

JOZEF RYBA[a], ANNA UJHELYIOVÁ[a], and PETER MICHLÍK[b]

[a] Department of Fibres and Textile Chemistry, Institute of Polymer Materials, Faculty of Chemical and Food Technology, Slovak University of Technology, Radlinského 9, 812 37 Bratislava, [b] Research Institute for Man-Made Fibres, a.s., Šturova 2, 059 21 Svit, Slovak Republic
jozef.ryba@stuba.sk

Synthetic fibers based on fiber-forming polymer blends belong to a special fiber group. A variability of properties in fibers can be reached using two or more components in the fiber –forming blend.

Ziegler-Natta (ZN) catalysts have been used to manufacture polypropylene (ZNPP) for over five decades[6,7]. These catalysts provide the preparation of ZNPP with a continuous growing of an application in all areas of an industry because their properties and price were very interested. The important increase of ZNPP application in the fibre and textile industry has been come after an introduction of the ZNPP degradation, which enabled the preparation of ZNPP with the lower molecular weight and narrower molecular distribution. These molecular characteristics of ZNPP provided the better processability of ZNPP at the spinning and drawing of PP fibres as well as the better unevenness of structure and mechanical-physical properties of ones.

The metallocene catalysts like the new generation of catalysts for polymerization of polyolefins generate polymers with narrower molecular weight distribution, lower melting temperature, tacticity, etc.[1–4].

These properties of metallocene polypropylene (mPP) could be to suffer their application at the preparation of oriented anisotropic materials – fibers with the important improvement of some properties, for an example the mechanical-physical properties (higher tenacity and Young's modulus) as well as with the use of better favourable spinning and drawing conditions. Generally, there are the fibers with the lower linear density, higher tenacity, lower elongation at the break and higher Young's modulus[5].

Metallocene polyethylene (mPE) and mPP form thermodynamically incompatible blended fibres with two melting peaks on the DSC thermograms corresponded with the melting temperatures of individual components – mPE and mPP (Table I). However, blended fibres prepared from mPP and ZNPP are thermodynamically compatible with the one double peak on the DSC thermograms. At the fibres from the PP with the lower MFI (12 g/10 min – N) the melting temperature of

Table I
The melting temperatures of components in the blended fiber obtained from the 1st heating (heating rate was 10 °C min^{-1})

Sample	$C_{PE(mPP)}$ [wt.%]	1st heating		
		T_{PE} [°C]	T_{mPP} [°C]	T_{ZN} [°C]
mPE	100	113.5	–	–
mPE/mPP-N	50	113.3	145.0	–
mPP-N	100	–	146.3	–
mPE/mPP-R	50	114.5	146.3	–
mPP-R	100	–	146.5	–
mPP-N/ZN-HG	50	–	144.3	156.0
ZNHG	–	–	–	161.3
mPP-R/ZN-HT	50	–	155.3	–
ZN-HT	–	–	–	161.0

mPP corresponds with the melting temperature of individual mPP, but the melting temperature of ZNPP component is shifted to the lower values in comparison with the melting temperature of individual ZNPP. At the fibres prepared from PP with the higher MFI (26 g/10 min – R) it is vice-versa.

Total melting enthalpies of blended fibres prepared from mPE/mPP as well as from mPP/ZNPP are lower than the theoretically calculated from their additive composition, what can predict slower crystallization ability of components at the preparation (Table II). It is very interested, that the decrease of crystallization ability of mPE resp. mPP is higher than the ZNPP.

Table II
The melting enthalpies of components in the blended fibers obtained from the 1st heating (heating rate = 10 °C min^{-1})

Sample	1st heating				
	$_{\Delta}H_{PE}$ [J g^{-1}]	$_{\Delta}H_{mPP}$ [J g^{-1}]	$_{\Delta}H_{ZN}$ [J g^{-1}]	$\Sigma_{\Delta}H$ [J g^{-1}]	$\Sigma_{\Delta}H_{teor}$ [J g^{-1}]
mPE	67.6	–	–	67.6	67.6
mPE/mPP-N	22.0	28.6	–	50.7	72.0
mPP-N	–	76.3	–	76.3	76.3
mPE/mPP-R	24.6	27.2	–	51.8	66.9
mPP-R	–	66.3	–	66.3	66.3
mPP-N/ZN-HG	–	16.4	55.4	71.8	88.8
ZN-HG	–	–	101.2	101.2	101.2
mPP-R/ZN-HT	–	68.4	–	68.4	76.6
ZN-HT	–	–	87.0	87.0	87.0

This work was supported by the Slovak Research and Development Agency under the contract No. APVV -0226-06.

REFERENCES

1. Arranz-Andres J.: Eur. Polymer J. *43*, 2357 (2007).
2. Bubeck R. A.: Mater. Sci. and Eng. R. *39*, 1 (2002).
3. Gomez-Elvira J. M.: Polymer Dagrad. Stab. *85*, 873 (2004).
4. Choon K. Ch.: Polymer *44*, 773 (2003).
5. http://www.engr.utk.edu/mse/pages/Textiles/Olefin%20fibers.htm
6. Folvarcikova K.: *Book of Preceeding of the International conference "Polymer Materials", 29.-30. October 2003, Bratislava*.
7. Razavi-Nouri M., Hay J. N.: Iranian Polymer J. *16*, 105 (2007).

P-25
INFLUENCE OF MAGNESIUM HYDROXIDE MODIFICATION WITH POLYPEROXIDES ON THE PROPERTIES OF POLYMER COMPOSITES

OLEH SHEVCHUK[a*], VIKTOR TOKAREV[a], SVEN WIESSNER[b], UDO WAGENKNECHT[b], NATALYA BUKARTYK[a], and ROMANNA MONCIBOVICH[a]

[a] Lviv Polytechnic National University, S. Bandera Str., 12, Lviv, Ukraine, 79013, [b] Institute of Polymer Researches, Hohe Str. 6, Dresden, Germany, 01069
oshevch@polynet.lviv.ua

Semicrystalline polyolefins such as polypropylene, high-density polyethylene are widely used in industry because of their advantage properties: easy processing, low density, corrosion resistance, low costs, high ultimate elongation before tensile fracture. However these polymers have a number of defects – low flame resistance, emission of smoke and poisonous gases while burning. Metal hydroxides (magnesium or aluminium hydroxides) are well known as acid and halogen-free flame-retardants for polymer composites. But their introduction into polymer matrix causes the decrease of composite physico-mechanical properties. Thus, the most important task is to increase the compatibility of these fillers and polyolefine matrix to improve their dispersability and as a result composite characteristics.

In order to solve this problem we have proposed the method of modification of magnesium hydroxide (MH) with peroxide-containing copolymers (PCC). This allows to form compatibilizing polymer layer on the surface of filler particles decreasing significantly surface energy on the phase boundary. From the other hand the presence of peroxide groups in the copolymer structure provides the grafting of the chains of polymer matrix to the filler surface during filled composite formation. Copolymers on the basis of 5-*tert*-butylperoxy-5--methyl-1-hexene-3-yne were used as surface modifiers. They have been synthesized both by copolymerization of initial monomers and by polymer-analogous transformation that allows to include into the PCC structure the fragments that facilitate the increase of polypropylene crystallinity degree (dibenzylidene sorbitol).

Modification of MH surface with these PCC causes the decrease of filler surface energy from 48 to 27÷30 mJ m^{-2}. Rheological tests of obtained composites witness about the formation of supramolecular structures in the composite, evidently, as a result of the bonds formed on the phase boundary due to PCC peroxide fragments. The flammability of obtained composites (LOI index) slightly depends of the nature of modifier. At the same time physico-mechanical characteristics of the filled composites on the basis of peroxidized MH are higher as compared with unmodified samples.

Hence, obtained results witness that the peroxidic modification of magnesium hydroxide is the prospective route to obtain incombustible polymer composites with improved physico-mechanical properties.

P-26
SYNTHESIS AND FUNCTIONALIZATION OF SUPERPARAMAGNETIC NANOPARTICLES FOR NEW POLYMERIC MATERIALS

TIMO STEINKE, ULRIKE ASSMANN, DENISA BELLUSOVÀ, and ROBERT H. SCHUSTER

Deutsches Institut für Kautschuktechnologie e.V., Eupener Straße 33, D-30519 Hannover
Timo.Steinke@DIKautschuk.de;
Robert.Schuster@DIKautschuk.de

Magnetic particles are widely studied for their applications in various fields in chemistry, biology and medicine. One application of scientific and technological interest is the use of composite materials like ferrofluides or magnetic rubbers as adjustable dampers. The damping properties of such a material can be varied by an external magnetic field.

In this text the synthesis, functionalization and analysis of magnetite nanoparticles with superparamagnetic properties and the synthesis of composite materials is presented.

Introduction

In this work magnetite nanoparticles were prepared with a diameter about 15 nm, which are coated with silica or a near monolayer of silanes with organic groups like acrylate or vinyl. The particles are incorporated as a superparamagnetic filler in PMMA and butadiene rubber (BR) to get organic-inorganic hybrid materials. These nano composites are characterized by using FT-IR-spectroscopy, thermal analysis (TGA / DSC), TEM, SEM, XRD, SQUID and DLS.

In a second part, the magnetite nanoparticles are dispersed in various solved polymers and used in an electrospinning process. The received hybrid nano fibres can be used as a filler for different rubbers.

Experimental

Magnetite particles are prepared by the usual co-precipitation method, adding 5 mol l^{-1} NaOH solution into the mixed solutions of $FeCl_2$ (0.25 mol l^{-1}) and $FeCl_3$ (0.5 mol l^{-1}) with a molar ratio of 1:2. The NaOH solution is slowly added drop wise under rapid stirring up to pH 11 at room temperature.

The slurry is washed by magnetic separation up to pH 7.

The dry particles are dispersed in ethanol and mixed with TEOS (tetraethyl ortho silicate) or the silane (1 g / g particles) and functionalized at room temperature for 24 hours.

After functionalization with a methacrylic acid silane the dry particles are dispersed in THF and MMA, then the mixture is polymerized and cleaned. A TEM image of the product is shown in Fig. 1.

The particles are dispersed in solved BR and after drying the mixture is vulcanized and characterized using TEM, AFM and TGA. A AFM image of the product is shown in Fig. 2.

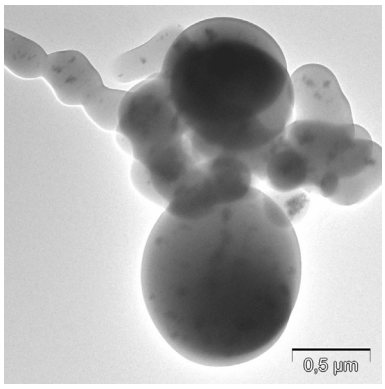

Fig. 1. **TEM image of magnetite nanoparticles in PMMA**

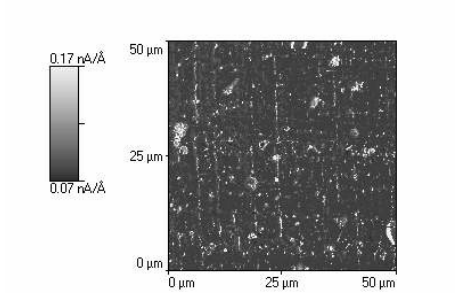

Fig. 2. **AFM image of magnetite nanoparticles in BR**

Results and discussion

The diameter of the dry magnetite particles is determined by TEM image to 9–17 nm. The diameter in ethanol is about 1.66 µm due to agglomeration.

After functionalization with TEOS the diameter in ethanol is about 144 nm. This shows a better separation of the core-shell particles.

The TGA measurements show that the acrylate functionalized particles have about 1.5 wt.% organic groups on the surface. At 192 °C the magnetite oxidizes to magnesite. This

is shown as well by a changing of the particle color from black to red.

REFERENCES
1. Ma M., Zhang Y., Yu W., Shen H., Zhang H., Gu N.: Colloids Surf., A *212*, 219 (2003).
2. Zhao W., Gu J., Zhang L., Chen H., Shi J.: J. Am. Chem. Soc. *127*, 8916 (2005).

P-27
PLASMA TREATMENT OF REINFORCEMENTS MATERIALS FOR TIRES

V. ŠURIOVÁ , A. KARVAŠ , and P. ZMOLEK

Continental Matador Rubber, s.r.o., Púchov
viera.suriova@conti.sk

P-28
PROPERTIES AND STABILITY OF POLYTHIOPHENES SYNTHESIZED IN THE PRESENCE OF SURFACTANTS

AYSEGUL UYGUN[a]*, LUTFI OKSUZ[b], ERHAN ASLAN[c], AYSE GUL YAVUZ[a], SONGUL SEN[d], and MÁRIA OMASTOVÁ[e]

[a] Suleyman Demirel University, Arts and Science Faculty, Department of Chemistry, 32260 Isparta, Turkey; [b] Suleyman Demirel University, Arts and Science Faculty, Department of Physics, 32260 Isparta, Turkey; [c] Suleyman Demirel University, Research Centre, 32260 Isparta, Turkey; [d] Mehmet Akif Ersoy University, Arts and Science Faculty, Department of Chemistry, 15100, Burdur, Turkey; [e] Polymer Institute, Slovak Academy of Sciences, Dúbravská cesta 9, 842 36 Bratislava, Slovakia
aysegul@fef.sdu.edu.tr

Conjugated polymers represent a field of intensive scientific research due to the wide range of possible applications of these materials, as for example polymeric LEDs[1] and plastic photovoltaic devices[2]. Among conducting polymers, polythiophene (PT) is one of the most studied conducting polymers because of its good electrical conductivity, environmental stability and relative ease of synthesis. PT can be synthesized by electrochemical[3] or chemical[4] oxidation of thiophene in various organic solvents. The preparation conditions and various additives introduced into reaction mixture influence the properties of final conducting polymer[5]. The growing know-how on the electronic and technological properties of conducting polymers is generating a lot of interest for large scale industrial applications[6]. For hydrophobic materials a quite commonly employed processing method, alternative to the solvent-based one, is represented by the use of surfactants, i.e. surface-active molecules able to stabilize a mixture of two immiscible liquids by interacting concurrently with both interfaces. This strategy permits to handle and process hydrophobic materials in water, avoids the use of organic solvents and complies with the principles of green chemistry, and for these reasons is widely used in industrial applications.

In this work, PT homopolymers were synthesized in the presence of surfactants and their properties were compared. Tween 60 ($C_{28}H_{24}O_3$, M_A = 438.73 g mol^{-1}); sodium dodecylsulfate (SDS, $C_{12}H_{25}NaO_4S$, M_A = 288.38 g mol^{-1}); anthraquinone-2-sulfonic acid sodium salt monohydrate (ACS, $C_{14}H_7NaO_5S.H_2O$, M_A = 328.27 g mol^{-1}) were selected as nonionic and anionic surfactants, respectively. The molar ratios of monomer/surfactant and oxidant/monomer were taken as 7 and 2.3, respectively. Thiophene and surfactant were dissolved into chloroform in a reaction vessel containing a magnetic stirring bar. Anhydrous oxidant $FeCl_3$ dissolved into $CHCl_3$ was added to monomer-surfactant solution dropwise. Polymerization was carried out 24 h at 20 °C. After filtration and purification prepared powders were dried at 50 ° C under vacuum for 24 h.

PT without surfactant was synthesized using the same conditions without adding any additive.

FTIR spectra of prepared PTs were recorded in the range 400–4000 cm^{-1} with a 4 cm^{-1} resolution from KBr pellets on a Perkin Elmer Spectrum BX FTIR system (Beaconsfield, Buckinghamshire, UK). Thermal stability of PTs was investigated on a Perkin Elmer model thermal parametric analyser (Beaconsfield, Buckinghamshire, UK) under pure nitrogen at a flow rate of 25 ml min^{-1}. Sample morphology studied by scanning electron microscopy (SEM) with a Philips model.

Table I shows FTIR wavenumbers of PT samples. The bands at 1486 and 1432 cm^{-1} belong to C=C asymmetric and symmetric stretching vibrations of thiophene ring, respectively. The peaks at 1169 and 786 cm^{-1} represent in-plane and out-of-plane C–H aromatic bending vibrations of substituted thiophene ring[7]. The C–S stretching vibration of the thiophene is assigned at 835 cm^{-1}. Peak at 694 cm^{-1} may be the ring deformation of C–S–C in PT[8]. The presence of surfactants in the PT samples is verified by the FTIR spectra. The observed peak shifts show that there are some interactions between PT

Table I
Assignments of FTIR bands of PT samples

Assignments	Wavenumbers [cm^{-1}]			
	PT	PT/ ASC	PT/ SDS	PT/ Tw60
O–H stretching of water in KBr	3434	3463	3446	3433
C–H aromatic stretching	3059	3061	3056	3059
C–H aliphatic stretching	2919			2913
C= C asym. ring stretching	1486		1484	1486
C =C sym. ring stretching	1432		1436	1437
C–H in-plane deformation	1169	1169, 1122	1104	1100
C–S stretching	835	861		837
C–H out-of-plane deformation	786	784	781	784
C–S–C ring deformation	694	706, 627	685, 638	694, 643

and the surfactants.

X-Ray diffraction of PT-ASC showed only one broad peak at the Bragg angle of around 18° in the wide angle X-ray diffractogram, suggesting that polythiophene is amorphous polymer[9]. This result confirms that the product obtained is the real amorphous polymer rather than liquid monomer or ordered polymers. The X-Ray pattern of pure surfactants ASC and SDS reveals that they have typical crystalline arrangement. After preparing surfactant modified polythiophenes, these structures were rigorously modified to a mainly amorphous pattern. The peak intensities of ASC and SDS diminished because of polymerization of thiophene. Crystalline structure of PT-ASC has some small peaks which are almost similar to ASC. These results support the predominant formation of polythiophenes in reaction mixture.

a

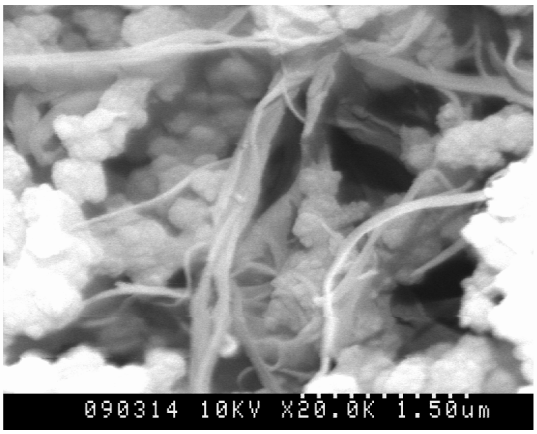

b

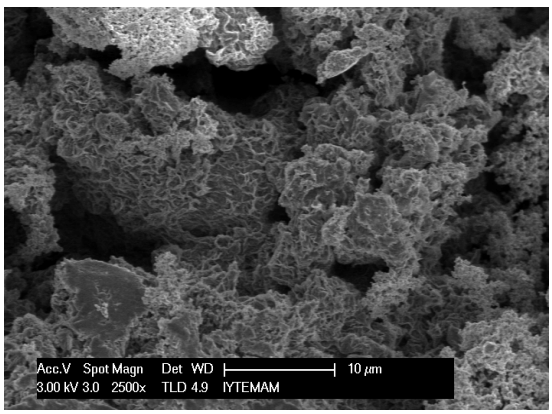

Fig. 1. **SEM image of surfactant free PT (a) and PT-ACS (b)**

Morphology of PT, PT-Tween 60, PT-SDS, and PT-ACS was investigated using SEM analysis. All surfactants influence the morphology of the corresponding polythiophenes. Surfactant-free PT has a globular structure but also some fibrils are visible, as shown in Fig. 1a. When compare the structure of samples at the same magnification, PT-Tween 60 has globular structure with smaller particle, PT-SDS presents a different structure which looks like flowers, and PT-ACS has a flat dense structure (Fig. 1b).

Besides the morphology changes, conductivity of samples changed when they were prepared in the presence of different surfactants. Conductivity increased linearly with decreasing the particle size of sample. As seen from Fig. 1b, PT-ACS has denser and smaller structure than other samples. This product showed also the highest conductivity $8.2 \cdot 10^{-5}$ S cm^{-1}.

The thermal stability of the PT-ACS sample is significantly higher than that of the other synthesized PTs.

This work is funded by the Scientific and Technological Research Council of Turkey (106T134), by the Scientific Grant Agency of the Ministry of Education of Slovakia and the Slovak Academy of Sciences (2/7103/27), and by Turkish-Slovak bilateral project No. 107T880.

REFERENCES

1. Friend R. H., Gymer R. W, Holmes A. B., Burroughes J. H., Marks R. N., Taliani C., Bradley D. D. C., Dos Santos D. A., Bredas J. L., Logdlund M., Salaneck W. R.: Nature. *397*, 121 (1999).
2. Brabec C. J., Sariciftci N. S., Hummelen J. C.: Adv. Funct. Mater. *11*, 15 (2001).
3. Toshima N., Hora S.: Prog. Polym. Sci. *20*, 155 (1995).
4. Fichou D. (ed.): *Handbook of Oligo- and Polythiophenes*, Wiley-VCH, Weinheirn 1999.
5. Kang H. C., Geckler K. E.: Polymer *41*, 6931 (2000).
6. Forrest S., Burrows P., Thompson M.: IEEE Spectrum. *37*, 29 (2000).
7. Gok A., Omastova M., Yavuz A.G.: Synth. Met. *157*, 23 (2007).
8. Nicho M. E., Hu H., Lopez-Mata C., Escalante J.: Sol. Energy Mater. Sol. Cells. *82*, 105 (2004).
9. Lin B. Z., Ding C., Xu B. H., Chen Z. J., Chen Y. L.: Mat. Res. Bul. *44*, 719 (2009).

P-29
MICROWAVE PLASMA AND ATMOSPHERIC PRESSURE MICROWAVE PLASMA TREATMENT OF RUBBER USING VARIOUS PLASMA GASES

LUTFI OKSUZ[a], ALI GULEC[a], SILVIA PODHRADSKÁ[b], AYSEGUL UYGUN[c], and MÁRIA OMASTOVÁ[b]

[a] Suleyman Demirel University, Arts and Science Faculty, Department of Physics, 32260 Isparta, Turkey; [b] Polymer Institute, Slovak Academy of Sciences, Dúbravská cesta 9, 842 36 Bratislava, Slovakia,[c] Suleyman Demirel University, Arts and Science Faculty, Department of Chemistry, 32260 Isparta, Turkey
aysegul@fef.sdu.edu.tr

The need to modify the surface or characteristics of materials is a growing issue for many industries. Plasma offers a novel approach for solving common surface problems[1]. Styrene butadiene rubber (SBR) is the largest volume synthetic rubber used in production. Styrene butadiene rubber is similar to natural rubber in its resistance to mild solvents and chemicals, like natural rubber. Butadiene rubber and styrene butadiene rubbers are widely used materials for the production of tires.

Oxygen, hydrogen and helium were used to treat SBR with the aim to modified surface and increase the surface energy and adhesion. SBR was treated by O_2 and H_2 plasma at 500 mTorr, while helium treatment was done under atmospheric pressure plasma. Plasma is generated using homemade microwave.

The changes of surface morphology of original sample and samples after plasma treatment were investigated using Scanning Electron Microscopy (SEM). Dynamic Mechanical Analysis (DMA) was used to study the behavior of SBR after plasma treatment. DMA Q800 (TA Instruments) mechanically deforms a sample and measures the sample response. The deformation was applied sinusoidally, in a constant (or step) fashion, or under a fixed rate. The response to the deformation was monitored as a function of temperature and time.

Fig. 1 indicates morphology of SBR without plasma treatment. Fig. 2 to 4 depict surface images of SBR-O_2 plasma, SBR-H_2 plasma, and SBR-He plasma samples, respectively.

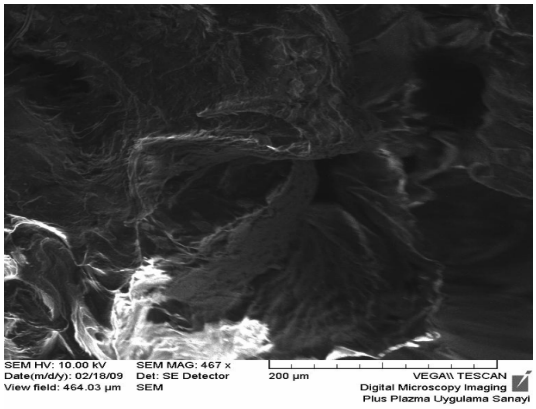

Fig. 1. **SEM image of SBR without plasma**

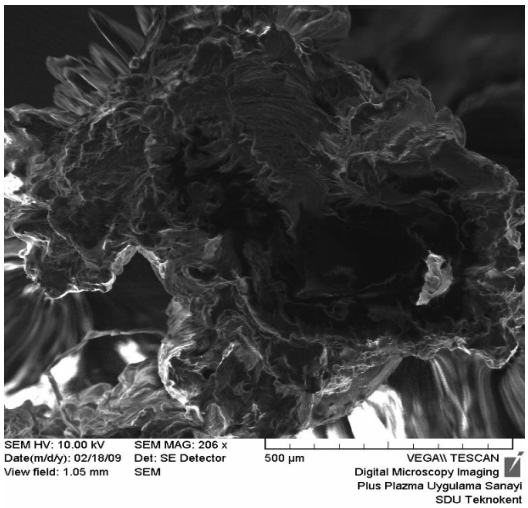

Fig. 2. **SEM image of SBR-O_2 plasma sample**

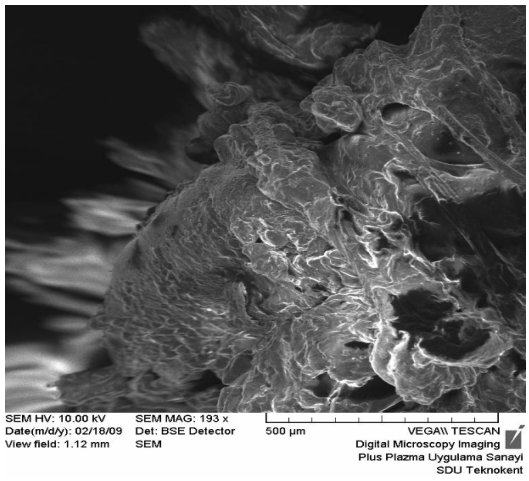

Fig. 3. **SEM image of SBR-H_2 plasma sample**

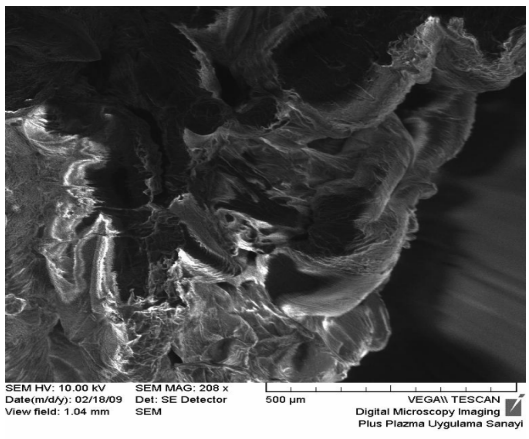

Fig. 4. **SEM image of SBR-He plasma sample**

The surface morphology of SBR was changed depending on plasma process. Especially, after O_2 plasma treatment, more structural breaking was observed from Fig. 2.

The influence of the time of the plasma treatment and the degree of surface oxidation were also studied. The differences when using oxygen plasma were detected by DMA and results are compared with untreated material.

This work is funded by DPT (2007-K-121310-DPT).

REFERENCE

1. Abdrashitov E. F., Ponomarev A. N.: High Energy Chemistry. *37*, *273* (2003).

P-30
IMMOBILISATION OF IRON OXIDE NANO-PARTICLES ONTO THE PLASMA-ACTIVATED POLYMER SURFACES

MAGDALENA WOLFOVA[a], LUDMILA CERNAKOVA[a], RENATA SZABOVA[a], and MIRKO CERNAK[b]

[a] Slovak University of Technology in Bratislava, Faculty of Chemical and Food Technology, Institute of Polymer Materials, Radlinského 9, 812 37 Bratislava, [b] Masaryk University, Department of Physical Electronics, Kotlářska 11, 611 37 Brno, Czech Republic
magdalena.wolfova@stuba.sk

The present development of textile market is connected with an ever increasing demand for new functionalities for highly specific applications. Given that background, surface modification became one of the most important topics to create new textiles.

One of the possibilities, for modifying the polymer surface is plasma treatment at atmospheric pressure. It is well known that this kind of modification leads to formation of various type functional groups on the surfaces, which are able to interact with modifying layer. As a result, the surface is modified and obtained specific properties such as magnetic properties, barrier properties, antibacterial properties etc.The plasma technique can be used for surface modification and thin film deposition for almost all substrates, including polymer, paper, glass and porous materials[1].

These surface modifications can produce long lasting or semi-permanent multi-use benefits that, in some embodiments, may include at least one of the following improved surface properties: cleaning, wettability, liquid strike-through, comfort, stain resistance, soil removal, malodor control, modification of surface friction, reduced damage to abrasion and color enhancement, relative to the surfaces unmodified with such nanoparticle systems.

This work is focused on the preparation of polypropylene nonwoven coated with iron oxide nanoparticles after plasma treatment. The surface of samples were treated by plasma in nitrogen or air atmosphere using surface dieletric barrier discharge (DCSBD)[2]. Consequently the polypropylene textiles were immersed in water dispersion of iron oxide nanoparticles under sonication.

The physical and chemical changes of polypropylene surfaces were studied by atomic force microscopy (AFM), scanning electron microscopy (SEM) and Fourier Transform Infrared Spectroscopy (FTIR).

It was find that about 3 wt.% of iron oxide were embedded at polypropylene nonwoven mainly as micrometer size aggregates than as nanoparticles.

This work was supported by Grant Agency of Slovak republic VEGA 1/4095/07 and Grant Agency of Czech Republic KAN 101630651.

REFERENCES

1. Shi D., He P., Wang S. X., Wim J. van Ooij, Wang L. M., Zhao J., Yu Zhou: J. Mater. Res. *17*, No. 5 (2002).
2. Černáková Ľ., Szabová R., Wolfová M., Buček A., Černák M.: Fibres Textiles in Eastern Europe *15*, 64 (2007).

P-31
EFFECT OF GRAFTED POLYETHYLENE ON THE MECHANICAL PROPERTIES OF THE ELASTOMER NANOCOMPOSITES

TERESA KLEPS, MALGORZATA PIASKIEWICZ, JAN MEZYNSKI, and MICHAL LEWANDOWSKI

Institute for Engineering of Polymer Materials and Dyes, Elastomer and Rubber Technology Division in Piastow, 05-820 Piastow, ul. Harcerska 30, Poland
t.kleps@ipgum.pl

The development of nanotechnology in the field of elastomers is associated primarily with the research aimed to be placed nanofillers in the elastomeric composites[1–4] instead of conventional used fillers such as carbon black, silica, metal oxides or carbonates in order to obtain significantly better properties of elastomer nanocomposites forming rubber compounds and rubber vulcanisates as useful rubber articles.

Fillers and nanofillers in the rubber composites are as important modifiers their properties such as abrasion resistance, tensile strength, tear resistance or multiple deformation. These properties depend essentially on the action of elastomers with fillers[3–6]. Strengthening as a results of fillers action is higher if the its particles are smaller, surface area is more and the relevant functional groups react with the rubber macromolecules.

Application of nanofillers, due to their extremely high surface area, should be radically increased strengthening action and bring much better results in comparison with conventional fillers. According to literature reports the results obtained in the field of elastomer nanocomposites[1–4], are not significantly adequate for the expectations of nanotechnology, in contrast to the nanocomposites of metal, ceramic, glass or even polymeric plastomers, which often obtained very good results.

In practice, there are significant difficulties in full and equal distribution of nanofillers in the elastomer matrix, which make impossible the achievement of good dispersion of nanofillers in elastomers. This is the cause of unfavorable morphology of elastomer nanocomposites and prevents exfoliation of nanofillers, what is a major interruption to obtaining better mechanical properties of nanocomposites. In the case of polymer composites, in order to improve mutual mixing of their components can be used the compatibilizators[3–5,7].

The purpose of our work was to study the effect on nanofillers dispersion and properties of elastomer nanocomposites containing montmorillonite, the compatibilizators type of polyethylene grafted with maleic anhydride – Fusabond EC 603D i Fusabond MG 423D. They are used primarily in the processing of polymers ABS and PA or PCA in order to improve the processing and properties of strength, particularly adhesion.

Mechanical properties of tested IR and EPDM nanocomosites containing Fusabonds in some cases have been positive changes (Fig. 1), in particular has improved tensile

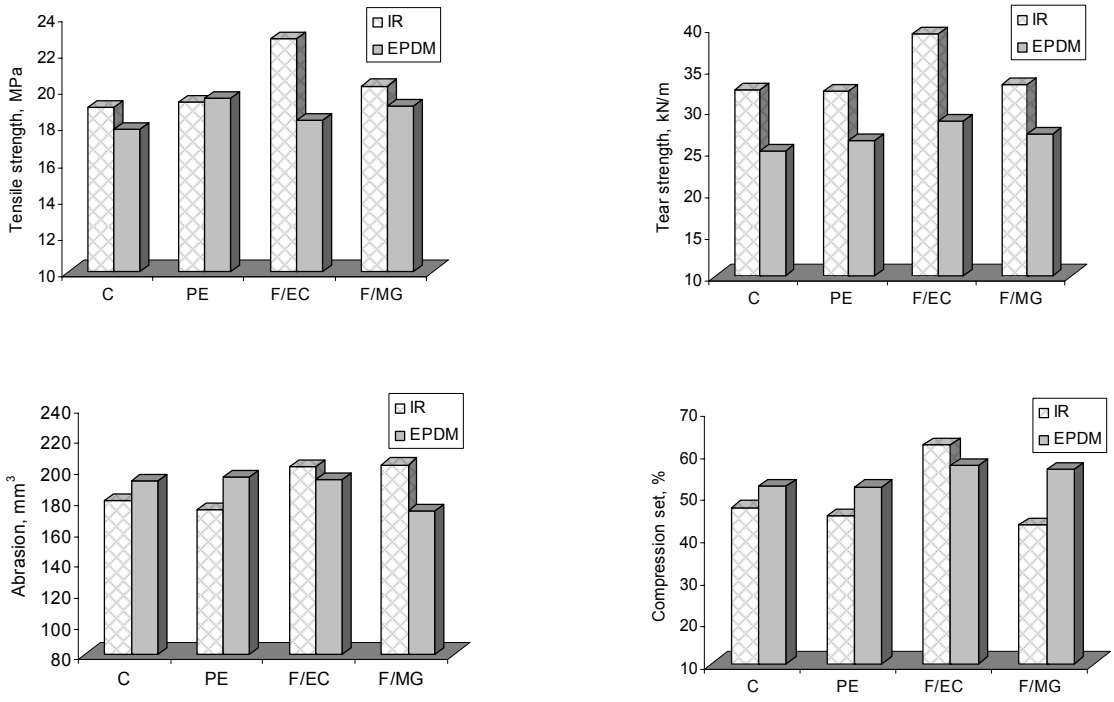

Fig. 1. **Effect of Fusabond E EC 603D and Fusabond A MG 423D on properties of IR and EPDM nanocomposites**

strength and tear resistance of nanocomposites containing Fusabond E EC-603D – about 15 %. Material also has improved thermal stability, in the case of IR composites with Fusabond EC-603D the value of T_5 increased around 25 °C; for EPDM about 90 °C.

Unfortunately, adverse effects were found in terms of compression set and resistance to abrasion of composites containing both modifiers. No beneficial effects on improving the resistance to heat aging were found too. Shore hardness and elongation at break developed slightly increased.

REFERENCES

1. Varghese S., Karger-Kocsis J.: J. Appl. Pol. Sci. *91*, 813 (2004).
2. Zheng H., Hang Y., Peng Z., Zhang Y.: J. Appl. Pol. Sci. *92*, 638 (2004).
3. Ahmadi S. A., Huang Y., Li W. : Comp. Sci. Technol. *65*, 1069 (2005).
4. Gołębiewski J., Różański A., Gałęski A.: Polimery *51*, 374 (2006).
5. Kunert A., Zaborski M.: cz. 2, Elastomery *10*, 3 (2006).
6. Ślusarski L., Zaborski M., Donnet J. B.: Kautsch. Gummi, Kunstst. *50*, 91 (1997).
7. Li W., Huang D., Ahmadi S. J.: J. Appl. Pol. Sci. *94*, 440 (2004).

P-32
EFFECT OF STRUCTURE ON MECHANICAL PROPERTIES OF PP-PTT BLEND FIBRES

ALENA HOFERÍKOVÁ*, MARCELA HRICOVÁ, ALEXANDRA ANDREJKOVÁ, and ANTON MARCINČIN

Slovak University of Technology in Bratislava, FCHFT, IPM, Department of Fibres and Textile Chemistry, Radlinského 9, 812 37 Bratislava, SK
alena.hoferikova@stuba.sk

Poly (trimethylene terephthalate) (PTT), which was recently commercialized[1], has similar molecular weight compared to other polyesters. It can be formed into fibres and films[2–4]. The characteristic properties for PTT are a flexible trimethylene repeat group in the polymer chain, lower melting temperature (238 °C), glass transition of about 55 °C and lower water absorption relative to PET[2]. PTT fibres display su-perior elasticity and recovery properties relative to PET[1–4].

In our previous work, the phase structure and properties of PP/PET and PP/PBT blends and blend fibres were investigated[5–7]. In this paper the rheological properties of the polymers and PP/ (PTT/PET) blends and the phase structure, morphology and selected properties of PP/PES fibres are presented. The compatibility during processing of polymers for spinning was evaluated by using a statistical evaluation of the external and internal non-uniformity of the blend fibres. Fi-

nally, the relationship between morphological parameters of the blend fibres and MB composition (rheological properties) as well as mechanical properties and phase structure characteristics are discussed.

Experimental

Polymers used in the study were:

Polypropylene TG 920 (PP), MFI = 10.5 g/10 min, Slovnaft
Poly (trimethylene Terephthalate) (PTT), $\eta_{\gamma=100\ s-1}$ = 260 Pa s, Du Pont
Poly (ethylene Terephthalate) (PET), IV = 0.55 l g^{-1}, SH Senica
"Master batch" composition: PP+PTT+PET (Table I)

Table I
The composition of the "master batch" MB

Master batch	PP [%]	PTT [%]	PET [%]
MB1	–	100	–
MB2	–	–	100
MB3	–	30	70
MB4	–	70	30
MB5	30	70	–
MB6	70	30	–
MB7	30	21	49
MB8	30	49	21
MB9	70	9	21
MB10	70	21	9

Preparation of the MB and blend fibres

PP/ (PTT/PET) fibres were prepared in two steps:
a) Mixing of the powder polymer components of the MB in a high a speed mixer. Powder mixtures were melted using twin-screw extruder (Werner Pfleiderer) f = 28 mm at 275 °C. The extrudate was cooled and cut into blend chips.
b) In the second step the blend PP/PES fibres were prepared by melt spinning of the polymer mixture of PP and MB, using a laboratory spinning equipment with an extruder f = 30 mm. The parameters of the spinning process were: temperature 275 °C and take up speed of 400 m min^{-1}. The linear density of the undrawn fibres was Tdt = 750 dtex. Multifilaments were drawn using the laboratory drawing equipment. The draw ratio was 3x at a temperature 110 °C. The linear density of the drawn multi filaments was Tdt = 250 dtex f40 (40 filaments).

Methods

Rheological properties of blends were measured using a capillary extrusiometer Göttfert N 6967.

A light microscope Olympus BH-2 with software Quick Photo Micro 2.0 was used for measurements of the size and shape of the separated PES microfibres upon dissolving of the PP matrix in xylene at 140 °C.

An Instron 1122 was used for determination of the mechanical properties, (tenacity and elongation) of the PP/PES blend fibres. Statistical evaluation of the tensile strength and elongation at break and their variation coefficients was used for determination of the internal (structural) unevenness of the PP/PES blend fibres.

Results and discussion

Rheology of polymer components and FPA

Experimental results of the rheological measurements indicate that in spite of the approximately three times higher viscosity of PTT relative to PET, its deviation from the Newtonian behavior was negligible (n = 0.99). The higher deviation was found for PET (n = 0.93) (Table II).

"Master batch" based on miscible PTT/PET blend exhibits the lowest both viscosity and viscosity ratio K in comparison with additive contribution of individual polymers, as indicated in the Table II. Immiscible binary blends PP/PTT exhibit the highest blend viscosity due to high PTT viscosity. Ternary blends PP/ (PTT/PET) provide viscosity between miscible PTT/PET and immiscible PP/PTT blends. Ternary MB blends also exhibit the highest deviation from Newtonian flow, with flow behavior similar to PP (Table II). It can be expected the higher viscosity of MB and viscosity ratio K, the more favourable conditions for deformation of MB and creating the PES microfibres in PP matrix. The balance between break and coalescence of the PES particles will determine their length and diameter.

Phase structure of the blend PP/ (PTT/PET) fibres

The diameter and length of the PES dispersed phase in the PP matrix define the phase structure of the PP/PES fibres.

Analysis of the separated PES micro-fibres shows uni-

Table II
Rheological parameters (n, k, K and η on Newton and Ostwald de Waele laws) of polymers and master batches (MB)

Master batch	k	n	η [Pa.s]		$K = \eta_d/\eta_m$	
			γ=100 s^{-1}	γ=300 s^{-1}	γ=100 s^{-1}	γ=300 s^{-1}
PP	3709	0.44	283	153	–	–
PTT	269	0.99	260	258	0.92	1.69
PET	134	0.93	97	89	0.34	0.58
MB3	92	0.97	80	77	0.28	0.50
MB4	133	0.93	98	91	0.35	0.59
MB5	452	0.78	164	129	0.58	0.84
MB6	2191	0.52	241	142	0.85	0.93
MB7	627	0.67	138	96	0.48	0.63
MB8	559	0.70	143	103	0.51	0.67
MB9	1563	0.53	180	107	0.64	0.70
MB10	2022	0.50	201	116	0.71	0.76

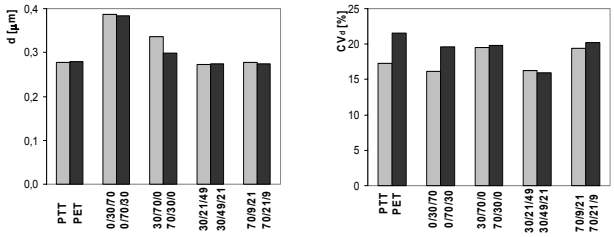

Fig. 1. **Impact of MB composition (PP/PTT/PET) on change in diameter (d) and coefficient of variation of diameter CVd for PES microfibres separated from PP matrix**

form thickness but wide distribution in length. Average values of both the diameter and length of the micro-fibres in PP matrix for spun and drawn fibres are given in the Fig. 1, 2. The results show, that the higher diameter (d) of the PES microfibres is characteristic for blend fibres prepared when using PP and a binary blend of MB such as PTT/PET and PP/PTT.

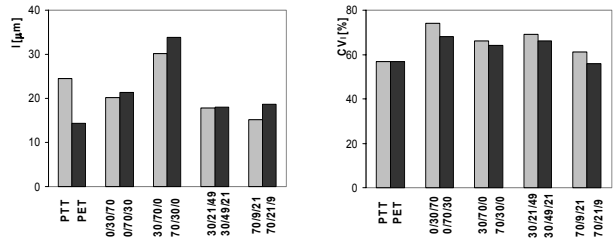

Fig. 2. **Impact of MB composition (PP/PTT/PET) on change in length (l) and coefficient of variation in length CVl for PES microfibres separated from PP matrix**

Lower diameter of the PES micro-fibres was obtained when PP and the ternary blend PP/ (PTT/PET) of MB was used in spinning. The longest PES micro-fibres were obtained for blend fibres obtained from PP and MB based on binary PP/PTT blend. Medium lengths are obtained by PTT/PET blend while the shortest micro-fibres were formed in spinning of the PP with PET and ternary PP/PTT/PET blend as MB. PTT component in PES dispersed phase contributes to an increase in both diameter and length of the dispersed PES phase. Taking into account fibres based on PP and pure PTT or PET or binary MB of PTT/PET, the length of the PES micro-fibres in PP matrix increases with increasing viscosity ratio (K) of MB to PP (Table II, Fig. 1, 2). The coefficient of variation of the diameter of microfibres ranges between 16 and 21 %, the lowest for PTT and the highest for PET microfibres. The phase structure with the smallest diameter and length was formed when ternary MB was added during spinning of PP/PES blend fibres (Fig. 1, 2).

The influence of the MB composition on processing the PP/PES blends during melting and spinning can be quantified by non-uniformity of the blend fibres. The coefficient of variation of the tenacity of fibres is a measure of internal non-uniformity of the fibres (Table III).

The higher uniformity in phase structure may result in lower mechanical properties of the blend fibres. As indicated

Table III
Tenacity (T) and elongation (E) of PP/PES blend fibers and their coefficients of variation. Content of PES in PP fibres 8.0 wt.%

Fiber	Composition of fiber	T [cN/ dtex]	CV_T [%]	E [%]	CV_E [%]
1	MB1 (100PTT)	1.52	1.49	28.2	3.47
2	MB2 (100PET)	1.27	2.16	26.7	5.93
3	MB3 (30PTT/70PET)	1.35	1.51	29.5	5.64
4	MB4 (70PTT/30PET)	1.50	1.52	28.0	8.46
5	MB5 (30PP/70PTT)	1.61	1.89	26.7	5.34
6	MB6 (70PP/30PTT)	1.57	1.40	28.0	4.23
7	MB7 (30PP/21PTT/49PET)	1.39	1.59	27.5	3.62
8	MB8 (30PP/49PTT/21PET)	1.44	1.36	26.7	4.17
9	MB9 (70PP/9PTT/21PET)	1.32	2.07	27.9	3.35
10	MB10 (70PP/29PTT/9PET)	1.37	1.26	27.7	4.53

in the Table III, higher tensile strength was obtained for PP/PTT fibres and fibres based on PP and binary MB with higher external and internal non-uniformity of blend fibres. Finer phase structure of the PP/PES blend fibres leads to increased PP/PES interphase and lower tensile strength of the fibres.

Fig. 3a indicates relationships between tenacity of the blend PP/PES fibres and viscosity ratio K of the MB to PP. The impact of length of PES micro-fibres in PP matrix on tensile strength of blend fibres is shown in Fig. 3b. The results also indicate the positive impact of the difference between power law index n of PP and MB on both internal and external non-uniformity of the blend fibres (Tables II, III).

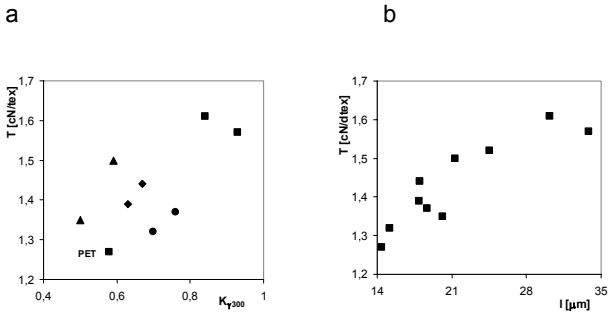

Fig. 3. **Impact of (a) viscosity ratio K of the MB to PP and (b) length of PES micro-fibres in PP matrix on tensile strength of the PP/PES blend fibres containing 8 wt.% of PES**

Conclusions

Phase structure of the blend fibres expressed by diameter (d) and length (l) of the PES micro-fibres in PP matrix is im-

pacted by the composition of the MB and viscosity of the polymer components. The relationship between the dimensions of the micro-fibres and viscosity ratio (K) of the MB to PP was obtained with the pure polyesters and binary MB used during spinning.

The relationship between the dimensions of the PES micro-fibres and tensile strength of the PP/PES blend fibres was established.

Fibres obtained from PP and ternary blends of PP/PES, (MB), indicate reduced micro-fibers dimensions of length, diameter and their coefficient of variation. In addition the non-uniformity of fibres were reduced.

Support of the grant agencies of Slovak Republic, APVV – 0226-06 and VEGA – 1/4456/07, is appreciated.

REFERENCES

1. Brown H. S.: Chem. Fiber. Int. *47*, 72 (1997).
2. Hwo CH. C.: Nonwovens from PTT staple, Shell Chemical Company, Publication No SC 3002-00, 10 (2000).
3. Tae-Kyung K., Young A. S., Yong J. L.: Dyes and Pigments *67*, 229 (2005).
4. Chuah H.: Chem. Fiber. Int. *46*, 424 (1996).
5. Marcinčin A., Ujhelyiová A., Marcinčinová T. Macromol. Symp. *176*, 65 (2001).
6. Körmendy E., Marcinčin A, Hricová M., Kovačič V.: Fibres Textiles in Eastern Europe *13*, 20 (2005).
7. Marcinčin A., Körmendy E., Hricova M., Rusnák A., Aneja A. P.: J. Appl. Polym. Sci. *102*, 4222 (2006).

P-33
SOLID PHASE GRAFTING OF iPP POWDER

AGNESA FIEDLEROVÁ, ŠTEFAN CHMELA, IVICA JANIGOVÁ, and IGOR NOVÁK

Polymer Institute, Slovak Academy of Sciences, Dubravska cesta 9, 842 36 Bratislava, Slovak Republic
Agnesa.Fiedlerova@savba.sk

The search for effective grafting methods of isotactic polypropylene (iPP) is already a fifty years history[1,2]. The aim of this effort is, in most cases, to suppress the nonpolar character of iPP by attaching to it polar functional groups or chains. This has led to methodologies for preparing multicomponent polymer systems based on iPP. Continued commercial applications (e.g. in automotive industry) for modified iPP such as nanocomposites containing dispersed nanoparticles, supports the need for further development. Currently, the iPP compatibilizer with highest efficiency in mixing with inorganic fillers, metal and polar polymers is iPP grafted with maleic anhydride – MAN[3].

This work is a continuation in our studies of grafting in the solid state[4,5] for which we have also tested the transfer of heat from a liquid medium (water) to the reacting solid iPP instead of inert gas with some vapor of present monomer. The usual procedure for solid phase grafting consists of a mixture of powdered iPP containing an adsorbed mixture of peroxide and monomer in amorphous part of iPP particles, where the main reaction of grafting is realized[4]. This represents a heterogeneous material, in which heat transfer is realized slowly. Thermal equilibrium of the reaction mixture is reached very slowly. Therefore, in this study we have used water as a heat transfer medium. The main aim of this study is to check the possible role of water as heat transfer medium, to investigate the influence of alkyl chain in the ester group of the series of methacrylic monomers on the efficiency of iPP chain grafting and also on the hydrophilicity of the grafted iPP.

The samples of grafted iPP with three different concentrations of each type of MA monomer (10, 20 and 30 wt.%) relating to iPP and at constant concentration of peroxide $1.39 \cdot 10^{-2}$ mol 100 g iPP in water medium were prepared. Methyl- (MMA), ethyl- (EMA), butyl- (BMA), ethyl hexyl- (EHMA), and dodecyl (DMA) methacrylate were used as comonomers. Because of the aqueous medium, the reaction temperature of iPP grafting was limited to ≤ 100 °C. 7 half-lives of the used peroxide (*tert*-butyl peroxy-pivalate – TBPPI) was chosen as sufficient time for complete peroxide decomposition. After elimination of alkyl-methacrylate homopolymer from prepared samples grafted iPP films (thickness ca 0.1 mm) were pressed. Pressed films of grafted iPP were scanned with a Nicolet Impact 400 Infrared spectrometer with 32 scans and with differentiation 4 cm^{-1}. The ratio of carbonyl absorption peak at wavelength 1730 cm^{-1}

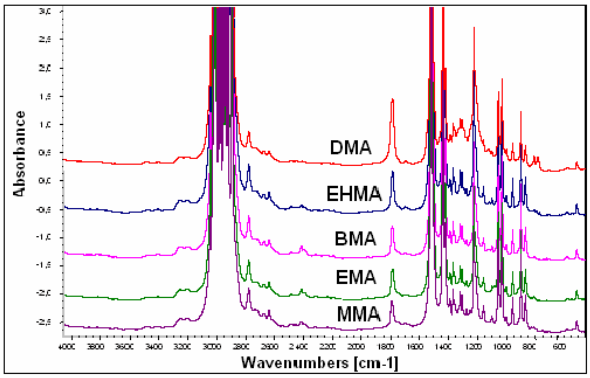

Fig. 1. **FTIR spectra of iPP grafted by different methacrylates**

Table I
Amount of methacrylate grafted onto iPP determined by FTIR spectroscopy

Type of comonomer	MA in reaction mixture [wt.%]		
	10	20	30
	Grafted methacrylate [wt.%]		
MMA	0.9	4.3	22.3
EMA	5.8	5.6	17.0
BMA	7.4	6.6	9.4
EHMA	3.5	7.4	13.0
DMA	13.4	19.6	29.5
Gel for polyDMA [wt.%]	2.1	21.5	34.7

and peak at wavelength 898 cm^{-1} (Fig. 1) was calculated. DSC measurements were done and the surface energy of grafted iPP copolymer was also determined.

The content of corresponding polymethacrylate in grafted sample was determined from calibration curve.

We have found out that the grafting degree is not a simple function of the alkyl chain length in MA monomer at grafting on iPP The highest influence on degree of grafting was observed at conditions of the gel effect of MMA and EMA (at levels of 20 to 30 wt.% of the monomer). Grafting of iPP with DMA resulted in a partial crosslinking of the grafted polymer chains. An increase of surface energy was found due to grafting of methacrylic monomer. The highest polarity was achieved in the case of iPP grafted with MMA.

The authors thank Grant Agency VEGA for financial support through grant 2/0082/08.

REFERENCES

1. Suhm J., Heinemann J., Wörner C., Müller P., Stricker F., Kressler J., Okada J., Mülhaupt R.: Macromol. Symp. *129*, 1 (1998).
2. Lazár M., Rado R., Pavlinec J.: J. Polym. Sci. *53*, 163 (1961).
3. Wang Q., Liu Ch., Chen Zh.: Polym. J. *33(7),* 522 (2001).
4. Borsig E., Lazár M., Fiedlerová A., Hrčková Ľ., Rätzsch M., Marcinčin, A.: Macromol. Symp. *176*, 289 (2001).
5. Lazár M., Hrčková Ľ., Borsig E., Marcinčin A., Reichelt N., Rätzsch M.: J. Appl. Polym. Sci. *78*, 886 (2000).

P-34
MATERIAL SELECTION FOR PRODUCTION OF PASSENGER CARS OIL FILTERS BOTTOMS

MAREK SZOSTAK

Poznan University of Technology, Institute of Materials Technology, Piotrowo street 3, 61-138 Poznan, Poland
Marek.Szostak@put.poznan.pl

In the work the comparison of mechanical properties of four materials which can be used in production of oil filters bottoms for passenger cars has been presented. For comparison the following materials: PA6 + 35 %GF – Itamid 35 (Xenon), PA6 + 40 %GF – Technyl C216 V40 (Rhodia), PC – Novarex 7020/S85 (Mitsubishi) and PBT – Crastin S600F 10 NC 010 (DuPont) has been chosen.

In literature we can find only a few articles describing the materials used for casing and membranes for car oil filters. A. Jha and A. Bhowmick[1] described the mechanical and thermal properties of PBT with acryl rubber used for oil membranes and mechanical and rheological properties of PA6 used for oil filter casing[3]. Z. Xu, T. Chung and Y. Huang[2] described the PEI/PVP blends. They have been tested the mechanical properties, mass weight, morphology and water separation of that blends. L. White and A. Nitsch[4] have been tested the filtration properties of PI membranes in correlation of types of oil used and types of impurities.

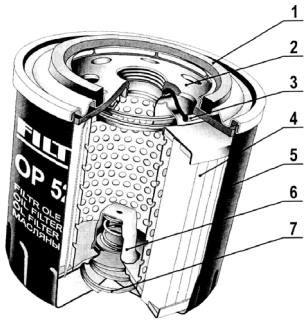

Fig. 1. **Spin–on oil filter;** 1 –sheet rubber gasket, 2 – cover, 3 – anti-drain back valve, 4 – filter pack, 5 – casing, 6 – by-pass valve, 7 – compression spring (ref.[5])

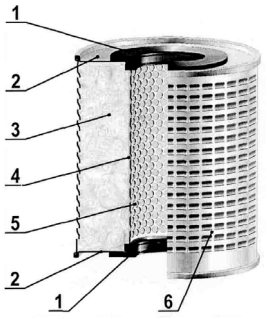

Fig. 2. **Unwoven fabric oil filter;** 1 – sheet rubber gasket, 2 – bottom, 3 – unwoven fabric, 4 – filter pack, 5 –steel core, 6 – perforated steel cover (ref.[5])

Below has been shown the samples of two types of oil filters for passenger cars: spin oil filter (Fig. 1) and unwoven fabric oil filter (Fig. 2) produced in Wix Filtron Company in Gostyn (Poland).

The measurements results of mechanical properties (max. tensile strength – δ_{max}, elongation at break – ε, Charpy's impact strength – I_{charpy} and Brinell Hardness – HB) are presented in Table I while the results of rheological (Melt Flow Index) and thermal resistant (Vicat softening temperature) properties tests in Table II.

Table I
Results of mechanical properties testing

Material	δ_m [MPa]	ε [%]	HB [MPa]	I_{charpy} [kJ m^{-2}]
PA6+35GF	156,7	8,2	36,9	18,7
PA6+40GF	180,9	5,8	39,8	11,1
PC	63,6	110,1	26,5	78,1
PBT	51,1	352,6	16,7	19,0

Table II
Results of rheological (Melt Flow Index) and thermal resistant (Vicat softening temperature) tests

Material	MFI [g/10 min]	Vicat softening temperature [°C]
PA6+35GF	4,29	218
PA6+40GF	3,09	221
PC	3,94	147
PBT	15,94	183

The results of the measurements shows that all materials have very good mechanical properties (tensile strength above 50 MPa, impact strength above 11 kJ m^{-2}), good procesability – MFI above 3 g/10 min (PBT very good – MFI above 15 g/10 min) and high thermal resistant (Vicat softening temperature above 145 °C for PC and PBT and above 200 °C for PA with glass fibers) what is very important for the materials used in the car engine chamber. Due to the market price for the production purposes the cheapest material – PA6 + 35 % GF have been selected.

Author thanks "Wix Filtron" company for financing of the project: "Plastic materials selection for passenger cars oil filters".

REFERENCES

1. Jha A., Bhowick A. K: J. Appl. Polymer Sci. *75*, 1001 (2000).
2. Xu Z., Chung T., Huang Y: J. Appl. Polymer Sci. *74*, 220 (1999).
3. Jha A., Dutta B., Bhowick A. K: J. Appl. Polymer Sci. *74*, 490 (1999).
4. White L., Nitsch A. R: J. Membr. Sci. *179*, 267 (2000).
5. Wix Filtron – producer data (2007).

P-35
INJECTION MOLD COOLING SYSTEM BY DMLS

ŠTĚPÁN ŠANDA, MIROSLAV MAŇAS, MICHAL STANĚK, DAVID MAŇAS, and LUBOŠ ROZKOŠNÝ

Tomas Bata University in Zlín, Faculty of Technology, Department of Production Engineering, nám. TGM 275, 762 72 Zlín, Czech Republic
sanda@ft.utb.cz

Abstract

This article deals with a problem of the injection mold cooling. Two designs of cooling system for the same injection mold cavity are compared with the help of the CAE application. Classical design created by drilling holes is confront with design created by DMLS (Direct Metal Laser Sintering) technology.

Introduction

Cooling system is very important part of the injection mold. Design of cooling system depends on the shape of injected product. Cooling system represent unique problem that includes many variables: material and shape of product, material of mold, etc. Uniform temperature field is fundamental principle inside the injection mold cavity. This principle is possible to realize in different ways. From this point of view designer has to be familiar with individual requirements before the injection mold project started.

Injection mold cooling system has significant effect on product quality, injection cycle duration and cost of injection mold. Mold design is created according the experiences of designer or recommendation from the technical books. He is able to review his own cooling system design using different types of CAE applications. He is able to evaluate quality of designed cooling system but he is not able to know whether the structural design of the cooling system is suitable for this injection mold.

Classical design of cooling system is usually done as drilled holes or milled channels. Tools material is very often substituted for the materials with very good thermal conductivity which are placed in the positions where it is very difficult to take of the heat. The cores are cooled with the help of baffles, cooling spirals or thermal pins. Designers very often solve problems with the position of cooling channels in order to provide the correct operation. Especially difficult is positioning of cooling channels or holes in case of complex shape products. Additional limitations are in location of ejectors and gate systems, mold strength and stiffness. Disadvantage of classical cooling system is necessity of channels sealing by reason of prevention of coolant leakage.

There are not many possibilities how to cool complex mold cavity. Use of DMLS technology (Direct Metal Laser Sintering) is one of them. DMLS is ranked among the Rapid tooling or Rapid prototyping technologies. There is possible create any geometry of cooling system with the help of DMLS technology. DMLS makes possible to create cooling channels in the case of complex cavity geometries even in positions where it would be impossible to use classical design.

Compared design

Cooling systems in the same mold cavity created both by classical and DMLS technology have been compared. For the comparison the corner part for the packaging has been used. Two-plate design of injection mold with cold runner system and cylindrical ejector pin has been used. Cooling system was created in core only (left side of the injection mold).

Classical design of cooling system is created by the drilled holes with diameter of 8 millimeters and two baffles which enable cool internal area of mold cavity. All drilled holes are sealed with plugs or O-rings. Positioning of ejectors bring many limitations for cooling system design. Classical design (Fig. 1) of the cooling system is created only by periphery of the core and from this point of view it is difficult to carry off the heat from the cavity.

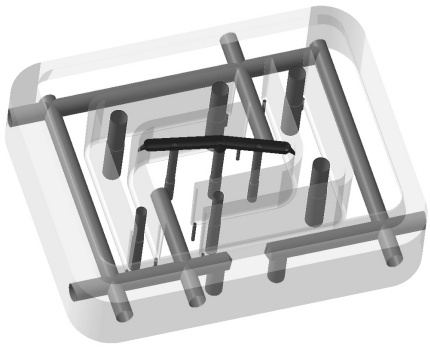

Fig. 1. **Cooling system – classical design**

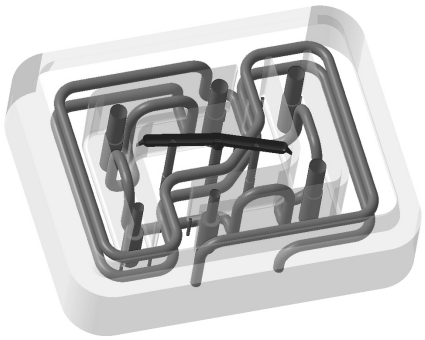

Fig. 2. **Cooling system – DMLS technology**

With the help of DMLS technology the complex shape of cooling channel is created. This channel in diameter of 5 millimeters covers very well the internal area of mold cavity. The channel is created even in these areas of mold cavity where it would be impossible to machine, e.g. by drilling or milling. The cooling channel made by DMLS technology has no intersection, has only input and output sealed by O-rings.

Cooling analyses

Moldflow Plastics Insight 6.2 has been used for cooling analyses. In this CAE application also the cavity, gating and cooling system of the mold has been defined. Two types of mashes (Dual Domain – 2.5D and Solid – 3D) have been used. All necessary correction in design of the mold cavity has been done to be able to obtain the best results. The both cooling systems were analyzed using Cool-Fill-Pack-Warp analysis sequence.

DMLS technology

Direct Metal Laser Sintering (DMLS) is a generative technology which creates product in individual layers. Thus it is possible to build very fast and effectively any geometric shape without cutting. 3D CAD model of product is necessary. DMLS builds product by layers according the 3D CAD model. Laser melts metal powder just in area of product. Materials used for DMLS: bronze, steel, stainless steel, titanium and Co-Cr. Product of DMLS is fully functional and homogenous metal part.

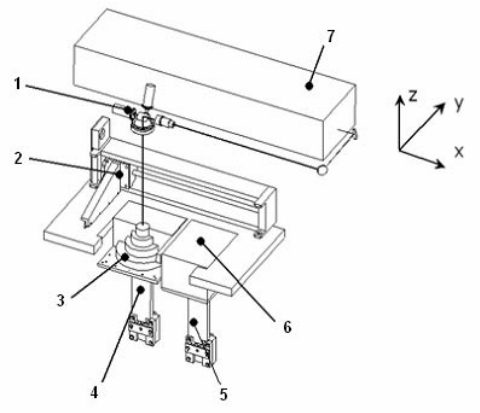

Fig. 3. **DMLS technology – principle;** 1 – galvanometer-scanner with f-Theta lens; 2 – laminated system; 3 – product of DMLS; 4 – structural platform; 5 – storage bin platform; 6 – storage bin; 7 – laser

Discussion

Cooling analyses show considerable differences between both designs of cooling systems results.

Cooling channels are more or less heat stressed from mold cavity where the polymer is cooled. Temperature of cooling channel surface represents heat stress which it is changed over the length of channel depending on position of mold cavity. It is necessary to ensure less temperature difference over the length of cooling channel than 5 °C. Higher temperature difference induces overloading of cooling channel. Classical structural design of cooling channel is overloading in baffles. Cooling channel created by DMLS technology does not have this problem because position of channel was more uniform and heat removal was more intensive. It is show on coolant temperature difference (input vs. output). Cooling channel by DMLS reached 2.25 °C and classical design reached 0.82 °C.

Either design of the cooling systems show difference intensity of heat removal from the mold cavity. This intensity of heat removal depends on distance of channel from the cavity, value of Reynolds number and temperature difference between the coolant and channel wall. The channel created by DMLS technology showed much more efficiency of heat removal because covers very well the internal area of mold cavity in compare with classical design. This statement was supported by comparison of temperature field from the both designs. Temperature differences both temperature fields had value almost 26 °C in individual areas of mold cavity. This fact has influence on rate of solidification of polymer in cavity and number of frozen polymer layers over the thickness of product wall.

Conclusion

Classical design of the injection mold cooling system represents available and cheap solution. However, classical design does not make uniform temperature field possible and therefore it was impossible to remove effectively the heat from the mold cavity. The results of cooling analyses confirmed that the new design of cooling system of injection mold is very useful. DMLS technology is important for practical applications and enables production of complicated geometry of product or several products simultaneously. DMLS is new flexible method for Rapid prototyping and Rapid tooling and production of tools with complex shapes of mold cavity in comparison with commonly used methods.

This article was financially supported by the Ministry of Youth and Education in the Czech Republic as a project of "Modeling Processes of Machining Natural and Synthetic Polymers". No. MSM 7088352102.

REFERENCES

1. Moldflow Plastics Insight [počítačový program]. Ver. 6.2 Academic Edition Revision 3. Moldflow Corporation, 2008 [cit. 2009-01-23]. Dostupný z WWW: <http://www.moldflow.com/stp/>.
2. Rees H.: *Mold Engineering*. 2nd edition. xxiii, 688 s. Carl Hanser Verlag, Munich 2002.
3. DMLS − Direct Metal Laser Sintering: Kovové prototypy [online]. c2007 [cit. 2009-02-02]. Dostupný z WWW: <http://www.dmls.cz/>.

CONTENTS

Main Lectures

Key Lectures

Contributed Lectures

Posters

AUTHOR INDEX